

The Quark-Gluon Plasma
in the AdS/CFT Correspondence and Thermal Perturbative QCD

by

Kiminad Abebe Mamo
B.Sc. (Addis Ababa University) 2008

Thesis submitted in partial fulfillment of the requirements
for the degree of Doctor of Philosophy in Physics
in the Graduate College of the
University of Illinois at Chicago, 2017

Chicago, Illinois

Defense Committee:
Ho-Ung Yee, Chair and Advisor
David Hofman
Matthias Kaminski, University of Alabama
Wai-Yee Keung
Misha Stephanov

Copyright by
Kiminad Abebe Mamo
2017

To

my grandma (Abaye)

ACKNOWLEDGMENTS

First and foremost, I would like to express my deep gratitude to my advisor Prof. Ho-Ung Yee for his continuous support, guidance and patience.

I would like to thank Profs. David Hofman, Wai-Yee Keung, Tom Imbo, whose course I took at UIC, and especially to Prof. Misha Stephanov for his deep and insightful questions, and Prof. Arthur Licht for various courses I took with him at UIC. Moreover, I would like to thank Prof. Matthias Kaminski for joining my committee.

I would also like to thank Deginet Admassu, Meseret Asrat, Ahmet Gulec, Saleh Hamdan, Tigran Kalaydzhyan, Shiyong Li, Pablo Morales, Jean-Francois Paquet, Tadas Paulauskas, Meisam Razaei, Francisco Restrepo, Andrey Sadofyev, Enrico Speranza, Qingyun Wang for various discussions about physics and beyond.

I would like to acknowledge ICTP Spring School on Superstring Theory and Related Topics (2014); ECT* Doctoral Training Program (2014); Brookhaven National Laboratory for hospitality; UIC dean's scholar fellowship which supported part of the research reported in this dissertation.

CONTRIBUTION OF AUTHORS

Parts of this dissertation are based on my previous publications: Chap. 2, Sec. 3.1, Sec. 4.3, Chap. 6, Chap. 7 are based on my single-authored papers (51), (210), (211), (196), (360) and (361), respectively.

ACKNOWLEDGMENTS (Continued)

Sec. 3.2, Sec. 3.3, Sec. 3.4, Chap. 5 are based on my papers with Ho-Ung Yee (362), (154), (155), (322), respectively. In this papers, I helped formulate the problems and did part of the calculations.

Sec. 4.1 and Sec. 4.2 are based on my paper with Shiyong Li and Ho-Ung Yee (206). In this paper, I helped formulate the problem and did part of the calculations.

All reproduction of part of my previous publications in this dissertation is in accordance with the copyright policies of the corresponding publishers.

TABLE OF CONTENTS

<u>CHAPTER</u>		<u>PAGE</u>
1	INTRODUCTION	1
2	SHEAR VISCOSITIES OF STRONGLY COUPLED ANISOTROPIC PLASMA	13
2.1	Effective Action for Gravitational Shear Mode Fluctuations .	14
2.2	Holographic RG Flow Equation for Shear Viscosities	16
2.3	Anisotropic Black Hole in Type IIB Supergravity and Its Shear Viscosities	19
3	ELECROMAGNETIC PROBES OF QUARK-GLUON PLASMA	31
3.1	Soft Electromagnetic Probes of Strongly Magnetized Plasma at Strong Coupling	32
3.1.1	DC Conductivities of Strongly Magnetized Plasma at Strong Coupling	35
3.2	Velocity Gradient Correction to Photon Production Rate at Strong Coupling	56
3.3	Spin Polarized Photons and Dileptons of Axially Charged Plasma at Strong Coupling	62
3.4	Spin Polarized Photons of Axially Charged Plasma at Weak Coupling	75
4	HARD PROBES OF STRONGLY MAGNETIZED QUARK-GLUON PLASMA	135
4.1	Jet Quenching Parameter at Weak Coupling	138
4.2	Jet Quenching Parameter at Strong Coupling	162
4.3	Energy Loss of Heavy Quark at Strong Coupling	185
4.3.1	Drag Force	189
5	THERMALIZATION OF MAGNETIZED QUARK-GLUON PLASMA	198
6	CONFINEMENT-DECONFINEMENT PHASE TRANSITION IN EXTERNAL MAGNETIC FIELD	211
6.1	Einstein-Maxwell Theory in 5D	215
6.2	Hard-Wall AdS/QCD	224
6.3	Unflavored $\mathcal{N}=4$ SYM Plasma on Compact Space	226
6.4	Flavored $\mathcal{N}=4$ SYM Plasma on Compact Space	227

TABLE OF CONTENTS (Continued)

<u>CHAPTER</u>		<u>PAGE</u>
7	$\mathcal{N}=4$ SUPER YANG-MILLS GAUGE THEORY ON THE COULOMB	
	BRANCH	230
7.1	Thermodynamics and a Second-Order Phase Transition	232
7.2	Cornell Potential and Glueball Mass Spectrum	235
7.3	Hadronization	242
7.4	Transport Coefficients	247
7.5	Hard Probes	250
	APPENDICES	260
	CITED LITERATURE	263
	VITA	308

LIST OF TABLES

<u>TABLE</u>		<u>PAGE</u>
I	(AdS ₅) Parameters of our numerical solutions for RHIC with a late-time temperature $T = 300$ MeV and several exemplar values of $B = 0; 0.08 \text{ GeV}^2; 0.2 \text{ GeV}^2; 1 \text{ GeV}^2; 2 \text{ GeV}^2$	206

LIST OF FIGURES

<u>FIGURE</u>		<u>PAGE</u>
1	Time evolution of a heavy-ion collision.	2
2	The Schwinger-Keldysh contour.	10
3	Penrose diagram of AdS black-hole geometry.	11
4	Shear viscosity $\eta \equiv \text{Re}(\eta^i_z)$ over $s/4\pi$ as a function of the radial coordinate ϵ with $u_h = 0.50$, $a = 0.1$, and $T = 0.64$	29
5	Shear viscosity $\eta \equiv \text{Re}(\eta^i_z)$ over $s/4\pi$ as a function of the anisotropy parameter a/T at the horizon $\epsilon = u_h = 0.50$, and at the boundary $\epsilon = 0$ for $a \ll T$	29
6	Thermal photon production at any frequency (Equation 3.1.50) [<i>solid lines</i>] and at low-frequency (Equation 3.1.51) [<i>dashed lines</i>] for $B = 0$	49
7	The ratio of thermal photon production at any frequency (Equation 3.1.50) and at low-frequency (Equation 3.1.51) for $B = 0$	50
8	Thermal photon production in the absence of the magnetic field $B = 0$ (Equation 3.1.52) [<i>solid lines</i>] and in the presence of the strong magnetic field $B \gg T^2$ (Equation 3.1.53) [<i>dashed lines</i>]. In (a) we used (Equation 3.1.32) to get $B = B_{SYM} = (6.8 \frac{B_{RHIC}}{T^2}) \times B_{RHIC} = 10.90 \times 4m_\pi^2$, $T = 1.58m_\pi$ and $b = \frac{1}{4\pi^2} \frac{B}{T^2} = 0.44$ at RHIC . In (b) we used (Equation 3.1.32) to get $B = B_{SYM} = (6.8 \frac{B_{LHC}}{T^2}) \times B_{LHC} = 21.46 \times 15m_\pi^2$, $T = 2.18m_\pi$ and $b = \frac{1}{4\pi^2} \frac{B}{T^2} = 1.72$ at LHC	51
9	Thermal dilepton production in the absence of the magnetic field $B = 0$ (Equation 3.1.71) [<i>solid lines</i>] and in the presence the strong magnetic field $B \gg T^2$ (Equation 3.1.72) [<i>dashed lines</i>] as a function of the intermediate-mass $1\text{GeV} \leq M \leq 3.2 \text{ GeV}$ of the dileptons. In (a) we used $p_T = 1\text{GeV}$, also used (Equation 3.1.32) to get $B = B_{SYM} = (6.8 \frac{B_{RHIC}}{T^2}) \times B_{RHIC} = 10.90 \times 4m_\pi^2$, $T = 1.58m_\pi$, $b = \frac{1}{4\pi^2} \frac{B}{T^2} = 0.44$ at RHIC . In (b) we used $p_T = 1\text{GeV}$, also used (Equation 3.1.32) to get $B = B_{SYM} = (6.8 \frac{B_{LHC}}{T^2}) \times B_{LHC} = 21.46 \times 15m_\pi^2$, $T = 2.18m_\pi$ and $b = \frac{1}{4\pi^2} \frac{B}{T^2} = 1.72$ at LHC	55
10	The plot of $R^{(1)} = \Gamma^{(1)}(\omega)/\Gamma^{(0)}(\omega)$ as a function of ω/T	61
11	A schematic illustration of the lepton (\vec{p}_1) and anti-lepton (\vec{p}_2) momenta in the di-lepton emission from an isotropic axially charged plasma.	67
12	The photon circular polarization asymmetry $A_{\pm\gamma}$ from an axially charged plasma as a function of frequency ω , where $T = 300 \text{ MeV}$ with $\mu_A = 100 \text{ MeV}$ (solid) and $\mu_A = 50 \text{ MeV}$ (dashed).	74

LIST OF FIGURES (Continued)

FIGURE

PAGE

13	The di-lepton spin polarization asymmetry $A_{\pm ll}$ from an axially charged plasma as a function of one lepton momentum $p = \vec{p} $ for the case of muon, where $T = 300$ MeV with $\mu_A = 100$ MeV (solid) and $\mu_A = 50$ MeV (dashed). The relative angle between muon and anti-muon pair is taken to be $2\theta = \frac{\pi}{2}$	75
14	Pair Annihilation diagrams with hard momentum exchanges.	83
15	Compton scattering diagrams with hard momentum exchanges.	86
16	The geometry of t-channel parametrization. $(\hat{q}, \hat{x}^1, \hat{x}^2)$ form an orthonormal basis rotated by θ_{qk} , and \mathbf{p}'' is a projection of \mathbf{p}' onto the (\hat{x}^1, \hat{x}^2) plane.	91
17	The integration domain of (q^0, \mathbf{q}) (shaded blue). The domain for $ \mathbf{p}' $ is $ \mathbf{p}' > (\mathbf{q} - q^0)/2$. The soft region A (shaded red) is responsible for leading log IR divergence, and the region B produces the energy logarithm that is described in the following.	92
18	Two real-time Feynman diagrams for $G_{\mu\nu}^{ra}(k)$ in the “ra”-basis.	101
19	Leading log contributions from soft t- or u-channel exchanges: a hard fermion making conversion to a collinear photon. The blob represents Hard Thermal Loop (HTL) re-summed propagator.	109
20	Angular momentum conservation in leading log spin polarized emission rates.	111
21	Ladder diagrams to be summed over to get the correct leading order LPM contribution to (our P-odd) photon emission rate.	112
22	Two types of real-time ladder diagrams for leading order LPM contributions. The shaded part represents the re-summed rr-type current vertex $\Lambda^i(p, k)$. The rr-type gluon lines are the HTL re-summed ones.	113
23	The real-time Schwinger-Dyson equation for the re-summed vertex $\Lambda^i(p, k)$	115
24	Numerical results for $C_{2\leftrightarrow 2}^{odd,(1)}(\omega/T)$, $C_{LPM}^{odd,(1)}(\omega/T)$ for $N_F = 2$ QCD.	134
25	The imaginary cut of the jet self-energy is equal to the damping rate, that is, the total scattering rate with thermal (hard) particles, especially the lowest Landau level quarks. The exchanged gluon line is Debye screened by the same hard LLL states.	141
26	(AdS ₅) Thermalization history of falling mass shell for RHIC (left) and LHC (right). The late-time temperature is fixed to be $T = 300$ (400) MeV for RHIC (LHC), and the magnetic fields are $B = 0$ (0) (<i>solid blue</i>); 0.08 (0.3) (<i>orange</i>); 0.2 (<i>green</i>); 1 (<i>red</i>); 2 (<i>purple</i>) GeV^2 for RHIC (LHC). Thermalization time is when the curve reaches its plateau at the horizon.	208
27	(AdS ₅) Thermalization history of falling mass shell for fixed energy density, and varying magnetic field $B = 0$ (<i>solid blue</i>); 0.08 (<i>orange</i>); 0.2 (<i>green</i>); 1 (<i>red</i>); 2 (<i>purple</i>) GeV^2 for RHIC.	209

LIST OF FIGURES (Continued)

FIGURE		PAGE
28	(AdS ₄) Thermalization history of falling mass shell in AdS_4 for a late-time temperature of $T = 300$, and the magnetic fields are $B = 0$ (<i>solid blue</i>); 0.08 (<i>orange</i>); 0.2 (<i>green</i>) GeV^2	210
29	Critical temperature $T_c(B)$ of the hard-wall AdS/QCD with $r_0 = \frac{m_\rho}{2.405} = 0.323$ GeV Note: $\mathcal{B} = \sqrt{3}B$ is the physical magnetic field at the boundary.	225
30	Critical temperature $T_c(B)$ of flavored $\mathcal{N} = 4$ SYM on $R^3 \times S^1$ (Equation 6.4.34) using $T_c^0 = 0.175$ GeV and $\lambda_h = 23 \times \frac{N_c}{N_f}$	229
31	Hawking temperature (Equation 7.1.4).	234
32	The free energy density $\frac{f}{\Lambda^4 N_c^2}$ of $\mathcal{N} = 4$ cSYM plasma (Equation 7.1.7) for the large and small black holes.	235
33	The free energy density $\frac{f_{sphere}}{(\Lambda_{sphere})^4 N_c^2}$ of $\mathcal{N} = 4$ SYM plasma on 3-sphere of radius R (Equation 7.3.16) for the large and small black holes.	236
34	The energy density $\frac{\epsilon}{T^4}$, entropy density $\frac{3}{4} \frac{s}{T^3 N_c^2}$, and pressure $\frac{3p}{T^4 N_c^2}$ of $\mathcal{N} = 4$ cSYM plasma for the large and small black holes.	237
35	The trace anomaly $\frac{\epsilon - 3p}{T^4 N_c^2}$ of $\mathcal{N} = 4$ cSYM plasma for the large and small black holes.	238
36	The specific heat C_Λ of $\mathcal{N} = 4$ cSYM plasma for the large and small black holes.	238
37	The speed of sound c_s^2 of $\mathcal{N} = 4$ cSYM plasma for the large and small black holes.	239
38	The bulk viscosity to entropy density ratio $\frac{\zeta}{s}$ of $\mathcal{N} = 4$ SYM plasma on the Coulomb branch for both large and small black holes (Equation 7.4.28).	249
39	The conductivity $\frac{\sigma_f}{TN_c N_f}$ of a $U(1)$ flavor charge (Equation 7.4.29), and $\frac{\sigma_R}{TN_c^2}$ of a single R-charge (Equation 7.4.30) of flavored and unflavored $\mathcal{N} = 4$ SYM plasma, respectively, on the Coulomb branch for both large and small black holes.	251
40	The drag forces $\frac{F_{drag}}{F_{drag}^0}$ (Equation 7.5.41), and $\frac{F_{drag}^{(10)}}{F_{drag}^0}$ of $\mathcal{N} = 4$ SYM plasma on the Coulomb branch for both large and small black holes, normalized by the drag force $F_{drag}^0 = -\frac{1}{2}\sqrt{\lambda}\pi T^2 \gamma v$ of the conformal $\mathcal{N} = 4$ SYM plasma.	254
41	The transverse and longitudinal momentum diffusion constants $\frac{\kappa^\perp(0)}{\kappa_0(v)}$ (Equation 7.5.42) and $\frac{\kappa^\parallel(0)}{\kappa_0(0)}$ (Equation 7.5.43), respectively, of $\mathcal{N} = 4$ SYM plasma on the Coulomb branch for both large and small black holes, normalized by the momentum diffusion constant $\kappa_0 = \kappa_0^\perp(0) = \kappa_0^\parallel(0) = \sqrt{\lambda}\pi T^3$ of the conformal $\mathcal{N} = 4$ SYM plasma.	255

LIST OF FIGURES (Continued)

<u>FIGURE</u>		<u>PAGE</u>
42	The jet quenching parameter $\frac{\hat{q}}{\hat{q}_0}$ (Equation 7.5.45) and entropy density $\frac{s}{s_0}$ of $\mathcal{N} = 4$ SYM plasma on the Coulomb branch for both large and small black holes, normalized by the jet quenching parameter $\hat{q}_0 = \frac{\pi^{3/4}\Gamma(3/4)}{\sqrt{2}\Gamma(5/4)}\sqrt{\lambda}T^3$ and entropy density $s_0 = \frac{1}{2}\pi^2 N_c^2 T^3$ of the conformal $\mathcal{N} = 4$ SYM plasma.	256
43	Copyright agreement for JHEP.	261
44	Copyright agreement for PRD.	262

LIST OF ABBREVIATIONS

SYM	Super Yang-Mills
cSYM	Super Yang-Mills on the Coulomb branch
QGP	Quark-Gluon Plasma
QCD	Quantum Chromodynamics
pQCD	Perturbative Quantum Chromodynamics
CME	Chiral Magnetic Effect
AdS	Anti-de Sitter
CFT	Conformal Field Theory
RG	Renormalization Group
IR	Infrared
UV	Ultraviolet
VEV	Vacuum Expectation Value
KSS	Kovtun-Son-Starinets
LPM	Landau-Pomeranchuk-Migdal
RHIC	Relativistic Heavy-ion Collider
LHC	Large Hadron Collider

SUMMARY

In this dissertation, I present my research on different aspects of the quark-gluon plasma (QGP) by using the AdS/CFT correspondence, and thermal perturbative QCD approaches. The effects of external magnetic field on the thermalization of the QGP (dual to black hole formation in AdS space), and the critical temperature of the confinement-deconfinement phase transition of the QGP (dual to Hawking-Page phase transition in AdS space) will be studied. The violation of the KSS viscosity bound in anisotropic QGP or anisotropic black hole geometries in AdS space will be shown. Moreover, using the holographic RG flow and Schwinger-Keldysh formalisms in the AdS/CFT correspondence, as well as thermal perturbative QCD, the electromagnetic probes of the QGP will be investigated by taking into account the effects of external magnetic field, velocity gradient correction, and axial anomaly. The hard probes of the strongly magnetized QGP, such as jet quenching and energy loss of a heavy quark, will also be investigated by using thermal perturbative QCD, and string theory in AdS space. Finally, different aspects of $\mathcal{N} = 4$ super Yang-Mills theory on the Coulomb branch will be explored by using its string theory dual, and will be shown to have most of the properties expected from pure Yang-Mills theory at strong coupling. In addition, a new holographic mechanism for hadronization or particle production from the QGP will be proposed, and shown to be equivalent to the well-known Cooper-Frye formula in the hydrodynamic or low frequency limit.

CHAPTER 1

INTRODUCTION

Due to the asymptotic freedom of the QCD coupling constant at very high temperature $T > T_c \sim 120 \text{ MeV}$, a quark-gluon plasma (QGP) is expected to be formed in ultra-relativistic heavy-ion (such as gold-gold or lead-lead) collision experiments. See the cartoon diagram Figure 1 that depicts the entire time flow of a heavy-ion collision experiment (1).

In this dissertation, we will investigate the properties, formation, and hadronization of the quark-gluon plasma (QGP) using thermal perturbative QCD, see for example (7), and the AdS/CFT correspondence (2; 3; 4), see also (5; 6).

In Chapter 2, a non-trivial holographic RG flow equation of the shear viscosity in anisotropic black hole geometry (dual to anisotropic QGP) will be derived. After solving the RG flow equation analytically, we show that the KSS viscosity bound is violated in anisotropic black hole geometries.

In Chapter 3, different aspects of the electromagnetic probes of the QGP will be investigated. In section 3.1, the thermal emission of soft photons and dileptons of a magnetic black hole geometry (dual to a magnetized QGP) will be computed analytically, and it will be shown that a strong magnetic field enhances both the soft photon and dilepton production rates of the QGP.

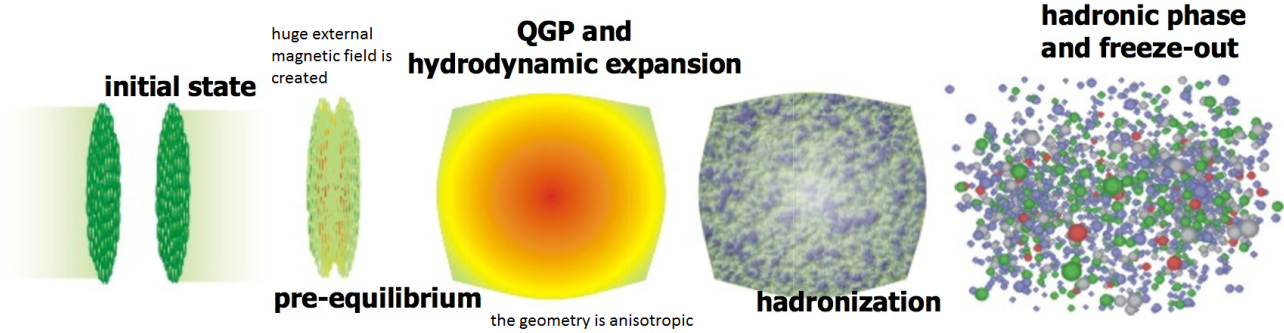


Figure 1. Time evolution of a heavy-ion collision.

In section 3.2, by using the Schwinger-Keldysh formalism in the AdS/CFT correspondence, we compute the velocity gradient correction to the photon emission rate of the QGP. We will show that the first order velocity gradient correction enhances the photon emission rate.

In section 3.3, the thermal photons and dileptons, from axially charged black hole or QGP, will be shown to have a spin polarized emission rates. The spin polarization asymmetry will be computed, both at strong coupling (in the holographic Sakai-Sugimoto model) in section 3.3, and at weak coupling (in the thermal perturbative QCD: to complete leading order which includes the LPM resummation) in section 3.4, and found to be a percent level.

In Chapter 4, the effects of strong magnetic field on hard probes of the QGP will also be investigated using thermal perturbative QCD for weak coupling regime in section 4.1, and string theory in AdS space for strong coupling regime in section 4.2. For both weak and strong

coupling regimes, it will be shown that a strong magnetic field enhances both the jet quenching parameter and energy loss of a heavy quark moving through a magnetized QGP.

In Chapter 5, using the AdS/CFT correspondence, we will show that the presence of external magnetic field speeds up the formation of black hole in the AdS background or thermalization of the QGP.

In Chapter 6, we will show that weak magnetic field decreases (while strong magnetic field increases) the critical temperature of the confinement-deconfinement phase transition in various confining holographic models of QCD.

Finally in Chapter 7, the holographic or string theory dual to the Coulomb branch of $\mathcal{N} = 4$ super Yang-Mills theory (where the conformal symmetry is broken due to the Higgs mechanism) will be studied. For particular choice of the VEVs (or for a particular point in its moduli space), we will show that $\mathcal{N} = 4$ super Yang-Mills theory on the Coulomb branch (cSYM) has most of the properties expected from pure Yang-Mills theory at strong coupling, i.e., confinement (Cornell potential), mass gap (with quantized mass spectrum for the scalar and spin-2 glueballs), an equation of state where the pressure vanishes at critical temperature T_c . We will also show that $\mathcal{N} = 4$ cSYM has a physical small black hole branch where the pressure is still positive. In addition, a new holographic mechanism for hadronization or particle production (which reduces to Cooper-Frye formula in the hydrodynamic or low frequency limit) will be proposed in section 7.3. The hydrodynamic transport coefficients and hard probe parameters of $\mathcal{N} = 4$ cSYM will also be computed in section 7.4 and 7.5, and will be shown to be consistent with the presence of particle production in the small black hole branch.

The AdS/CFT Correspondence

In what follows, we will provide a quick introduction to the tools of the AdS/CFT correspondence that we need in the subsequent chapters of the dissertation.

The AdS/CFT correspondence (2) (in its weakest form) is a holographic duality between *a weakly coupled supergravity in AdS space and strongly coupled gauge theory at the boundary of the AdS space.*

For example, Type IIB supergravity in AdS_5 space is equivalent to $\mathcal{N} = 4$ Super-Yang Mills (SYM) gauge theory at the boundary of the AdS_5 space with the following parameter mappings (2):

$$\frac{\alpha'^2}{R^4} = \frac{1}{\lambda}, \quad (1.0.1)$$

$$\frac{G_5}{R^3} = \frac{\pi/2}{N_c^2}, \quad (1.0.2)$$

where the parameters of Type IIB supergravity are: R (the radius of the 5-dimensional AdS_5 space), $\alpha' = \ell_s^2$ (the string length scale), and G_5 (the 5-dimensional Newton's gravitational coupling constant), while the parameters of $\mathcal{N} = 4$ Super-Yang Mills (SYM) gauge theory are: $\lambda = g_{YM}^2 N_c$ (the 't Hooft coupling constant), g_{YM} (the gauge theory coupling constant), and N_c (the number of colors).

Moreover, weakly coupled supergravity in the AdS black hole geometry is equivalent to strongly coupled gauge theory at finite temperature at the boundary of the AdS black hole geometry where, for example, the temperature T_{bh} of the AdS black hole is identified with the

temperature T of the thermal gauge theory, and the entropy density s_{bh} of the AdS black hole is identified with the entropy density s of the thermal gauge theory (4).

Formulations of the AdS/CFT Correspondence

The partition function for a gauge theory in Euclidean signature (where, for example, $t \rightarrow -i\tau$, $\omega \rightarrow i\omega_E$, and the action $iS \rightarrow -S_E$) is

$$Z_{\text{gauge}}(J; N_c, \lambda) = \int \mathcal{D}(\text{fields}) e^{-S_{\text{gauge}}(\text{fields}; N_c, \lambda) + \int d^d x J \mathcal{O}} \quad (1.0.3)$$

where J is the source function for the corresponding operator \mathcal{O} . And, the partition function for a supergravity theory in Euclidean signature is

$$Z_{\text{gravity}}(\phi_0; G_{d+1}, \frac{\alpha'}{R^2}) = \int \mathcal{D}\phi e^{-S_{\text{gravity}}(\phi; G_{d+1}, \frac{\alpha'}{R^2})}, \quad (1.0.4)$$

where $\phi_0(\tau, x, y, z)$ is the boundary value of $\phi(\tau, x, y, z, u)$, i.e., $\phi_0(\tau, x, y, z) = \phi(\tau, x, y, z, u = 0)$.

Therefore, according to the AdS/CFT correspondence (in its strongest form) (2; 4), we have the equivalence of the partition functions

$$Z_{\text{gauge}}(J; N_c, \lambda) \equiv Z_{\text{gravity}}(\phi_0; G_{d+1}, \frac{\alpha'}{R^2}), \quad (1.0.5)$$

where J is mapped to ϕ_0 , i.e., $J = \phi_0$.

And, in its weakest form, using $\mathcal{N}=4$ SYM as an example, we have

$$Z_{SYM_4}(J; N_c \gg 1, \lambda \rightarrow \infty) \equiv e^{-S_{gravity_5}(\phi_{cl}; G_{d+1} \ll 1, \frac{\alpha'}{R^2} \rightarrow 0)}, \quad (1.0.6)$$

where

$$\phi_{cl}(\omega_E, \mathbf{k}, u) = F(\omega_E, \mathbf{k}, u) \phi_0(\omega_E, \mathbf{k}), \quad (1.0.7)$$

is the classical solution for equation of motion of the scalar field ϕ in the AdS_5 space with the boundary condition $F(\omega_E, \mathbf{k}, u=0) = 1$.

As a specific example, we will consider the gravity action

$$S_{gravity_5}(\phi; G_5, \frac{\alpha'}{R^2} \rightarrow 0) = \frac{1}{2} \frac{1}{16\pi G_5} \int d^5x \sqrt{-g} g^{\mu\mu} \partial_\mu \phi \partial_\mu \phi, \quad (1.0.8)$$

on the AdS_5 space with the metric $g_{\mu\nu}$ given by

$$ds^2 = \frac{\pi^2 T^2 R^2}{u} ((1-u^2)d\tau^2 + dx^2 + dy^2 + dz^2) + \frac{R^2}{4(1-u^2)u^2} du^2. \quad (1.0.9)$$

And, the on-shell gravity action $S_{\text{on-shell}}$ found by inserting $\phi_{cl}(\omega_E, \mathbf{k}, u) = F(\omega_E, \mathbf{k}, u) \phi_0(\omega_E, \mathbf{k})$

into the gravity action Equation 1.0.8, and integrating by parts, is given by

$$S_{\text{on-shell}} = \frac{1}{4} \frac{1}{16\pi G_5} \int d^4k \sqrt{-g} g^{uu} F_E(-k, u) \partial_u F_E(k, u) \phi_0(-k) \phi_0(k)|_{u=0}. \quad (1.0.10)$$

Using the on-shell action Equation 1.0.10, and the mapping of the source function $J = \phi_0$, we can determine the one-point and two-point functions of the corresponding operator \mathcal{O} as (3; 4)

$$\langle \mathcal{O} \rangle_E = \frac{\delta Z_{\text{SYM}}}{\delta J} = -\frac{\delta S_{\text{on-shell}}}{\delta \phi_0} = -\frac{1}{2} \frac{1}{16\pi G_5} \sqrt{-g} g^{uu} F_E(-k, u) \partial_u F_E(k, u) \phi_0(-k)|_{u=0}, \quad (1.0.11)$$

$$G_E(\omega_E, \mathbf{k}) = \langle \mathcal{O} \mathcal{O} \rangle_E = \frac{\delta^2 Z_{\text{SYM}}}{\delta J \delta J} = \frac{\delta^2 S_{\text{on-shell}}}{\delta \phi_0 \delta \phi_0} = \frac{1}{16\pi G_5} \sqrt{-g} g^{uu} F_E(-k, u) \partial_u F_E(k, u)|_{u=0}. \quad (1.0.12)$$

And, we can determine the retarded Green's function $G_R = (-i)\theta(t) \langle [\mathcal{O}(t, \mathbf{x}), \mathcal{O}(0)] \rangle$ in real-time to be (5; 6)

$$G_R(\omega, \mathbf{k}) = G_E(\omega_E, \mathbf{k})|_{\omega_E = -i\omega} = \frac{1}{16\pi G_5} \sqrt{-g} g^{uu} F(k, u) \partial_u F(k, u)|_{u=0}. \quad (1.0.13)$$

Therefore, the prescription for computing the real-time retarded Green's function $G_R(\omega, \mathbf{k})$ can be stated as (5): *solve the classical equation of motion for the scalar field $\phi(\omega, \mathbf{k}, u)$ in AdS space with real-time signature, and with the boundary condition $\phi_{cl}(\omega, \mathbf{k}, u) = F(\omega, \mathbf{k}, u)\phi_0(\omega, \mathbf{k})|_{u=0} = \phi_0(\omega, \mathbf{k})$, then the retarded Green's function $G_R(\omega, \mathbf{k})$ is simply given by*

$$G_R(\omega, \mathbf{k}) = \frac{1}{16\pi G_5} \sqrt{-g} g^{uu} F(k, u) \partial_u F(k, u)|_{u=0}. \quad (1.0.14)$$

Though the above prescription to compute $G_R(\omega, \mathbf{k})$ is straightforward, it requires solving a linear second-order differential equation for the scalar field $\phi(\omega, \mathbf{k}, u)$

$$\partial_u \Pi = (\mathcal{N}^{tt} \omega^2 + \mathcal{N}^{xx} k_x^2) \phi, \quad (1.0.15)$$

where $\mathcal{N}^{\mu\mu}(u) = \frac{1}{16\pi G_5} \sqrt{-g} g^{\mu\mu}$, and the conjugate momenta $\Pi = \frac{\delta S_{gravity_5}}{\delta \partial_u \phi} = \mathcal{N}^{uu} \partial_u \phi$.

However, one can avoid solving the linear second-order differential equation Equation 1.0.15, by defining a 5-dimensional retarded Green's function $G_R(\omega, \mathbf{k}, u) = \frac{\Pi}{\phi(\omega, \mathbf{k}, u)}$, and recasting Equation 1.0.15 as a non-linear first-order differential equation (also known as holographic RG flow equation) for $G_R(\omega, \mathbf{k}, u)$, i.e.,(6)

$$\partial_u G_R(\omega, k_x, u) = -\frac{G_R(\omega, k_x, u)^2}{\mathcal{N}^{uu}} + \mathcal{N}^{tt} \omega^2 + \mathcal{N}^{xx} k_x^2. \quad (1.0.16)$$

Then, the retarded Green's function $G_R(\omega, \mathbf{k}) = G_R(\omega, \mathbf{k}, u = 0)$. In this formalism, the interpretation of the extra radial dimension u as the energy scale of the field theory becomes apparent (2; 8; 9). We will use the holographic RG flow equations when we compute the shear viscosities in Chapter 2 and section 7.4, electric conductivities in section 3.1 and 7.4, and jet quenching parameters in section 4.2 and 7.5.

In addition to the retarded Green's function $G_R(\omega, \mathbf{k})$, we can use the AdS/CFT correspondence to compute the Schwinger-Keldysh propagators $G_{11}(\omega, \mathbf{k})$, $G_{22}(\omega, \mathbf{k})$, $G_{12}(\omega, \mathbf{k})$, and

$G_{21}(\omega, \mathbf{k})$ (13; 14; 15), on the contour shown in Figure 2 with $\sigma = \beta/2 = 1/2T$, by generalizing the prescription to compute $G_R(\omega, \mathbf{k})$ as (14)

$$\phi(k, u_a) = \phi_b(k) \mathcal{G}_{ba}(k, u), \quad (1.0.17)$$

where the indices a and b take the values 1 and 2 (where 1 corresponds to the R quadrant, and 2 the L quadrant of the Penrose diagram shown in Figure 3 with two boundaries of the AdS space located at $u_R = u_L = 0$),

$$\phi_1(k) = \lim_{u_R \rightarrow 0} \phi(k, u_R) \quad \phi_2(k) = \lim_{u_L \rightarrow 0} \phi(k, u_L), \quad (1.0.18)$$

and \mathcal{G}_{ab} are bulk-to-boundary Schwinger-Keldysh propagators

$$\begin{aligned} \mathcal{G}_{11}(\omega, \mathbf{k}, u) &= \frac{e^{\omega/T}}{e^{\omega/T} - 1} F(k, u_R) - \frac{1}{e^{2\omega\pi} - 1} F(-k, u_R), \\ \mathcal{G}_{21}(\omega, \mathbf{k}, u) &= 2i \frac{e^{\omega\pi}}{e^{\omega/T} - 1} \text{Im } F(-k, u_R), \\ \mathcal{G}_{12}(\omega, \mathbf{k}, u) &= -2i \frac{e^{\omega/2T}}{e^{\omega/T} - 1} \text{Im } F(-k, u_L), \\ \mathcal{G}_{22}(\omega, \mathbf{k}, u) &= \frac{e^{\omega/T}}{e^{\omega/T} - 1} F(-k, u_L) - \frac{1}{e^{\omega/T} - 1} F(k, u_L), \end{aligned} \quad (1.0.19)$$

and the retarded bulk-to-boundary Green's function $\mathcal{G}_R(\omega, \mathbf{k}, u) = F(k, u)$, with the property $\mathcal{G}_R^*(k, u) = \mathcal{G}_R(-k, u)$.

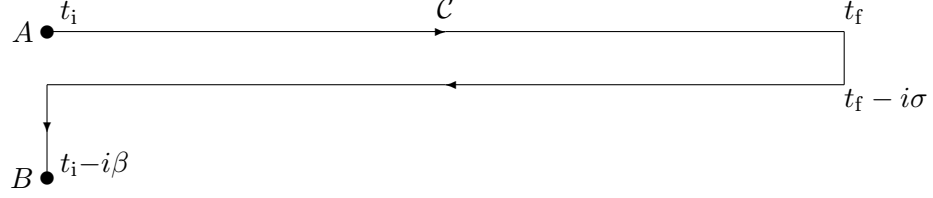


Figure 2. The Schwinger-Keldysh contour.

Then the Schwinger-Keldysh (boundary-to-boundary) propagators $G_{ab}(\omega, \mathbf{k})$ are

$$G_{ab}(k_1, k_2) = -(-1)^{a+b} \frac{\delta^2 S_0}{\delta \phi_a(k_1) \delta \phi_b(k_2)}, \quad (1.0.20)$$

where

$$S_{gravity_5} = \frac{1}{2} \frac{1}{16\pi G_5} \int_R d^5x \sqrt{-g} g^{\mu\nu} \partial_\mu \phi \partial_\nu \phi - \frac{1}{2} \frac{1}{16\pi G_5} \int_L d^5x \sqrt{-g} g^{\mu\nu} \partial_\mu \phi \partial_\nu \phi. \quad (1.0.21)$$

After taking the functional derivatives in Equation 1.0.20, we find

$$\begin{aligned} G_{11}(\omega, \mathbf{k}) &= \mathcal{N}^{uu}(u) \frac{(e^{\omega/T} - 1)F(k, u) \partial_u F(k, u) + (e^{-\omega/T} - 1)F(-k, u) \partial_u F(-k, u)}{(e^{2\omega\pi} - 1)(e^{-2\omega\pi} - 1)} \Big|_{u=0}, \\ G_{12}(\omega, \mathbf{k}) &= \mathcal{N}^{uu}(u) \frac{e^{\omega/2T}}{e^{\omega/T} - 1} \left(F(-k, u) \partial_u F(-k, u) - F(k, u) \partial_u F(k, u) \right) \Big|_{u=0}, \\ G_{21}(\omega, \mathbf{k}) &= -G_{12}^*(\omega, \mathbf{k}), \\ G_{22} &= -G_{11}^*(\omega, \mathbf{k}), \end{aligned} \quad (1.0.22)$$

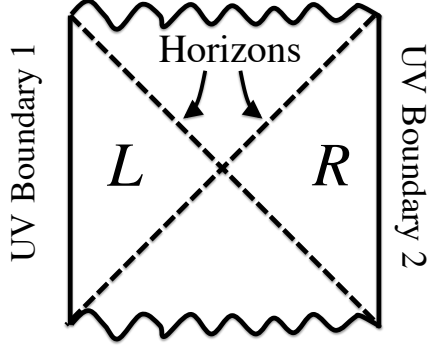


Figure 3. Penrose diagram of AdS black-hole geometry.

and the retarded boundary-to-boundary Green's function $G_R(\omega, \mathbf{k}) = \mathcal{N}^{uu}(u)F(k, u)\partial_u F(k, u)|_{u=0}$ as in Equation 1.0.14. Note that the Schwinger-Keldysh (boundary-to-boundary) propagators $G_{ab}(\omega, \mathbf{k})$ satisfy the KMS identities

$$G_{ab}^* = -G_{\bar{a}\bar{b}}, \quad (1.0.23)$$

where $\bar{1} = 2$ and $\bar{2} = 1$, as long as the bulk-to-boundary propagators \mathcal{G}_{ab} have the property

$$\mathcal{G}_{ab} = \mathcal{G}_{\bar{a}\bar{b}}^*. \quad (1.0.24)$$

And, using the fact that $\mathcal{G}_R^*(k, u) = \mathcal{G}_R(-k, u)$ or $F^*(k, u) = F(-k, u)$, and $2i\text{Im}G_R = G_R - G_R^*$, one can derive the fluctuation-dissipation relations

$$\begin{aligned} G^<(\omega, \mathbf{k}) &= -ie^{\frac{\omega}{2T}} G_{12}(\omega, \mathbf{k}) = -2n_B(\omega) \text{Im}G_R(\omega, \mathbf{k}), \\ G^>(\omega, \mathbf{k}) &= -ie^{-\frac{\omega}{2T}} G_{21}(\omega, \mathbf{k}) = -2n_B(\omega) e^{\frac{\omega}{T}} \text{Im}G_R(\omega, \mathbf{k}), \end{aligned} \quad (1.0.25)$$

where $n_B(\omega) = \frac{1}{e^{\omega/T} - 1}$ is the Bose-Einstein distribution, while $G^<(k) = \int d^4x e^{-ikx} \langle \mathcal{O}(0) \mathcal{O}(x) \rangle$ and $G^>(k) = \int d^4x e^{-ikx} \langle \mathcal{O}(x) \mathcal{O}(0) \rangle$ are the Wightman functions.

Note that the fluctuation-dissipation relations Equation 1.0.25 still hold in a space-time dependent bulk metric of the form $g_{\mu\nu}(t, \mathbf{x}, u) = \bar{g}_{\mu\nu}(u) + \delta g_{ij}(t, \mathbf{x}, u)$ as long as the bulk-to-boundary propagators \mathcal{G}_{ab} or $\mathcal{G}_R = F(k, u)$ are constructed only from the background metric $\bar{g}_{\mu\nu}(u)$, and has the property $\mathcal{G}_{ab} = \mathcal{G}_{\bar{a}\bar{b}}^*$ or $\mathcal{G}_R^*(k, u) = \mathcal{G}_R(-k, u)$. This fact will especially be important for us in section 3.2, where we will compute the velocity gradient correction to the photon emission rate.

CHAPTER 2

SHEAR VISCOSITIES OF STRONGLY COUPLED ANISOTROPIC PLASMA

(Previously published as Kiminad A. Mamo, “Holographic RG flow of the shear viscosity to entropy density ratio in strongly coupled anisotropic plasma,” JHEP 1210, 070 (2012))

Since, the strongly coupled quark gluon plasma created in the heavy ion collision (16; 17) is anisotropic (32; 33), it is important to study the anisotropic version of $\mathcal{N} = 4$ $SU(N_c)$ super-Yang-Mills plasma by using its type IIB supergravity dual (34; 35). For example, the trace of the energy-momentum tensor of the anisotropic $\mathcal{N} = 4$ plasma has been calculated in (35), by using its gravity dual, and it turned out to be proportional to the anisotropy parameter a , more precisely, $\langle T^b_b \rangle = \frac{N_c^2 a^4}{48\pi^4}$. This shows that there is conformal anomaly in the anisotropic $\mathcal{N} = 4$ plasma due to the anisotropy. Hence, the Callan-Symanzik RG flow equation for the two-point function, consequently, the RG flow of some components of the shear viscosity tensor $\eta^b_a{}^b_a$ must be non-trivial. In fact, in this chapter, we show that an independent component of the shear viscosity tensor, $\eta^i{}_z{}^i{}_z$, has a non-trivial RG flow while the other independent components of the shear viscosity tensor, $\eta^j{}_i{}^j{}_i$ and $\eta^z{}_i{}^z{}_i$, have a trivial RG flow.

In this chapter, we derive the non-trivial holographic RG flow equation of the shear viscosity $\eta^i{}_z{}^i{}_z$ of the anisotropic $\mathcal{N} = 4$ plasma, using the equation of motion for the shear mode gravitational fluctuations, we find analytical solution up to first order in the anisotropy parameter a , and show that the Kovtun-Son-Starinets (KSS) shear viscosity bound is violated.

2.1 Effective Action for Gravitational Shear Mode Fluctuations

As shown in (21), later in (6), and more recently in (43) the relevant equations for gravitational shear mode fluctuations can be mapped onto an electromagnetic problem. Consider a metric perturbation of the form

$$g_{aN}(r) \rightarrow g_{aN}(r) + g_{aa}h^a{}_N(x_M \neq a) \quad (2.1.1)$$

in isotropic bulk spacetime

$$ds^2 = g_{MN}dx^M dx^N = g_{tt}dt^2 + g_{aa}dx^a dx^a + g_{uu}du^2. \quad (2.1.2)$$

Indices: $\{L, M, N, \}$ run over the full 5-dimensional bulk; $\{a, b, c\}$ run over all spatial coordinates x , y , and z . And, throughout this paper the Einstein summation convention will apply only for indices $\{L, M, N, \}$ but not for $\{a, b, c\}$. Comparing this to the standard problem of Kaluza-Klein dimensional reduction along the a spatial direction, setting $A_N^a \equiv h^a{}_N$, and using the gauge $h_{NN} = h_{uN} = 0$, the Einstein-Hilbert action

$$S_{bulk} = \frac{1}{2\kappa^2} \int_{\mathcal{M}} \sqrt{-g} R, \quad (2.1.3)$$

after expanding it to second order in the gravitational shear mode fluctuations $h^a{}_N$, with gravitational coupling $\frac{1}{2\kappa^2} = \frac{1}{16\pi G}$, can be mapped onto Maxwell's action for the gauge fields A^a_N , with an effective gauge coupling $\frac{1}{g_{effa}^2} = \frac{1}{2\kappa^2}g_{aa} = \frac{1}{2\kappa^2}g_{xx} = \frac{1}{2\kappa^2}g_{yy} = \frac{1}{2\kappa^2}g_{zz}$ (21; 6)

$$S_{eff} = -\frac{1}{4} \int d^5x \mathcal{N}_a^{MN} F_{MN}^a F_{MN}^a, \quad (2.1.4)$$

where

$$F_{MN}^a = \partial_M A_N^a - \partial_N A_M^a, \quad (2.1.5)$$

$$A_N^a = h^a{}_N = g^{aa} h_{aN}(t, u, c \neq a), \quad (2.1.6)$$

$$\mathcal{N}_a^{MN}(u) = \frac{1}{2\kappa^2} g_{aa} \sqrt{-g} g^{MM} g^{NN}. \quad (2.1.7)$$

The effective action for A_N^a with the effective gauge coupling g_{effa} can be further mapped on to an action for scalar fields $\psi_b^a \equiv A_b^a$

$$S_{eff} = -\frac{1}{2} \int d^5x \mathcal{N}_a^{Mb} \partial_M \psi_b^a \partial_M \psi_b^a. \quad (2.1.8)$$

which upon variation gives the equation of motion for the shear mode gravitational fluctuations

ψ_b^a

$$\partial_M (\mathcal{N}_a^{Mb}(u) \partial_M \psi_b^a) = 0. \quad (2.1.9)$$

2.2 Holographic RG Flow Equation for Shear Viscosities

The fact that classical equations of motion in the bulk corresponds to RG flow equations in the field theory side was anticipated at the early stage of AdS/CFT (41). Therefore, for example, the holographic RG flow equations for the shear viscosity tensor $\eta^b{}_a \equiv \eta^b{}_a{}^b{}_a$, and conductivity σ were derived, using the equations of motion for the scalar modes of the gravitational fluctuations, and Maxwell's equations of motion, respectively, for an electrically neutral isotropic black hole background (6), which were trivial in the hydrodynamic limit. And, recently, (42) has derived the same flow equation, for the conductivity, using the holographic Wilsonian renormalization group method (37; 38), and has provided the proof for the equivalence of the two methods in a general black hole background. Also, (43) has derived the holographic RG flow equation for σ , using the equations of motion for U(1) gauge fields in a charged black hole background, which is non-trivial even in the hydrodynamics limit, and is in agreement with the one derived in (45) using Kubo's formula.

Now, we derive the RG flow equation for the shear viscosity tensor $\eta^b{}_a \equiv \eta^b{}_a{}^b{}_a$, which is extracted from the correlation function $\langle T^b{}_a T^b{}_a \rangle$ where $T^b{}_a$ is dual to $h^a{}_b$, in isotropic bulk spacetime using the equation of motion (Equation 2.1.9). To this end, integrating by parts the bulk action (Equation 2.1.8), and using the equation of motion (Equation 2.1.9), we'll be left with the on-shell boundary action

$$S_{eff} = -S_B[\epsilon], \quad (2.2.10)$$

where the boundary action at $u = \epsilon$, $S_B[\epsilon]$, is

$$S_B[\epsilon] = -\frac{1}{2} \int_{u=\epsilon} d^4x \mathcal{N}_a^{ub} \psi_b^a \partial_u \psi_b^a. \quad (2.2.11)$$

And, the canonical conjugate momentum along the radial direction Π is

$$\Pi = \frac{\delta S_B}{\delta \psi_b^a} = -\mathcal{N}_a^{ub} \partial_u \psi_b^a. \quad (2.2.12)$$

In terms of Π (Equation 2.2.12) the equation of motion (Equation 2.1.9) can be re-written, in the momentum space, as

$$\partial_u \Pi = -(\mathcal{N}_a^{tb} \omega^2 + \mathcal{N}_a^{cb} k_c^2) \psi_b^a. \quad (2.2.13)$$

Note that $a \neq c$. The shear viscosity tensor $\eta^b{}_a$ is defined by $\eta^b{}_a \equiv \frac{\Pi}{i\omega \psi_b^a}$, and taking its first derivative with respect to ϵ , we'll get

$$\partial_\epsilon \eta^b{}_a = \frac{\partial_u \Pi}{i\omega \psi_b^a} - \frac{\Pi \partial_u \psi_b^a}{i\omega (\psi_b^a)^2}. \quad (2.2.14)$$

Then, using (Equation 2.2.13) and (Equation 2.2.12) in (Equation 2.2.14), we'll find the holographic RG flow equation for $\eta^b{}_a$ to be

$$\partial_\epsilon \eta^b{}_a = i\omega \left(\frac{(\eta^b{}_a)^2}{\mathcal{N}_a^{ub}} + \mathcal{N}_a^{tb} \right) + \frac{i}{\omega} \mathcal{N}_a^{cb} k_c^2, \quad (2.2.15)$$

One can see that the RG flow equation (Equation 2.2.15) is trivial in the hydrodynamics limit $k_c = 0$, and $\omega \rightarrow 0$. Hence, the shear viscosity tensor $\eta^b{}_a$ takes the same value at any hypersurface $u = \epsilon$. And, the initial data at the horizon is provided by requiring regularity at the horizon $\epsilon = u_h$ (6). Since $\frac{1}{\mathcal{N}_a^{ub}}$ and \mathcal{N}_a^{tb} diverge at the horizon $\epsilon = u_h$, for the solution to be regular at the horizon, the right hand side of (Equation 2.2.15) has to vanish at $\epsilon = u_h$. From which we recover, the frequency and momentum independent result

$$\eta^b{}_a(\epsilon = u_h) = \sqrt{-\mathcal{N}_a^{ub}\mathcal{N}_a^{tb}} = \frac{1}{2\kappa^2} \sqrt{\frac{g(u_h)}{g_{uu}(u_h)g_{tt}(u_h)}} \frac{g_{aa}(u_h)}{g_{bb}(u_h)}. \quad (2.2.16)$$

And, using the entropy density $s = \frac{1}{4G} \sqrt{\frac{g(u_h)}{g_{uu}(u_h)g_{tt}(u_h)}}$, the shear viscosity to entropy density ratio at the horizon $\epsilon = u_h$ will be

$$\frac{\eta^b{}_a(\epsilon = u_h)}{s} = \frac{1}{4\pi} \frac{g_{aa}(u_h)}{g_{bb}(u_h)} = \frac{1}{4\pi}, \quad (2.2.17)$$

where we used the fact that $g_{aa} = g_{bb}$, for any a and b in isotropic spacetime. And, since the RG flow is trivial, in the hydrodynamic limit, the shear viscosity to entropy density ratio $\frac{\eta^b{}_a(\epsilon)}{s}$ will be given by (Equation 2.2.17) at any hypersurface $u = \epsilon$, i.e.,

$$\frac{\eta^b{}_a(\epsilon)}{s} = \frac{\eta^b{}_a(\epsilon = u_h)}{s} = \frac{\eta^b{}_a(\epsilon = 0)}{s} = \frac{1}{4\pi}. \quad (2.2.18)$$

This proves the universality of $\frac{\eta^b{}_a(\epsilon)}{s}$, in isotropic bulk spacetime. But, we'll see, later on, that the universality of $\frac{\eta^b{}_a}{s}$ is no more valid in anisotropic bulk spacetime where different components

of the shear viscosity tensor $\eta^b{}_a$, hence $\frac{\eta^b{}_a}{s}$, will take different values, and some components of it will RG flow non-trivially, i.e., their value at the horizon (IR) will be different from the one at the boundary (UV).

2.3 Anisotropic Black Hole in Type IIB Supergravity and Its Shear Viscosities

Our five dimensional axion-dilaton gravity bulk action, which is a type IIB supergravity action where the Ramond-Ramond (RR) field, the axion, is a 0-form potential which is the 'magnetic' dual of the 8-form potential which couples to D7-branes 'electrically', is (34; 35; 36)

$$S_{bulk} = \frac{1}{2\kappa^2} \int_{\mathcal{M}} \sqrt{-g} \left(R + 12 - \frac{(\partial\phi)^2}{2} - e^{2\phi} \frac{(\partial\chi)^2}{2} \right), \quad (2.3.19)$$

where $\kappa^2 = 8\pi G = \frac{4\pi^2}{N_c^2}$. The background solutions for the equation of motions resulting from the variation of this action are (35)

$$\chi = az, \quad (2.3.20)$$

$$\begin{aligned} ds^2 &= g_{MN} dx^M dx^N = g_{tt} dt^2 + g_{aa} dx^a dx^a + g_{uu} du^2 = g_{tt} dt^2 + g_{ii} dx^i dx^i + g_{zz} dz^2 + g_{uu} du^2 \\ &= \frac{e^{-\phi(u)/2}}{u^2} \left(-\mathcal{F}(u)\mathcal{B}(u) dt^2 + \frac{du^2}{\mathcal{F}(u)} + dx^2 + dy^2 + \mathcal{H}(u) dz^2 \right) \end{aligned} \quad (2.3.21)$$

Indices: $\{L, M, N, \}$ run over the full 5-dimensional bulk; $\{a, b, c\}$ run over all spatial coordinates x, y , and z ; $\{i, j\}$ stand for x and y only. Also, throughout this paper the Einstein summation convention will apply only for indices $\{L, M, N, \}$ but not for $\{a, b, c\}$ and $\{i, j\}$. And,

$$\phi(u) = -\frac{a^2 u_h^2}{4} \log\left(1 + \frac{u^2}{u_h^2}\right) + O(a^4), \quad (2.3.22)$$

$$\mathcal{F}(u) = 1 - \frac{u^4}{u_h^4} + \frac{a^2}{24u_h^2} [8u^2(u_h^2 - u^2) - 10u^4 \log 2 + (3u_h^4 + 7u^4) \log(1 + \frac{u^2}{u_h^2})] + O(a^4), \quad (2.3.23)$$

$$\mathcal{B}(u) = 1 - \frac{a^2 u_h^2}{24} \left[\frac{10u^2}{u_h^2 + u^2} + \log\left(1 + \frac{u^2}{u_h^2}\right) \right] + O(a^4), \quad (2.3.24)$$

$$\mathcal{H}(u) = e^{-\phi(u)}, \quad (2.3.25)$$

for $a \ll T$. And, the horizon u_h and the entropy density s are related to the temperature T by

(35)

$$u_h = \frac{1}{\pi T} + \frac{5 \log 2 - 2}{48\pi^3 T^3} a^2 + O(a^4), \quad (2.3.26)$$

$$s = \frac{1}{4G} \sqrt{\frac{g(u_h)}{g_{uu}(u_h)g_{tt}(u_h)}} = \frac{\pi^2 N_c^2 T^3}{2} + \frac{N_c^2 T}{16} a^2 + O(a^4). \quad (2.3.27)$$

Turning on only the metric fluctuations h_{MN} about the background solution g_{MN}^0 (Equation 2.3.21), i.e. $g_{MN} = g_{MN}^0 + h_{MN}$, expanding the bulk action (Equation 6.1.2) to second order in h_{MN} , and also using the gauge $h_{Mu} = 0$, we'll have (36)

$$S^{(2)} = \frac{1}{16\pi G} \int d^5x \left[\sqrt{-g}^{(2)} 2A^{(0)} + \sqrt{-g}^{(0)} \left(R^{(2)} - \frac{1}{2} e^{2\phi} a^2 g^{zz(2)} \right) \right], \quad (2.3.28)$$

where

$$A^{(0)} = -\frac{1}{2}\left(8 + \frac{1}{2}\phi'^2 g^{uu} + \frac{1}{2}e^{2\phi}a^2 g^{zz}\right)^{(0)}, \quad (2.3.29)$$

$$g^{zz(2)} = g^{LL(0)} g^{zz(0)} g^{zz(0)} h_{Lz} h_{Lz}. \quad (2.3.30)$$

Using the trick of (21; 6) of Kaluza-Klein dimensional reduction in the a direction, considering only $h_{Na} = h_{Na}(x_M \neq a)$, and using the gauge $h_{NN} = h_{uN} = 0$, we'll get the effective action

$$S_{eff}^{(2)} = \int d^5x \left(-\frac{1}{4} \mathcal{N}_a^{MN} F_{MN}^a F_{MN}^a - \frac{1}{2} \mathcal{M}^L A_L^z A_L^z \right), \quad (2.3.31)$$

where

$$F_{MN}^a = \partial_M A_N^a - \partial_N A_M^a, \quad (2.3.32)$$

$$A_N^a = h^a{}_N = g^{aa(0)} h_{aN}, \quad (2.3.33)$$

$$\mathcal{N}_a^{MN}(u) = \frac{1}{2\kappa^2} g_{aa}^{(0)} \sqrt{-g}^{(0)} g^{MM(0)} g^{NN(0)}, \quad (2.3.34)$$

$$\mathcal{M}^L(u) = \frac{1}{2\kappa^2} a^2 e^{2\phi} \sqrt{-g}^{(0)} g^{LL(0)}. \quad (2.3.35)$$

Note that this action, as emphasized in (6), is exactly in the form of the standard Maxwell's action with an effective coupling for the gauge fields

$$\frac{1}{g_{eff_a}^2} = \frac{1}{2\kappa^2} g_{aa}^{(0)}. \quad (2.3.36)$$

It's obvious from the above relationship that the effective coupling $g_{eff_i} \neq g_{eff_z}$ since $g_{ii} \neq g_{zz}$. Hence, we have two distinct effective theories depending on which coupling and gauge fields we use. The gauge fields A_N^i are coupled by g_{eff_i} , and the gauge fields A_N^z are coupled by g_{eff_z} . For example, using the effective theory with the g_{eff_i} we can extract the shear viscosity tensor $\eta^b{}_i{}^b{}_i$ from the correlation function $\langle T^b{}_i T^b{}_i \rangle$ where $T^b{}_i$ is dual to $h^i{}_b$. Similarly, using the effective theory with the g_{eff_z} we can extract the shear viscosity tensor $\eta^b{}_z{}^b{}_z$ from the correlation function $\langle T^b{}_z T^b{}_z \rangle$ where $T^b{}_z$ is dual to $h^z{}_b$. Therefore, there are three independent components of the shear viscosity tensor $\eta^b{}_a{}^b{}_a$, in the bulk, namely

$$\begin{aligned}
\eta^j{}_i &\equiv \eta^j{}_i{}^j{}_i &= \eta^x{}_y{}^x{}_y = \eta^y{}_x{}^y{}_x, \\
\eta^z{}_i &\equiv \eta^z{}_i{}^z{}_i &= \eta^z{}_x{}^z{}_x = \eta^z{}_y{}^z{}_y, \\
\eta^i{}_z &\equiv \eta^i{}_z{}^i{}_z &= \eta^x{}_z{}^x{}_z = \eta^y{}_z{}^y{}_z.
\end{aligned} \tag{2.3.37}$$

However, we observe that two of the three independent components of the shear viscosity tensor in the bulk, $\eta^z{}_i$, and $\eta^i{}_z$, take the same value at the boundary, hence, we have only two independent components of the shear viscosity tensor at the boundary. This is consistent with the fact that the one index up and one index down energy-momentum tensor operator at the boundary is symmetric, and the shear viscosity tensor has only two independent components at the boundary (31).

Now, we start studying the properties of the shear viscosities using their corresponding effective actions. The effective action for A_i^z with the effective gauge coupling g_{eff_z} can be found from the action (Equation 6.1.1) by setting $a = z$, $N = i$, and $L = i$

$$S_{eff}^{(2)} = \int d^5x \left(-\frac{1}{2} \mathcal{N}_z^{Mi} \partial_M \psi_i^z \partial_M \psi_i^z - \frac{1}{2} \mathcal{M}^i \psi_i^z \psi_i^z \right) \quad (2.3.38)$$

where

$$\mathcal{N}_z^{Mi} = \frac{1}{2\kappa^2} g_{zz}^{(0)} \sqrt{-g}^{(0)} g^{MM(0)} g^{ii(0)}, \quad (2.3.39)$$

$$\mathcal{M}^i = \frac{1}{2\kappa^2} a^2 e^{2\phi} \sqrt{-g}^{(0)} g^{ii(0)}, \quad (2.3.40)$$

$$\psi_i^z(t, u, y) = A_i^z(t, u, y) = h^z{}_i(t, u, y). \quad (2.3.41)$$

Similarly, the effective action for A_b^i with the effective gauge coupling g_{eff_i} can be found from the action (Equation 6.1.1) by setting $a = i$, $N = b$, and $L = b$

$$S_{eff}^{(2)} = \int d^5x \left(-\frac{1}{2} \mathcal{N}_i^{Mb} \partial_M \psi_b^i \partial_M \psi_b^i \right) \quad (2.3.42)$$

where

$$\mathcal{N}_i^{Mb} = \frac{1}{2\kappa^2} g_{ii}^{(0)} \sqrt{-g}^{(0)} g^{MM(0)} g^{bb(0)}, \quad (2.3.43)$$

$$\mathcal{M}^i = \frac{1}{2\kappa^2} a^2 e^{2\phi} \sqrt{-g}^{(0)} g^{ii(0)}, \quad (2.3.44)$$

$$\psi_b^i(t, u, z) = A_b^i(t, u, z) = h^i{}_b(t, u, z). \quad (2.3.45)$$

Note that we have dropped the mass-like term $\frac{1}{2}\mathcal{M}^b\psi_b^z\psi_b^z$ from (Equation 2.3.42) since it doesn't affect the equation of motion for ψ_b^i . Also, since (Equation 2.3.42) is the same effective action as the isotropic one (Equation 2.1.4) discussed in the previous section, we can immediately observe that $\eta^b{}_i$ has a trivial RG flow, and the components of $\frac{\eta^b{}_i}{s}$ take the values

$$\frac{\eta^j{}_i(\epsilon)}{s} = \frac{1}{4\pi} \frac{g_{ii}}{g_{jj}} = \frac{1}{4\pi}, \quad (2.3.46)$$

and,

$$\frac{\eta^z{}_i(\epsilon)}{s} = \frac{1}{4\pi} \frac{g_{ii}(u_h)}{g_{zz}(u_h)} = \frac{1}{4\pi\mathcal{H}(u_h)} = \frac{1}{4\pi} \left(1 - \frac{\log 2}{4\pi^2} \left(\frac{a}{T}\right)^2 + O(a^4)\right) < \frac{1}{4\pi} \quad (2.3.47)$$

for $a \neq 0$. Equations (Equation 2.3.46), and (Equation 2.3.47) are exactly Eq.14, and Eq.17 of reference (36), respectively, derived using the membrane paradigm approach.

But, in order to calculate $\eta^i{}_z$ one has to solve the RG flow equation that we'll get from the corresponding effective action (Equation 2.3.38).

Using the equation of motion for the shear modes of gravitational fluctuations, we derive the holographic RG flow equation for the shear viscosity $\eta^i{}_z$. Varying the effective action (Equation 2.3.38), we find the equation of motion

$$\partial_M(\mathcal{N}_z^{Mi}\partial_M\psi_i^z) - \mathcal{M}^i\psi_i^z = 0. \quad (2.3.48)$$

Using the equation of motion (Equation 2.3.48) in the bulk action (Equation 2.3.38), we get the on-shell action

$$S_{eff}^{(2)} = -S_B[\epsilon], \quad (2.3.49)$$

where the boundary action at $u = \epsilon$, $S_B[\epsilon]$, is

$$S_B[\epsilon] = -\frac{1}{2} \int_{u=\epsilon} d^4x \mathcal{N}_z^{ui} \psi_i^z \partial_u \psi_i^z. \quad (2.3.50)$$

And, the canonical conjugate momentum along the radial direction Π is

$$\Pi = \frac{\delta S_B}{\delta \psi_i^z} = -\mathcal{N}_z^{ui} \partial_u \psi_i^z. \quad (2.3.51)$$

In terms of Π (Equation 2.3.51) the equation of motion (Equation 2.3.48) can be re-written, in the momentum space, as

$$\partial_u \Pi = -(\mathcal{N}_z^{ti} \omega^2 + \mathcal{N}_z^{yi} k_y^2 + \mathcal{M}^i) \psi_i^z. \quad (2.3.52)$$

The shear viscosity tensor $\eta^i{}_z$ is defined by $\eta^i{}_z \equiv \frac{\Pi}{i\omega \psi_i^z}$, and taking its first derivative with respect to ϵ , we'll get

$$\partial_\epsilon \eta^i{}_z = \frac{\partial_u \Pi}{i\omega \psi_i^z} - \frac{\Pi \partial_u \psi_i^z}{i\omega (\psi_i^z)^2}. \quad (2.3.53)$$

Then, using (Equation 2.3.52) and (Equation 2.3.51) in (Equation 2.3.53), we find the holographic RG flow equation for η^i_z to be

$$\partial_\epsilon \eta^i_z = i\omega \left(\frac{(\eta^i_z)^2}{\mathcal{N}_z^{ui}} + \mathcal{N}_z^{ti} \right) + \frac{i}{\omega} (\mathcal{N}_z^{yi} k_y^2 + \mathcal{M}^i), \quad (2.3.54)$$

which is non trivial even in the hydrodynamics limit $k_y = 0$ and $\omega \rightarrow 0$. One can also see that at $a = 0$, which makes $\mathcal{M}^i = 0$, the flow equation (Equation 2.3.54) reduces to the isotropic one (Equation 2.2.15).

We solve the flow equations (Equation 2.3.54) analytically up to second order in the anisotropy parameter a . The initial data at the horizon is provided by requiring regularity at the horizon $\epsilon = u_h$ (6). Since $\frac{1}{\mathcal{N}_z^{ui}}$ and \mathcal{N}_z^{ti} diverge at $\epsilon = u_h$, in order for the solution to be regular at the horizon, the right hand side of (Equation 2.3.54) has to vanish at $\epsilon = u_h$. From which we recover frequency, momentum and mass-like term \mathcal{M}^i independent result

$$\eta^i_z(\epsilon = u_h) = \sqrt{-\mathcal{N}_z^{ui} \mathcal{N}_z^{ti}} = \frac{1}{2\kappa^2} \sqrt{\frac{g(u_h)}{g_{uu}(u_h)g_{tt}(u_h)}} \frac{g_{zz}(u_h)}{g_{ii}(u_h)}. \quad (2.3.55)$$

And, using (Equation 2.3.27), the shear viscosity to entropy density ratio at the horizon $\epsilon = u_h$ will be

$$\frac{\eta^i_z(\epsilon = u_h)}{s} = \frac{1}{4\pi} \frac{g_{zz}(u_h)}{g_{ii}(u_h)} = \frac{1}{4\pi} \mathcal{H}(u_h) = \frac{1}{4\pi} \left(1 + \frac{\log 2}{4\pi^2} \left(\frac{a}{T} \right)^2 + O(a^4) \right) > \frac{1}{4\pi} \quad (2.3.56)$$

for $a \neq 0$. Writing out $\eta^j_z = \text{Re}(\eta^i_z) + i\text{Im}(\eta^i_z)$ in (Equation 2.3.54), taking $\omega \rightarrow 0$ limit, setting $k_y = 0$, and writing out the metric components explicitly, we'll get

$$\partial_\epsilon \text{Im}(\eta^i_z) - \frac{a^2}{2\kappa^2\omega} \frac{e^{\frac{3}{4}\phi(\epsilon)} \sqrt{\mathcal{B}(\epsilon)}}{\epsilon^3} = 0, \quad (2.3.57)$$

$$\partial_\epsilon \text{Re}(\eta^i_z) + 4\omega\kappa^2 \frac{e^{\frac{9}{4}\phi(\epsilon)} \epsilon^3}{\mathcal{F}(\epsilon) \sqrt{\mathcal{B}(\epsilon)}} \text{Im}(\eta^i_z) \text{Re}(\eta^i_z) = 0. \quad (2.3.58)$$

Since, we are interested only up to second order in a , we'll take $\mathcal{B} = e^\phi = 1 + O(a^2)$, and $\mathcal{F}(u) = 1 - \frac{u^4}{u_h^4} + O(a^2) = \frac{(u_h^2 + u^2)(u_h^2 - u^2)}{u_h^4} + O(a^2)$. Therefore, up to a second order in a , the flow equation for $\text{Im}(\eta^i_z)$ can be written as

$$\partial_\epsilon \text{Im}(\eta^i_z) = \frac{a^2}{2\kappa^2\omega} \frac{1}{\epsilon^3} + O(a^4). \quad (2.3.59)$$

Solving (Equation 2.3.59), using the initial condition at the horizon $\text{Im}(\eta^j_z(\epsilon = u_h)) = 0$, and using it in (Equation 2.3.58), we'll get

$$\partial_\epsilon \text{Re}(\eta^i_z) - \left[\frac{u_h^2 \epsilon}{\epsilon^2 + u_h^2} a^2 + O(a^4) \right] \text{Re}(\eta^i_z) = 0. \quad (2.3.60)$$

Note that ω is canceled out. Solving (Equation 2.3.60), and setting $\text{Re}(\eta^i_z) \equiv \eta(\epsilon)$, we'll get

$$\eta(\epsilon) = \eta(u_h) \left(\frac{\epsilon^2 + u_h^2}{2u_h^2} \right)^{\frac{a^2 u_h^2}{2}} + O(a^4) = \eta(u_h) \left(1 + \frac{1}{2} a^2 u_h^2 \log \left[\frac{\epsilon^2 + u_h^2}{2u_h^2} \right] \right) + O(a^4) \quad (2.3.61)$$

which, after using (Equation 2.3.55), and (Equation 2.3.26), becomes

$$\eta(\epsilon) = \frac{\pi N_c^2 T^3}{8} + \left(1 + \log\left[\frac{1}{4}(1 + \pi^2 T^2 \epsilon^2)^4\right]\right) \frac{N_c^2 T}{64\pi} a^2 + O(a^4). \quad (2.3.62)$$

Note that at $a = 0$ (Equation 4.3.149) reduces to the isotropic case calculated in (20). And, using (Equation 2.3.27), the shear viscosity to entropy density ratio at any hypersurface $u = \epsilon$ will be

$$\frac{\eta(\epsilon)}{s} = \frac{1}{4\pi} \left(1 + \frac{\log\left[\frac{1}{2}(1 + \pi^2 T^2 \epsilon^2)^2\right]}{4\pi^2} \left(\frac{a}{T}\right)^2 + O(a^4)\right). \quad (2.3.63)$$

Note again that when $a = 0$ in (Equation 2.3.63) $\frac{\eta(\epsilon)}{s}$ will take the universal value $\frac{1}{4\pi}$. We've plotted the holographic RG flow of $\frac{\eta(\epsilon)}{s}$ (Equation 2.3.63), for a fixed value of a and T , in Figure 4.

As we can see from (Equation 2.3.63), the shear viscosity to entropy density ratio at the boundary $\epsilon = 0$ becomes

$$\frac{\eta(\epsilon = 0)}{s} = \frac{1}{4\pi} \left(1 - \frac{\log 2}{4\pi^2} \left(\frac{a}{T}\right)^2 + O(a^4)\right) < \frac{1}{4\pi}. \quad (2.3.64)$$

Note that (Equation 2.3.64) is equivalent to (Equation 2.3.47) as advertised. And, at the horizon $\epsilon^2 = u_h^2 = \frac{1}{\pi^2 T^2}$, (Equation 2.3.63) reproduces (Equation 2.3.56), as expected,

$$\frac{\eta(\epsilon = u_h)}{s} = \frac{1}{4\pi} \left(1 + \frac{\log 2}{4\pi^2} \left(\frac{a}{T}\right)^2 + O(a^4)\right) > \frac{1}{4\pi}. \quad (2.3.65)$$

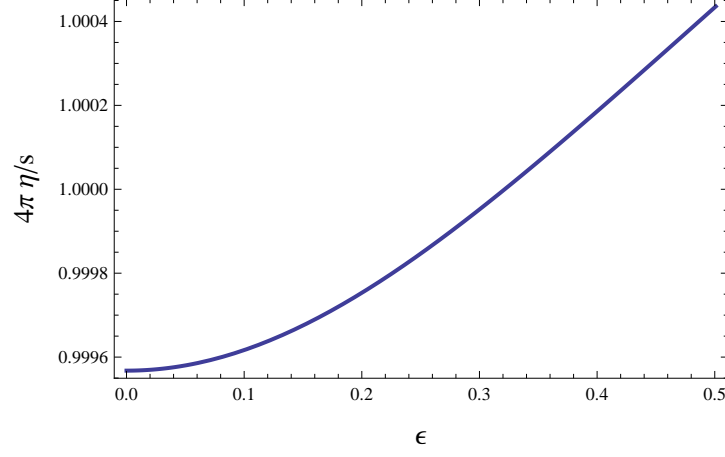


Figure 4. Shear viscosity $\eta \equiv \text{Re}(\eta^i_z)$ over $s/4\pi$ as a function of the radial coordinate ϵ with $u_h = 0.50$, $a = 0.1$, and $T = 0.64$.

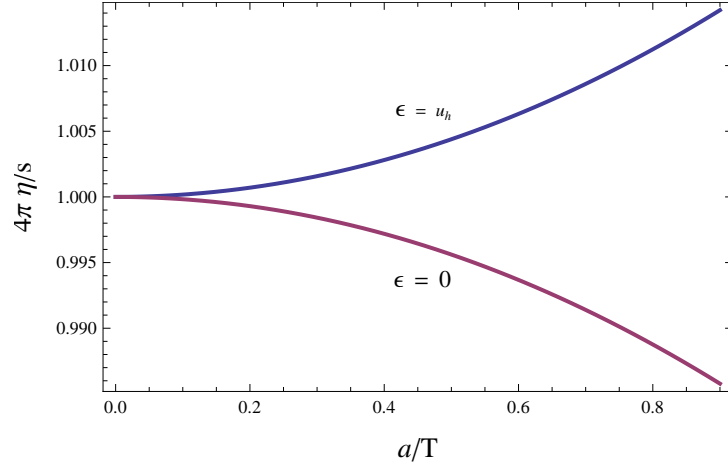


Figure 5. Shear viscosity $\eta \equiv \text{Re}(\eta^i_z)$ over $s/4\pi$ as a function of the anisotropy parameter a/T at the horizon $\epsilon = u_h = 0.50$, and at the boundary $\epsilon = 0$ for $a \ll T$.

We've plotted the temperature flows of $\frac{\eta(\epsilon=u_h)}{s}$ (Equation 2.3.65), and $\frac{\eta(\epsilon=0)}{s}$ (Equation 2.3.64) in Figure 5.

CHAPTER 3

ELECTROMAGNETIC PROBES OF QUARK-GLUON PLASMA

(Previously published as Kiminad A. Mamo, “Enhanced thermal photon and dilepton production in strongly coupled $N = 4$ SYM plasma in strong magnetic field,” *JHEP* 1308, 083 (2013), Kiminad A. Mamo and Ho-Ung Yee, “Gradient Correction to Photon Emission Rate at Strong Coupling,” *Phys. Rev. D* 91, no. 8, 086011 (2015), Kiminad A. Mamo and Ho-Ung Yee, “Spin polarized photons and dileptons from axially charged plasma,” *Phys. Rev. D* 88, no. 11, 114029 (2013), Kiminad A. Mamo and Ho-Ung Yee, “Spin polarized photons from an axially charged plasma at weak coupling: Complete leading order,” *Phys. Rev. D* 93, no. 6, 065053 (2016))

Electromagnetic probes, such as thermal photons and dileptons, are defined as direct photons and dileptons produced from interactions other than decay process in the presence of thermal background or quark-gluon plasma (QGP), and cover the low-momentum $p_T < 2\text{GeV}$ (68) and intermediate-mass $1\text{GeV} \leq M \leq 3.2\text{ GeV}$ (69) region of the total direct photon and dilepton production spectrums, respectively, in the heavy-ion collision experiments.

Thermal photons and dileptons, in heavy-ion collisions are valuable observables that can provide important information on the properties of quark-gluon plasma. Since the emitted photons and dileptons rarely interact with the background plasma again, their signals are expected to faithfully describe the state of the quark-gluon plasma at the time of their emissions.

The experimentally measured thermal photon and dilepton productions at **RHIC** (70; 71; 72) have shown significant enhancement in comparison to the thermal perturbative QCD (166; 74; 75) and relativistic hydrodynamics (68; 74; 75; 69) predictions, and the enhancements increase in more non-central collisions (74; 75) where the magnetic field is expected to be stronger. In addition, the experimental measurements show that, the enhancement of the thermal dilepton production increases with the decreasing of its invariant mass (69). Thus, in this chapter, we will explore different effects which might enhance the thermal photon and dilepton production rates of the QGP. We will also propose and compute the spin polarization asymmetries of thermal photons and dileptons as a probe to the topological charge of QCD vacuum.

3.1 Soft Electromagnetic Probes of Strongly Magnetized Plasma at Strong Coupling

In this section, we will apply the AdS/CFT correspondence, to compute soft-thermal photon and dilepton production rates in strongly coupled $\mathcal{N} = 4$ super-Yang-Mills (SYM) plasma in the presence of strong external magnetic field $B \gg T^2$ hoping to find qualitative insights into the quark-gluon plasma produced at **RHIC** and **LHC** which were recently found to contain a strong magnetic field background at the order of $B \sim 4m_\pi^2$ at **RHIC** (152) and $B \sim 15m_\pi^2$ at **LHC** (54), produced during the early times of the non-central heavy-ion collisions. The effects of this strong magnetic field backgrounds on different signatures of the quark-gluon plasma has recently been explored in different contexts (153; 152; 57; 161; 59; 60; 61; 62; 213; 64; 65; 66), see (67) for a review.

Previous studies of the thermal photon and dilepton production rates at strong coupling without magnetic field include: $\mathcal{N} = 4$ super-Yang-Mills plasma with zero (77) and non-zero chemical potential (78); a strongly coupled plasma with flavor and with zero (364) and non-zero baryon chemical potential (80); finite 't Hooft coupling corrections (81; 82; 83); prompt photon production rate (84; 85); strongly coupled anisotropic plasma (86; 87).

In thermal equilibrium, if we let the photon interaction with matter be of the form $eJ_\mu A^\mu$, and Γ_γ denotes the number of photons emitted per unit time per unit volume, the photon emission rate will be given by (77)

$$\frac{d\Gamma_\gamma}{d^3k} = Q_\gamma \eta_{\mu\nu} \chi^{\mu\nu}(K) \Big|_{k^0=|\mathbf{k}|} , \quad (3.1.1)$$

where $\chi^{\mu\nu}(K)$ is the spectral function, proportional to the imaginary part of the retarded current-current correlation function

$$\chi^{\mu\nu}(K) = -2 \text{Im} C^{\mu\nu}(K) , \quad (3.1.2)$$

where $C^{\mu\nu}$ is the retarded two-point function of conserved current J^ν

$$C^{\mu\nu}(K) = -i \int d^4X e^{-iK \cdot X} \theta(t) \langle [J^\mu(X), J^\nu(0)] \rangle . \quad (3.1.3)$$

And, $Q_\gamma = \frac{e^2}{16\pi^3|\mathbf{k}|} n_b(k^0)$ where $n_b(k^0) = 1/(e^{\frac{k^0}{T}} - 1)$ is the Bose-Einstein distribution function, T is the thermal equilibrium temperature of the plasma, $\eta_{\mu\nu} = \text{diag}(-+++)$ is the Minkowski metric, and K is a null four-momentum vector with $k^0 = |\mathbf{k}| = \omega$.

We can also re-write (Equation 3.1.1) as

$$\frac{d\Gamma_\gamma}{d\omega} = \overline{Q}_\gamma \chi_\mu^\mu(\omega) , \quad (3.1.4)$$

where $\overline{Q}_\gamma = \frac{\alpha_{EM} T}{\pi} \frac{\frac{\omega}{T}}{e^{\frac{\omega}{T}} - 1}$. And, for soft photons the spectral function $\chi^{\mu\nu}(\omega)$ is given in terms of the frequency independent conductivity (DC conductivity) $\sigma^{\mu\nu}$ as (333)

$$\chi^{\mu\nu}(\omega) \cong 2\omega \sigma^{\mu\nu} , \quad (3.1.5)$$

for small ω . Note that equation (Equation 3.1.5) can be obtained by inverting the Kubo's formula for DC conductivity $\sigma^{\mu\nu}$ (333)

$$\sigma^{\mu\nu} = \lim_{\omega \rightarrow 0} \frac{1}{2\omega} \int dt d\mathbf{x} e^{i\omega t} \langle [J^\mu(x), J^\nu(0)] \rangle = \lim_{\omega \rightarrow 0} \frac{1}{2\omega} \chi^{\mu\nu}(\omega). \quad (3.1.6)$$

If we also add to the above theory massive leptons which carry only electric charge, then the thermal system will also emit these leptons, produced by virtual photon decay. Therefore, the

same electromagnetic current-current correlation function, evaluated for spacelike and timelike momenta $K^2 = -M^2$, gives the dilepton production rate, (77)

$$\frac{d\Gamma_{\ell\bar{\ell}}}{d^4K} = Q_{\ell\bar{\ell}} \chi_\mu^\mu(K), \quad (3.1.7)$$

where

$$\begin{aligned} Q_{\ell\bar{\ell}} &= \frac{1}{(2\pi)^4} \frac{e^2 e_\ell^2}{6\pi|K^2|^{5/2}} \Theta(k^0) \Theta(-K^2 - 4m^2) \\ &\times [-K^2 - 4m^2]^{1/2} (-K^2 + 2m^2) n_b(k^0), \end{aligned} \quad (3.1.8)$$

and, e_ℓ is the electric charge of the lepton, m is lepton mass, and $\Theta(x)$ denotes a unit step function. Expressions (Equation 3.1.1) and (Equation 3.1.7) for the production rates are true to leading order in the electromagnetic couplings e and e_ℓ , but are valid non-perturbatively in all other interactions. And, for soft dileptons the spectral functions are given by the same equation as the soft photons (Equation 3.1.5).

3.1.1 DC Conductivities of Strongly Magnetized Plasma at Strong Coupling

In this subsection, we will calculate the DC conductivities of the $\mathcal{N} = 4$ super-Yang-Mills plasma both in the absence $B = 0$ and presence $B \gg T^2$ of the external magnetic field. For the case, where the external magnetic field is present, we calculate the DC conductivities separately when the momentum is parallel $k_z \parallel B_z$ and perpendicular $k_x \perp B_z$ to the magnetic field $B_z = B$.

DC Conductivity for $B = 0$

The gravity dual of $\mathcal{N} = 4$ super-Yang-Mills plasma at strong coupling and large N_c limit is studied in an asymptotically AdS_5 metric (77)

$$ds^2 = g_{\mu\nu}dx^\mu dx^\nu = \frac{\pi^2 T^2 R^2}{u} (-f(u)dt^2 + dx^2 + dy^2 + dz^2) + \frac{R^2}{4f(u)u^2} du^2, \quad (3.1.9)$$

where $T = \frac{r_0}{\pi R^2}$ is the Hawking temperature which is conjectured to be the thermal equilibrium temperature of the plasma in section 2, $R^4 = \lambda \ell_s^4$ is the radius of the AdS_5 spacetime, $\lambda = g_{YM}^2 N_c$ is the 't Hooft coupling, $u = r_0^2/r^2$, $f(u) = 1 - u^2$, the horizon corresponds to $u = 1$, the boundary to $u = 0$, and the entropy density s is given by

$$s = \frac{1}{4G_5} \sqrt{g_{xx}g_{yy}g_{zz}} = \frac{1}{2} \pi^2 N_c^2 T^3, \quad (3.1.10)$$

where $G_5 = \frac{\pi R^3}{2N_c^2}$ is Newton's constant. So, the energy density $\epsilon = \frac{3}{4}sT$ at infinite coupling $\lambda = \infty$ is

$$\epsilon = \frac{3}{8} \pi^2 N_c^2 T^4, \quad (3.1.11)$$

while the zero coupling $\lambda = 0$ result is

$$\epsilon_{\lambda=0} = \frac{4}{3} \epsilon = \frac{1}{2} \pi^2 N_c^2 T^4. \quad (3.1.12)$$

In contrast, for the large- N_c QCD plasma at zero coupling, see for example (91), we've

$$\epsilon_{QCD} = \frac{\pi^2}{60}(4N_c^2 + 7N_f N_c)T^4, \quad (3.1.13)$$

and, comparing (Equation 3.1.13) and (Equation 3.1.12) for $N_c = 3$ and $N_f = 3$, we can infer that $\epsilon_{SYM} = 2.73\epsilon_{QCD}$ at zero coupling and similar difference can be expected at strong coupling $1 \ll \lambda \ll N_c$ limit. Therefore, we have to take this qualitative difference between QCD and $\mathcal{N} = 4$ SYM plasma in consideration, whenever we try to compare the AdS/CFT correspondence computations in this paper with the heavy-ion collision experiments at **RHIC** and **LHC**.

The gauge fluctuation A_μ is governed by the Maxwell's action

$$S = -\frac{1}{4g_5^2} \int d^{d+1}x \sqrt{-g} F_{MN} F^{MN}, \quad (3.1.14)$$

where $g_5^2 = \frac{16\pi^2 R}{N_c^2}$ (77).

Choosing a gauge at which $A_u = 0$ and choosing the wave to move in the z direction only, i.e., $K = (\omega, 0, 0, k_z)$, the equation of motion for the transversal component A_x derived from the action (Equation 3.1.14) can be written as

$$\partial_u \left(\frac{1}{g_5^2} \sqrt{-g} g^{uu} g^{xx} A'_x \right) - \frac{1}{g_5^2} \sqrt{-g} g^{xx} A_x (\omega^2 g^{tt} + k_z^2 g^{zz}) = 0. \quad (3.1.15)$$

One also finds the current or the conjugate momentum to be

$$J^x = \frac{\partial \mathcal{L}}{\partial \partial_u A_x} = -\frac{1}{g_5^2} \sqrt{-g} F^{ux} = -\frac{1}{g_5^2} \sqrt{-g} g^{uu} g^{xx} A'_x. \quad (3.1.16)$$

Then, using Ohm's law, defining the transversal frequency and momentum dependent (AC) conductivities at finite UV cut-off $u = \epsilon$ as $\sigma_T^{yy}(\epsilon, \omega, k_z) = \sigma_T^{xx}(\epsilon, \omega, k_z) = \frac{J^x}{i\omega A_x}$, one can derive the RG flow equation for the transversal AC conductivity $\sigma_T^{xx}(\epsilon, \omega, k_z)$ using (Equation 3.1.15) as (6)

$$\partial_\epsilon \sigma_T^{xx} = \omega \sqrt{\frac{g_{uu}}{g_{tt}}} \left[\frac{(\sigma_T^{xx})^2}{\Sigma^{xx}(\epsilon)} - \Sigma^{xx}(\epsilon) \left(1 + \frac{k_z^2 g^{zz}}{\omega^2 g^{tt}} \right) \right], \quad (3.1.17)$$

where

$$\Sigma^{xx}(u) = \frac{1}{g_5^2} \sqrt{\frac{g}{g_{uu} g_{tt}}} g^{xx}. \quad (3.1.18)$$

Since the right hand side of (Equation 3.1.17) is divergent at the horizon $u = 1$, requiring them to vanish there, due to the regularity condition at the horizon, we'll get, the momentum and frequency independent (DC) conductivities $\sigma_T^{yy}(\epsilon = 1, \omega, k_z) = \sigma_T^{xx}(\epsilon = 1, \omega, k_z)$ (6)

$$\sigma_T^{xx}(\epsilon = 1, \omega, k_z) = \sigma_T^{yy}(\epsilon = 1, \omega, k_z) = \Sigma^{xx}(\epsilon = 1) = \frac{1}{g_5^2} \sqrt{g_{xx}(1) g_{yy}(1) g_{zz}(1)} g^{xx}(1) = \frac{N_c^2 T}{16\pi} = \sigma(1). \quad (3.1.19)$$

Similarly, if the wave is chosen to move in the x -direction, we'll have the transversal DC conductivities $\sigma_T^{zz}(\epsilon = 1, \omega, k_x) = \sigma_T^{yy}(\epsilon = 1, \omega, k_x)$

$$\sigma_T^{zz}(\epsilon = 1, \omega, k_x) = \Sigma^{zz}(\epsilon = 1) = \frac{1}{g_5^2} \sqrt{g_{xx}(1)g_{yy}(1)g_{zz}(1)} g^{zz}(1) = \frac{N_c^2 T}{16\pi} = \sigma(1) . \quad (3.1.20)$$

We can also find the RG flow equation for the longitudinal component of the conductivity $\sigma_L^{zz}(\epsilon, \omega, k_z)$, for example when the momentum is in the z direction, from the equations of motion for the longitudinal component A_z and the time component A_t accompanied by the equation for the conservation of the current $J^z = -\frac{1}{g_5^2} \sqrt{-g} F^{uz}$ and the Bianchi identity as (6)

$$\partial_\epsilon \sigma_L^{zz} = \omega \sqrt{\frac{g_{uu}}{g_{tt}}} \left[\frac{(\sigma_L^{zz})^2}{\Sigma^{zz}(\epsilon)} \left(1 + \frac{k_z^2 g^{zz}}{\omega^2 g^{tt}} \right) - \Sigma^{zz}(\epsilon) \right] , \quad (3.1.21)$$

where

$$\Sigma^{zz}(\epsilon) = \frac{1}{g_5^2} \sqrt{\frac{g}{g_{uu}g_{tt}}} g^{zz} . \quad (3.1.22)$$

Since the right hand side of (Equation 3.1.21) are divergent when the UV cut-off is at the horizon $\epsilon = 1$, requiring them to vanish there, due to the regularity condition at the horizon, we'll get, the momentum and frequency independent (DC) longitudinal conductivity $\sigma_L^{zz}(\epsilon = 1, \omega, k_z)$ (6)

$$\sigma_L^{zz}(\epsilon = 1, \omega, k_z) = \Sigma^L(\epsilon = 1) = \frac{1}{g_5^2} \sqrt{g_{xx}(1)g_{yy}(1)g_{zz}(1)} g^{zz}(1) = \frac{N_c^2 T}{16\pi} = \sigma(1) . \quad (3.1.23)$$

Similarly, if the wave is chosen to move in the x -direction, we get the longitudinal DC conductivity $\sigma_L^{xx}(\epsilon = 1, \omega, k_x)$

$$\sigma_L^{xx}(\epsilon = 1, \omega, k_x) = \Sigma^{xx}(1) = \frac{1}{g_5^2} \sqrt{g_{xx}(1)g_{yy}(1)g_{zz}(1)} g^{xx}(1) = \frac{N_c^2 T}{16\pi} = \sigma(1) . \quad (3.1.24)$$

Note that, throughout this paper, we work in the limit $k_x \approx \omega \ll T$ where the diffusion constant $D = 0$.

DC Conductivities for $B \gg T^2$

Recently, a magnetic brane solution has been found in (280; 93) which interpolates between the AdS_5 spacetime (Equation 3.1.9) in the UV or near the boundary and the $AdS_3 \times T^2$ spacetime in the IR or near the horizon for $B \gg T^2$. Near the boundary, i.e., for $B \ll T^2$ the magnetic brane solution can be given as a perturbation series around the AdS_5 space (Equation 3.1.9) in powers of $\frac{B}{T^2}$ (280; 93; 213) while the metric in the strong magnetic field $B \gg T^2$ regime is given by $AdS_3 \times T^2$ metric (280; 93; 213)

$$ds^2 = g_{\mu\nu}^B dx^\mu dx^\nu = \frac{r^2}{(\frac{R}{\sqrt{3}})^2} (-f_B(r) dt^2 + dz^2) + \frac{(\frac{R}{\sqrt{3}})^2}{r^2 f_B(r)} dr^2 + \left(\frac{R}{\sqrt{3}}\right)^2 (\sqrt{3} B dx^2 + \sqrt{3} B dy^2) , \quad (3.1.25)$$

where $f_B(r) = 1 - \frac{r_h^2}{r^2}$, the horizon corresponds to $r = r_h$, the boundary to $r = \infty$, $R^4 = \lambda \ell_s^4$ is the radius of the AdS_5 spacetime, and we can identify $\frac{R}{\sqrt{3}}$ as the radius of the AdS_3 spacetime.

Introducing $u = r_h^2/r^2$, we can re-write the metric (Equation 3.1.25) in more convenient form as

$$ds^2 = g_{\mu\nu}^B dx^\mu dx^\nu = \frac{\frac{4}{3}\pi^2 T^2 R^2}{u} (-f_B(u) dt^2 + dz^2) + \frac{R^2}{12f_B(u)u^2} du^2 + B \frac{R^2}{\sqrt{3}} (dx^2 + dy^2) , \quad (3.1.26)$$

where $T = \frac{r_h}{\frac{2}{3}\pi R^2}$ is the Hawking temperature (213), $\lambda = g_{YM}^2 N_c$, $f_B(u) = 1 - u$, and the horizon corresponds to $u = 1$. The entropy density s_B is given by (280; 93)

$$s_B = \frac{1}{4G_5} \sqrt{g_{xx}^B g_{yy}^B g_{zz}^B} = \frac{1}{3} N_c^2 B T , \quad (3.1.27)$$

where $G_5 = \frac{\pi R^3}{2N_c^2}$ is Newton's constant. Comparing (Equation 3.1.27) and (Equation 4.3.147), one can see that

$$s_B = \frac{2}{3\pi^2} \frac{B}{T^2} s = \frac{8}{3} b s , \quad (3.1.28)$$

where we've defined the dimensionless quantity $b = \frac{B}{4\pi^2 T^2}$, and the ratio of the energy densities $\epsilon_B = \frac{3}{4} T s_B$ and $\epsilon = \frac{3}{4} T s$, at infinite coupling $\lambda = \infty$, will be

$$\frac{\epsilon_B}{\epsilon} = \frac{2}{3\pi^2} \frac{B}{T^2} \simeq 0.07 \frac{B}{T^2} , \quad (3.1.29)$$

which can be compared to the zero coupling $\lambda = 0$ result (280; 93)

$$\frac{\epsilon_B^{\lambda=0}}{\epsilon^{\lambda=0}} = \frac{\sqrt{3}}{2} \frac{3}{4} \frac{\epsilon_B}{\epsilon} \simeq 0.05 \frac{B}{T^2} . \quad (3.1.30)$$

So, for $\mathcal{N} = 4$ super-Yang-Mills plasma, the ratio of the energy densities interpolates between $0.05 \frac{B}{T^2}$ at zero coupling to $0.07 \frac{B}{T^2}$ at infinite coupling.

In contrast, using the fact that for QCD plasma $\epsilon_{QCD}^B = \frac{B^2}{8\pi\alpha_{EM}}$ in the presence of the magnetic field B at zero coupling, see for example (66), we can infer that

$$\frac{\epsilon_{QCD}^B}{\epsilon_{QCD}} \simeq (6.8 \frac{B}{T^2}) \times \frac{\epsilon_{SYM}^B}{\epsilon_{SYM}} = 0.05 \frac{(6.8 \frac{B}{T^2}) \times B}{T^2} . \quad (3.1.31)$$

Thus, one can see that equation Equation 3.1.30 and Equation 3.1.31 are equivalent with the replacement of

$$B \leftrightarrow (6.8 \frac{B}{T^2}) \times B. \quad (3.1.32)$$

Therefore, whenever we compare the AdS/CFT correspondence computations in this paper with the heavy-ion collision experiments at RHIC and LHC, we have to use about $6.8 \frac{B}{T^2}$ times stronger magnetic field than actually produced at those experiments, i.e., $B = B_{SYM} = (6.8 \frac{B_{actual}}{T^2}) \times B_{actual}$. Note that we are making the above conclusion based on an observation at weak coupling but we expect the same conclusion to hold in the strong coupling limit $1 \ll \lambda \ll N_c$, at least qualitatively.

The equation of motion and the RG flow equations for $B \gg T^2$ are still given by (Equation 3.1.15) and (Equation 3.1.17), respectively, but this time using the $AdS_3 \times T^2$ metric $g_{\mu\nu}^B$ (Equation 3.1.26). So, if we take the momentum k_z to be in the z -direction, which is parallel

to the direction of the magnetic field $B = B_z \parallel k_z$, then the transversal DC conductivities

$\sigma_T^{xxB\parallel}(1) = \sigma_T^{yyB\parallel}(1)$ will be

$$\sigma_T^{xxB\parallel}(1) = \frac{1}{g_5^2} \sqrt{g_{xx}^B(1)g_{yy}^B(1)g_{zz}^B(1)} g_B^{xx}(1) = \frac{2}{\sqrt{3}} \frac{N_c^2 T}{16\pi} = \frac{2}{\sqrt{3}} \sigma(1) , \quad (3.1.33)$$

while the longitudinal DC conductivity $\sigma_L^{zzB\parallel}(1)$ will be

$$\sigma_L^{zzB\parallel}(1) = \frac{1}{g_5^2} \sqrt{g_{xx}^B(1)g_{yy}^B(1)g_{zz}^B(1)} g_B^{zz}(1) = \frac{1}{2} \frac{N_c^2 B}{16\pi^3 T} = 2b\sigma(1) , \quad (3.1.34)$$

where we used $\sigma(1) = \frac{N_c^2 T}{16\pi}$ to get the last line. Therefore, one can see that the DC conductivity

$\sigma_T^{xxB\parallel}(1)$ is independent of B and has increased by a factor of $\frac{2}{\sqrt{3}}$ when the momentum is

parallel to the magnetic field $B_z \parallel k_z$.

Similarly, if we take the momentum k_x in the x -direction, which is perpendicular to the direction of the magnetic field $B = B_z \perp k_x$, then the transversal DC conductivities $\sigma_T^{yyB\perp}(1) \neq$

$\sigma_T^{zzB\perp}(1)$ will be

$$\sigma_T^{yyB\perp}(1) = \frac{1}{g_5^2} \sqrt{g_{xx}^B(1)g_{yy}^B(1)g_{zz}^B(1)} g_B^{yy}(1) = \frac{2}{\sqrt{3}} \frac{N_c^2 T}{16\pi} = \frac{2}{\sqrt{3}} \sigma(1) , \quad (3.1.35)$$

and

$$\sigma_T^{zzB\perp}(1) = \frac{1}{g_5^2} \sqrt{g_{xx}^B(1)g_{yy}^B(1)g_{zz}^B(1)} g_B^{zz}(1) = \frac{1}{2} \frac{N_c^2 B}{16\pi^3 T} = 2b\sigma(1) , \quad (3.1.36)$$

while the longitudinal DC conductivity $\sigma_L^{xxB_\perp}(1)$ will be

$$\sigma_L^{xxB_\perp}(1) = \frac{1}{g_5^2} \sqrt{g_{xx}^B(1)g_{yy}^B(1)g_{zz}^B(1)g_B^{xx}(1)} = \frac{2}{\sqrt{3}} \frac{N_c^2 T}{16\pi} = \frac{2}{\sqrt{3}} \sigma(1) . \quad (3.1.37)$$

Note that $\sigma_T^{yyB_\perp}(1)$ is independent of B and has increased by a factor of $\frac{2}{\sqrt{3}}$ while $\sigma_T^{zzB_\perp}(1)$ has increased linearly with $b = \frac{B}{4\pi^2 T^2}$. The fact that the DC conductivities $\sigma_T^{xxB_\perp}(1) = \sigma_T^{yyB_\perp}(1)$ are independent of the magnetic field $B = B_z$ while $\sigma_T^{zzB_\perp}(1)$ increases linearly with $B = B_z$ has already been observed in the lattice computations for $T = 0$ (see Figure 3 of (88) and Figure 2 of (89), see also (94; 95) which is consistent with our strong magnetic field or low temperature regime $T \ll \sqrt{B}$.

Production Rate of Longitudinal Photons

We'll compute the spectral functions of photons in the low-frequency limit, $\omega \ll T$ for $B = 0$ or $\omega \ll \sqrt{B}$ for $B \gg T^2$, using the DC conductivities.

Photon Spectral Functions for $B = 0$

Using (Equation 3.1.5) and choosing the momentum of the photon to lie in the z -direction $K = (\omega, 0, 0, k_z = \omega)$, we find the transversal components of the spectral function $\chi^{xx}(\omega)$ and $\chi^{yy}(\omega)$ to be

$$\chi^{xx}(\omega) = \chi^{yy}(\omega) = 2\omega\sigma_T^{xx}(1) = 2\omega\sigma(1) . \quad (3.1.38)$$

Then, we can calculate the trace of the spectral function $\chi_\mu^\mu(\omega)$ as

$$\chi_\mu^\mu(\omega) = \chi_t^t(\omega) + \chi_z^z(\omega) + \chi_x^x(\omega) + \chi_y^y(\omega) = \chi_x^x(\omega) + \chi_y^y(\omega) = 4\omega\sigma(1) , \quad (3.1.39)$$

where we used the Ward identity $\frac{k_z^2}{\omega^2}\chi^{zz} = \chi^{tt}$, at light like momentum $k_z = \omega$, to eliminate the time and longitudinal components of the spectral function from its trace. The fact that only the transversal components of the spectral function contribute for the photon production rate has already been observed, for example in (77).

Similarly, by making the momentum of the photon to lie in the x -direction $K = (\omega, k_x = \omega, 0, 0)$, one can find the transversal components of the spectral function $\chi^{yy}(\omega)$ and $\chi^{zz}(\omega)$ to be

$$\chi^{yy}(\omega) = \chi^{zz}(\omega) = 2\omega\sigma_T^{yy}(1) = 2\omega\sigma(1) . \quad (3.1.40)$$

Hence, the trace of the spectral function $\chi_\mu^\mu(\omega)$ becomes

$$\chi_\mu^\mu(\omega) = \chi_y^y(\omega) + \chi_z^z(\omega) = 4\omega\sigma(1) . \quad (3.1.41)$$

For $B = 0$, one can also calculate the trace of the spectral function $\chi_\mu^\mu(\omega)$ exactly at any frequency ω , as it was first done in (77), giving us an opportunity to compare our low-frequency result with the exact one. The exact result is (77)

$$\chi_\mu^\mu(\omega) = \chi_y^y(\omega) + \chi_z^z(\omega) = |{}_2F_1(1 - (1+i)\frac{\omega}{4\pi T}, 1 + (1-i)\frac{\omega}{4\pi T}; 1 - i\frac{\omega}{2\pi T}; -1)|^{-2} \omega \sigma(1) . \quad (3.1.42)$$

So, using the identity ${}_2F_1(1, 1; 1; -1) = \frac{1}{2}$ for Gauss's hypergeometric function ${}_2F_1(a, b; c; z)$, it's clear that the exact result (Equation 3.1.42) reduces to our low-frequency result (Equation 3.1.41) in the $\frac{\omega}{T} \rightarrow 0$ limit.

Photon Spectral Functions for $B \gg T^2$

Since, we have external magnetic field $B = B_z$ in the z -direction which creates anisotropy in our system, we'll carefully and separately study the spectral functions when the momentum is parallel and perpendicular to the direction of the magnetic field B_z .

Using (Equation 3.1.5) and choosing the momentum of the photon to lie in the z -direction $K = (\omega, 0, 0, k_z = \omega)$, which is parallel to the magnetic field B_z , we find the transversal components of the spectral function $\chi^{xxB_\parallel}(\omega)$ and $\chi^{yyB_\parallel}(\omega)$ to be

$$\chi^{xxB_\parallel}(\omega) = \chi^{yyB_\parallel}(\omega) = 2\omega\sigma_T^{xxB_\parallel}(1) = \frac{4}{\sqrt{3}}\omega\sigma(1) , \quad (3.1.43)$$

which means that the trace of the spectral function $\chi_\mu^{\mu B_\parallel}(\omega)$ becomes

$$\chi_\mu^{\mu B_\parallel}(\omega) = \chi_x^{xB_\parallel}(\omega) + \chi_y^{yB_\parallel}(\omega) = 4\omega\sigma_T^{xxB_\parallel}(1) = \frac{8}{\sqrt{3}}\omega\sigma(1) . \quad (3.1.44)$$

In the presence of strong external magnetic field $B_z = B \gg T^2$, for the photons with momentum $k_z = \omega$ parallel to the direction of the magnetic field B_z , the photon production rate (Equation 3.1.4) using the trace of the spectral function (Equation 3.1.44) becomes

$$\left. \frac{d\Gamma_\gamma^{B_\parallel}}{d\omega} \right|_{\omega \ll \sqrt{B}} = \frac{8}{\sqrt{3}} \overline{Q}_\gamma \omega \sigma(1). \quad (3.1.45)$$

Production Rate of Transverse Photons

Using (Equation 3.1.5) and choosing the momentum of the photon to lie in the x -direction $K = (\omega, k_x = \omega, 0, 0)$, which is perpendicular to the magnetic field B_z , we find the transversal components of the spectral function $\chi^{yyB_\perp}(\omega)$ and $\chi^{zzB_\perp}(\omega)$ to be

$$\chi^{yyB_\perp}(\omega) = 2\omega \sigma_T^{B_\perp, yy}(1) = \frac{4}{\sqrt{3}} \omega \sigma(1), \quad (3.1.46)$$

$$\chi^{zzB_\perp}(\omega) = 2\omega \sigma_T^{B_\perp, zz}(1) = 4b\omega \sigma(1). \quad (3.1.47)$$

So, the trace of the spectral function $\chi_\mu^{\mu B_\perp}(\omega)$ becomes

$$\chi_\mu^{\mu B_\perp}(\omega) = \chi_y^{yB_\perp}(\omega) + \chi_z^{zB_\perp}(\omega) = 2\omega \sigma_T^{B_\perp, yy}(1) + 2\omega \sigma_T^{B_\perp, zz}(1) = \left(\frac{4}{\sqrt{3}} + 4b\right) \omega \sigma(1). \quad (3.1.48)$$

Note that our low-frequency limit results (Equation 3.1.44) and (Equation 3.1.48) should be considered as a large magnetic field $B \gg T^2$ and low frequency $\omega \ll \sqrt{B}$ limits of a yet undetermined spectral functions at an arbitrary magnetic field B and frequency ω . Unfortunately,

we couldn't find the exact spectral functions here since the exact bulk metric which interpolates between the $AdS_3 \times T^2$ metric near the horizon for $B \gg T^2$, which we used in this paper, and the AdS_5 metric near the boundary is lacking (280).

For the photons with momentum $k_x = \omega$ perpendicular to the magnetic field B_z , the photon production rate (Equation 3.1.4) using the trace of the spectral function (Equation 3.1.48) becomes

$$\left. \frac{d\Gamma_\gamma^{B_\perp}}{d\omega} \right|_{\omega \ll \sqrt{B}} = \left(\frac{4}{\sqrt{3}} + 4b \right) \overline{Q}_\gamma \omega \sigma(1). \quad (3.1.49)$$

The photon production rates for $B = 0$ are found from (Equation 3.1.4) using the trace of the spectral functions (Equation 3.1.42) and (Equation 3.1.41), therefore, they are given by

$$\frac{d\Gamma_\gamma^{B=0}}{d\omega} = |{}_2F_1(1 - (1+i)\frac{\omega}{4\pi T}, 1 + (1-i)\frac{\omega}{4\pi T}; 1 - i\frac{\omega}{2\pi T}; -1)|^{-2} \overline{Q}_\gamma \omega \sigma(1), \quad (3.1.50)$$

for any frequency ω , and

$$\left. \frac{d\Gamma_\gamma^{B=0}}{d\omega} \right|_{\omega \ll T} = 4\overline{Q}_\gamma \omega \sigma(1), \quad (3.1.51)$$

for a small frequency $\omega \ll T$. We've compared the low-frequency result (Equation 3.1.51) and the exact result (Equation 3.1.50) in Figure 6. Note that, in Figure 6, we've multiplied both (Equation 3.1.51) and (Equation 3.1.50) by a factor of 2 in order to find the total thermal photon production rate in the x and z directions. Also, note that $\overline{Q}_\gamma \omega \sigma(1) = \frac{\alpha_{EM} N_c^2 T^3}{16\pi^2} \frac{(\frac{\omega}{T})^2}{e^{\frac{\omega}{T}} - 1}$.

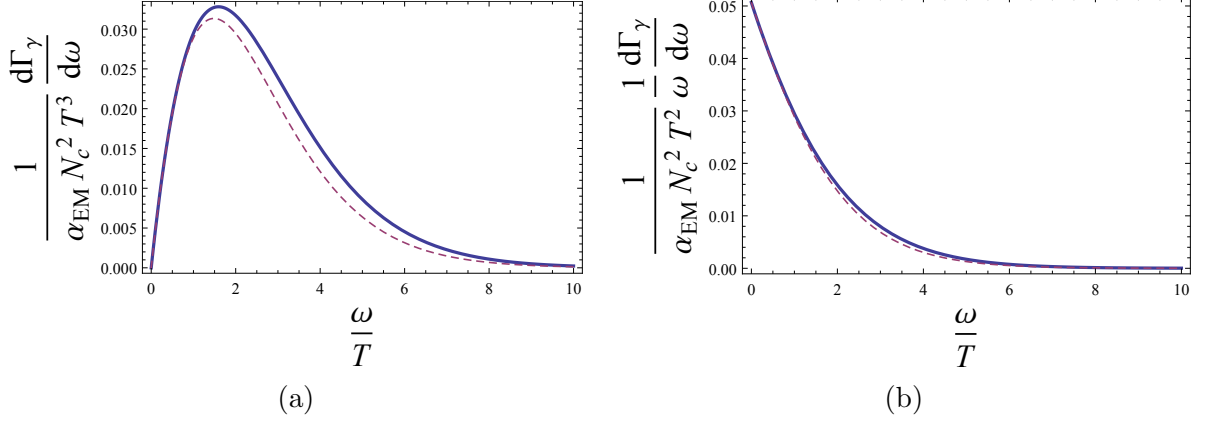


Figure 6. Thermal photon production at any frequency (Equation 3.1.50) [*solid lines*] and at low-frequency (Equation 3.1.51) [*dashed lines*] for $B = 0$.

Finally, the total thermal photon production rates $\frac{d\Gamma_{\gamma(Total)}^{B=0}}{d\omega}$ and $\frac{d\Gamma_{\gamma(Total)}^B}{d\omega}$ become

$$\left. \frac{d\Gamma_{\gamma(Total)}^{B=0}}{d\omega} \right|_{\omega \ll T} = 2 \left. \frac{d\Gamma_{\gamma}^{B=0}}{d\omega} \right|_{\omega \ll T} = 8\bar{Q}_{\gamma}\omega\sigma(1), \quad (3.1.52)$$

and

$$\left. \frac{d\Gamma_{\gamma(Total)}^B}{d\omega} \right|_{\omega \ll \sqrt{B}} = \left. \frac{d\Gamma_{\gamma}^{B_{\parallel}}}{d\omega} \right|_{\omega \ll \sqrt{B}} + \left. \frac{d\Gamma_{\gamma}^{B_{\perp}}}{d\omega} \right|_{\omega \ll \sqrt{B}} = \left(\frac{12}{\sqrt{3}} + 4b \right) \bar{Q}_{\gamma}\omega\sigma(1). \quad (3.1.53)$$

We have plotted the total thermal photon production rates (Equation 3.1.52) and (Equation 3.1.53) together in Figure 8. Note also that $\bar{Q}_{\gamma}\omega\sigma(1) = \frac{\alpha_{EM}N_c^2T^3}{16\pi^2} \frac{(\frac{\omega}{T})^2}{e^{\frac{\omega}{T}} - 1}$.

Production Rate of Longitudinal Dileptons

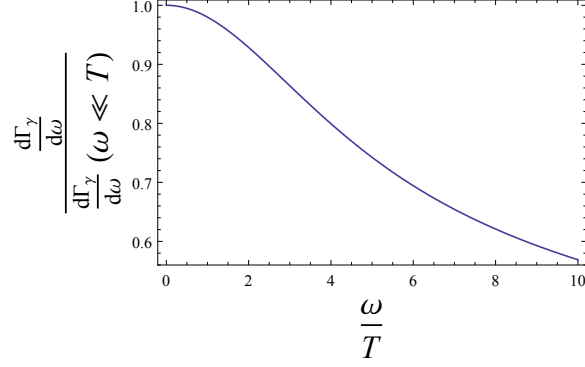


Figure 7. The ratio of thermal photon production at any frequency (Equation 3.1.50) and at low-frequency (Equation 3.1.51) for $B = 0$.

We will compute the spectral functions of soft or low-frequency dileptons, $\omega \ll T$ for $B = 0$ or $\omega \ll \sqrt{B}$ for $B \gg T^2$, using the DC conductivities.

Dilepton Spectral Functions for $B = 0$

Using (Equation 3.1.5) and choosing the momentum of the dilepton to lie in the z -direction $K = (\omega, 0, 0, k_z)$, we find the longitudinal and time components of the spectral function $\chi^{zz}(\omega, k_z)$ and $\chi^{tt}(\omega, k_z)$, respectively, to be

$$\chi^{zz}(\omega, k_z) = 2\omega\sigma_L^{zz}(1) = 2\omega\sigma(1), \quad (3.1.54)$$

and

$$\chi^{tt}(\omega, k_z) = \frac{k_z^2}{\omega^2}\chi^{zz}(\omega, k_z) = 2\frac{k_z^2}{\omega}\sigma(1), \quad (3.1.55)$$

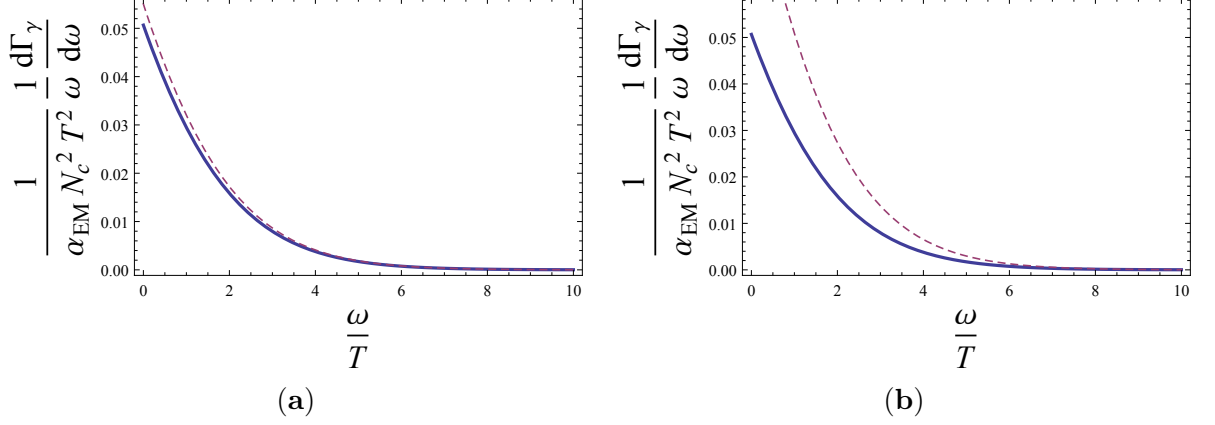


Figure 8. Thermal photon production in the absence of the magnetic field $B = 0$ (Equation 3.1.52) [*solid lines*] and in the presence of the strong magnetic field $B \gg T^2$ (Equation 3.1.53) [*dashed lines*]. In (a) we used (Equation 3.1.32) to get $B = B_{SYM} = (6.8 \frac{B_{RHIC}}{T^2}) \times B_{RHIC} = 10.90 \times 4m_\pi^2$, $T = 1.58m_\pi$ and $b = \frac{1}{4\pi^2} \frac{B}{T^2} = 0.44$ at **RHIC**. In (b) we used (Equation 3.1.32) to get $B = B_{SYM} = (6.8 \frac{B_{LHC}}{T^2}) \times B_{LHC} = 21.46 \times 15m_\pi^2$, $T = 2.18m_\pi$ and $b = \frac{1}{4\pi^2} \frac{B}{T^2} = 1.72$ at **LHC**.

where we used the Ward identity to find the time component of the spectral function $\chi^{tt}(\omega, k_z)$ from the longitudinal one $\chi^{zz}(\omega, k_z)$. Again, using (Equation 3.1.5), we can find the transversal components of the spectral function for the dileptons to be

$$\chi^{xx}(\omega, k_z) = \chi^{yy}(\omega, k_z) = 2\omega\sigma_T^{xx}(1) = 2\omega\sigma(1). \quad (3.1.56)$$

So, the trace of the spectral function for the dileptons $\chi_\mu^\mu(\omega, k_z)$ becomes

$$\chi_\mu^\mu(\omega, k_z) = \chi_t^t(\omega, k_z) + \chi_z^z(\omega, k_z) + \chi_x^x(\omega, k_z) + \chi_y^y(\omega, k_z) = -2\frac{k_z^2}{\omega}\sigma(1) + 6\omega\sigma(1). \quad (3.1.57)$$

Similarly, when the momentum of the dileptons lies in the x -direction $K = (\omega, k_x = \omega, 0, 0)$, the trace of their spectral function $\chi_\mu^\mu(\omega, k_z)$ becomes

$$\chi_\mu^\mu(\omega, k_x) = \chi_t^t(\omega, k_x) + \chi_x^x(\omega, k_x) + \chi_y^y(\omega, k_x) + \chi_z^z(\omega, k_x) = -2\frac{k_x^2}{\omega}\sigma(1) + 6\omega\sigma(1) . \quad (3.1.58)$$

Dilepton Spectral Functions for $B \gg T^2$

Using (Equation 3.1.5) and choosing the momentum of the dileptons to lie in the z -direction $K = (\omega, 0, 0, k_z)$, which is parallel to the magnetic field B_z , we find the longitudinal and time components of the spectral function $\chi^{zzB_\parallel}(\omega, k_z)$ and $\chi^{ttB_\parallel}(\omega, k_z)$, respectively, to be

$$\chi^{zzB_\parallel}(\omega, k_z) = 2\omega\sigma_L^{zzB_\parallel}(1) = 4b\omega\sigma(1), \quad (3.1.59)$$

and

$$\chi^{ttB_\parallel}(\omega, k_z) = \frac{k_z^2}{\omega^2}\chi^{zzB_\parallel}(\omega, k_z) = 4b\frac{k_z^2}{\omega}\sigma(1). \quad (3.1.60)$$

We can also find the transversal components of the spectral function for the dileptons $\chi^{xxB_\parallel}(\omega, k_z)$ and $\chi^{yyB_\parallel}(\omega, k_z)$ to be

$$\chi^{xxB_\parallel}(\omega, k_z) = \chi^{yyB_\parallel}(\omega, k_z) = 2\omega\sigma_T^{xxB_\parallel}(1) = \frac{4}{\sqrt{3}}\omega\sigma(1), \quad (3.1.61)$$

which means that the trace of their spectral function $\chi_\mu^{\mu B_\parallel}(\omega, k_z)$ becomes

$$\chi_\mu^{\mu B_\parallel}(\omega, k_z) = \chi_t^{t B_\parallel}(\omega, k_z) + \chi_z^{z B_\parallel}(\omega, k_z) + \chi_x^{x B_\parallel}(\omega, k_z) + \chi_y^{y B_\parallel}(\omega, k_z) = -4b \frac{k_z^2}{\omega} \sigma(1) + 4b\omega \sigma(1) + \frac{8}{\sqrt{3}} \omega \sigma(1). \quad (3.1.62)$$

The thermal dilepton production rate for $B = 0$ is found from (Equation 3.1.7) using the trace of the spectral function (Equation 3.1.57), thus, it's given by

$$\left. \frac{d\Gamma_{\ell\bar{\ell}}^{B=0}}{d^4K} \right|_{\omega \ll T} = (-2 \frac{k_z^2}{\omega^2} + 6) Q_{\ell\bar{\ell}} \omega \sigma(1). \quad (3.1.63)$$

Therefore, in the presence of strong external magnetic field $B = B_z \gg T^2$, for the dileptons with momentum k_z which is parallel to the direction of the magnetic field B_z , the thermal dilepton production rate (Equation 3.1.7) using the trace of the spectral function (Equation 3.1.62) becomes

$$\left. \frac{d\Gamma_{\ell\bar{\ell}}^{B_\parallel}}{d^4K} \right|_{\omega \ll \sqrt{B}} = (-4b \frac{k_z^2}{\omega^2} + 4b + \frac{8}{\sqrt{3}}) Q_{\ell\bar{\ell}} \omega \sigma(1). \quad (3.1.64)$$

Production Rate of Transverse Dileptons

Using (Equation 3.1.5) and choosing the momentum of the dileptons to lie in the x -direction $K = (\omega, k_x, 0, 0)$, which is perpendicular to the magnetic field B_z , we find the longitudinal and time components of the spectral function $\chi^{xx B_\perp}(\omega, k_x)$ and $\chi^{tt B_\perp}(\omega, k_x)$, respectively, to be

$$\chi^{xx B_\perp}(\omega, k_x) = 2\omega \sigma_L^{xx B_\perp}(1) = \frac{4}{\sqrt{3}} \omega \sigma(1), \quad (3.1.65)$$

and

$$\chi^{ttB\perp}(\omega, k_x) = \frac{k_x^2}{\omega^2} \chi^{xxB\perp}(\omega, k_x) = \frac{4}{\sqrt{3}} \frac{k_x^2}{\omega} \sigma(1). \quad (3.1.66)$$

We can also find the transversal components of the spectral function for the dileptons $\chi^{yyB\perp}(\omega, k_x)$ and $\chi^{zzB\perp}(\omega, k_x)$, respectively, to be

$$\chi^{yyB\perp}(\omega, k_x) = 2\omega \sigma_T^{yyB\perp}(1) = \frac{4}{\sqrt{3}} \omega \sigma(1), \quad (3.1.67)$$

and

$$\chi^{zzB\perp}(\omega, k_x) = 2\omega \sigma_T^{zzB\perp}(1) = 4b\omega \sigma(1). \quad (3.1.68)$$

So, the trace of the spectral function for the dileptons $\chi_\mu^{\mu B\perp}(\omega, k_x)$ becomes

$$\chi_\mu^{\mu B\perp}(\omega, k_x) = \chi_t^{tB\perp}(\omega, k_x) + \chi_x^{xB\perp}(\omega, k_x) + \chi_y^{yB\perp}(\omega, k_x) + \chi_z^{zB\perp}(\omega, k_x) = -\frac{4}{\sqrt{3}} \frac{k_z^2}{\omega} \sigma(1) + \frac{8}{\sqrt{3}} \omega \sigma(1) + 4b\omega \sigma(1). \quad (3.1.69)$$

for the dileptons with momentum k_x perpendicular to the direction of the magnetic field B_z , the dilepton production rate (Equation 3.1.7), using the trace of the spectral function (Equation 3.1.69), becomes

$$\frac{d\Gamma_{\ell\bar{\ell}}^{B\perp}}{d^4K} \Big|_{\omega \ll \sqrt{B}} = \left(-\frac{4}{\sqrt{3}} \frac{k_x^2}{\omega^2} + \frac{8}{\sqrt{3}} + 4b \right) Q_{\ell\bar{\ell}} \omega \sigma(1). \quad (3.1.70)$$

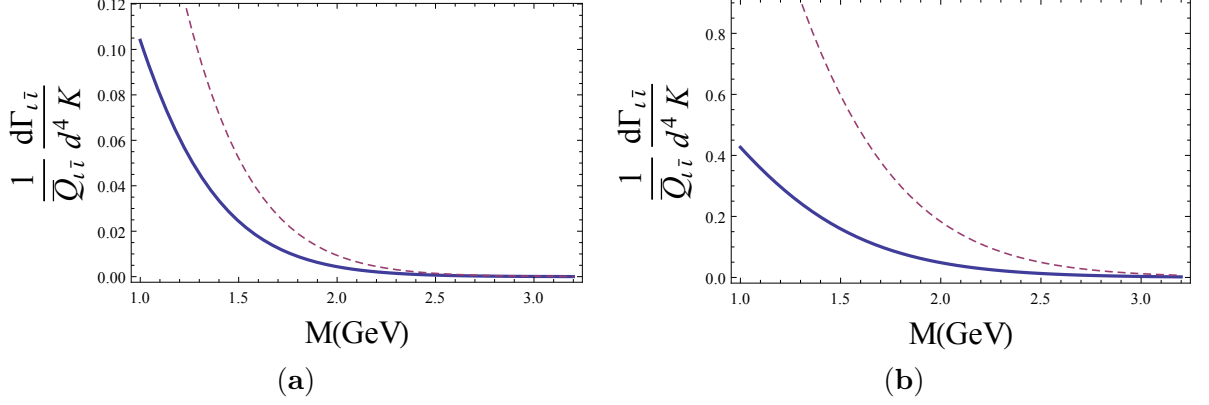


Figure 9. Thermal dilepton production in the absence of the magnetic field $B = 0$ (Equation 3.1.71) [*solid lines*] and in the presence the strong magnetic field $B \gg T^2$ (Equation 3.1.72) [*dashed lines*] as a function of the intermediate-mass $1\text{GeV} \leq M \leq 3.2\text{ GeV}$ of the dileptons. In (a) we used $p_T = 1\text{GeV}$, also used (Equation 3.1.32) to get $B = B_{SYM} = (6.8 \frac{B_{RHIC}}{T^2}) \times B_{RHIC} = 10.90 \times 4m_\pi^2$, $T = 1.58m_\pi$, $b = \frac{1}{4\pi^2} \frac{B}{T^2} = 0.44$ at **RHIC**. In (b) we used $p_T = 1\text{GeV}$, also used (Equation 3.1.32) to get $B = B_{SYM} = (6.8 \frac{B_{LHC}}{T^2}) \times B_{LHC} = 21.46 \times 15m_\pi^2$, $T = 2.18m_\pi$ and $b = \frac{1}{4\pi^2} \frac{B}{T^2} = 1.72$ at **LHC**.

Finally, the total thermal dilepton production rates $\frac{d\Gamma_{\ell\bar{\ell}}^{B=0}(Total)}{d^4K}$ and $\frac{d\Gamma_{\ell\bar{\ell}}^B(Total)}{d^4K}$ are

$$\left. \frac{d\Gamma_{\ell\bar{\ell}}^{B=0}(Total)}{d^4K} \right|_{\omega \ll T} = 2 \left. \frac{d\Gamma_{\ell\bar{\ell}}^{B=0}}{d^4K} \right|_{\omega \ll T} = 2(-2\frac{p_T^2}{\omega^2} + 6)Q_{\ell\bar{\ell}}\omega\sigma(1), \quad (3.1.71)$$

and

$$\left. \frac{d\Gamma_{\ell\bar{\ell}}^B(Total)}{d^4K} \right|_{\omega \ll \sqrt{B}} = \left. \frac{d\Gamma_{\ell\bar{\ell}}^{B_{\parallel}}}{d^4K} \right|_{\omega \ll \sqrt{B}} + \left. \frac{d\Gamma_{\ell\bar{\ell}}^{B_{\perp}}}{d^4K} \right|_{\omega \ll \sqrt{B}} = (-4(b + \frac{1}{\sqrt{3}})\frac{p_T^2}{\omega^2} + 8b + \frac{16}{\sqrt{3}})Q_{\ell\bar{\ell}}\omega\sigma(1), \quad (3.1.72)$$

where we used $p_T^2 = k_x^2 + k_z^2$. We've plotted the total soft-thermal dilepton production rates (Equation 3.1.71) and (Equation 3.1.72) in Figure 9. Also, note that in Figure 9 $\overline{Q}_{\ell\bar{\ell}} = \frac{Q_{\ell\bar{\ell}}\sigma(1)T}{n_b(k^0)}$, and $\omega^2 = p_T^2 + M^2$.

3.2 Velocity Gradient Correction to Photon Production Rate at Strong Coupling

In this section, using the AdS/CFT correspondence, we will compute the velocity gradient correction to photon emission rate of the QGP

$$\frac{d\Gamma}{d^3\vec{k}}(\epsilon^\mu) = \frac{e^2}{(2\pi)^3 2|\vec{k}|} \epsilon^\mu (\epsilon^\nu)^* G_{\mu\nu}^<(k) \Big|_{k^0=|\vec{k}|}, \quad (3.2.73)$$

where

$$G_{\mu\nu}^<(k) = \int d^4x e^{-ikx} \langle J_\mu(0) J_\nu(x) \rangle. \quad (3.2.74)$$

Considering rotational invariance, the correction to the emission rate at local rest frame should take the form

$$\frac{d\Gamma^{shear}}{d^3\vec{k}} = \frac{e^2}{T} \Gamma^{(1)}(\omega) \hat{k}^i \hat{k}^j \sigma_{ij}, \quad (3.2.75)$$

where \hat{k}^i is the unit vector parallel to the momentum direction of the emitted photons, and T is the temperature.

We note that for a static equilibrium QGP, the photon emission rate was computed both at strong (77) and weak coupling (163; 164; 166; 132). In addition, in the weak coupling regime, (135) has computed the correction to photon emission rate arising from non-vanishing shear

component of velocity gradients, and has been implemented in realistic numerical simulations of heavy-ion collisions in (136; 137; 138; 139). We also note that (220) has computed the similar gradient correction to the drag force on heavy quark, and (84) has computed the photon emission rate in far out-of-equilibrium geometry of falling mass shell (141).

In the AdS/CFT correspondence, computing the velocity gradient correction boils down to computing the Wightman function $G_{\mu\nu}^<(k)$ in a bulk metric with velocity gradient correction $g_{\mu\nu}(t, \mathbf{x}, r) = \bar{g}_{\mu\nu}(r) + \delta g_{\mu\nu}(t, \mathbf{x}, r)$, that is,

$$ds^2 = \frac{dr^2}{f(r, T)r^2} + r^2 (-f(r, T)u_\mu u_\nu dx^\mu dx^\nu + (\eta_{\mu\nu} - u_\mu u_\nu) dx^\mu dx^\nu) + \delta g_{\mu\nu} dx^\mu dx^\nu, \quad (3.2.76)$$

with

$$\delta g_{ij}(r) = S(r)\sigma_{ij}, \quad (3.2.77)$$

where (147; 148)

$$S(r) = \frac{r^2}{2} \frac{1}{\pi T} \left(\pi - 2 \arctan\left(\frac{r}{\pi T}\right) + \log \left[\left(1 + \left(\frac{\pi T}{r}\right)\right)^2 \left(1 + \left(\frac{\pi T}{r}\right)^2\right) \right] \right), \quad (3.2.78)$$

$$\sigma_{ij} = \frac{1}{2} \left(\partial_i u_j + \partial_j u_i - \frac{2}{3} \left(\partial^k u_k \right) \right), \quad (3.2.79)$$

is the shear component of velocity gradient with u_μ slowly varying in space-time, hence we will assume σ_{ij} and u_μ to be constant,

$$f(r, T) = 1 - \left(\frac{\pi T}{r} \right)^4, \quad (3.2.80)$$

is the blackening factor of the black hole with the local temperature T , representing hydrodynamic evolution of the gauge theory plasma close to equilibrium.

Since, in our computation, the bulk-to-boundary propagators \mathcal{G}_{ab} and \mathcal{G}_R are constructed from the background metric $\bar{g}_{\mu\nu}$ in thermal equilibrium, as we have showed in Chapter 1, the fluctuation-dissipation relations Equation 1.0.25 still hold, specifically, $G_{\mu\nu}^< = -2n_B(\omega)ImG_{\mu\nu}^R$. Therefore, we only need to compute the velocity gradient correction to the retarded Green's function $G_{\mu\nu}^R$.

Linearizing the 5-dimensional Maxwell's gravitational action, for $g_{\mu\nu}(t, \mathbf{x}, r) = \bar{g}_{\mu\nu}(r) + \delta g_{\mu\nu}(t, \mathbf{x}, r)$, we find

$$S_5 = -\frac{1}{16\pi G_5} \int d^5x \sqrt{-g_5} \left(\frac{1}{8} F_{MN} F^{MN} - \frac{1}{2} \sigma_{ij} \frac{S(r)}{r^4} F_{iN} F^{jQ} g^{NQ} \right). \quad (3.2.81)$$

Note that we have dropped the bar from the background metric $\bar{g}_{\mu\nu}$ after linearizing the action.

The Maxwell's equation of motion for the transverse component of $A_\nu(k, r) = (\epsilon_\nu)^* \mathcal{G}_{\mu\nu}^R(k, r) \phi_0(k)$ (where we use the transverse photon polarization tensor ϵ^μ with $\epsilon^0 = 0$ and $\vec{\epsilon} \cdot \vec{k} = \epsilon^i k_i = 0$) is given by

$$\left[\partial_r (r^3 f(r) \partial_r) + \frac{1}{r} \left(\frac{\omega^2}{f(r)} - |\vec{k}|^2 \right) \right] A_\nu(k, r) = 0, \quad (3.2.82)$$

$A_\nu(k, r)$ satisfies the UV boundary condition $A_\nu(k, r \rightarrow \infty) = (\epsilon_\nu)^* \phi_0(k)$.

The exact analytic solution of Equation 3.2.82, for light-like on-shell momenta with $|\vec{k}| = \omega$ is given, in terms of hypergeometric function ${}_2F_1(a, b; c; z)$, as (77)

$$A_\nu(k, r) = -i(\epsilon_\nu)^* \left(1 - \left(\frac{\pi T}{r}\right)^2\right)^{-i\frac{\omega}{4\pi T}} \left(1 + \left(\frac{\pi T}{r}\right)^2\right)^{-\frac{\omega}{2\pi T}} \quad (3.2.83)$$

$$\begin{aligned} & \times \frac{{}_2F_1\left(1 - \frac{1}{2}(1+i)\frac{\omega}{2\pi T}, -\frac{1}{2}(1+i)\frac{\omega}{2\pi T}; 1 - i\frac{\omega}{2\pi T}; \frac{1}{2}\left(1 - \left(\frac{\pi T}{r}\right)^2\right)\right)}{{}_2F_1\left(1 - \frac{1}{2}(1+i)\frac{\omega}{2\pi T}, -\frac{1}{2}(1+i)\frac{\omega}{2\pi T}; 1 - i\frac{\omega}{2\pi T}; \frac{1}{2}\right)} \phi_0(k) \\ & = (\epsilon_\nu)^* \mathcal{G}_{\mu\nu}^R(k, r) \phi_0(k). \end{aligned} \quad (3.2.84)$$

Similarly, we have

$$A_\mu(k, r) = -i\epsilon_\mu \left(1 - \left(\frac{\pi T}{r}\right)^2\right)^{-i\frac{\omega}{4\pi T}} \left(1 + \left(\frac{\pi T}{r}\right)^2\right)^{-\frac{\omega}{2\pi T}} \quad (3.2.85)$$

$$\begin{aligned} & \times \frac{{}_2F_1\left(1 - \frac{1}{2}(1+i)\frac{\omega}{2\pi T}, -\frac{1}{2}(1+i)\frac{\omega}{2\pi T}; 1 - i\frac{\omega}{2\pi T}; \frac{1}{2}\left(1 - \left(\frac{\pi T}{r}\right)^2\right)\right)}{{}_2F_1\left(1 - \frac{1}{2}(1+i)\frac{\omega}{2\pi T}, -\frac{1}{2}(1+i)\frac{\omega}{2\pi T}; 1 - i\frac{\omega}{2\pi T}; \frac{1}{2}\right)} \phi_0(k) \\ & = (\epsilon_\nu)^* \mathcal{G}_{\mu\nu}^R(k, r) \phi_0(k). \end{aligned} \quad (3.2.86)$$

Using the above solutions in the action Equation 3.2.81 and taking the functional derivative twice with the boundary value $A_\nu(k, r \rightarrow \infty) = (\epsilon_\nu)^* \phi_0(k)$, we determine the velocity gradient correction to the retarded Green's function $\delta G_{\mu\nu}^R(k)$ to be

$$\begin{aligned} \delta G_{\mu\nu}^R(k) &= \frac{1}{32\pi G_5} \sigma_{ij} \int_{r_H}^{\infty} dr \frac{S(r)}{r} \left[(\partial_r \mathcal{G}_{i\nu}^R(k, r)) (\partial_r \mathcal{G}_{\mu j}^R(k, r)) g^{rr} \right. \\ &\quad \left. + (k_i \mathcal{G}_{\rho\nu}^R(k, r) - k_\rho \mathcal{G}_{i\nu}^R(k, r)) (k_j \mathcal{G}_{\mu\sigma}^R(k, r) - k_\sigma \mathcal{G}_{\mu j}^R(k, r)) g^{\rho\sigma} \right], \end{aligned} \quad (3.2.87)$$

which after integrating by parts, and contracting it with the photon polarization tensors, becomes

$$\delta G^R(k) = \frac{\sigma_{ij}}{32\pi G_5 C^2} \int_{r_H}^{\infty} dr \left[\epsilon_i(\epsilon_j)^* \partial_r \left(\frac{S(r)}{r^2} \right) r^3 f(r) H(r) \partial_r H(r) - k_i k_j \frac{S(r) H(r)^2}{r^3} \right], \quad (3.2.88)$$

where $\delta G^R(k) = \epsilon^\mu(\epsilon^\nu)^* \delta G_{\mu\nu}^R(k)$,

$$\begin{aligned} H(r) &\equiv \left(1 - \left(\frac{\pi T}{r} \right)^2 \right)^{-i \frac{\omega}{4\pi T}} \left(1 + \left(\frac{\pi T}{r} \right)^2 \right)^{-\frac{\omega}{2\pi T}} \\ &\times {}_2F_1 \left(1 - \frac{1}{2}(1+i) \frac{\omega}{2\pi T}, -\frac{1}{2}(1+i) \frac{\omega}{2\pi T}; 1 - i \frac{\omega}{2\pi T}; \frac{1}{2} \left(1 - \left(\frac{\pi T}{r} \right)^2 \right) \right), \end{aligned} \quad (3.2.89)$$

$$C \equiv {}_2F_1 \left(1 - \frac{1}{2}(1+i) \frac{\omega}{2\pi T}, -\frac{1}{2}(1+i) \frac{\omega}{2\pi T}; 1 - i \frac{\omega}{2\pi T}; \frac{1}{2} \right), \quad (3.2.90)$$

and we have used the fact that the boundary term from the integration by part,

$$- \frac{i}{32\pi G_5 C^2} \epsilon_i(\epsilon_j)^* \left(\frac{S(r)}{r^2} r^3 f(r) H(r) \partial_r H(r) \right) \Big|_{r_H}^{\infty}, \quad (3.2.91)$$

vanishes both at $r = \infty$ and $r = r_H$.

Therefore, the expression for the correction to the photon emission rate

$$\frac{d\Gamma^{shear}}{d^3\vec{k}}(\epsilon^\mu) = \frac{e^2}{(2\pi)^3 2\omega} \epsilon^\mu(\epsilon^\nu)^* \delta G_{\mu\nu}^<(k) = - \frac{e^2}{(2\pi)^3 2\omega} 2n_B(\omega) \text{Im} [\delta G^R(k)], \quad (3.2.92)$$

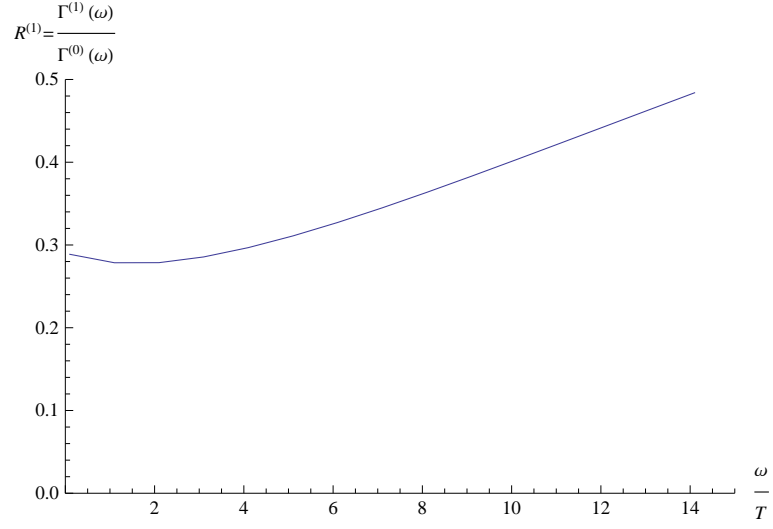


Figure 10. The plot of $R^{(1)} = \Gamma^{(1)}(\omega)/\Gamma^{(0)}(\omega)$ as a function of ω/T .

after using

$$\epsilon_i(\epsilon_j)^* \rightarrow \delta_{ij} - \hat{k}_i \hat{k}_j, \quad (3.2.93)$$

in Equation 3.2.88, becomes

$$\frac{d\Gamma^{shear}}{d^3\vec{k}} = \frac{e^2}{T} \Gamma^{(1)}(\omega) \hat{k}^i \hat{k}^j \sigma_{ij}, \quad (3.2.94)$$

where

$$\begin{aligned} \Gamma^{(1)}(\omega) &= \frac{1}{(2\pi)^3 2\omega} 2n_B(\omega) \frac{N_c^2 T}{16\pi^2} \\ &\times \text{Im} \left[\frac{1}{C^2} \int_{r_H}^{\infty} dr \left[\partial_r \left(\frac{S(r)}{r^2} \right) r^3 f(r) H(r) \partial_r H(r) + \omega^2 \frac{S(r) H(r)^2}{r^3} \right] \right]. \end{aligned} \quad (3.2.95)$$

Finally, the total photon emission rate including the velocity gradient correction becomes

$$\frac{d\Gamma}{d^3\vec{k}} = e^2\Gamma^{(0)}(\omega) + \frac{e^2}{T}\Gamma^{(1)}(\omega)\hat{k}^i\hat{k}^j\sigma_{ij} + \dots, \quad (3.2.96)$$

where (77)

$$\begin{aligned} \Gamma^{(0)}(\omega) &= \frac{1}{(2\pi)^3 2\omega} \epsilon^\mu (\epsilon^\nu)^* G_{\mu\nu}^<(k) \Big|_{\omega=|\vec{k}|} \times 2 \\ &= -\frac{1}{(2\pi)^3 \omega} 2n_B(\omega) \text{Im} [\epsilon^\mu (\epsilon^\nu)^* G_{\mu\nu}^R(k)] \\ &= \frac{1}{(2\pi)^3 \omega} n_B(\omega) \frac{N_c^2 T \omega}{32\pi} \left| {}_2F_1 \left(1 - \frac{1}{2}(1+i)\frac{\omega}{2\pi T}, 1 + \frac{1}{2}(1-i)\frac{\omega}{2\pi T}; 1 - i\frac{\omega}{2\pi T}; -1 \right) \right|^{-2} \end{aligned}$$

where the last factor 2 in the first line comes from the polarization summation. We have plotted

the dimensionless ratio $R^{(1)} \equiv \frac{\Gamma^{(1)}(\omega)}{\Gamma^{(0)}(\omega)}$ in Figure 10.

3.3 Spin Polarized Photons and Dileptons of Axially Charged Plasma at Strong Coupling

So far, in the previous sections of this chapter, we have explored the effects of magnetic field, and fluid velocity gradient on the thermal photon and/or dilepton emission rates of the QGP. In this section, we will investigate the effect of chiral (axial) anomaly on the thermal photons and dileptons emitted from the QGP.

An $SU(N)$ Yang-Mills theory, such as QCD, in addition to infinite number of degenerate vacua, can also has gauge field configurations with topological charge $Q = \frac{g^2}{32\pi^2} \int d^4x F_a^{\mu\nu} \tilde{F}_{\mu\nu}^a$ which is quantized as an integer if these configurations interpolate between two of the infinite

number of degenerate vacua. In the presence of axial anomaly in $SU(N)$ Yang-Mills theory coupled to massless fermions (quarks), i.e.,

$$\partial_\mu J_A^\mu = -\frac{N_f g^2}{16\pi^2} F_a^{\mu\nu} \tilde{F}_{\mu\nu}^a, \quad (3.3.97)$$

it can be shown that the change in axial charge or chirality (where chirality is the difference between the number of particles (plus antiparticles) with right-handed and left-handed helicity) over time ΔJ_A^0 is proportional to the topological charge Q , i.e.,

$$\frac{dJ_A^0}{dt} = -\frac{g^2 N_f}{16\pi^2} \int d^3x F_a^{\mu\nu} \tilde{F}_{\mu\nu}^a, \quad (3.3.98)$$

where the axial charge $J_A^0 = N(q_L) + N(\bar{q}_L) - N(q_R) - N(\bar{q}_R)$. Therefore, Equation 3.3.98 implies that the $Q \neq 0$ fields can induce parity (\mathcal{P}) and charge-parity (\mathcal{CP}) odd effects by interacting with the fermions.

In off-central heavy-ion collisions, axial charges may be created event-by-event either by the glasma color fields in the early stage of collisions or by thermal sphaleron transitions in a later stage (152; 150; 100). Moreover, the ultra-relativistic heavy-ion projectiles can create a huge magnetic field which provides an ideal set-up for Chiral Magnetic Effect (CME) (152)

$$\vec{J} = \frac{e^2 \mu_A}{2\pi^2} \vec{B}, \quad (3.3.99)$$

where μ_A is the axial chemical potential. The induced event-by-event charge separation from the CME may lead to some experimental signatures (101) that indeed seem to be consistent with the observations in RHIC (102) and LHC (103). However, as the proposed signal is roughly the square of the charge separations in order to avoid event-averaging to zero, the signal is in fact P-even and may get additional contributions from other background effects unrelated to triangle anomaly (104; 105; 106; 107), which makes it hard to draw definite conclusions on the CME in heavy-ion collisions.

Another related phenomenon is the Chiral Magnetic Wave (CMW) (60; 61) which is a gapless sound-like propagation of chiral (that is, left-handed or right-handed) charges along the direction of the magnetic field. The CMW may lead to a non-zero electric quadrupole moment in the plasma fireball (108; 109; 110) that can explain the experimentally observed (111; 112) charge-dependent elliptic flows of pions at RHIC (109; 110). Although this is quite suggestive to the existence of the phenomenon, similarly to CME the observable is sensitive to other background effects not originating from triangle anomaly (113; 114; 115; 90; 116).

The proposed observables sensitive to the presence of the axial charge J_A^0 in the quark-gluon plasma (QGP), such as charge separation by Chiral Magnetic Effect rely on the presence of background magnetic field B . However, thermal photon and dilepton emission rates are directly sensitive to the axial charge J_A^0 , even in the absence of background magnetic field B .

For example, in the presence of axial charge J_A^0 , the difference in the photon emission rates between $+$ and $-$ circularly polarized states ("circular polarization asymmetry")

$$A_{\pm\gamma} \equiv \frac{\frac{d\Gamma}{d^3\vec{k}}(\epsilon_+) - \frac{d\Gamma}{d^3\vec{k}}(\epsilon_-)}{\frac{d\Gamma}{d^3\vec{k}}(\epsilon_+) + \frac{d\Gamma}{d^3\vec{k}}(\epsilon_-)}, \quad (3.3.100)$$

is given by

$$A_{\pm\gamma} = \frac{Im G_+^R - Im G_-^R}{Im G_+^R + Im G_-^R} \Big|_{k^0=|\vec{k}|} = \frac{Re G_{12}^R}{Im G_{11}^R} \Big|_{k^0=|\vec{k}|} = \frac{2Re G_{12}^R}{Im Tr G^R} \Big|_{k^0=|\vec{k}|} = \frac{Im \sigma_\chi(k^0)}{Re \sigma_{11}(k^0)}, \quad (3.3.101)$$

where we used the photon emission rate per unit volume $d\Gamma/d^3\vec{k}(\epsilon^\mu)$ to be

$$\frac{d\Gamma}{d^3\vec{k}}(\epsilon^\mu) = \frac{e^2}{(2\pi)^3 2|\vec{k}|} \frac{-2}{e^{\beta|\vec{k}|} - 1} Im [\epsilon^\mu (\epsilon^\nu)^* G_{\nu\mu}^R(k)] \Big|_{k^0=|\vec{k}|}, \quad (3.3.102)$$

with the retarded correlation functions

$$G_{\mu\nu}^R(k) \equiv -i \int d^4x e^{-ikx} \theta(x^0) \langle [J_\mu(x), J_\nu(0)] \rangle, \quad (3.3.103)$$

which after choosing the momentum of the emitted photons to be $\vec{k} = k\hat{x}^3$, and contracting with the circular polarization vectors $\epsilon_\pm^\mu = (\epsilon^0, \epsilon^1, \epsilon^2, \epsilon^3) = \frac{1}{\sqrt{2}}(0, 1, \pm i, 0)$, becomes

$$\epsilon_\pm^\mu (\epsilon_\pm^\nu)^* G_{\nu\mu}^R = (G_{11}^R \pm i G_{12}^R) \equiv G_\pm^R. \quad (3.3.104)$$

To get the last line, we have also used $G_{12}^R \sim ik^0 \sigma_\chi(k^0)$ and $G_{11}^R \sim -ik^0 \sigma_{11}(k^0)$ where

$$G_{ij}^{R,-} = i\sigma_\chi(\omega, k)\epsilon_{ijk}k^k, \quad i, j, k = 1, 2, 3, \quad (3.3.105)$$

and $\sigma_\chi(\omega, k)$ is the coefficient of the CME Equation 3.3.99 at finite frequency-momentum,

$$\vec{J} = e^2 \sigma_\chi(\omega, k) \vec{B}(\omega, k). \quad (3.3.106)$$

Since in the zero frequency limit, the chiral magnetic conductivity $\sigma_\chi(k^0)$ is given by

$$\lim_{k^0 \rightarrow 0} \sigma_\chi(k^0) = \frac{e^2 \mu_A}{2\pi^2}, \quad (3.3.107)$$

which is real, we expect the imaginary part of the chiral magnetic conductivity hence the circular polarization asymmetry $A_{\pm\gamma}$ Equation 3.3.101 to vanish in the zero frequency limit of our numerical computation. We also expect the circular polarization asymmetry $A_{\pm\gamma}$ to be proportional to the axial chemical potential μ_A .

Similarly, for dileptons, one can show that their spin polarization asymmetry $A_{\pm l\bar{l}}$ is given by (154)

$$A_{\pm l\bar{l}} = \left(\frac{2 \cos \theta}{1 + \cos^2 \theta} \right) \cdot \frac{\text{Im } G_+^R - \text{Im } G_-^R}{\text{Im } G_+^R + \text{Im } G_-^R} \bigg|_{p^\mu = p_f^\mu = p_1^\mu + p_2^\mu}, \quad (3.3.108)$$

where $\vec{p}_1 = p(-\sin \theta, 0, \cos \theta)$ and $\vec{p}_2 = p(\sin \theta, 0, \cos \theta)$ are the two momenta of the lepton and anti-lepton with the same magnitude $p = |\vec{p}_1| = |\vec{p}_2|$, and an angle 2θ between them as shown in Figure 11, $p_f^\mu = (2E = 2\sqrt{p^2 + m^2}, 0, 0, 2p \cos \theta)$ is the total center of mass four-momentum

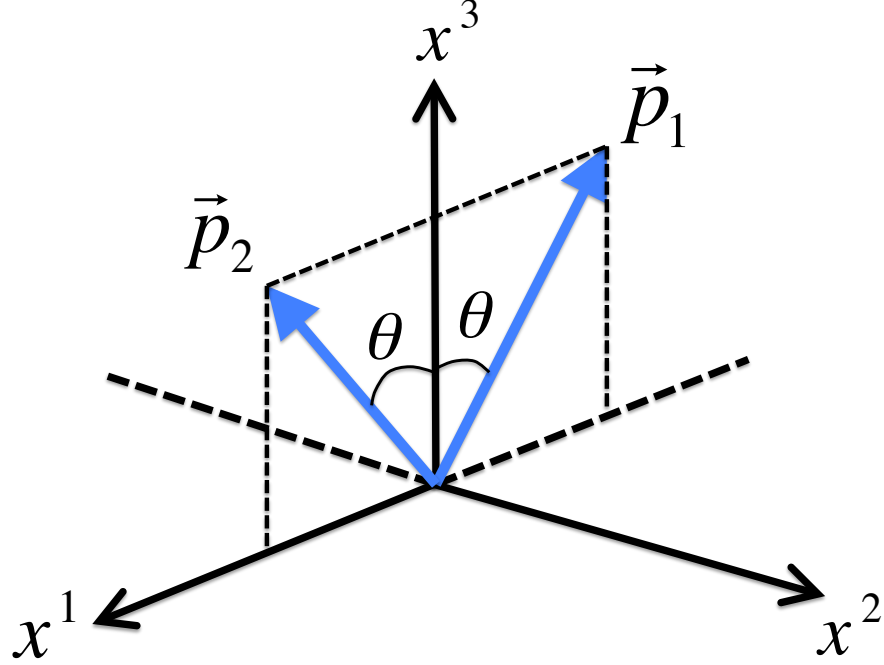


Figure 11. A schematic illustration of the lepton (\vec{p}_1) and anti-lepton (\vec{p}_2) momenta in the di-lepton emission from an isotropic axially charged plasma.

that is carried by the virtual photons, and m is the mass of the lepton species. Note that Equation 3.3.108 is similar to the expression Equation 3.3.101 for $A_{\pm\gamma}$, except for an additional angular factor and a different kinematic domain probed.

An interesting observation on the effect of triangle anomaly to the photons interacting with the plasma was previously made in Ref.(126), showing that the photon field with a particular polarization is unstable and seems to grow. The physics is based on the same P- and CP-odd

part of the retarded correlation functions (Equation 3.3.105), now entering the dispersion relation of photon field interacting with the plasma medium. Although this is quite interesting, for this instability to be realized, the time scale should be long enough to allow multiple interactions between photons and the plasma. Due to a smallness of electromagnetic coupling $\alpha_{EM} \ll 1$, this required time scale is parametrically long (proportional to α_{EM}^{-1}), and based on this, it has been typically assumed that the photons in heavy-ion collisions once emitted from the plasma do not interact with the plasma again before they leave out the fireball, and the well-known photon emission rate is based on this premise. In this case, the more plausible phenomenon happening in real heavy-ion collisions seems to be a simple asymmetry in the emission rates for different spins we discuss.

In what follows, we will compute the spin polarization asymmetries Equation 3.3.101 and Equation 3.3.108 in strongly coupled regime, using the AdS/CFT correspondence in Sakai-Sugimoto model (300).

Spin Polarized Photons and Dileptons in Sakai-Sugimoto Model

Sakai-Sugimoto holographic model of QCD (300)(for detailed discussion of Sakai-Sugimoto model, see for example, the section 5 of (161) and section 3 of (124)) lives in a 5 dimensional space-time, (x^μ, U) where U is an extra holographic dimension. There are two 5 dimensional U(1) gauge fields, A_V and A_a , corresponding to the vector and axial symmetry of the massless quark species in the QCD side, whose 5 dimensional dynamics describes the chiral dynamics

of the massless quark holographically. Especially, there are 5 dimensional Chern-Simons terms that are the holographic manifestation of the triangle anomaly in the QCD side

$$S_{CS} = \frac{N_c}{96\pi^2} \int d^4x dU \epsilon^{MNPQR} [-(A_L)_M (F_L)_{NP} (F_L)_{QR} + (A_R)_M (F_R)_{NP} (F_R)_{QR}] , \quad (3.3.109)$$

where we introduce chiral gauge fields defined by

$$A_L = A_V - A_a , \quad A_R = A_V + A_a . \quad (3.3.110)$$

The QCD plasma with a finite axial charge is described in the model by a non-zero background configuration of the axial gauge field A_a which is

$$(F_a)_{tU}^{(0)} = -\frac{\alpha}{\sqrt{U^5 + \alpha^2}} , \quad (3.3.111)$$

where the parameter α is related to the axial chemical potential μ_A by the relation

$$\mu_A = \int_{U_T}^{\infty} dU \frac{\alpha}{\sqrt{U^5 + \alpha^2}} = \frac{2\alpha}{3U_T^{\frac{3}{2}}} {}_2F_1 \left(\frac{3}{10}, \frac{1}{2}, \frac{13}{10}, -\frac{\alpha^2}{U_T^5} \right) . \quad (3.3.112)$$

The parameter U_T in the above in turn is determined by the temperature T by

$$U_T = R^3 \left(\frac{4\pi T}{3} \right)^2 , \quad (3.3.113)$$

with a numerical value $R^3 = 1.44$ in units of GeV. The U_T is in fact the location of the black-hole horizon at $U = U_T$ in the background holographic space-time describing a finite temperature plasma, and the holographic coordinate U has a range $U_T < U < \infty$ where $U = \infty$ is the region corresponding to the UV regime of the QCD side.

Our main interest is to compute retarded (vector) current correlation functions in the axially charged plasma described above. To do this in holography, one first solves the linearized equations of motion for the vector gauge field A_V fluctuations from the background solution given by (Equation 3.3.111) (161)

$$\partial_U(A(U)F_{tU}) - B(U)(\partial_i F_{Ui}) = 0, \quad (3.3.114)$$

$$A(U)(\partial_t F_{tU}) + B(U)(\partial_i F_{ti}) + C(U)(\partial_i F_{Ui}) = 0,$$

$$B(U)(\partial_t F_{Ui}) + \partial_U(B(U)F_{ti} + C(U)F_{Ui}) + D(U)\partial_j F_{ji} - \frac{N_c}{8\pi^2 C}(F_a)_{tU}^{(0)}\epsilon^{ijk}F_{jk} = 0,$$

where $i, j, k = 1, 2, 3$, $C = 0.0211$ in units of GeV, and the functions $A(U), B(U), C(U), D(U)$ are given by

$$\begin{aligned} A(U) &= U^{-5} (U^5 + \alpha^2)^{\frac{3}{2}}, & B(U) &= \left(\frac{R}{U}\right)^{\frac{3}{2}} (U^5 + \alpha^2)^{\frac{1}{2}}, \\ C(U) &= f(U) (U^5 + \alpha^2)^{\frac{1}{2}}, & D(U) &= \left(\frac{R}{U}\right)^3 U^5 (U^5 + \alpha^2)^{-\frac{1}{2}}, \end{aligned} \quad (3.3.115)$$

with

$$f(U) = 1 - \left(\frac{U_T}{U}\right)^3. \quad (3.3.116)$$

Note that the last term in the third equation in (Equation 3.3.114) is from the 5 dimensional Chern-Simons term which is a consequence of triangle anomaly. The solution has a near $U \rightarrow \infty$ behavior given by

$$A_\mu = A_\mu^{(0)} + \frac{A_\mu^{(1)}}{U^{\frac{1}{2}}} + \frac{A_\mu^{(2)}}{U} + \frac{\tilde{A}_\mu}{U^{\frac{3}{2}}} + \dots, \quad (3.3.117)$$

with

$$A_t^{(1)} = 0, \quad A_i^{(1)} = 2R^{\frac{3}{2}} F_{ti}^{(0)}, \quad A_t^{(2)} = -2R^3 \partial_j F_{tj}^{(0)}, \quad A_i^{(2)} = -2R^3 \partial_j F_{ij}^{(0)}, \quad (3.3.118)$$

where $A_\mu^{(0)}$ is a free parameter (the UV boundary condition) acting as a source for the QCD vector current J^μ , while the \tilde{A}_μ is a dynamically determined quantity which encodes the expectation value of the current in the presence of the source $A_\mu^{(0)}$ by (124)

$$\begin{aligned} \langle J_t \rangle &= 3C \left(\tilde{A}_t + \frac{8}{3} R^{\frac{9}{2}} \partial_t \partial_j F_{tj}^{(0)} \right), \\ \langle J_i \rangle &= 3C \left(\tilde{A}_i + 4R^{\frac{9}{2}} \left(\partial_t \partial_j F_{ij}^{(0)} + \frac{2}{3} \partial_t^2 F_{ti}^{(0)} - \frac{1}{3} \partial_i \partial_j F_{tj}^{(0)} \right) \right). \end{aligned} \quad (3.3.119)$$

The solution with a given source $A_\mu^{(0)}$ and the incoming boundary condition at the horizon $U = U_T$ is unique and it is proportional to $A_\mu^{(0)}$, and hence the current expectation value (Equation 3.3.119) is a linear function of $A_\mu^{(0)}$ from which we finally obtain our desired retarded correlation functions as

$$\langle J_\mu \rangle = -G_\mu^{R \nu} A_\nu^{(0)}. \quad (3.3.120)$$

Since we are interested in computing only the transverse part of the correlation functions, we can consistently turn on $A_{1,2}$ components only, after taking the frequency-momentum $(\omega, \vec{k} = k\hat{x}^3)$, so that $\partial_t = -i\omega$, $\partial_i = ik\delta_{i3}$. The relevant equation of motion is the third equation in (Equation 3.3.114),

$$-i\omega B(U)\partial_U A_i + \partial_U (-i\omega B(U)A_i + C(U)\partial_U A_i) - k^2 D(U)A_i + ik\frac{N_c}{8\pi^2 C}(F_a)_{tU}^{(0)}\epsilon^{ij}A_j = 0, \quad (3.3.121)$$

with $i, j = 1, 2$ and $\epsilon^{12} = -\epsilon^{21} = +1$. From the structure of the above equation, it is natural to work with a helicity basis

$$A_{\pm} = \frac{1}{\sqrt{2}}(A_1 \mp iA_2), \quad (3.3.122)$$

in terms of which the equation of motion diagonalizes as

$$-i\omega B(U)\partial_U A_{\pm} + \partial_U (-i\omega B(U)A_{\pm} + C(U)\partial_U A_{\pm}) - k^2 D(U)A_{\pm} \mp k\frac{N_c}{8\pi^2 C}(F_a)_{tU}^{(0)}A_{\pm} = 0. \quad (3.3.123)$$

Once we find the solution of A_{\pm} , we can read off the source $A_{\pm}^{(0)} = 1/\sqrt{2}(A_1^{(0)} \mp A_2^{(0)})$ and the expectation value via (Equation 3.3.119)

$$\langle J^{\pm} \rangle = \frac{1}{\sqrt{2}}(J^1 \mp iJ^2) = 3C \left(\tilde{A}_{\pm} + 4R^{\frac{9}{2}}(-i\omega) \left(k^2 - \frac{2}{3}\omega^2 \right) A_{\pm}^{(0)} \right). \quad (3.3.124)$$

From the relation $\langle J^i \rangle = -G^{Rij} A_j^{(0)}$, and the rotational symmetry $G_{11}^R = G_{22}^R$ and $G_{12}^R = -G_{21}^R$, it is straight forward to see that

$$\langle J^\pm \rangle = - (G_{11}^R \pm iG_{12}^R) A_\pm^{(0)} = -G_\pm^R A_\pm^{(0)}, \quad (3.3.125)$$

so that we can naturally obtain our desired G_\pm^R , entering our expressions (??) and (??) for $A_{\pm\gamma}$ and $A_{\pm\bar{l}}$, from the solutions of A_\pm .

Numerically, what we do is to solve the equation (Equation 3.3.123) from the horizon $U = U_T$ up to a UV maximum U_{max} and then compare its value and derivative at U_{max} with the UV expansion (Equation 3.3.117),

$$\begin{aligned} A_\pm(U_{max}) &= A_\pm^{(0)} + \frac{2R^{\frac{3}{2}}(-i\omega)}{U_{max}^{\frac{1}{2}}} A_\pm^{(0)} + \frac{-2R^3 k^2}{U_{max}} A_\pm^{(0)} + \frac{\tilde{A}_\pm}{U_{max}^{\frac{3}{2}}}, \\ \partial_U A_\pm(U_{max}) &= -\frac{1}{2} \frac{2R^{\frac{3}{2}}(-i\omega)}{U_{max}^{\frac{3}{2}}} A_\pm^{(0)} + \frac{2R^3 k^2}{U_{max}^2} A_\pm^{(0)} - \frac{3}{2} \frac{\tilde{A}_\pm}{U_{max}^{\frac{5}{2}}}, \end{aligned} \quad (3.3.126)$$

to obtain $A_\pm^{(0)}$ and \tilde{A}_\pm . We then compute $\langle J^\pm \rangle$ from (Equation 3.3.124), and finally get G_\pm^R from

$$G_\pm^R = -\frac{\langle J^\pm \rangle}{A_\pm^{(0)}}. \quad (3.3.127)$$

Figure 12 shows our numerical results of photon circular polarization asymmetry $A_{\pm\gamma}$ as a function of frequency, where $T = 300$ MeV with $\mu_A = 100$ MeV (solid) and $\mu_A = 50$ MeV (dashed). Since the model is trustable only up to a few GeV's, we compute $A_{\pm\gamma}$ only for $\omega < 2$ GeV. We observe that the asymmetry is about a percent level with a peak around $\omega = 1$ GeV.

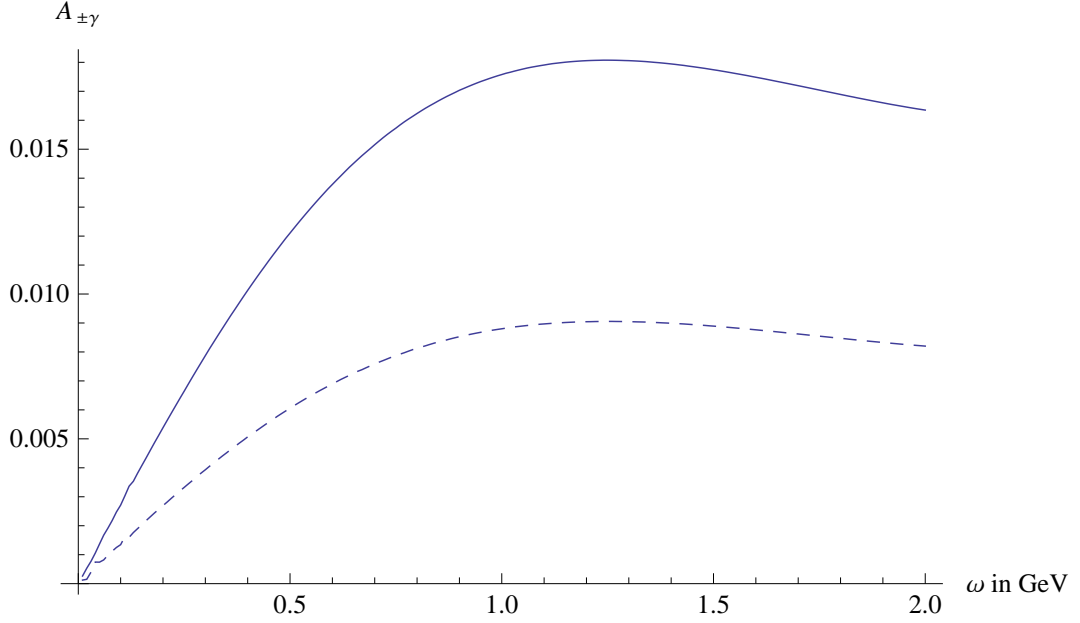


Figure 12. The photon circular polarization asymmetry $A_{\pm\gamma}$ from an axially charged plasma as a function of frequency ω , where $T = 300$ MeV with $\mu_A = 100$ MeV (solid) and $\mu_A = 50$ MeV (dashed).

It is easy to check that the result is absent without the Chern-Simons term (triangle anomaly) and the effect is roughly proportional to the axial chemical potential.

Figure 13 shows our numerical results for the di-lepton spin polarization asymmetry $A_{\pm l\bar{l}}$ in the case of di-muon pair with a relative angle $2\theta = \frac{\pi}{2}$ as a function of the muon momentum $p = |\vec{p}|$ (see Figure 11). Note that the p_f^μ which probes the plasma is

$$p_f^0 = 2\sqrt{p^2 + m_\mu^2}, \quad m_\mu = 100 \text{ MeV}, \quad |\vec{p}_f| = 2p \cos \theta. \quad (3.3.128)$$

We observe again that the effect is about a percent level.

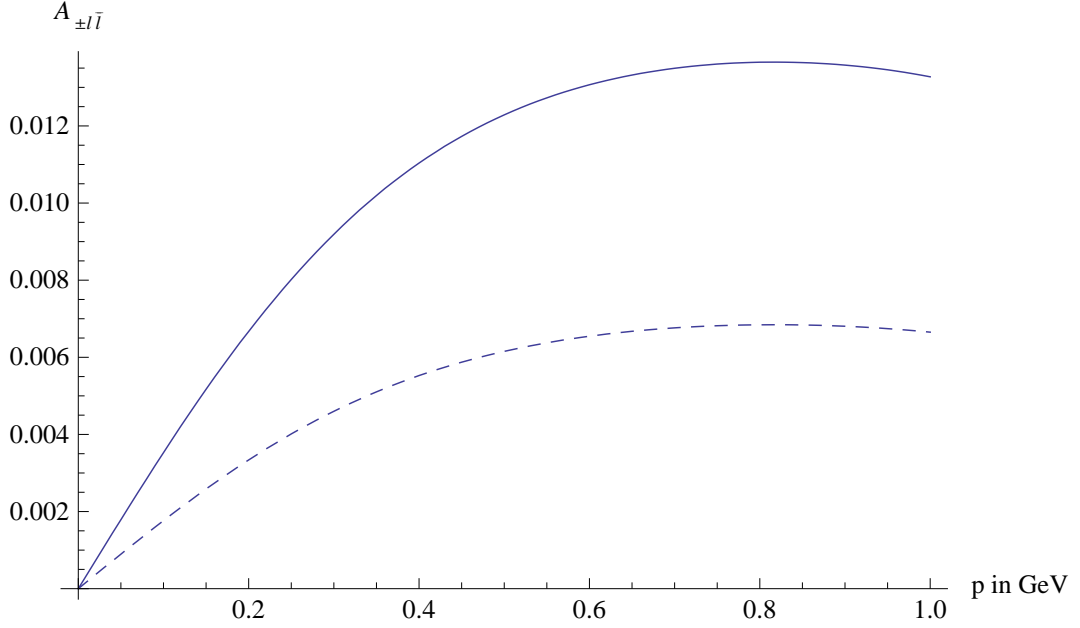


Figure 13. The di-lepton spin polarization asymmetry $A_{\pm l \bar{l}}$ from an axially charged plasma as a function of one lepton momentum $p = |\vec{p}|$ for the case of muon, where $T = 300$ MeV with $\mu_A = 100$ MeV (solid) and $\mu_A = 50$ MeV (dashed). The relative angle between muon and anti-muon pair is taken to be $2\theta = \frac{\pi}{2}$.

3.4 Spin Polarized Photons of Axially Charged Plasma at Weak Coupling

In this section, we will compute the spin or circular polarization asymmetry of photons Equation 3.3.101 in the weakly coupled regime of thermal QCD, by using the concept of “P-odd spectral density”, first introduced in (182) (see Appendix 1 of that reference).

We will compute it in real-time Schwinger-Keldysh formalism, where we have two time contours joined at future infinity, one is going forward in time (labeled as contour 1) and the other is going backward (contour 2). Initial thermal density matrix is realized by attaching an imaginary time thermal contour at the beginning time (at past infinity). By placing operators

in suitable positions in the two contours, one can generate all kinds of time orderings for correlation functions. In terms of “ra”-variables defined by

$$O_r = \frac{1}{2}(O_1 + O_2) , \quad O_a = O_1 - O_2 , \quad (3.4.129)$$

our starting point is the thermal relation for the current-current correlation functions

$$G_{ij}^{rr}(k) = \left(\frac{1}{2} + n_B(k^0) \right) (G_{ij}^{ra}(k) - G_{ij}^{ar}(k)) . \quad (3.4.130)$$

The retarded Green’s function is given in this notation by

$$G_{ij}^R(k) = -iG_{ij}^{ra}(k) , \quad (3.4.131)$$

and by hermiticity of the current operator, the retarded Green’s function should be real-valued in coordinate space. This requires to have $(G_{ij}^R(k))^* = G_{ij}^R(-k)$ in momentum space, or equivalently

$$(G_{ij}^{ra}(k))^* = -G_{ij}^{ra}(-k) . \quad (3.4.132)$$

On the other hand, by definition, $G_{ij}^{ra}(x) = G_{ji}^{ar}(-x)$, so that in momentum space we have

$$G_{ij}^{ar}(k) = G_{ji}^{ra}(-k) = -(G_{ji}^{ra}(k))^* , \quad (3.4.133)$$

where the last equality comes from (Equation 3.4.132).

In the relation (Equation 6.1.13), the left-hand side means the fluctuation amplitude, and the right-hand side, besides the statistical factor, represents the spectral density

$$G_{ij}^{rr}(k) = \left(\frac{1}{2} + n_B(k^0) \right) \rho_{ij}(k), \quad \rho_{ij}(k) \equiv G_{ij}^{ra}(k) - G_{ij}^{ar}(k). \quad (3.4.134)$$

The relation (Equation 3.4.133) gives us

$$\rho_{ij}(k) = G_{ij}^{ra}(k) + (G_{ji}^{ra}(k))^*, \quad (3.4.135)$$

so that the spectral density is twice of the hermitian part of $G_{ij}^{ra}(k)$ in terms of spatial i, j indices. In a P-even ensemble, rotational invariance dictates that $G_{ij}^{ra}(k)$ be proportional to δ^{ij} or $\mathbf{k}^i \mathbf{k}^j$, and hence be symmetric with respect to i, j . The resulting spectral density from this should then be real-valued by (Equation 3.4.135).

In a P-odd ensemble, such as with axial chemical potential, rotational invariance allows us to have a purely imaginary and anti-symmetric (and hence hermitian) spectral density,

$$\rho_{ij}(k) \sim \rho^{odd}(k) i \epsilon^{ijl} \mathbf{k}^l, \quad (3.4.136)$$

with a real valued function $\rho^{odd}(k)$. From (??), we have $\rho^{odd}(k) = -2Im\sigma_\chi(k)$, that is, the P-odd spectral density is in fact the imaginary part of chiral magnetic conductivity. We see that the imaginary part of chiral magnetic conductivity governs P-odd thermal fluctuations of currents, while the topological real part at zero momentum limit (??) does not contribute to

thermal fluctuations. This gives some intuition why $Im\sigma_\chi(k)$ is subject to microscopic real-time dynamics of the theory.

From (Equation 3.4.132), and (Equation 3.4.135), we have

$$\rho^{odd}(-k) = -\rho^{odd}(k). \quad (3.4.137)$$

Rotational invariance dictates that $\rho^{odd}(k)$ be a function of $|\mathbf{k}|$, so $\rho^{odd}(\omega, |\mathbf{k}|)$ is an odd function on ω , similarly to P-even spectral densities. In small frequency, zero momentum limit we expect to have

$$\rho^{odd}(\omega, \mathbf{0}) \sim 2\xi_5\omega + \dots, \quad \omega \rightarrow 0, \quad (3.4.138)$$

where the hydrodynamic transport coefficient ξ_5 has the meaning of (??). As the sign of ξ_5 depends both on the chirality and the axial chemical potential, there seems to be no concept of positivity constraint on it, contrary to electric conductivity. However, explicit computations indicate that the “relative” sign between σ_0 (defined in (??)) and ξ_5 is always negative, reminiscent of magnetic induction (182). We are not yet aware of any formal proof on this.

Our P-odd photon emission rate is related to the P-odd spectral density via (??) by

$$\frac{d\Gamma^{odd}}{d^3\mathbf{k}} = -\frac{e^2}{(2\pi)^3}n_B(\omega)\rho^{odd}(\omega, \mathbf{k})\big|_{\omega=|\mathbf{k}|}, \quad (3.4.139)$$

which explains that the P-odd photon emission rate, while it is P- and CP-odd, is a dynamics driven observable.

We will compute the P-odd photon emission rate at complete leading order in QCD coupling

α_s ,

$$\frac{d\Gamma^{odd}}{d^3\mathbf{k}} \equiv \frac{d\Gamma^+}{d^3\mathbf{k}} - \frac{d\Gamma^-}{d^3\mathbf{k}} \sim \alpha_{EM}\alpha_s(\log(1/\alpha_s) + c), \quad (3.4.140)$$

with an (approximate) axial chemical potential μ_A in the chiral limit of QCD.

The leading order rate consists of three distinct contributions: 1) Compton and Pair Annihilation with hard (that is, comparable to T) momentum exchanges, 2) Soft (that is, much less than T) t-channel exchange contribution with IR divergence regulated by Hard Thermal Loop (HTL) re-summation of exchanged fermion line, and 3) collinear Bremsstrahlung and pair-annihilation contributions induced by multiple scatterings with soft thermal gluons, referred to as Landau-Pomeranchuk-Migdal (LPM) effect. The leading log result in α_s is produced by 1) and 2), and the matching of the two logarithms from 1) and 2) to have the cut-off dependence removed is an important consistency check for the computation. We will see that this happens for our result.

Our methods of computation for the above three contributions closely follow the well-known ones in literature (163; 164; 165; 166), and we apply them to our case of P-odd emission rate, modulo a few subtleties. The complexity of numerical evaluation is somewhat heavier than the P-even total emission rate.

A massless Dirac quark consists of a pair of left- and right-handed Weyl fermions. At leading order in α_s , the QCD interaction between them gives a higher order correction to the photon emission rate, and hence we can treat them independently. This will be clear in the Feynman diagrams we compute in the following. The only effect of having the other chiral Weyl

fermion appears in the value of Debye mass m_D^2 in the gluon Hard Thermal Loop self-energy which enters the Landau-Pomeranchuk-Migdal (LPM) resummation of collinear Bremsstrahlung and pair-annihilation. We therefore present our computational details only for the right-handed Weyl fermion with its chemical potential $\mu = \mu_A$. The other left-handed Weyl fermion then has $\mu = -\mu_A$, and the total contribution to our P-odd photon emission rate is simply twice of that from the right-handed Weyl fermion, up to the above mentioned modification of m_D^2 . We assume our Dirac quark has a electromagnetic charge $Q = +1$, and the full result for two flavor QCD is simply

$$Q_u^2 + Q_d^2 = \frac{5}{9}, \quad (3.4.141)$$

times of the result for $Q = +1$ (where again m_D^2 has to include two flavor contributions).

We briefly summarize our notation and convention for a right-handed Weyl fermion theory. Our metric convention is $\eta = (-, +, +, +)$. Let us define

$$\sigma^\mu = (1, \boldsymbol{\sigma}), \quad \bar{\sigma}^\mu = (1, -\boldsymbol{\sigma}), \quad (3.4.142)$$

which satisfy

$$\sigma^\mu \bar{\sigma}^\nu + \bar{\sigma}^\mu \sigma^\nu = -2\eta^{\mu\nu}. \quad (3.4.143)$$

The equation

$$(p \cdot \sigma)(p \cdot \bar{\sigma}) = -p^2 = (p^0)^2 - |\mathbf{p}|^2, \quad (3.4.144)$$

and the following trace formula will be useful,

$$Tr(\sigma^\mu \bar{\sigma}^\nu \sigma^\alpha \bar{\sigma}^\beta) = 2(\eta^{\mu\nu} \eta^{\alpha\beta} + \eta^{\mu\beta} \eta^{\nu\alpha} - \eta^{\mu\alpha} \eta^{\nu\beta} + i\epsilon^{\mu\nu\alpha\beta}). \quad (3.4.145)$$

The right-handed Weyl fermion action with QCD coupling g is

$$L = i\psi^\dagger \sigma^\mu (\partial_\mu - ig t^a A_\mu^a) \psi, \quad (3.4.146)$$

Upon quantization, we have

$$\psi(x) = \int \frac{d^3\mathbf{p}}{\sqrt{2|\mathbf{p}|}} \left(u(\mathbf{p}) a_{\mathbf{p}} e^{-i|\mathbf{p}|t + i\mathbf{p}\cdot\mathbf{x}} + v(\mathbf{p}) b_{-\mathbf{p}}^\dagger e^{i|\mathbf{p}|t + i\mathbf{p}\cdot\mathbf{x}} \right), \quad (3.4.147)$$

where particle and antiparticle spinors are defined by

$$(1 - \boldsymbol{\sigma} \cdot \hat{\mathbf{p}})u(\mathbf{p}) = 0, \quad (1 + \boldsymbol{\sigma} \cdot \hat{\mathbf{p}})v(\mathbf{p}) = 0, \quad \hat{\mathbf{p}} \equiv \frac{\mathbf{p}}{|\mathbf{p}|}, \quad (3.4.148)$$

with normalization

$$u(\mathbf{p})u^\dagger(\mathbf{p}) = -p \cdot \bar{\sigma}, \quad v(\mathbf{p})v^\dagger(\mathbf{p}) = -p \cdot \sigma, \quad p^\mu = (|\mathbf{p}|, \mathbf{p}). \quad (3.4.149)$$

Note also that $v(-\mathbf{p})v^\dagger(-\mathbf{p}) = -p \cdot \bar{\sigma}$. It will be convenient to define spin projection operators to quark/anti-quark states

$$P_s(\mathbf{p}) \equiv \frac{1}{2}(1 + s\hat{\mathbf{p}} \cdot \boldsymbol{\sigma}) = -s \frac{p_s \cdot \bar{\sigma}}{2|\mathbf{p}|}, \quad p_s \equiv (s|\mathbf{p}|, \mathbf{p}), \quad s = \pm 1, \quad (3.4.150)$$

in terms of which the (bare) real-time propagators in “r/a” basis are

$$\begin{aligned} S^{ra}(p) &= i \frac{p \cdot \bar{\sigma}}{p^2} \Big|_{p^0 \rightarrow p^0 + i\epsilon} = \sum_{s=\pm} \frac{i}{p^0 - s|\mathbf{p}| + i\epsilon} P_s(\mathbf{p}), \\ S^{ar}(p) &= \sum_{s=\pm} \frac{i}{p^0 - s|\mathbf{p}| - i\epsilon} P_s(\mathbf{p}), \\ S^{rr}(p) &= \left(\frac{1}{2} - n_+(p^0) \right) (S^{ra}(p) - S^{ar}(p)) = \left(\frac{1}{2} - n_+(p^0) \right) \rho_F(p), \end{aligned} \quad (3.4.151)$$

where $n_\pm(p^0) = 1/(e^{\beta(p^0 \mp \mu)} + 1)$ and the (bare) fermionic spectral density is

$$\rho_F(p) = (2\pi) \sum_{s=\pm} \delta(p^0 - s|\mathbf{p}|) P_s(\mathbf{p}). \quad (3.4.152)$$

The Feynman rules are as usual, for example, for incoming (out-going) quark of momentum \mathbf{p} , we have $u(\mathbf{p})$ ($u^\dagger(\mathbf{p})$), and for the incoming (out-going) antiquark of momentum \mathbf{p} , we have $v^\dagger(-\mathbf{p})$ ($v(-\mathbf{p})$). We remind ourselves of the rules for polarization states as it is important to get the correct sign for our P-odd photon emission rate. For out-going photon of polarization ϵ_μ , we attach $(\epsilon_\mu)^*$ contracted with the photon vertex $ie\sigma^\mu$ in the diagram. The same is true for

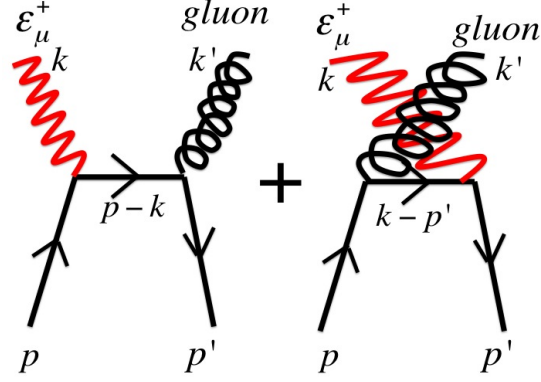


Figure 14. Pair Annihilation diagrams with hard momentum exchanges.

gluons. For incoming gluon of polarization $\tilde{\epsilon}_\mu$, we attach $\tilde{\epsilon}_\mu$ contracted with the gluon vertex $igt^a\sigma^\mu$. Finally, with these normalizations, the natural momentum integration measure is

$$\int \frac{d^3\mathbf{p}}{(2\pi)^3 2|\mathbf{p}|}. \quad (3.4.153)$$

Hard Compton and Pair Annihilation Contributions

Let the final photon momentum be k . For Pair Annihilation we label the momenta of incoming quark and antiquark pair by p and p' respectively, and let k' be the momentum of out-going gluon of polarization $\tilde{\epsilon}^\mu$ and color a . There are two Feynman diagrams as in Figure 14 with the total amplitude given as

$$M^{pair}(\epsilon_\pm) = -ieg v^\dagger(-\mathbf{p}') \left[t^a \sigma^\nu \frac{(p-k) \cdot \bar{\sigma}}{(p-k)^2} \sigma^\mu + \sigma^\mu \frac{(k-p') \cdot \bar{\sigma}}{(k-p')^2} t^a \sigma^\nu \right] u(\mathbf{p}) (\epsilon_\mu^\pm)^* (\tilde{\epsilon}_\nu)^*, \quad (3.4.154)$$

where ϵ_{\pm}^{μ} are the spin polarized photon states. Summing over colors in the squared amplitude produces a simple color factor

$$\sum_a \text{tr}(t^a t^a) = C_2(R) d_R = \frac{1}{2}(N_c^2 - 1), \quad (3.4.155)$$

for the fundamental representation of $SU(N_c)$. The summation over gluon polarization can be replaced by

$$\sum_{\tilde{\epsilon}} (\tilde{\epsilon}_{\nu})^* \tilde{\epsilon}_{\nu'} \rightarrow \eta_{\nu\nu'}, \quad (3.4.156)$$

thanks to Ward identities. Since our P-odd photon emission rate is the difference between the rates with ϵ_+ and ϵ_- , what we need is the difference

$$|M^{pair}(\epsilon_+)|^2 - |M^{pair}(\epsilon_-)|^2 \equiv |M^{pair}|_{odd}^2, \quad (3.4.157)$$

and the Pair Annihilation contribution to the P-odd photon emission rate is written as

$$\begin{aligned} (2\pi)^3 2\omega \frac{d\Gamma^{odd}}{d^3\mathbf{k}} &= \int \frac{d^3\mathbf{p}}{(2\pi)^3 2|\mathbf{p}|} \int \frac{d^3\mathbf{p}'}{(2\pi)^3 2|\mathbf{p}'|} \int \frac{d^3\mathbf{k}'}{(2\pi)^3 2|\mathbf{k}'|} (2\pi)^4 \delta(p + p' - k - k') \\ &\times |M^{pair}|_{odd}^2 n_+(|\mathbf{p}|) n_-(|\mathbf{p}'|) (1 + n_B(|\mathbf{k}'|)). \end{aligned} \quad (3.4.158)$$

The computation of P-odd amplitude $|M^{pair}|_{odd}^2$ is algebraically complicated, although conceptually straightforward. Using (Equation 3.4.149) and (Equation 4.1.27), and the polarization vectors

$$\epsilon_{\pm}^{\mu} = \frac{1}{\sqrt{2}}(0, 1, \pm i, 0), \quad (3.4.159)$$

after choosing $\mathbf{k} = |\mathbf{k}|\hat{\mathbf{x}}^3$, it reduces to computing traces of 8 σ matrices. After some amount of efforts, we obtain a compact expression

$$|M^{pair}|_{odd}^2 = C_2(R)d_R \cdot 4e^2g^2(t-u) \left(\frac{1}{t} + \frac{1}{u} - 2 \left(\frac{\mathbf{p}_{\perp}}{t} - \frac{\mathbf{p}'_{\perp}}{u} \right)^2 \right), \quad (3.4.160)$$

where $t \equiv (p-k)^2$, $u \equiv (k-p')^2$, and \mathbf{p}_{\perp} is the component of \mathbf{p} perpendicular to the photon momentum \mathbf{k} .

The momentum integration in the emission rate (Equation 3.4.158) with the above P-odd amplitude possesses logarithmic IR divergences near $t \sim 0$ and $u \sim 0$, corresponding to soft fermion exchanges. From the diagrams in Figure Figure 14, it is clearly seen that the $u \sim 0$ divergence is the same type of divergence near $t \sim 0$ with a simple interchange of quark and anti-quark. We can explore this symmetry of interchanging quark and anti-quark to simplify our computation: the kinematics is identical under the interchange

$$\mathbf{p} \longleftrightarrow \mathbf{p}', \quad t \longleftrightarrow u, \quad n_{+}(|\mathbf{p}|) \longleftrightarrow n_{-}(|\mathbf{p}'|), \quad (3.4.161)$$

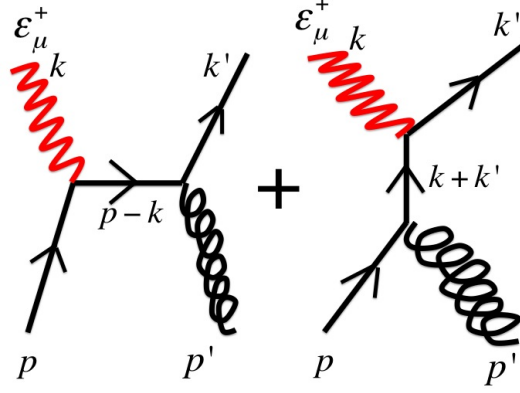


Figure 15. Compton scattering diagrams with hard momentum exchanges.

and we can replace singular $\sim 1/u$ terms in the amplitude with $\sim 1/t$ terms, so that the IR divergence appears in the new expression only around $t \sim 0$. Explicitly, we can have a replacement

$$\begin{aligned}
 & |M^{pair}|_{odd}^2 n_+(|\mathbf{p}|) n_-(|\mathbf{p}'|) (1 + n_B(|\mathbf{k}'|)) \\
 \longrightarrow & C_2(R) d_R \cdot 4e^2 g^2 \left(-\frac{u}{t} - 2(t-u) \left(\frac{\mathbf{p}_\perp^2}{t^2} - \frac{\mathbf{p}_\perp \cdot \mathbf{p}'_\perp}{tu} \right) \right) \\
 \times & (n_+(|\mathbf{p}|) n_-(|\mathbf{p}'|) - n_-(|\mathbf{p}|) n_+(|\mathbf{p}'|)) (1 + n_B(|\mathbf{k}'|)). \tag{3.4.162}
 \end{aligned}$$

The integral with the above new expression has an additional advantage besides the absence of IR divergence near $u \sim 0$: from the new structure of distribution function factor, the fact that the result is an odd function on the chemical potential μ is manifest.

For Compton scatterings, let us first consider the Compton scattering with incoming quark of momentum p and incoming gluon of momentum p' . The momentum of out-going quark will then be k' . The kinematics is identical to the Pair Annihilation case with the same definitions of $t \equiv (p - k)^2$, $u \equiv (k - p')^2$ and $s \equiv (k + k')^2$. Note that

$$t + u + s = 0. \quad (3.4.163)$$

There are two Feynman diagrams as in Figure 15 with the amplitude

$$M_{quark}^{Compton}(\epsilon_{\pm}) = -ieg u^{\dagger}(\mathbf{k}') \left[\sigma^{\nu} \frac{(p - k) \cdot \bar{\sigma}}{(p - k)^2} \sigma^{\mu} + \sigma^{\mu} \frac{(k + k') \cdot \bar{\sigma}}{(k + k')^2} \sigma^{\nu} \right] u(\mathbf{p})(\epsilon_{\mu}^{\pm})^* \tilde{\epsilon}_{\nu}, \quad (3.4.164)$$

where we omit color generators as it produces the same $C_2(R)d_R$ factor in the final result. The P-odd amplitude square is then computed after some amount of algebra as

$$\begin{aligned} |M_{quark}^{Compton}|_{odd}^2 &\equiv |M_{quark}^{Compton}(\epsilon_+)|^2 - |M_{quark}^{Compton}(\epsilon_-)|^2 \\ &= C_2(R)d_R \cdot 4e^2 g^2 (s - t) \left(\frac{1}{t} + \frac{1}{s} - 2 \left(\frac{\mathbf{p}_{\perp}}{t} + \frac{\mathbf{k}'_{\perp}}{s} \right)^2 \right). \end{aligned} \quad (3.4.165)$$

The P-odd emission rate with this Compton amplitude for quarks is given by

$$\begin{aligned} (2\pi)^3 2\omega \frac{d\Gamma^{odd}}{d^3\mathbf{k}} &= \int \frac{d^3\mathbf{p}}{(2\pi)^3 2|\mathbf{p}|} \int \frac{d^3\mathbf{p}'}{(2\pi)^3 2|\mathbf{p}'|} \int \frac{d^3\mathbf{k}'}{(2\pi)^3 2|\mathbf{k}'|} (2\pi)^4 \delta(p + p' - k - k') \\ &\times |M_{quark}^{Compton}|_{odd}^2 n_+(|\mathbf{p}|)(1 - n_+(|\mathbf{k}'|))n_B(|\mathbf{p}'|). \end{aligned} \quad (3.4.166)$$

There arises a logarithmic divergence near $t \sim 0$ only, which can be treated together with the one from the Pair Annihilation contribution.

The Compton scatterings with anti-quark has the P-odd amplitude square which is precisely negative to the above. This could be expected simply from the fact that anti-quark has the opposite chirality (helicity) to that of quark, so P-odd observable has to flip sign between them. We confirmed this expectation by an explicit computation, but just for reference we present the Compton amplitude with anti-quark,

$$M_{anti\text{quark}}^{Compton}(\epsilon_{\pm}) = -ieg v^{\dagger}(-\mathbf{p}) \left[\sigma^{\mu} \frac{(k-p) \cdot \bar{\sigma}}{(k-p)^2} \sigma^{\nu} + \sigma^{\nu} \frac{(-k-k') \cdot \bar{\sigma}}{(k+k')^2} \sigma^{\mu} \right] v(-\mathbf{k}') (\epsilon_{\mu}^{\pm})^* \tilde{\epsilon}_{\nu}. \quad (3.4.167)$$

Besides to this sign flip compared to the quark Compton contribution, the distribution function n_{+} in (Equation 3.4.166) has to be replaced by n_{-} for anti-quarks, so the final Compton rate is given as

$$\begin{aligned} (2\pi)^3 2\omega \frac{d\Gamma^{odd}}{d^3\mathbf{k}} &= \int \frac{d^3\mathbf{p}}{(2\pi)^3 2|\mathbf{p}|} \int \frac{d^3\mathbf{p}'}{(2\pi)^3 2|\mathbf{p}'|} \int \frac{d^3\mathbf{k}'}{(2\pi)^3 2|\mathbf{k}'|} (2\pi)^4 \delta(p+p'-k-k') \\ &\times |M_{quark}^{Compton}|_{odd}^2 (n_{+}(|\mathbf{p}|)(1-n_{+}(|\mathbf{k}'|)) - n_{-}(|\mathbf{p}|)(1-n_{-}(|\mathbf{k}'|))) n_B(|\mathbf{p}'|). \end{aligned} \quad (3.4.168)$$

The fact the the result is an odd function on the chemical potential is also apparent here.

To perform the phase space integrations in (Equation 3.4.158) and (Equation 3.4.168) with P-odd amplitudes (Equation 3.4.160) and (Equation 3.4.165), we follow the technique nicely

introduced and explained in Refs.(167; 168). The idea is to introduce auxiliary energy variable q^0 corresponding to either t-channel energy transfer (“t-channel parametrization” according to Ref.(168)), or s-channel energy transfer (“s-channel parametrization”). Its essential role is to trade the angular integration, coming from the energy δ -function, for a scalar integration of q^0 . The price to pay is a somewhat complicated, but manageable integration domain. The choice between t-channel and s-channel parametrizations is simply for convenience: t-channel parametrization is convenient for terms with $1/t$, and vice versa for s-parametrization.

We will give a brief summary on these parametrizations that one can also find in the original Refs.(167; 168). Let us focus on the common phase space integration measure in (Equation 3.4.158) and (Equation 3.4.168),

$$\int \frac{d^3\mathbf{p}}{(2\pi)^3 2|\mathbf{p}|} \int \frac{d^3\mathbf{p}'}{(2\pi)^3 2|\mathbf{p}'|} \int \frac{d^3\mathbf{k}'}{(2\pi)^3 2|\mathbf{k}'|} (2\pi)^4 \delta(p + p' - k - k'). \quad (3.4.169)$$

For t-channel parametrization, we perform $d^3\mathbf{k}'$ integration, and shift the integration variable \mathbf{p} to $\mathbf{q} \equiv \mathbf{p} - \mathbf{k}$ to obtain

$$\int \frac{d^3\mathbf{q}}{(2\pi)^3 2|\mathbf{q} + \mathbf{k}|} \int \frac{d^3\mathbf{p}'}{(2\pi)^3 2|\mathbf{p}'|} \frac{1}{2|\mathbf{q} + \mathbf{p}'|} (2\pi) \delta(|\mathbf{q} + \mathbf{k}| + |\mathbf{p}'| - |\mathbf{k}| - |\mathbf{q} + \mathbf{p}'|) . \quad (3.4.170)$$

We then introduce a variable q^0 to write the energy δ function as

$$\delta(|\mathbf{q} + \mathbf{k}| + |\mathbf{p}'| - |\mathbf{k}| - |\mathbf{q} + \mathbf{p}'|) = \int_{-\infty}^{+\infty} dq^0 \delta(|\mathbf{q} + \mathbf{k}| - |\mathbf{k}| - q^0) \delta(q^0 + |\mathbf{p}'| - |\mathbf{q} + \mathbf{p}'|) , \quad (3.4.171)$$

where the meaning of $Q \equiv (q^0, \mathbf{q})$ as the t-channel exchange momentum is obvious.

The next step is to express the energy δ -functions in terms of angle variables. Denoting the angle between \mathbf{q} and \mathbf{k} as θ , we have

$$\delta(|\mathbf{q} + \mathbf{k}| - |\mathbf{k}| - q^0) = \frac{|\mathbf{k}| + q^0}{|\mathbf{q}||\mathbf{k}|} \delta(\cos \theta - \cos \theta_{\mathbf{q}\mathbf{k}}), \quad (3.4.172)$$

where

$$\cos \theta_{\mathbf{q}\mathbf{k}} = \frac{(q^0)^2 - |\mathbf{q}|^2 + 2|\mathbf{k}|q^0}{2|\mathbf{q}||\mathbf{k}|}. \quad (3.4.173)$$

There appears constraints on $(q^0, |\mathbf{q}|)$ simply from the requirement that $|\cos \theta_{\mathbf{q}\mathbf{k}}| \leq 1$, which restricts the final integration domain that will be described shortly. Similarly, for the angle θ' between \mathbf{q} and \mathbf{p}' we have

$$\delta(q^0 + |\mathbf{p}'| - |\mathbf{q} + \mathbf{p}'|) = \frac{|\mathbf{p}'| + q^0}{|\mathbf{p}'||\mathbf{q}|} \delta(\cos \theta' - \cos \theta_{\mathbf{p}'\mathbf{q}}), \quad (3.4.174)$$

with

$$\cos \theta_{\mathbf{p}'\mathbf{q}} = \frac{(q^0)^2 - |\mathbf{q}|^2 + 2|\mathbf{p}'|q^0}{2|\mathbf{p}'||\mathbf{q}|}. \quad (3.4.175)$$

Using these, one can perform the angular integrals of $\cos \theta$ from $d^3\mathbf{q}$ and $\cos \theta'$ from $d^3\mathbf{p}'$, localizing $\cos \theta$ and $\cos \theta'$ to the values $\cos \theta_{\mathbf{q}\mathbf{k}}$ and $\cos \theta_{\mathbf{p}'\mathbf{q}}$. Since we need to compute $\mathbf{p}_\perp = \mathbf{q}_\perp$ and \mathbf{p}'_\perp that appear in the P-odd amplitudes, it is convenient to fix the photon momentum direction to be along $\hat{\mathbf{x}}^3$, and using the overall rotational symmetry in (x^1, x^2) -plane, we can align \mathbf{q} to be in (x^1, x^3) plane. See Figure 16 for the illustration. This alignment will produce

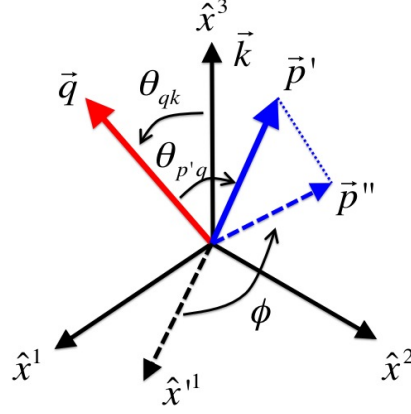


Figure 16. The geometry of t-channel parametrization. $(\hat{\mathbf{q}}, \hat{\mathbf{x}}^1, \hat{\mathbf{x}}^2)$ form an orthonormal basis rotated by θ_{qk} , and \mathbf{p}'' is a projection of \mathbf{p}' onto the $(\hat{\mathbf{x}}^1, \hat{\mathbf{x}}^2)$ plane.

a trivial (2π) azimuthal integration factor in the integral of $d^3\mathbf{q}$. Note that the azimuthal angle ϕ of \mathbf{p}' with respect to \mathbf{q} as defined in Figure ?? still has to be integrated explicitly. From the geometry in Figure 16, we have

$$\mathbf{q}_\perp = (|\mathbf{q}| \sin \theta_{qk}, 0), \quad (3.4.176)$$

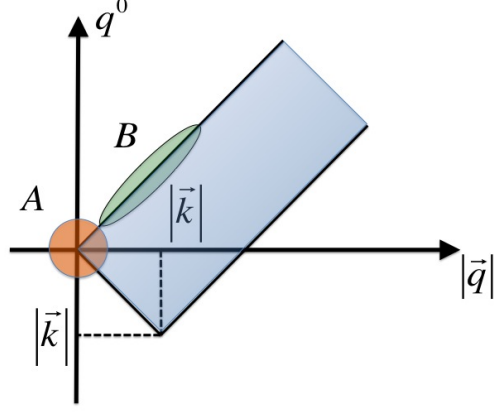


Figure 17. The integration domain of $(q^0, |\mathbf{q}|)$ (shaded blue). The domain for $|\mathbf{p}'|$ is $|\mathbf{p}'| > (|\mathbf{q}| - q^0)/2$. The soft region A (shaded red) is responsible for leading log IR divergence, and the region B produces the energy logarithm that is described in the following.

in (x^1, x^2) plane, and the \mathbf{p}' in (x^1, x^2, x^3) -basis is given as

$$\begin{aligned}
 \mathbf{p}' &= |\mathbf{p}'| \begin{pmatrix} \cos \theta_{\mathbf{q}\mathbf{k}} & 0 & \sin \theta_{\mathbf{q}\mathbf{k}} \\ 0 & 1 & 0 \\ -\sin \theta_{\mathbf{q}\mathbf{k}} & 0 & \cos \theta_{\mathbf{q}\mathbf{k}} \end{pmatrix} \begin{pmatrix} \sin \theta_{\mathbf{p}'\mathbf{q}} \cos \phi \\ \sin \theta_{\mathbf{p}'\mathbf{q}} \sin \phi \\ \cos \theta_{\mathbf{p}'\mathbf{q}} \end{pmatrix} \\
 &= |\mathbf{p}'| \begin{pmatrix} \cos \theta_{\mathbf{q}\mathbf{k}} \sin \theta_{\mathbf{p}'\mathbf{q}} \cos \phi + \sin \theta_{\mathbf{q}\mathbf{k}} \cos \theta_{\mathbf{p}'\mathbf{q}} \\ \sin \theta_{\mathbf{p}'\mathbf{q}} \sin \phi \\ -\sin \theta_{\mathbf{q}\mathbf{k}} \sin \theta_{\mathbf{p}'\mathbf{q}} \cos \phi + \cos \theta_{\mathbf{q}\mathbf{k}} \cos \theta_{\mathbf{p}'\mathbf{q}} \end{pmatrix}, \quad (3.4.177)
 \end{aligned}$$

which will be used in computing the P-odd amplitudes (Equation 3.4.160) and (Equation 3.4.165).

Finally, the integration domain for $(q^0, |\mathbf{q}|, |\mathbf{p}'|)$ is depicted in Figure 17.

From all these, the phase space integration in the t-channel parametrization becomes

$$\begin{aligned}
& \int \frac{d^3 \mathbf{p}}{(2\pi)^3 2|\mathbf{p}|} \int \frac{d^3 \mathbf{p}'}{(2\pi)^3 2|\mathbf{p}'|} \int \frac{d^3 \mathbf{k}'}{(2\pi)^3 2|\mathbf{k}'|} (2\pi)^4 \delta(p + p' - k - k') \\
&= \frac{1}{8(2\pi)^4 |\mathbf{k}|} \int_0^\infty d|\mathbf{q}| \int_{\max(-|\mathbf{q}|, |\mathbf{q}| - 2|\mathbf{k}|)}^{|\mathbf{q}|} dq^0 \int_{\frac{|\mathbf{q}| - q^0}{2}}^\infty d|\mathbf{p}'| \int_0^{2\pi} d\phi. \quad (3.4.178)
\end{aligned}$$

For the amplitudes, we need to express various quantities in terms of integration variables and the angles $\theta_{\mathbf{k}\mathbf{q}}$ and $\theta_{\mathbf{p}'\mathbf{q}}$. The following expressions can be derived from (Equation 3.4.176) and (Equation 3.4.177) and the previous definitions:

$$\begin{aligned}
t &= -(q^0)^2 + |\mathbf{q}|^2, \quad u = 2|\mathbf{k}||\mathbf{p}'| (1 + \sin \theta_{\mathbf{q}\mathbf{k}} \sin \theta_{\mathbf{p}'\mathbf{q}} \cos \phi - \cos \theta_{\mathbf{q}\mathbf{k}} \cos \theta_{\mathbf{p}'\mathbf{q}}), \\
\mathbf{q}_\perp^2 &= |\mathbf{q}|^2 \sin^2 \theta_{\mathbf{q}\mathbf{k}}, \quad \mathbf{q}_\perp \cdot \mathbf{p}'_\perp = |\mathbf{q}||\mathbf{p}'| (\sin \theta_{\mathbf{q}\mathbf{k}} \cos \theta_{\mathbf{q}\mathbf{k}} \sin \theta_{\mathbf{p}'\mathbf{q}} \cos \phi + \sin^2 \theta_{\mathbf{q}\mathbf{k}} \cos \theta_{\mathbf{p}'\mathbf{q}}), \\
s &= -t - u, \quad \mathbf{p}_\perp = \mathbf{q}_\perp, \quad \mathbf{k}'_\perp = \mathbf{q}_\perp + \mathbf{p}'_\perp, \quad (3.4.179)
\end{aligned}$$

where $\theta_{\mathbf{k}\mathbf{q}}$ and $\theta_{\mathbf{p}'\mathbf{q}}$ are given by (Equation 3.4.173) and (Equation 3.4.175). Finally, for the arguments that enter the distribution functions, we have

$$|\mathbf{p}| = q^0 + |\mathbf{k}|, \quad |\mathbf{k}'| = q^0 + |\mathbf{p}'|. \quad (3.4.180)$$

The above data are enough, at least numerically, to compute the phase space integrations in (Equation 3.4.158) and (Equation 3.4.168) to obtain our P-odd emission rate from the hard Compton and Pair Annihilation processes. This t-channel parametrization is not efficient for the terms of $\sim 1/s$ or $\sim 1/s^2$ type, for which we use s-channel parametrization.

The geometry of s-channel parametrization is similar, so we simply summarize it. The phase space measure becomes

$$\begin{aligned}
& \int \frac{d^3 \mathbf{p}}{(2\pi)^3 2|\mathbf{p}|} \int \frac{d^3 \mathbf{p}'}{(2\pi)^3 2|\mathbf{p}'|} \int \frac{d^3 \mathbf{k}'}{(2\pi)^3 2|\mathbf{k}'|} (2\pi)^4 \delta(p + p' - k - k') \\
&= \frac{1}{8(2\pi)^4 |\mathbf{k}|} \int_{|\mathbf{k}|}^{\infty} dq^0 \int_{|2|\mathbf{k}| - q^0|}^{q^0} d|\mathbf{q}| \int_{\frac{q^0 - |\mathbf{q}|}{2}}^{\frac{q^0 + |\mathbf{q}|}{2}} d|\mathbf{p}| \int_0^{2\pi} d\phi,
\end{aligned} \tag{3.4.181}$$

and we have

$$\begin{aligned}
s &= -(q^0)^2 + |\mathbf{q}|^2, \quad t = 2|\mathbf{k}||\mathbf{p}| (1 + \sin \theta_{\mathbf{qk}} \sin \theta_{\mathbf{pq}} \cos \phi - \cos \theta_{\mathbf{qk}} \cos \theta_{\mathbf{pq}}), \\
\mathbf{q}_{\perp}^2 &= |\mathbf{q}|^2 \sin^2 \theta_{\mathbf{qk}}, \quad \mathbf{p}_{\perp} \cdot \mathbf{q}_{\perp} = |\mathbf{p}||\mathbf{q}| (\sin \theta_{\mathbf{qk}} \cos \theta_{\mathbf{qk}} \sin \theta_{\mathbf{pq}} \cos \phi + \sin^2 \theta_{\mathbf{qk}} \cos \theta_{\mathbf{pq}}), \\
\mathbf{k}'_{\perp} &= \mathbf{q}_{\perp},
\end{aligned} \tag{3.4.182}$$

where

$$\cos \theta_{\mathbf{qk}} = \frac{|\mathbf{q}|^2 - (q^0)^2 + 2q^0|\mathbf{k}|}{2|\mathbf{q}||\mathbf{k}|}, \quad \cos \theta_{\mathbf{pq}} = \frac{|\mathbf{q}|^2 - (q^0)^2 + 2q^0|\mathbf{p}|}{2|\mathbf{q}||\mathbf{p}|}, \tag{3.4.183}$$

and finally, we have to replace

$$|\mathbf{p}'| \rightarrow q^0 - |\mathbf{p}|, \quad |\mathbf{k}'| \rightarrow q^0 - |\mathbf{k}|, \tag{3.4.184}$$

in the arguments of distribution functions.

The ϕ integrations in both t-channel and s-channel methods are at most of the type

$$\int_0^{2\pi} d\phi \frac{A + B \cos \phi}{C + D \cos \phi}, \quad (3.4.185)$$

which can be done analytically. The rest parts of the integration have to be done numerically, but we can identify the leading log parts of $\log(1/\alpha_s)$ and $\log(\omega/T)$ for $\omega \gg T$ analytically (recall $\omega = |\mathbf{k}|$), which we now describe.

Leading Log

The Pair Annihilation contribution (Equation 3.4.158) with (Equation 3.4.160) has a logarithmic IR divergence near $t \sim 0$, or when $(q^0, |\mathbf{q}|) \ll |\mathbf{k}|, |\mathbf{p}'|$ in the t-channel parametrization. The same is true for the Compton rate (Equation 3.4.168) with (Equation 3.4.165). These divergences are regulated by including HTL self-energy (169) in the t-channel fermion propagator, which screens the fermion exchange for soft momenta $(q^0, |\mathbf{q}|) \lesssim gT$ (“soft region”). When $(q^0, |\mathbf{q}|) \gg gT$ (“hard region”), the HTL correction is sub-leading in α_s and what we have in the above as hard Compton and Pair Annihilation contributions give the leading order result.

A practical way to organize the leading order contributions from both regions is to introduce an intermediate scale $gT \ll q^* \ll T$ (183), which serves as a t-channel IR cutoff for the above hard Compton and Pair Annihilation rates in the hard region, and as a t-channel UV cutoff for the same rates in the soft region with now the HTL self-energy included in the fermion propagator. The two logs of $\log q^*$ from both regions have to match to produce a final result independent of q^* : after identifying $\log q^*$ from each region, we neglect q^*/T and $(gT)/q^*$

corrections in the rest parts of the two regions by sending $q^* \rightarrow 0$ in the hard region and $q^* \rightarrow \infty$ in the soft region. The resulting (numerical) constant is the leading order constant under the log.

Let us identify the leading log from the hard region in this subsection. The t-channel parametrization is most efficient for this purpose. The q^* is introduced as an IR cutoff of $d|\mathbf{q}|$ -integral in (Equation 3.4.178)

$$(2\pi)^3 2\omega \frac{d\Gamma_{hard}^{odd}}{d^3\mathbf{k}} = \frac{1}{8(2\pi)^4 |\mathbf{k}|} \int_{q^*}^{\infty} d|\mathbf{q}| \int_{\max(-|\mathbf{q}|, |\mathbf{q}|-2|\mathbf{k}|)}^{|\mathbf{q}|} dq^0 \int_{\frac{|\mathbf{q}|-q^0}{2}}^{\infty} d|\mathbf{p}'| \int_0^{2\pi} d\phi I, \quad (3.4.186)$$

where I is the sum of the integrands in (Equation 3.4.162) and (Equation 3.4.168) from the Compton and Pair Annihilation processes:

$$\begin{aligned} I &= C_2(R) d_R \cdot 4e^2 g^2 \left(-\frac{u}{t} - 2(t-u) \left(\frac{\mathbf{q}_{\perp}^2}{t^2} - \frac{\mathbf{q}_{\perp} \cdot \mathbf{p}'_{\perp}}{tu} \right) \right) \\ &\times (n_+(q^0 + |\mathbf{k}|) n_- (|\mathbf{p}'|) - n_-(q^0 + |\mathbf{k}|) n_+ (|\mathbf{p}'|)) (1 + n_B(q^0 + |\mathbf{p}'|)) \\ &+ C_2(R) d_R \cdot 4e^2 g^2 (s-t) \left(\frac{1}{t} + \frac{1}{s} - 2 \left(\frac{\mathbf{q}_{\perp}}{t} + \frac{(\mathbf{q}_{\perp} + \mathbf{p}'_{\perp})}{s} \right)^2 \right) \\ &\times (n_+(q^0 + |\mathbf{k}|) (1 - n_+(q^0 + |\mathbf{p}'|)) - n_-(q^0 + |\mathbf{k}|) (1 - n_-(q^0 + |\mathbf{p}'|))) n_B (|\mathbf{p}'|), \end{aligned} \quad (3.4.187)$$

with the use of expressions in (Equation 3.4.179) and (Equation 3.4.180) for the t-channel parametrization.

From the distribution functions, $|\mathbf{p}'|$ integral is dominated by $|\mathbf{p}'| \sim T$. The log divergence appears in small $(q^0, |\mathbf{q}|) \ll |\mathbf{k}|, |\mathbf{p}'| \sim T$ since we assume hard photons $T \lesssim |\mathbf{k}|$. Figure 17 shows this region (region A). In this case, from (Equation 3.4.173) and (Equation 3.4.175), we have

$$\cos \theta_{\mathbf{q}\mathbf{k}} \approx \cos \theta_{\mathbf{p}'\mathbf{q}} \approx \frac{q^0}{|\mathbf{q}|}, \quad (3.4.188)$$

and the leading behavior in A comes from the terms of $(u, s)/t$ or $(u, s)\mathbf{q}_\perp^2/t^2$ types, which gives after some algebra,

$$\begin{aligned} I &\sim C_2(R)d_R \cdot 8e^2g^2 \frac{|\mathbf{k}||\mathbf{p}'|}{|\mathbf{q}|^2} (1 + \cos \phi) \\ &\times (n_+(|\mathbf{k}|)n_-(|\mathbf{p}'|)(1 + n_B(|\mathbf{p}'|)) + n_+(|\mathbf{k}|)n_B(|\mathbf{p}'|)(1 - n_+(|\mathbf{p}'|)) - (n_+ \leftrightarrow n_-)) \\ &= C_2(R)d_R \cdot 8e^2g^2 \frac{|\mathbf{k}||\mathbf{p}'|}{|\mathbf{q}|^2} (1 + \cos \phi) \\ &\times (n_+(|\mathbf{k}|)n_-(0) - n_-(|\mathbf{k}|)n_+(0)) (n_+(|\mathbf{p}'|) + n_-(|\mathbf{p}'|) + 2n_B(|\mathbf{p}'|)) , \end{aligned} \quad (3.4.189)$$

where in the last line, we use an interesting identity

$$n_\mp(|\mathbf{p}'|)(1 + n_B(|\mathbf{p}'|)) + n_B(|\mathbf{p}'|)(1 - n_\pm(|\mathbf{p}'|)) = n_\mp(0) (n_+(|\mathbf{p}'|) + n_-(|\mathbf{p}'|) + 2n_B(|\mathbf{p}'|)) . \quad (3.4.190)$$

We then have a leading log behavior

$$\begin{aligned}
(2\pi)^3 2\omega \frac{d\Gamma_{hard}^{odd}}{d^3\mathbf{k}} &\sim C_2(R) d_R \cdot \frac{e^2 g^2}{(2\pi)^3} (n_+(|\mathbf{k}|)n_-(0) - n_- (|\mathbf{k}|)n_+(0)) \\
&\times \int_{q^*}^{\sim T} d|\mathbf{q}| \frac{1}{|\mathbf{q}|^2} \int_{-|\mathbf{q}|}^{|\mathbf{q}|} dq^0 \int_0^\infty d|\mathbf{p}'| |\mathbf{p}'| (n_+(|\mathbf{p}'|) + n_-(|\mathbf{p}'|) + 2n_B(|\mathbf{p}'|)) \\
&\sim C_2(R) d_R \cdot \frac{e^2 g^2}{(2\pi)^3} (\pi^2 T^2 + \mu^2) (n_+(|\mathbf{k}|)n_-(0) - n_- (|\mathbf{k}|)n_+(0)) \log(T/q^*) \\
&= d_R \frac{e^2}{(2\pi)} m_f^2 (n_+(|\mathbf{k}|)n_-(0) - n_- (|\mathbf{k}|)n_+(0)) \log(T/q^*) , \tag{3.4.191}
\end{aligned}$$

where we use

$$\int_0^\infty d|\mathbf{p}'| |\mathbf{p}'| (n_+(|\mathbf{p}'|) + n_-(|\mathbf{p}'|) + 2n_B(|\mathbf{p}'|)) = \frac{1}{2} (\pi^2 T^2 + \mu^2) , \tag{3.4.192}$$

and in the last line we write the result in terms of the asymptotic fermion thermal mass

$$m_f^2 = C_2(R) \frac{g^2}{4} \left(T^2 + \frac{\mu^2}{\pi^2} \right) . \tag{3.4.193}$$

We will check that the leading log from the hard Compton and Pair Annihilation given in (Equation 3.4.191) nicely matches to the soft region result with HTL re-summation in the next subsection.

For an ultra-hard photon energy $\omega = |\mathbf{k}| \gg T$, there appears a logarithmic rise of $\log(\omega/T)$ in the energy dependence of the leading order constant under the log. We close this subsection

by identifying this “energy logarithm”. For this aim, it is convenient to work with the light cone variables

$$q^\pm \equiv \frac{|\mathbf{q}| \pm q^0}{2}, \quad (3.4.194)$$

with the measure change $d|\mathbf{q}|dq^0 = 2dq^+dq^-$. The energy logarithm appears in the domain where

$$q^- \lesssim |\mathbf{p}'| \sim T \ll q^+ \ll |\mathbf{k}| = \omega, \quad (3.4.195)$$

which is also indicated in Figure 17 (region B). In this case, we have

$$\cos \theta_{\mathbf{q}\mathbf{k}} \approx \frac{q^0}{|\mathbf{q}|} \approx 1, \quad \cos \theta_{\mathbf{p}'\mathbf{q}} = \frac{-4q^+q^- + 2q^0|\mathbf{p}'|}{2|\mathbf{p}'||\mathbf{q}|} \approx 1 - \frac{2q^-}{|\mathbf{p}'|}, \quad (3.4.196)$$

and the leading behavior in A arises again from the same $(u, s)/t$ or $(u, s)\mathbf{q}_\perp^2/t^2$ terms, with

$$I \sim C_2(R)d_R \cdot 4e^2g^2 \frac{|\mathbf{k}|}{q^+} \left(n_+(|\mathbf{k}|) (n_-(|\mathbf{p}'|) + n_B(|\mathbf{p}'|)) - (n_+ \leftrightarrow n_-) \right), \quad (3.4.197)$$

so that we have

$$\begin{aligned} (2\pi)^3 2\omega \frac{d\Gamma_{hard}^{odd}}{d^3\mathbf{k}} &\sim C_2(R)d_R \frac{e^2g^2}{(2\pi)^3} \int_{\sim T}^{|\mathbf{k}|} dq^+ \frac{1}{q^+} \int_0^\infty dq^- \int_{q^-}^\infty d|\mathbf{p}'| \\ &\times \left(n_+(|\mathbf{k}|) (n_-(|\mathbf{p}'|) + n_B(|\mathbf{p}'|)) - (n_+ \leftrightarrow n_-) \right) \\ &= C_2(R)d_R \frac{e^2g^2}{(2\pi)^3} \log(|\mathbf{k}|/T) \left(n_+(|\mathbf{k}|) \int_0^\infty dq^- q^- (n_-(q^-) + n_B(q^-)) - (n_+ \leftrightarrow n_-) \right), \end{aligned} \quad (3.4.198)$$

where in the first line, we can safely let the upper cutoff of q^- be infinity, due to the presence of effective cutoff by the distribution functions (more precisely, the cutoff is given by $\sim q^+ \gg T$).

The integrals that appear in the above

$$\int_0^\infty dq^- q^- (n_{\mp}(q^-) + n_B(q^-)) = \frac{T^2}{6} \left(\pi^2 - 6 \operatorname{Li}_2 \left(-e^{\mp\mu/T} \right) \right), \quad (3.4.199)$$

are not simple polynomials in T and μ , contrary to the case of leading log in coupling (Equation 3.4.191).

Soft t-Channel Contribution: Hard Thermal Loop

We compute the soft t-channel contributions from Compton and Pair Annihilation processes, whose IR divergence is regulated by re-summing fermion HTL self-energy in the fermion exchange line. Following the original treatment in Refs.(163; 164), we compute this directly in terms of 1-loop current-current correlation functions that enter the emission rate formula (??) or (??), with one internal fermion line being soft, and hence HTL re-summed, corresponding to soft t-channel exchange. The emission rate written in (??) is given by suitable imaginary part of the correlation functions, and by applying the cutting-rule, it is easy to see that the result should be equivalent to that from computing Feynman diagrams of only t-channel Compton and Pair Annihilation processes (with the HTL re-summed propagator) that we described in the previous subsection.

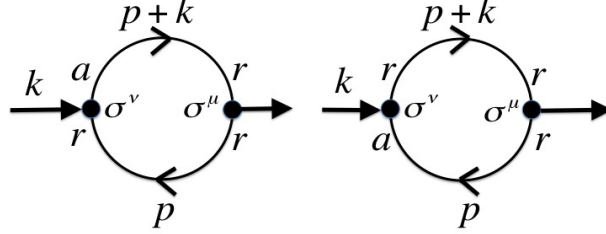


Figure 18. Two real-time Feynman diagrams for $G_{\mu\nu}^{ra}(k)$ in the “ra”-basis.

We compute the following with the soft t-channel momentum with an UV cutoff q^* ,

$$(2\pi)^3 2\omega \frac{d\Gamma(\epsilon_{\pm})}{d^3\mathbf{k}} = e^2 n_B(\omega) (-2) \text{Im} [(\epsilon_{\pm}^{\mu})^* \epsilon_{\pm}^{\nu} G_{\mu\nu}^R(k)] = e^2 n_B(\omega) 2 \text{Re} [(\epsilon_{\pm}^{\mu})^* \epsilon_{\pm}^{\nu} G_{\mu\nu}^{ra}(k)] . \quad (3.4.200)$$

Since $(\epsilon_{\pm}^{\mu})^* \epsilon_{\pm}^{\nu}$ is a hermitian matrix in terms of μ, ν indices, the emission rate picks up only the hermitian part of $G_{\mu\nu}^{ra}(k)$. There are two real-time Feynman diagrams for $G_{\mu\nu}^{ra}(k)$ depicted in Figure 18, which gives

$$G_{\mu\nu}^{ra}(k) = (-1) d_R \int \frac{d^4 p}{(2\pi)^4} \text{tr} [\sigma^{\nu} S^{rr}(p) \sigma^{\mu} S^{ra}(p+k) + \sigma^{\nu} S^{ar}(p) \sigma^{\mu} S^{rr}(p+k)] , \quad (3.4.201)$$

where d_R is the dimension of color representation. Recall the thermal relation

$$S^{rr}(p) = \left(\frac{1}{2} - n_+(p^0) \right) (S^{ra}(p) - S^{ar}(p)) \equiv \left(\frac{1}{2} - n_+(p^0) \right) \rho_F(p), \quad (3.4.202)$$

and by the reality property $S^{ar}(p)^\dagger = -S^{ra}(p)$, $S^{rr}(p)$ and $\rho_F(p)$ are hermitian matrices in terms of 2 component spinor indices. Using the same relations and the hermiticity of σ^μ , it is easy to find the hermitian part of $G_{\mu\nu}^{ra}(k)$ as (we denote $\omega \equiv k^0 = |\mathbf{k}|$)

$$G_{\mu\nu}^{ra}(k) + (G_{\nu\mu}^{ra}(k))^* = d_R \int \frac{d^4 p}{(2\pi)^4} (n_+(p^0) - n_+(p^0 + \omega)) \text{tr} [\sigma^\nu \rho_F(p) \sigma^\mu \rho_F(p + k)] . \quad (3.4.203)$$

The emission rate is given solely by (fermion) spectral density ρ_F , which conforms to the expectation from cutting rules.

Bare fermion spectral density is easy to read off from (Equation 3.4.151) or (Equation 3.4.152):

$$\rho_F^{bare}(p) = (2\pi) \sum_{s=\pm} \delta(p^0 - s|\mathbf{p}|) P_s(\mathbf{p}), \quad (3.4.204)$$

with the projection operators we repeat here for convenience,

$$P_s(\mathbf{p}) = \frac{1}{2} (1 + s\hat{\mathbf{p}}) = -s \frac{\bar{\sigma} \cdot \mathbf{p}_s}{2|\mathbf{p}|}, \quad p_s^\mu \equiv (s|\mathbf{p}|, \mathbf{p}). \quad (3.4.205)$$

In general, fermion spectral density in a Weyl fermion theory including HTL self-energy is written as (see Appendix 2 of Ref.(182)),

$$\rho_F^{HTL}(p) = \sum_s \rho_s^{HTL}(p) P_s(\mathbf{p}), \quad \rho_s^{HTL}(p) = -2 \operatorname{Im} \left[\frac{1}{p^0 - s|\mathbf{p}| + \Sigma_s^{R,HTL}(p)} \right], \quad (3.4.206)$$

where the HTL self-energy is given by

$$\Sigma_s^{R,HTL}(p) = -\frac{m_f^2}{4|\mathbf{p}|} \left(2s + \left(1 - s \frac{p^0}{|\mathbf{p}|} \right) \log \left(\frac{p^0 + |\mathbf{p}| + i\epsilon}{p^0 - |\mathbf{p}| + i\epsilon} \right) \right), \quad (3.4.207)$$

with the asymptotic fermion thermal mass that is introduced before in (Equation 3.4.193),

$$m_f^2 = C_2(R) \frac{g^2}{4} \left(T^2 + \frac{\mu^2}{\pi^2} \right). \quad (3.4.208)$$

Inserting (Equation 3.4.203) into (Equation 3.4.200), choosing the direction of $\mathbf{k} = |\mathbf{k}| \hat{\mathbf{x}}^3$ explicitly and computing the σ -matrix traces using (Equation 3.4.145), we end up to an expression for our P-odd emission rate as

$$\begin{aligned} (2\pi)^3 2\omega \frac{d\Gamma^{odd}}{d^3\mathbf{k}} &= d_R e^2 n_B(\omega) \int \frac{d^4 p}{(2\pi)^4} (n_+(p^0) - n_+(p^0 + \omega)) \\ &\times \sum_{s,t} \rho_s(p) \rho_t(p+k) \left(t \frac{(\mathbf{p}_3 + |\mathbf{k}|)}{|\mathbf{p} + \mathbf{k}|} - s \frac{\mathbf{p}_3}{|\mathbf{p}|} \right), \end{aligned} \quad (3.4.209)$$

where $\rho_{s,t}$ in the above can be either bare or HTL, depending on whether the momentum argument is hard or soft. We should consider the region of p where one of the two momenta, p or $p+k$, is soft, corresponding to soft t- or u-channel processes.

It would be convenient to combine the two soft regions into one, say soft p region. That is, for soft $p+k$ region, let us change the variable $p \rightarrow -p-k$, so that in the new variable, p is soft. Under this transform, we have

$$n_+(p^0) - n_+(p^0 + \omega) \rightarrow n_-(p^0) - n_-(p^0 + \omega), \quad \rho_s(p) \rightarrow \rho_{-s}(p+k), \quad \rho_t(p+k) \rightarrow \rho_{-t}(p), \quad (3.4.210)$$

and relabeling $-t \rightarrow s$ and $-s \rightarrow t$, we arrive at the precisely the same form as in (Equation 3.4.212), with the replacement

$$(n_+(p^0) - n_+(p^0 + \omega)) \rightarrow -(n_-(p^0) - n_-(p^0 + \omega)), \quad (3.4.211)$$

therefore, we can study only the soft p region of the following expression

$$\begin{aligned} (2\pi)^3 2\omega \frac{d\Gamma_{soft}^{odd}}{d^3\mathbf{k}} &= d_R e^2 n_B(\omega) \int \frac{d^4 p}{(2\pi)^4} (n_+(p^0) - n_+(p^0 + \omega) - (n_+ \leftrightarrow n_-)) \\ &\times \sum_{s,t} \rho_s^{HTL}(p) \rho_t^{bare}(p+k) \left(t \frac{(\mathbf{p}_3 + |\mathbf{k}|)}{|\mathbf{p} + \mathbf{k}|} - s \frac{\mathbf{p}_3}{|\mathbf{p}|} \right), \end{aligned} \quad (3.4.212)$$

where we explicitly indicated the HTL (bare) spectral density for soft (hard) p ($p+k$). An additional bonus is that the result is manifestly an odd function in the chemical potential.

This is reminiscent of what happens in our previous computation of hard Compton and Pair Annihilation processes.

From

$$\rho_t^{bare}(p+k) = (2\pi)\delta(p^0 + |\mathbf{k}| - t|\mathbf{p} + \mathbf{k}|), \quad (3.4.213)$$

and since p is soft while $(\omega = |\mathbf{k}|, \mathbf{k})$ is hard, we see that only $t = 1$ contributes. The total integrand has a rotational symmetry on (x^1, x^2) -plane, so the azimuthal integral of \mathbf{p} around \mathbf{k} will trivially give (2π) . The polar integration can be done by the same technique we use in (Equation 3.4.173): for $p \ll k$, we can write the integral measure including the energy δ -function as

$$\int \frac{d^4p}{(2\pi)^4} (2\pi)\delta(p^0 + |\mathbf{k}| - |\mathbf{p} + \mathbf{k}|) = \frac{1}{(2\pi)^2} \int_0^\infty d|\mathbf{p}| |\mathbf{p}| \int_{-|\mathbf{p}|}^{|\mathbf{p}|} dp^0 \left(1 + \frac{p^0}{|\mathbf{k}|}\right) \Big|_{\mathbf{p}_3 \rightarrow |\mathbf{p}| \cos \theta_{\mathbf{p}\mathbf{k}}}, \quad (3.4.214)$$

where

$$\cos \theta_{\mathbf{p}\mathbf{k}} = \frac{(p^0)^2 - |\mathbf{p}|^2 + 2p^0|\mathbf{k}|}{2|\mathbf{p}||\mathbf{k}|}. \quad (3.4.215)$$

Using this, our P-odd rate (Equation 3.4.212) from soft region is compactly written as

$$\begin{aligned} (2\pi)^3 2\omega \frac{d\Gamma_{soft}^{odd}}{d^3\mathbf{k}} &= d_R \frac{e^2}{(2\pi)^2} n_B(\omega) \int_0^{q^*} d|\mathbf{p}| |\mathbf{p}| \int_{-|\mathbf{p}|}^{|\mathbf{p}|} dp^0 \left(1 + \frac{p^0}{|\mathbf{k}|}\right) \\ &\times (n_+(p^0) - n_+(p^0 + \omega) - (n_+ \leftrightarrow n_-)) \\ &\times \sum_s \rho_s^{HTL}(p^0, |\mathbf{p}|) \left(\frac{|\mathbf{p}| \cos \theta_{\mathbf{p}\mathbf{k}} + |\mathbf{k}|}{p^0 + |\mathbf{k}|} - s \cos \theta_{\mathbf{p}\mathbf{k}} \right), \end{aligned} \quad (3.4.216)$$

where we introduce the UV cutoff q^* for the t-channel momentum integral of $|\mathbf{p}|$ to regulate the logarithmic divergence. The meaning of q^* here is identical to that used in the hard Compton and Pair Annihilation rates in the previous subsection, which is important to get the correct leading order constant under the log.

Since the cutoff is $q^* \ll T \lesssim |\mathbf{k}|$ (while $q^* \gg m_f \sim gT$), we have a further simplification at leading order to

$$\cos \theta_{\mathbf{p}\mathbf{k}} \approx \frac{p^0}{|\mathbf{p}|}, \quad \left(\frac{|\mathbf{p}| \cos \theta_{\mathbf{p}\mathbf{k}} + |\mathbf{k}|}{p^0 + |\mathbf{k}|} - s \cos \theta_{\mathbf{p}\mathbf{k}} \right) \approx 1 - s \frac{p^0}{|\mathbf{p}|}, \quad (3.4.217)$$

and we arrive at

$$\begin{aligned} (2\pi)^3 2\omega \frac{d\Gamma_{soft}^{odd}}{d^3\mathbf{k}} &\approx d_R \frac{e^2}{(2\pi)^2} n_B(\omega) (n_+(0) - n_+(\omega) - (n_+ \leftrightarrow n_-)) \\ &\times \int_0^{q^*} d|\mathbf{p}| |\mathbf{p}| \int_{-|\mathbf{p}|}^{|\mathbf{p}|} dp^0 \sum_s \rho_s^{HTL}(p^0, |\mathbf{p}|) \left(1 - s \frac{p^0}{|\mathbf{p}|} \right) \\ &= d_R \frac{e^2}{(2\pi)^2} (n_+(\omega) n_-(0) - n_-(\omega) n_+(0)) \\ &\times \int_0^{q^*} d|\mathbf{p}| |\mathbf{p}| \int_{-|\mathbf{p}|}^{|\mathbf{p}|} dp^0 \sum_s \rho_s^{HTL}(p^0, |\mathbf{p}|) \left(1 - s \frac{p^0}{|\mathbf{p}|} \right), \quad (3.4.218) \end{aligned}$$

where in the last line, we use an interesting identity

$$n_B(\omega)(n_{\pm}(0) - n_{\pm}(\omega)) = n_{\pm}(\omega)n_{\mp}(0). \quad (3.4.219)$$

As it happens, the remaining integral is something that has been already computed in literature: the same integral appears in the P-even total emission rate. In fact, a similar

manipulation in our language produces the usual P-even total emission rate from soft t-channel region at leading order as

$$(2\pi)^3 2\omega \frac{d\Gamma_{soft}^{total}}{d^3\mathbf{k}} \approx d_R \frac{e^2}{(2\pi)^2} (n_+(\omega)n_-(0) + n_-(\omega)n_+(0)) \times \int_0^{q^*} d|\mathbf{p}||\mathbf{p}| \int_{-|\mathbf{p}|}^{|\mathbf{p}|} dp^0 \sum_s \rho_s^{HTL}(p^0, |\mathbf{p}|) \left(1 - s \frac{p^0}{|\mathbf{p}|}\right), \quad (3.4.220)$$

and matching to the known results in Refs.(163; 166) when $\mu = 0$, we have at leading order

$$\int_0^{q^*} d|\mathbf{p}||\mathbf{p}| \int_{-|\mathbf{p}|}^{|\mathbf{p}|} dp^0 \sum_s \rho_s^{HTL}(p^0, |\mathbf{p}|) \left(1 - s \frac{p^0}{|\mathbf{p}|}\right) = (2\pi)m_f^2 (\log(q^*/m_f) - 1 + \log 2). \quad (3.4.221)$$

Using this in (Equation 3.4.218) we finally have the leading order expression for our P-odd emission rate as

$$(2\pi)^3 2\omega \frac{d\Gamma_{soft}^{odd}}{d^3\mathbf{k}} \approx d_R \frac{e^2}{(2\pi)} m_f^2 (n_+(\omega)n_-(0) - n_-(\omega)n_+(0)) (\log(q^*/m_f) - 1 + \log 2). \quad (3.4.222)$$

Nonetheless, it is instructive to see how the leading log arises from the above integral, using the sum rules for the fermion spectral densities ρ_s^{HTL} . The leading log comes from the region $m_f \ll |\mathbf{p}| \ll q^*$, and in this case, we have sum rules (see, for example, Refs.(171; 172))

$$\begin{aligned} \int_{-|\mathbf{p}|}^{|\mathbf{p}|} dp^0 \rho_s^{HTL}(p^0, |\mathbf{p}|) &= \frac{\pi}{2} \frac{m_f^2}{|\mathbf{p}|^2} \left(\log \left(\frac{4|\mathbf{p}|^2}{m_f^2} \right) - 1 \right), \\ \int_{-|\mathbf{p}|}^{|\mathbf{p}|} dp^0 p^0 \rho_s^{HTL}(p^0, |\mathbf{p}|) &= s \frac{\pi}{2} \frac{m_f^2}{|\mathbf{p}|^2} \left(\log \left(\frac{4|\mathbf{p}|^2}{m_f^2} \right) - 3 \right), \end{aligned} \quad (3.4.223)$$

which gives

$$\begin{aligned}
(2\pi)^3 2\omega \frac{d\Gamma_{soft}^{odd}}{d^3\mathbf{k}} &\approx d_R \frac{e^2}{(2\pi)} m_f^2 (n_+(\omega)n_-(0) - n_-(\omega)n_+(0)) \int_{m_f}^{q^*} d|\mathbf{p}| \frac{1}{|\mathbf{p}|} \\
&= d_R \frac{e^2}{(2\pi)} m_f^2 (n_+(\omega)n_-(0) - n_-(\omega)n_+(0)) \log(q^*/m_f). \quad (3.4.224)
\end{aligned}$$

Looking at the leading log from the hard Compton and Pair Annihilation processes (Equation 3.4.191),

$$(2\pi)^3 2\omega \frac{d\Gamma_{hard}^{odd}}{d^3\mathbf{k}} \approx d_R \frac{e^2}{(2\pi)} m_f^2 (n_+(|\mathbf{k}|)n_-(0) - n_- (|\mathbf{k}|)n_+(0)) \log(T/q^*), \quad (3.4.225)$$

we see that the $\log(q^*)$ nicely cancels in their sum, which is an important consistency check of our computation.

Physics of Leading Log Result

Looking at the leading log expressions for both P-even case (Equation 3.4.220) and the P-odd emission rate (Equation 3.4.222),

$$\begin{aligned}
(2\pi)^3 2\omega \frac{d\Gamma_{soft}^{total}}{d^3\mathbf{k}} &\approx d_R \frac{e^2}{(2\pi)} m_f^2 (n_+(\omega)n_-(0) + n_-(\omega)n_+(0)) \log(q^*/m_f), \\
(2\pi)^3 2\omega \frac{d\Gamma_{soft}^{odd}}{d^3\mathbf{k}} &\approx d_R \frac{e^2}{(2\pi)} m_f^2 (n_+(\omega)n_-(0) - n_-(\omega)n_+(0)) \log(q^*/m_f), \quad (3.4.226)
\end{aligned}$$

and recalling that they are given in terms of spin polarized emission rates as

$$\Gamma^{total} = \Gamma(\epsilon^+) + \Gamma(\epsilon^-), \quad \Gamma^{odd} = \Gamma(\epsilon^+) - \Gamma(\epsilon^-), \quad (3.4.227)$$

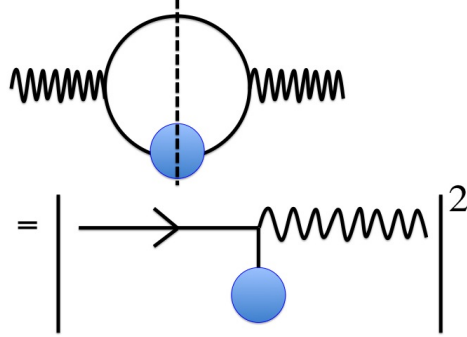


Figure 19. Leading log contributions from soft t- or u-channel exchanges: a hard fermion making conversion to a collinear photon. The blob represents Hard Thermal Loop (HTL) re-summed propagator.

we find that the leading log spin polarized emission rates are given, after matching the logarithmic dependence on q^* with the hard rate, as

$$(2\pi)^3 2\omega \frac{d\Gamma(\epsilon^\pm)}{d^3\mathbf{k}} \Big|_{\text{Leading Log}} = d_R \frac{e^2}{(2\pi)} m_f^2 n_\pm(\omega) n_\mp(0) \log(T/m_f), \quad (3.4.228)$$

which can be physically understood as follows.

Recall that the leading log comes from the soft t-channel fermion exchange, and the t-channel momentum is space-like as can be seen in the integral in (Equation 3.4.218); we have $p^0 < |\mathbf{p}|$. The spectral density in this kinematics is non-zero due to Landau damping that is captured by HTL self-energy, and represents thermally excited (fermionic) fluctuations of soft momentum that are present in the finite temperature plasma. The leading log process can be understood as a process of a hard fermion making conversion into a collinear photon after being

annihilated by a soft fermion of momentum gT , as in the Figure 19. At leading order, this gT momentum can be taken as zero.

For definite spin helicity of the final photon in $\Gamma(\epsilon^\pm)$, the conservation of angular momentum dictates that the incoming hard fermion which is collinear to the photon should have a spin $\pm 1/2$ aligned with the momentum direction: the other spin $\pm 1/2$ to make up the final spin ± 1 of the photon will be provided by the annihilating soft fermion. Since hard fermions have bare spectral density at leading order in coupling, they have definite helicities determined by their quantization in free limit: for our right-handed Weyl fermion field, a particle has helicity $+1/2$ and anti-particle has $-1/2$. This means that the leading log rate of $\Gamma(\epsilon^+)$ (for photons of spin helicity $+1$) can appear only from the incoming particle of helicity $+1/2$, while an incoming anti-particle of helicity $-1/2$ can not contribute to $\Gamma(\epsilon^+)$. Since the incoming particle can annihilate only with a soft anti-particle, the rate $\Gamma(\epsilon^+)$ should be proportional to $n_+(\omega)n_-(0)$, where the first factor is the number density of incoming particle and the second is the number density of annihilating anti-particle of zero (soft) momentum. See Figure 20. The precisely same logic tells us that the leading log rate of $\Gamma(\epsilon^-)$ should be proportional to $n_-(\omega)n_+(0)$. This argument nicely explains the result in (Equation 3.4.228). The overall m_f^2 is nothing but the strength of the fermionic spectral density in soft momentum range that arises from the HTL self-energy: the same self-energy also gives arise to the asymptotic thermal mass m_f^2 .

Collinear Bremsstrahlung and Pair Annihilation: LPM Resummation

We compute collinear Bremsstrahlung and Pair Annihilation contributions to the P-odd photon emission rate that are induced by multiple scatterings with soft thermal gluons in

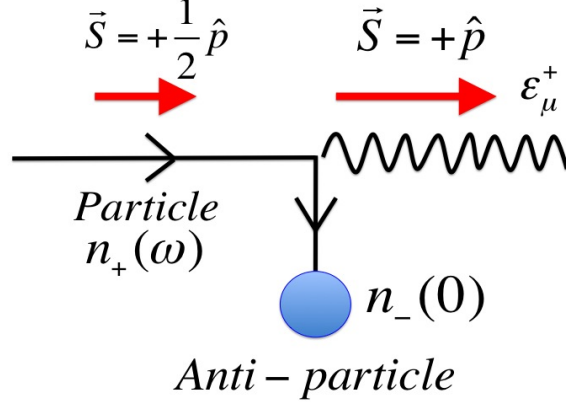


Figure 20. Angular momentum conservation in leading log spin polarized emission rates.

the plasma (165). The incoming quark or anti-quark of a hard momentum experiences soft transverse kicks by thermal gluons of momenta $\sim gT$, becoming off-shell by small amount g^2T , during which a nearly collinear photon is emitted, or quark-antiquark pair annihilates to a collinear photon. The rate of these soft scatterings is well-known to be $\sim g^2T$ (which causes the damping rate of $\sim g^2T$). The scattering gluons are genuine thermal effects: their momenta are space like and the non-zero spectral density in this kinematics arises only due to the Landau damping. Since the life time of the intermediate states dictated by small virtuality g^2T is of $1/(g^2T)$, which is comparable to the scattering rate, one has to sum over all multiple scatterings to get the correct leading order result, coined as the LPM re-summation (165). These contributions add to the leading order constant under the log. The effect of re-summation typically gives a suppression compared to the single scattering contribution.

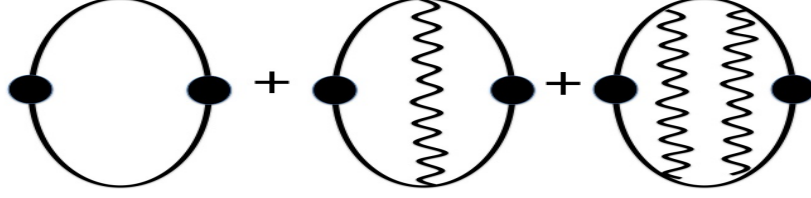


Figure 21. Ladder diagrams to be summed over to get the correct leading order LPM contribution to (our P-odd) photon emission rate.

In diagrammatic language, the LPM re-summation corresponds to summing over all ladder diagrams of the type depicted in Figure 21 for the retarded (or “ra”) current-current correlation functions that enter the photon emission rate formula (165). The reason why these multiple ladder diagrams are not suppressed by higher powers in coupling constant is the presence of collinear “pinch” singularities arising from nearly on-shell fermion propagators: the momentum transfer by exchanged gluon lines are soft, and each pair of fermion propagators, one from the upper line and the other from the lower line, are nearly on-shell and have an IR pinch singularity when the internal momentum is nearly collinear to the external photon momentum (the detail will become clear in the following). This singularity is regulated by soft transverse component of the fermion momentum, $\mathbf{p}_\perp^2 \sim g^2 T^2$, induced by soft kicks from thermal gluons. Then, one has to also include in the propagators the fermion thermal mass $m_f^2 \sim g^2 T^2$ and the leading order damping rate $\zeta \sim g^2 T$ which are of the same order as \mathbf{p}_\perp^2 .

Since the exchanged gluons have soft momenta for leading order contributions, we need to re-sum gluonic HTL self-energy in their propagators. To get a Bose-Einstein enhancement

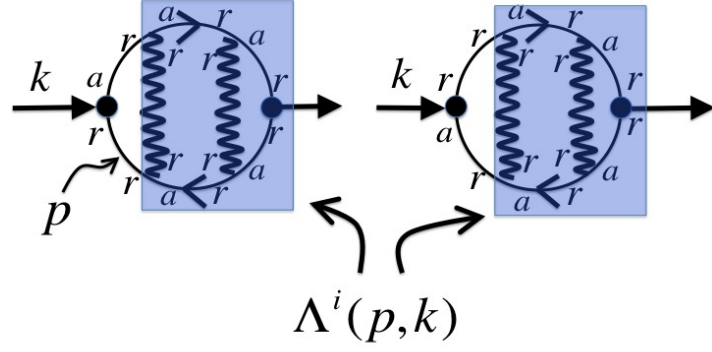


Figure 22. Two types of real-time ladder diagrams for leading order LPM contributions. The shaded part represents the re-summed rr-type current vertex $\Lambda^i(p, k)$. The rr-type gluon lines are the HTL re-summed ones.

$n_B(q^0) \sim T/q^0 \sim 1/g$ in the exchanged gluon lines, the gluon propagators need to be of the rr -type in the “ra”-basis of Schwinger-Keldysh formalism: only these diagrams give leading order contributions in g . Imposing this requirement and the maximal number of pinch singularities (that arise from a pair of S^{ra} and S^{ar} propagators), there are essentially two types of ladder diagrams to be summed over in the “ra”-basis as depicted in Figure 22. Defining the re-summed “rr”-type fermion-current vertex $\Lambda^i(p, k)$ which has two r-type fermions legs, the re-summed $G_{ij}^{ra}(k)$ current-current correlation function is written as

$$G_{ij}^{ra}(k) = (-1)d_R \int \frac{d^4 p}{(2\pi)^4} \text{tr} [S^{ra}(p+k)\sigma^j S^{rr}(p)\Lambda^i(p, k) + S^{rr}(p+k)\sigma^j S^{ar}(p)\Lambda^i(p, k)] . \quad (3.4.229)$$

Since the pinch singularity appears from a pair of S^{ra} and S^{ar} , and using the thermal relation $S^{rr}(p) = (1/2 - n_+(p^0))(S^{ra}(p) - S^{ar}(p))$, the singular part of $G_{ij}^{ra}(k)$ is given by ($\omega \equiv k^0 = |\mathbf{k}|$)

$$G_{ij}^{ra}(k) \approx d_R \int \frac{d^4 p}{(2\pi)^4} (n_+(p^0 + \omega) - n_+(p^0)) \text{tr} [S^{ra}(p+k) \sigma^j S^{ar}(p) \Lambda^i(p, k)] . \quad (3.4.230)$$

The re-summation of the vertex $\Lambda^i(p, k)$ is achieved by solving the Schwinger-Dyson equation described in the Figure 23,

$$\Lambda^i(p, k) = \sigma^i + (ig)^2 C_2(R) \int \frac{d^4 Q}{(2\pi)^4} \sigma^\beta S^{ar}(p+Q) \Lambda^i(p+Q, k) S^{ra}(p+Q+k) \sigma^\alpha G_{\alpha\beta}^{rr}(Q) , \quad (3.4.231)$$

where $G_{\alpha\beta}^{rr}$ is the HTL re-summed gluon propagator. We will solve this integral equation and compute $G_{ij}^{ra}(k)$ in leading collinear pinch singularity limit.

The real-time fermion propagators, including the thermal mass and the leading order damping rate, are given as

$$S^{ra}(p) = \sum_s \frac{iP_s(\mathbf{p})}{p^0 - s\sqrt{|\mathbf{p}|^2 + m_f^2} + \frac{i}{2}\zeta} = -(S^{ar}(p))^\dagger , \quad (3.4.232)$$

where the damping rate is independent of momentum p and the species s at leading order

$$\zeta = C_2(R) \frac{g^2}{2\pi} \log(1/g) T . \quad (3.4.233)$$

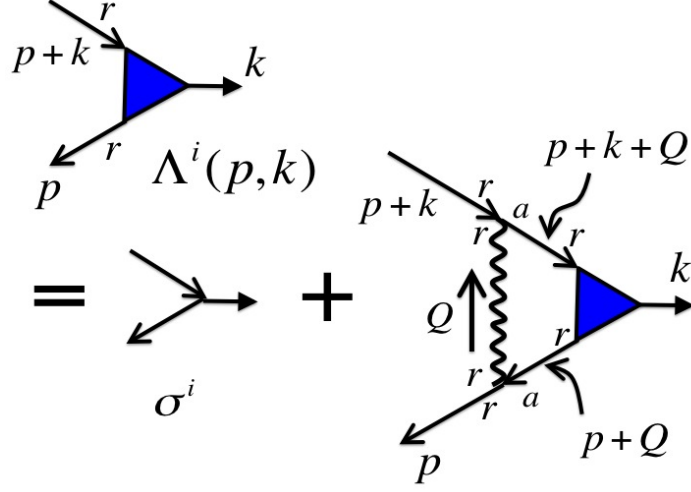


Figure 23. The real-time Schwinger-Dyson equation for the re-summed vertex $\Lambda^i(p, k)$.

Let's consider the pair of $S^{ra}(p+k)$ and $S^{ar}(p)$ in (Equation 3.4.230) to illustrate the pinch singularity and its leading order treatment. Looking at the expression

$$S^{ra}(p+k)S^{ar}(p) = \sum_{s,t} \frac{iP_s(\mathbf{p}+\mathbf{k})}{\left(p^0 + |\mathbf{k}| - s\sqrt{|\mathbf{p}+\mathbf{k}|^2 + m_f^2} + \frac{i}{2}\zeta\right)} \frac{iP_t(\mathbf{p})}{\left(p^0 - t\sqrt{|\mathbf{p}|^2 + m_f^2} - \frac{i}{2}\zeta\right)}, \quad (3.4.234)$$

the two poles in the complex p^0 -plane, one in the upper half plane and the other in the lower half plane,

$$p^0 = -|\mathbf{k}| + s\sqrt{|\mathbf{p}+\mathbf{k}|^2 + m_f^2} - \frac{i}{2}\zeta, \quad p^0 = t\sqrt{|\mathbf{p}|^2 + m_f^2} + \frac{i}{2}\zeta, \quad (3.4.235)$$

may be close to each other with a distance of $\sim g^2T$, if \mathbf{p} is nearly collinear to \mathbf{k} and $\mathbf{p}_\perp \sim gT$.

In computing p^0 integral, we close the p^0 integral contour, say, in the upper half plane, picking up the pole of $p^0 = t\sqrt{|\mathbf{p}|^2 + m_f^2} + i\zeta/2$, then the residue from the other pole is

$$\frac{1}{|\mathbf{k}| + t\sqrt{|\mathbf{p}|^2 + m_f^2} - s\sqrt{|\mathbf{p} + \mathbf{k}|^2 + m_f^2} + i\zeta}. \quad (3.4.236)$$

Let's fix the direction of \mathbf{k} to be along $\hat{\mathbf{z}} = \hat{\mathbf{x}}^3$ direction, and write the $\hat{\mathbf{z}}$ component of momentum \mathbf{p} as p_\parallel , and the perpendicular component as \mathbf{p}_\perp , so that we can expand up to order g^2T as

$$\sqrt{|\mathbf{p}|^2 + m_f^2} \approx |p_\parallel| + \frac{\mathbf{p}_\perp^2 + m_f^2}{2|p_\parallel|}, \quad \sqrt{|\mathbf{p} + \mathbf{k}|^2 + m_f^2} \approx |p_\parallel| + |\mathbf{k}| + \frac{\mathbf{p}_\perp^2 + m_f^2}{2|p_\parallel| + |\mathbf{k}|}. \quad (3.4.237)$$

The pinch singularity happens when the leading collinear terms in the denominator cancel with each other, that is $|\mathbf{k}| + t|p_\parallel| - s|p_\parallel| + |\mathbf{k}| = 0$, to result in $\sim g^2T$ in the denominator which enhances the contribution. There are three physically distinct cases where this happens:

1) $s = t = 1$: in this case, $|\mathbf{k}| + |p_\parallel| - |p_\parallel| + |\mathbf{k}| = 0$ is satisfied when $p_\parallel > 0$. Considering the kinematics, one easily sees that this case corresponds to quark of momentum $\mathbf{p} + \mathbf{k}$ emitting the collinear photon of momentum \mathbf{k} by Bremsstrahlung. The residue becomes

$$\frac{\mathbf{p}_\perp^2 + m_f^2}{2p_\parallel} - \frac{\mathbf{p}_\perp^2 + m_f^2}{2(p_\parallel + |\mathbf{k}|)} + i\zeta = \frac{|\mathbf{k}|(\mathbf{p}_\perp^2 + m_f^2)}{2p_\parallel(p_\parallel + |\mathbf{k}|)} + i\zeta \equiv \delta E(\mathbf{p}_\perp) + i\zeta. \quad (3.4.238)$$

2) $s = 1, t = -1$: the condition $|\mathbf{k}| - |p_{\parallel}| - |p_{\parallel}| + |\mathbf{k}| = 0$ is fulfilled when $-|\mathbf{k}| < p_{\parallel} < 0$, and this case corresponds to collinear pair annihilation of a quark of momentum $\mathbf{p} + \mathbf{k}$ and an anti-quark of momentum $-\mathbf{p}$. Considering signs of p_{\parallel} and $p_{\parallel} + |\mathbf{k}|$, one finds that the residue has the precisely the same expression, $\delta E + i\zeta$ with δE is defined as above.

3) $s = t = -1$: we have $p_{\parallel} < -|\mathbf{k}|$, which corresponds to Bremsstrahlung of anti-quark of momentum $\mathbf{p} + \mathbf{k}$. Again the residue has the precisely the same form as $\delta E + i\zeta$.

Note that in all three cases, (s, t) are correlated with p_{\parallel} in such a way that $s(p_{\parallel} + |\mathbf{k}|) > 0$ and $tp_{\parallel} > 0$. Since we only care about the above pinch singularity enhanced contributions, the (s, t) are uniquely chosen for each value of p_{\parallel} as above, and we consider only these terms in the following.

In leading order treatment, the location of the pole can be approximated as $p^0 = t\sqrt{|\mathbf{p}|^2 + m_f^2} + i\zeta/2 \approx t|p_{\parallel}| = p_{\parallel}$ in all other places in the integral once the above residues are correctly identified. In summary, we can replace the two poles in (Equation 3.4.234) by

$$\frac{1}{\left(p^0 + |\mathbf{k}| - s\sqrt{|\mathbf{p} + \mathbf{k}|^2 + m_f^2} + \frac{i}{2}\zeta\right)} \frac{1}{\left(p^0 - t\sqrt{|\mathbf{p}|^2 + m_f^2} - \frac{i}{2}\zeta\right)} \rightarrow \frac{(2\pi i)\delta(p^0 - p_{\parallel})}{\delta E + i\zeta}, \quad (3.4.239)$$

and depending on the value of $p_{\parallel} \in [-\infty, +\infty]$, the suitable (s, t) as described in the above has to be chosen. For example, we have for (Equation 3.4.230),

$$\begin{aligned} S^{ra}(p + k)\sigma^j S^{ar}(p) \rightarrow & \left(P_+(\mathbf{p} + \mathbf{k})\sigma^j P_+(\mathbf{p})\Theta(p_{\parallel}) + P_+(\mathbf{p} + \mathbf{k})\sigma^j P_-(\mathbf{p})\Theta(-p_{\parallel})\Theta(p_{\parallel} + |\mathbf{k}|) \right. \\ & \left. + P_-(\mathbf{p} + \mathbf{k})\sigma^j P_-(\mathbf{p})\Theta(-p_{\parallel} - |\mathbf{k}|) \right) \frac{-(2\pi i)\delta(p^0 - p_{\parallel})}{\delta E(\mathbf{p}_{\perp}) + i\zeta}. \end{aligned} \quad (3.4.240)$$

Since Q carried by exchange gluons is soft, we have an essentially same structure for $S^{ar}(p+Q)\Lambda^i(p+Q, k)S^{ra}(p+Q+k)$ appearing in the integral equation for $\Lambda^i(p, k)$ in (Equation 3.4.231),

$$\begin{aligned}
& S^{ra}(p+Q)\Lambda^i(p+Q, k)S^{ar}(p+Q+k) \\
& \rightarrow \left(P_+(\mathbf{p}+\mathbf{q})\Lambda^i(p+Q, k)P_+(\mathbf{p}+\mathbf{q}+\mathbf{k})\Theta(p_{\parallel}) \right. \\
& + P_-(\mathbf{p}+\mathbf{q})\Lambda^i(p+Q, k)P_+(\mathbf{p}+\mathbf{q}+\mathbf{k})\Theta(-p_{\parallel})\Theta(p_{\parallel}+|\mathbf{k}|) \\
& \left. + P_-(\mathbf{p}+\mathbf{q})\Lambda^i(p+Q, k)P_-(\mathbf{p}+\mathbf{q}+\mathbf{k})\Theta(-p_{\parallel}-|\mathbf{k}|) \right) \frac{-(2\pi i)\delta(q^0-q_{\parallel})}{\delta E(\mathbf{p}_{\perp}+\mathbf{q}_{\perp})+i\zeta},
\end{aligned} \tag{3.4.241}$$

the only difference of which are the argument $\mathbf{p}_{\perp}+\mathbf{q}_{\perp}$ in δE instead of \mathbf{p}_{\perp} . In writing the $\delta(q^0-q_{\parallel})$ factor, we used $p^0 = p_{\parallel}$ that is imposed by (Equation 3.4.240) when we compute the correlation function $G_{ij}^{ra}(k)$ by (Equation 3.4.230). We will solve the integral equation (Equation 3.4.231) for Λ^i , with the above replacement (Equation 3.4.241) that is enough for the leading order result.

Looking at (Equation 3.4.230), (Equation 3.4.240), and (Equation 3.4.241), what we need are the projected vertices

$$P_s(\mathbf{p}+\mathbf{k})\sigma^j P_t(\mathbf{p}) \equiv \Sigma_{st}^j(\mathbf{p}, \mathbf{k}) P_s(\mathbf{p}+\mathbf{k})P_t(\mathbf{p}), \tag{3.4.242}$$

and we define a vector function $F^i(\mathbf{p}_\perp)$ as (we ignore p_\parallel and $|\mathbf{k}|$ arguments in F^i as they are common in all subsequent expressions)

$$P_t(\mathbf{p})\Lambda^i(p, k)|_{p^0=p_\parallel}P_s(\mathbf{p}+\mathbf{k}) \equiv (\delta E(\mathbf{p}_\perp) + i\zeta) F^i(\mathbf{p}_\perp) P_t(\mathbf{p})P_s(\mathbf{p}+\mathbf{k}). \quad (3.4.243)$$

Here, we emphasize again that the (s, t) are the choice depending on the value of p_\parallel suitable for the pinch singularity that we discuss in the above. Note that Σ_{st}^j and F^i are complex valued functions, not 2×2 matrices. In terms of these functions, using (Equation 3.4.230), (Equation 3.4.240), (Equation 3.4.242) and (Equation 3.4.243), we have (recall $\omega \equiv k^0 = |\mathbf{k}|$)

$$\begin{aligned} G_{ij}^{ra}(k) &= d_R(-i) \int \frac{d^4p}{(2\pi)^4} (n_+(p^0 + \omega) - n_+(p^0)) \Sigma_{st}^j(\mathbf{p}, \mathbf{k}) F^i(\mathbf{p}_\perp) \text{tr}(P_s(\mathbf{p}+\mathbf{k})P_t(\mathbf{p})) \\ &\times (2\pi)\delta(p^0 - p_\parallel) \\ &\approx d_R(-i) \int \frac{d^4p}{(2\pi)^4} (n_+(p^0 + \omega) - n_+(p^0)) \Sigma_{st}^j(\mathbf{p}, \mathbf{k}) F^i(\mathbf{p}_\perp) (2\pi)\delta(p^0 - p_\parallel), \end{aligned} \quad (3.4.244)$$

where in the last line, we use

$$\text{tr}(P_s(\mathbf{p}+\mathbf{k})P_t(\mathbf{p})) = \frac{1}{2} \left(1 + st \hat{\mathbf{p}} \cdot \widehat{\mathbf{p}+\mathbf{k}} \right) \approx 1, \quad (3.4.245)$$

to leading order in $\mathbf{p}_\perp/p_\parallel \sim g$ and we use $tp_\parallel > 0$ and $s(p_\parallel + |\mathbf{k}|) > 0$.

Recall that our P-odd photon emission rate is given in terms of $G_{ij}^{ra}(k)$ as

$$(2\pi)^3 2\omega \frac{d\Gamma^{odd}}{d^3\mathbf{k}} = e^2 n_B(\omega) (-2) \text{Im} [G_{12}^{ra}(k) - G_{21}^{ra}(k)] , \quad (3.4.246)$$

given the choice of $\mathbf{k} = |\mathbf{k}|\hat{\mathbf{x}}^3$. Hence, we need only the transverse components of Σ_{st}^j and F^i .

A short computation from the definition (Equation 3.4.242) after taking the trace of the both sides gives

$$\Sigma_{st}^j(\mathbf{p}, \mathbf{k}) = \frac{s \widehat{\mathbf{p} + \mathbf{k}}^j + t \hat{\mathbf{p}}^j + ist \epsilon^{jlm} \hat{\mathbf{p}}^l \widehat{\mathbf{p} + \mathbf{k}}^m}{1 + st \hat{\mathbf{p}} \cdot \widehat{\mathbf{p} + \mathbf{k}}} , \quad (3.4.247)$$

and the integral equation (Equation 3.4.231) after being contracted with $P_t(\mathbf{p})$ on the left and $P_s(\mathbf{p} + \mathbf{k})$ on the right gives

$$(\delta E(\mathbf{p}_\perp) + i\zeta) F^i(\mathbf{p}_\perp) = (\Sigma_{st}^i(\mathbf{p}, \mathbf{k}))^* + g^2 C_2(R) \int \frac{d^4 Q}{(2\pi)^4} F^i(\mathbf{p}_\perp + \mathbf{q}_\perp) \hat{v}^\alpha \hat{v}^\beta G_{\alpha\beta}^{rr}(Q) (2\pi i) \delta(q^0 - q_\parallel) , \quad (3.4.248)$$

where in the integral kernel, we used an approximation

$$P_t(\mathbf{p}) \sigma^\beta P_t(\mathbf{p} + \mathbf{q}) \approx P_t(\mathbf{p}) \sigma^\beta P_t(\mathbf{p}) = p_t^\beta / |p_\parallel| P_t(\mathbf{p}) , \quad (3.4.249)$$

for soft Q , where $p_t^\alpha = (|\mathbf{p}|, t\mathbf{p}) \approx (|p_\parallel|, 0, 0, tp_\parallel)$ at leading order, so that $p_t^\alpha / |p_\parallel|$ is a light-like 4-velocity \hat{v}^α along the collinear vector $t\mathbf{p}$. Considering the correlation between p_\parallel and the

sign of t that we describe before, we see that $tp_{\parallel} > 0$ always, so that this 4-velocity is always $\hat{v}^{\alpha} = (1, 0, 0, 1)$. The same is true for $P_s(\mathbf{p} + \mathbf{q} + \mathbf{k})\sigma^{\alpha}P_s(\mathbf{p} + \mathbf{k})$ so that we have

$$P_t(\mathbf{p})\sigma^{\beta}P_t(\mathbf{p} + \mathbf{q})P_s(\mathbf{p} + \mathbf{q} + \mathbf{k})\sigma^{\alpha}P_s(\mathbf{p} + \mathbf{k}) \approx \hat{v}^{\alpha}\hat{v}^{\beta}P_t(\mathbf{p})P_s(\mathbf{p} + \mathbf{k}), \quad (3.4.250)$$

which has been used to arrive at our integral equation for F^i in (Equation 3.4.248). Since $F^i \sim 1/g$ and the both sides of (Equation 3.4.248) are of order $\sim g$, this approximation is enough for the leading order computation.

One subtle point is that the HTL gluon fluctuations in $G_{\alpha\beta}^{rr}$ contains a P-odd spectral density which is anti-symmetric in α and β , which could potentially contribute to our P-odd photon emission rate, if we keep Q corrections in (Equation 3.4.249). We estimated them to find that these corrections are higher order in g . The fluctuations contracted with light-like vector \hat{v}^{α} in (Equation 3.4.248), $\hat{v}^{\alpha}\hat{v}^{\beta}G_{\alpha\beta}^{rr}$ (which are the correlations along the Eikonalized light-like Wilson line) receive only the usual P-even longitudinal and transverse contributions.

As is well-known (165), the integral equation is further simplified due to the fact that the integral on the right in (Equation 3.4.248) without F^i is identical to the leading order damping rate ζ ,

$$\zeta = g^2 C_2(R) \int \frac{d^4 Q}{(2\pi)^4} \hat{v}^{\alpha}\hat{v}^{\beta} G_{\alpha\beta}^{rr}(Q) (2\pi) \delta(q^0 - q_{\parallel}), \quad (3.4.251)$$

so that we can move $i\zeta F^i(\mathbf{p}_\perp)$ term in the left to the right to arrive at

$$\begin{aligned} \delta E(\mathbf{p}_\perp) F^i(\mathbf{p}_\perp) &= (\Sigma_{st}^i(\mathbf{p}, \mathbf{k}))^* \\ &+ g^2 C_2(R) \int \frac{d^4 Q}{(2\pi)^4} (F^i(\mathbf{p}_\perp + \mathbf{q}_\perp) - F^i(\mathbf{p}_\perp)) \hat{v}^\alpha \hat{v}^\beta G_{\alpha\beta}^{rr}(Q) (2\pi i) \delta(q^0 - q_\parallel). \end{aligned} \quad (3.4.252)$$

This form has a good infrared behavior so that only the well-controlled soft scale $Q \sim gT$ contributes at leading order, while the magnetic scale of $g^2 T$ gives a finite, sub-leading contributions.

Finally, for soft Q we replace

$$G_{\alpha\beta}^{rr}(Q) = \left(\frac{1}{2} + n_B(q^0) \right) \rho_{\alpha\beta}^{gluon}(Q) \approx \frac{T}{q^0} \rho_{\alpha\beta}^{gluon}(Q), \quad (3.4.253)$$

for leading order, where $\rho_{\alpha\beta}^{gluon}$ is the gluon spectral density in HTL approximation, and the amazing sum rule in Ref.(173) gives the integral over (q^0, q_\parallel) as

$$T \int \frac{dq^0 dq_\parallel}{(2\pi)^2} \hat{v}^\alpha \hat{v}^\beta \frac{1}{q^0} \rho_{\alpha\beta}^{gluon}(Q) (2\pi) \delta(q^0 - q_\parallel) = \frac{T m_D^2}{\mathbf{q}_\perp^2 (\mathbf{q}_\perp^2 + m_D^2)}, \quad (3.4.254)$$

where

$$m_D^2 = g^2 \left(\frac{T^2}{3} + \frac{\mu^2}{\pi^2} \right) (T_A + N_F T_R) = g^2 \left(\frac{T^2}{3} + \frac{\mu^2}{\pi^2} \right) (N_c + N_F/2), \quad (3.4.255)$$

is the Debye mass for N_F Dirac quarks in fundamental representation, so that the integral equation for $F^i(\mathbf{p}_\perp)$ is finally recast to

$$\delta E(\mathbf{p}_\perp) F^i(\mathbf{p}_\perp) = (\Sigma_{st}^i(\mathbf{p}, \mathbf{k}))^* + i \int \frac{d^2 \mathbf{q}_\perp}{(2\pi)^2} C(\mathbf{q}_\perp) (F^i(\mathbf{p}_\perp + \mathbf{q}_\perp) - F^i(\mathbf{p}_\perp)) , \quad (3.4.256)$$

with

$$C(\mathbf{q}_\perp) = g^2 C_2(R) \frac{T m_D^2}{\mathbf{q}_\perp^2 (\mathbf{q}_\perp^2 + m_D^2)} . \quad (3.4.257)$$

Since we need only the transverse parts of (Equation 3.4.256) and (Equation 4.1.22) for $G_{ij}^{ra}(k)$, we expand $\Sigma_{st}^i(\mathbf{p}, \mathbf{k})$ given in (Equation 3.4.247) to linear order in $\mathbf{p}_\perp/p_\parallel \sim g$, which is enough for leading order,

$$\begin{aligned} \Sigma_{st}^i(\mathbf{p}, \mathbf{k}) &\approx \frac{1}{2} \left(\frac{1}{p_\parallel} + \frac{1}{p_\parallel + |\mathbf{k}|} \right) \mathbf{p}_\perp^i + \frac{i}{2} \left(\frac{1}{p_\parallel} - \frac{1}{p_\parallel + |\mathbf{k}|} \right) \epsilon_\perp^{il} \mathbf{p}_\perp^l \\ &= \frac{2p_\parallel + |\mathbf{k}|}{2p_\parallel(p_\parallel + |\mathbf{k}|)} \mathbf{p}_\perp^i + i \frac{|\mathbf{k}|}{2p_\parallel(p_\parallel + |\mathbf{k}|)} \epsilon_\perp^{il} \mathbf{p}_\perp^l , \end{aligned} \quad (3.4.258)$$

where we used the fact that $tp_\parallel > 0$ and $s(p_\parallel + |\mathbf{k}|) > 0$, and $\epsilon_\perp^{12} = -\epsilon_\perp^{21} = 1$. We use this expansion in both (Equation 4.1.22) and (Equation 3.4.256). From (Equation 3.4.256), we see that the solution for $F^i(\mathbf{p}_\perp)$ is given by

$$F^i(\mathbf{p}_\perp) = \frac{2p_\parallel + |\mathbf{k}|}{2p_\parallel(p_\parallel + |\mathbf{k}|)} f_\perp^i(\mathbf{p}_\perp) - i \frac{|\mathbf{k}|}{2p_\parallel(p_\parallel + |\mathbf{k}|)} \epsilon_\perp^{il} f_\perp^l(\mathbf{p}_\perp) , \quad (3.4.259)$$

where $f_{\perp}^i(\mathbf{p}_{\perp})$ is the solution of the integral equation

$$\delta E(\mathbf{p}_{\perp}) f_{\perp}^i(\mathbf{p}_{\perp}) = \mathbf{p}_{\perp}^i + i \int \frac{d^2 \mathbf{q}_{\perp}}{(2\pi)^2} C(\mathbf{q}_{\perp}) (f_{\perp}^i(\mathbf{p}_{\perp} + \mathbf{q}_{\perp}) - f_{\perp}^i(\mathbf{p}_{\perp})) . \quad (3.4.260)$$

This equation for $f_{\perp}^i(\mathbf{p}_{\perp})$ is identical to the integral equation obtained by Arnold-Moore-Yaffe in Ref.(165), with the identification

$$f_{\perp}^i(\mathbf{p}_{\perp}) = -\frac{i}{2} (f_{AMY}^i(\mathbf{p}_{\perp}))^* , \quad (3.4.261)$$

so that the techniques of solving this integral equation that are known in literature can be utilized to find our object $F^i(\mathbf{p}_{\perp})$. Using this expression for F^i and (Equation 4.1.22) for $G_{ij}^{ra}(k)$, we obtain after short manipulations,

$$G_{12}^{ra} - G_{21}^{ra}(k) = -\frac{d_R}{2} \int \frac{dp_{\parallel} d^2 \mathbf{p}_{\perp}}{(2\pi)^3} (n_+(p_{\parallel} + \omega) - n_+(p_{\parallel})) \frac{|\mathbf{k}|(2p_{\parallel} + |\mathbf{k}|)}{p_{\parallel}^2(p_{\parallel} + |\mathbf{k}|)^2} (\mathbf{p}_{\perp} \cdot \mathbf{f}_{\perp}) , \quad (3.4.262)$$

and using an interesting identity

$$n_B(\omega) (n_+(p_{\parallel} + \omega) - n_+(p_{\parallel})) = -n_+(p_{\parallel} + \omega) (1 - n_+(p_{\parallel})) , \quad (3.4.263)$$

we finally arrive at an expression for our P-odd photon emission rate in terms of the solution $\mathbf{f}_\perp(\mathbf{p}_\perp)$ of the integral equation (Equation 3.4.260) (recall $\omega = |\mathbf{k}|$),

$$(2\pi)^3 2\omega \frac{d\Gamma_{LPM}^{odd}}{d^3\mathbf{k}} = e^2 d_R \int \frac{dp_\parallel d^2\mathbf{p}_\perp}{(2\pi)^3} n_+(p_\parallel + \omega) (1 - n_+(p_\parallel)) \frac{\omega(2p_\parallel + \omega)}{p_\parallel^2(p_\parallel + \omega)^2} (-1) \text{Im}[(\mathbf{p}_\perp \cdot \mathbf{f}_\perp)] . \quad (3.4.264)$$

This is the main outcome of this section. Our numerical evaluation is based on this expression with the integral equation (Equation 3.4.260), where δE is given in (Equation 3.4.238) (see also (Equation 3.4.267)).

Although it is not manifestly obvious that the above expression is an odd function in (axial) chemical potential μ that enters the distribution function n_+ , one way to see this is to first observe that the factor $n_+(p_\parallel + \omega) (1 - n_+(p_\parallel))$ is easily recognized as the statistical factor for the collinear Bremsstrahlung process of a fermion of momentum $\mathbf{p} + \mathbf{k}$ emitting a photon of momentum \mathbf{k} , provided that $p_\parallel > 0$. In the case $p_\parallel < -|\mathbf{k}|$, using the identity

$$n_+(p_\parallel + \omega) (1 - n_+(p_\parallel)) = n_-(-p_\parallel) (1 - n_-(-p_\parallel - \omega)) \quad (3.4.265)$$

we see that the process is in fact the Bremsstrahlung of anti-fermion of momentum $-\mathbf{p}$ emitting a photon of momentum \mathbf{k} . It is more convenient to change the integration variable in this case to $p_\parallel \rightarrow -(\tilde{p}_\parallel + \omega)$ so that we have $\tilde{p}_\parallel > 0$ and the statistical factor becomes

$$n_-(-\tilde{p}_\parallel + \omega) (1 - n_-(-\tilde{p}_\parallel)) , \quad (3.4.266)$$

which makes the interpretation clearer. From the expression for δE in (Equation 3.4.238), we have

$$\delta E = \frac{\omega(\mathbf{p}_\perp^2 + m_f^2)}{2p_\parallel(p_\parallel + \omega)} = \frac{\omega(\mathbf{p}_\perp^2 + m_f^2)}{2\tilde{p}_\parallel(\tilde{p}_\parallel + \omega)}, \quad (3.4.267)$$

so that the integral equation (Equation 3.4.260) and hence the solution $\mathbf{f}_\perp(\mathbf{p}_\perp)$ is invariant under this change of variable, but the integral kernel in our P-odd emission rate in (Equation 3.4.264) changes sign under this transformation as

$$\frac{\omega(2p_\parallel + \omega)}{p_\parallel^2(p_\parallel + \omega)^2} \rightarrow -\frac{\omega(2\tilde{p}_\parallel + \omega)}{\tilde{p}_\parallel^2(\tilde{p}_\parallel + \omega)^2}, \quad (3.4.268)$$

so that the net sign of the contribution from anti-fermion Bremsstrahlung is opposite to the one from fermion Bremsstrahlung. This is expected since fermion and anti-fermion from our right-handed Weyl fermion field have opposite chirality, so their contributions to Γ^{odd} should be opposite. From the above, if we sum over $p_\parallel > 0$ and $\tilde{p}_\parallel > 0$ regions (and calling \tilde{p}_\parallel as p_\parallel), we see that the final result is proportional to

$$n_+(p_\parallel + \omega) (1 - n_+(p_\parallel)) - n_-(p_\parallel + \omega) (1 - n_-(p_\parallel)), \quad (3.4.269)$$

which is indeed an odd function on the (axial) chemical potential μ . More generally, by the change of variable from p_{\parallel} to \tilde{p}_{\parallel} for the entire range of p_{\parallel} , we can simply replace the statistical factor in our main formula (Equation 3.4.264) with the average

$$n_+(p_{\parallel} + \omega) (1 - n_+(p_{\parallel})) \rightarrow \frac{1}{2} (n_+(p_{\parallel} + \omega) (1 - n_+(p_{\parallel})) - n_-(p_{\parallel} + \omega) (1 - n_-(p_{\parallel}))) , \quad (3.4.270)$$

so that the LPM contribution to our P-odd emission rate, (Equation 3.4.264), is now manifestly an odd function in μ .

Following Ref.(174), the integral equation (Equation 3.4.260) can be transformed to the one in the transverse 2-dimensional coordinate space \mathbf{b} , which takes a form

$$\frac{\omega(-\nabla_{\mathbf{b}}^2 + m_f^2)}{2p_{\parallel}(p_{\parallel} + \omega)} \mathbf{f}_{\perp}^i(\mathbf{b}) = -i \nabla_{\mathbf{b}}^i \delta^{(2)}(\mathbf{b}) + i C(\mathbf{b}) \mathbf{f}_{\perp}^i(\mathbf{b}) , \quad (3.4.271)$$

where

$$\mathbf{f}_{\perp}^i(\mathbf{b}) = \int \frac{d^2 \mathbf{p}_{\perp}}{(2\pi)^2} e^{i\mathbf{b} \cdot \mathbf{p}_{\perp}} f_{\perp}^i(\mathbf{p}_{\perp}) , \quad (3.4.272)$$

and

$$C(\mathbf{b}) \equiv \int \frac{d^2 \mathbf{q}_{\perp}}{(2\pi)^2} C(\mathbf{q}_{\perp}) (e^{-i\mathbf{b} \cdot \mathbf{q}_{\perp}} - 1) = -\frac{g^2 C_2(R) T}{2\pi} (K_0(|\mathbf{b}| m_D) + \gamma_E + \log(|\mathbf{b}| m_D / 2)) . \quad (3.4.273)$$

From rotational symmetry, one can write

$$\mathbf{f}_{\perp}(\mathbf{b}) = \mathbf{b} f(b) , \quad b \equiv |\mathbf{b}| , \quad (3.4.274)$$

in terms of a scalar function $f(b)$ which satisfies the following second order differential equation

$$\frac{\omega}{2p_{\parallel}(p_{\parallel} + \omega)} \left(-\partial_b^2 - \frac{3}{b} \partial_b + m_f^2 \right) f(b) = i C(b) f(b), \quad (3.4.275)$$

with the boundary conditions

$$f(b \rightarrow 0) = -i \frac{p_{\parallel}(p_{\parallel} + \omega)}{\pi \omega b^2} + O(b^0), \quad f(b \rightarrow \infty) = 0. \quad (3.4.276)$$

In terms of the scalar function $f(b)$ which can be easily solved from the above differential equation, the \mathbf{p}_{\perp} integral in our P-odd emission rate (Equation 3.4.264) takes a simple form

$$\int \frac{d^2 \mathbf{p}_{\perp}}{(2\pi)^2} (-1) Im [\mathbf{p}_{\perp} \cdot \mathbf{f}_{\perp}(\mathbf{p}_{\perp})] = (-1) Im [(-i) \nabla_{\mathbf{b}} \cdot \mathbf{f}_{\perp}(\mathbf{b})] \Big|_{\mathbf{b} \rightarrow 0} = 2 Re f(0), \quad (3.4.277)$$

so that the final expression for the LPM contribution to the P-odd photon emission rate becomes

$$\begin{aligned} (2\pi)^3 2\omega \frac{d\Gamma_{LPM}^{odd}}{d^3 \mathbf{k}} &= e^2 d_R \int_{-\infty}^{+\infty} \frac{dp_{\parallel}}{2\pi} (n_+(p_{\parallel} + \omega) (1 - n_+(p_{\parallel})) - n_-(p_{\parallel} + \omega) (1 - n_-(p_{\parallel}))) \\ &\times \frac{\omega(2p_{\parallel} + \omega)}{p_{\parallel}^2(p_{\parallel} + \omega)^2} Re f(0). \end{aligned} \quad (3.4.278)$$

This is what we practically use for numerical evaluations, and the computation reduces to solving the second order differential equation (Equation 3.4.275) with the boundary conditions (Equation 3.4.276).

In summary, the leading order P-odd photon emission rate for a single species of right-handed Weyl fermion is a sum of the three contributions: 1) hard Compton and Pair Annihilation rate given by (in t-channel parametrization) the equation (Equation 3.4.186) with (Equation 3.4.187) where one has to use (Equation 3.4.179), 2) soft t- and u-channel contributions given in (Equation 3.4.222), 3) the LPM re-summed collinear Bremsstrahlung and Pair Annihilation contribution given in (Equation 3.4.278) with (Equation 3.4.275) and (Equation 3.4.276). For a theory with N_F Dirac fermions with an axial chemical potential μ_A , one has to multiply the above results by a factor

$$2 \left(\sum_F Q_F^2 \right), \quad (3.4.279)$$

with a replacement $\mu \rightarrow \mu_A$ in the distribution functions, where Q_F are electromagnetic charges of flavor F in units of e . Recall also that the Debye mass

$$m_D^2 = g^2 \left(\frac{T^2}{3} + \frac{\mu^2}{\pi^2} \right) (N_c + N_F/2), \quad (3.4.280)$$

has to be adjusted according to the number of flavors N_F .

We choose to present our result in a way similar to the existing literature. Define

$$A(\omega) \equiv 2 \alpha_{EM} \left(\sum_F Q_F^2 \right) d_R \frac{m_{f,(0)}^2}{\omega} n_f(\omega), \quad (3.4.281)$$

where $n_f(\omega)$ is the Fermi-Dirac distribution with zero chemical potential and $m_{f,(0)}^2 \equiv C_2(R)g^2T^2/4$ is the asymptotic fermion thermal mass at zero chemical potential that has to be compared to the full expression (Equation 3.4.193) in the presence of (axial) chemical potential

$$m_f^2 = C_2(R) \frac{g^2}{4} \left(T^2 + \frac{\mu_A^2}{\pi^2} \right). \quad (3.4.282)$$

The hard Compton and Pair Annihilation rate is then written as

$$(2\pi)^3 \frac{d\Gamma_{hard}^{odd}}{d^3\mathbf{k}} = A(\omega) \frac{2}{(2\pi)^3} \frac{T}{\omega} \frac{1}{n_f(\omega)} \int_{q^*}^{\infty} \frac{d|\mathbf{q}|}{T} \int_{\max(-|\mathbf{q}|, |\mathbf{q}|-2|\mathbf{k}|)}^{|\mathbf{q}|} \frac{dq^0}{T} \int_{\frac{|\mathbf{q}|-q^0}{2}}^{\infty} \frac{d|\mathbf{p}'|}{T} \int_0^{2\pi} d\phi \bar{I}, \quad (3.4.283)$$

where

$$\begin{aligned} \bar{I} &= \left(-\frac{u}{t} - 2(t-u) \left(\frac{\mathbf{q}_{\perp}^2}{t^2} - \frac{\mathbf{q}_{\perp} \cdot \mathbf{p}'_{\perp}}{tu} \right) \right) \\ &\times (n_+(q^0 + |\mathbf{k}|)n_- (|\mathbf{p}'|) - n_-(q^0 + |\mathbf{k}|)n_+ (|\mathbf{p}'|))(1 + n_B(q^0 + |\mathbf{p}'|)) \\ &+ (s-t) \left(\frac{1}{t} + \frac{1}{s} - 2 \left(\frac{\mathbf{q}_{\perp}}{t} + \frac{(\mathbf{q}_{\perp} + \mathbf{p}'_{\perp})}{s} \right)^2 \right) \\ &\times (n_+(q^0 + |\mathbf{k}|)(1 - n_+(q^0 + |\mathbf{p}'|)) - n_-(q^0 + |\mathbf{k}|)(1 - n_-(q^0 + |\mathbf{p}'|))) n_B(|\mathbf{p}'|). \end{aligned} \quad (3.4.284)$$

Note that what is multiplied to $A(\omega)$ is a dimensionless function on ω/T (recall $|\mathbf{k}| = \omega$), and the phase space integral as well as the integrand \bar{I} is in terms of dimensionless variables $|\mathbf{q}|/T$, etc. The soft t- and u-channel contribution is written as

$$(2\pi)^3 \frac{d\Gamma_{soft}^{odd}}{d^3\mathbf{k}} = A(\omega) \frac{m_f^2}{m_{f,(0)}^2} \frac{1}{n_f(\omega)} (n_+(\omega)n_-(0) - n_-(\omega)n_+(0)) (\log(q^*/m_f) - 1 + \log 2) . \quad (3.4.285)$$

Finally, the LPM contribution is

$$(2\pi)^3 \frac{d\Gamma_{LPM}^{odd}}{d^3\mathbf{k}} = A(\omega) \frac{1}{n_f(\omega)} \int_{-\infty}^{+\infty} d\bar{p}_{\parallel} (n_+(p_{\parallel} + \omega) (1 - n_+(p_{\parallel})) - n_-(p_{\parallel} + \omega) (1 - n_-(p_{\parallel}))) \\ \times \frac{\bar{\omega}(2\bar{p}_{\parallel} + \bar{\omega})}{\bar{p}_{\parallel}^2(\bar{p}_{\parallel} + \bar{\omega})^2} Re \bar{f}(0) , \quad (3.4.286)$$

where $\bar{p}_{\parallel} \equiv p_{\parallel}/T$ and $\bar{\omega} \equiv \omega/T$, and $\bar{f}(\bar{b})$ is the solution of the differential equation

$$\frac{\bar{\omega}}{2\bar{p}_{\parallel}(\bar{p}_{\parallel} + \bar{\omega})} \left(-\partial_{\bar{b}}^2 - \frac{3}{\bar{b}} \partial_{\bar{b}} + \frac{m_f^2}{m_D^2} \right) \bar{f}(\bar{b}) = -i \frac{2}{\pi} \frac{m_{f,(0)}^2}{m_D^2} (K_0(\bar{b}) + \gamma_E + \log(\bar{b}/2)) \bar{f}(\bar{b}) , \quad (3.4.287)$$

with the boundary conditions

$$\bar{f}(\bar{b} \rightarrow 0) = -i \frac{\bar{p}_{\parallel}(\bar{p}_{\parallel} + \bar{\omega})}{\pi \bar{\omega} \bar{b}^2} \frac{m_D^2}{m_{f,(0)}^2} , \quad \bar{f}(\bar{b} \rightarrow \infty) = 0 . \quad (3.4.288)$$

The final result can be recast to the form

$$(2\pi)^3 \frac{d\Gamma_{LO}^{odd}}{d^3\mathbf{k}} = A(\omega) \left(C_{Log}^{odd}(\omega/T) \log(T/m_f) + C_{2\leftrightarrow 2}^{odd}(\omega/T) + C_{LPM}^{odd}(\omega/T) \right) , \quad (3.4.289)$$

with the dimensionless functions C_{Log}^{odd} , $C_{2\leftrightarrow 2}^{odd}$, C_{LPM}^{odd} , where

$$\begin{aligned}
C_{Log}^{odd} &= \frac{m_f^2}{m_{f,(0)}^2} \frac{1}{n_f(\omega)} (n_+(\omega)n_-(0) - n_-(\omega)n_+(0)) , \\
C_{2\leftrightarrow 2}^{odd} &= \lim_{q^* \rightarrow 0} \left(\frac{2}{(2\pi)^3} \frac{T}{\omega} \frac{1}{n_f(\omega)} \int_{q^*}^{\infty} \frac{d|\mathbf{q}|}{T} \int_{\max(-|\mathbf{q}|, |\mathbf{q}|-2|\mathbf{k}|)}^{|\mathbf{q}|} \frac{dq^0}{T} \int_{\frac{|\mathbf{q}|-q^0}{2}}^{\infty} \frac{d|\mathbf{p}'|}{T} \int_0^{2\pi} d\phi \bar{I} \right. \\
&\quad \left. - C_{Log}^{odd}(\omega/T) (\log(T/q^*) + 1 - \log 2) \right) , \\
C_{LPM}^{odd} &= \frac{1}{n_f(\omega)} \int_{-\infty}^{+\infty} d\bar{p}_{\parallel} (n_+(p_{\parallel} + \omega) (1 - n_+(p_{\parallel})) - n_-(p_{\parallel} + \omega) (1 - n_-(p_{\parallel}))) \\
&\quad \times \frac{\bar{\omega}(2\bar{p}_{\parallel} + \bar{\omega})}{\bar{p}_{\parallel}^2(\bar{p}_{\parallel} + \bar{\omega})^2} Re \bar{f}(0) .
\end{aligned} \tag{3.4.290}$$

Note that we have not extracted out the energy logarithm given in (Equation 5.0.24), but one could choose to do so to redefine $C_{2\leftrightarrow 2}^{odd}$.

The above result is valid for full dependence in the axial chemical potential μ_A , but we will present our numerical evaluations only for its linear dependency by expanding the dimensionless functions C_{Log}^{odd} , $C_{2\leftrightarrow 2}^{odd}$, C_{LPM}^{odd} in linear order in μ_A/T . In this case, m_f^2 can be identified with $m_{f,(0)}^2$ and one can also neglect μ_A^2 in the Debye mass m_D^2 . Writing this linear expansion as

$$\begin{aligned}
(2\pi)^3 \frac{d\Gamma_{LO}^{odd}}{d^3\mathbf{k}} &\approx A(\omega) \left(C_{Log}^{odd,(1)}(\omega/T) \log(T/m_f) + C_{2\leftrightarrow 2}^{odd,(1)}(\omega/T) + C_{LPM}^{odd,(1)}(\omega/T) \right) \frac{\mu_A}{T} \\
&\quad + \mathcal{O}(\mu_A^3) ,
\end{aligned} \tag{3.4.291}$$

we have

$$C_{Log}^{odd,(1)} = \frac{1}{2} (1 - 2n_f(\omega)) , \tag{3.4.292}$$

while the other two functions, $C_{2\leftrightarrow 2}^{odd,(1)}$, $C_{LPM}^{odd,(1)}$, have to be evaluated numerically. The numerical evaluation involves three dimensional integrals and solving second order differential equation, and can be performed with a reasonable precision using Mathematica. We present our numerical results in Figure 24 for the range $0.5 < \omega/T < 3$. We see that the LPM contributions to the constant under the log is 2-3 times bigger than the one from $2 \leftrightarrow 2$ Compton and Pair Annihilation contributions in this range, but we should remember that the leading log contribution comes from these $2 \leftrightarrow 2$ processes.

Finally, recalling that

$$\Gamma^{total} = \Gamma(\epsilon^+) + \Gamma(\epsilon^-), \quad \Gamma^{odd} = \Gamma(\epsilon^+) - \Gamma(\epsilon^-), \quad (3.4.293)$$

we get

$$(2\pi)^3 \frac{d\Gamma_{LO}^{total}}{d^3\mathbf{k}} \approx A(\omega) \left(\log(T/m_f) + C_{2\leftrightarrow 2}^{total,(0)}(\omega/T) + C_{LPM}^{total,(0)}(\omega/T) \right) + \mathcal{O}(\mu_A^2), \quad (3.4.294)$$

where

$$\begin{aligned} C_{2\leftrightarrow 2}^{total,(0)}(\omega/T) &= \frac{1}{2} \ln \left(\frac{2\omega}{T} \right) + 0.041 \frac{T}{\omega} - 0.3615 + 1.01e^{-1.35\omega/T}, \\ &0.2 < \frac{\omega}{T}, \end{aligned} \quad (3.4.295)$$

$$\begin{aligned} C_{LPM}^{total,(0)}(\omega/T) &= 2 \left[\frac{0.316 \ln(12.18 + T/\omega)}{(\omega/T)^{3/2}} + \frac{0.0768\omega/T}{\sqrt{1 + \omega/(16.27T)}} \right], \\ &0.2 < \frac{\omega}{T} < 50, \end{aligned} \quad (3.4.296)$$

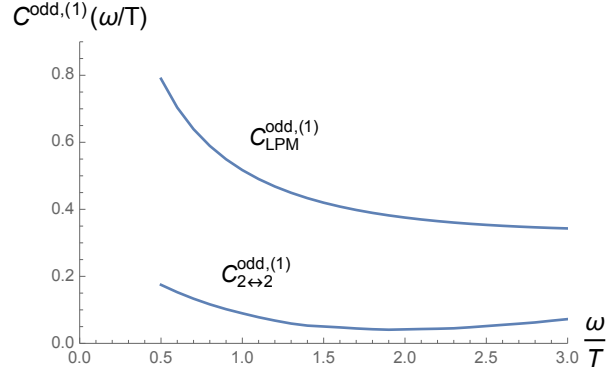


Figure 24. Numerical results for $C^{odd,(1)}_{2\leftrightarrow 2}(\omega/T)$, $C^{odd,(1)}_{LPM}(\omega/T)$ for $N_F = 2$ QCD.

which is nothing but AMY's result for $\mu_A = 0$ (166).

Therefore, the circular polarization asymmetry $A_{\pm\gamma} = \frac{\Gamma^{odd}}{\Gamma^{total}} \approx 0.03$ for $\omega/T = 2$, $\alpha_s = 0.2$, and $\mu_A/T = 0.1$ which is about three times more than the strong coupling result $A_{\pm\gamma} \approx 0.01$ that we found in Sakai-Sugimoto model using AdS/CFT correspondence, see Figure 12.

CHAPTER 4

HARD PROBES OF STRONGLY MAGNETIZED QUARK-GLUON PLASMA

(Previously published as Shiyong Li, Kiminad A. Mamo, and Ho-Ung Yee, “Jet quenching parameter of the quark-gluon plasma in a strong magnetic field: Perturbative QCD and AdS/CFT correspondence,” Phys. Rev. D 94, no. 8, 085016 (2016), and Kiminad A. Mamo, “Energy loss of a nonaccelerating quark moving through a strongly coupled N=4 super Yang-Mills vacuum or plasma in strong magnetic field,” Phys. Rev. D 94, no. 4, 041901 (2016))

In this chapter, we will investigate the energy loss of a high energy jet in a strongly magnetized plasma both at weak and strong coupling regimes.

The energy loss of a high energy jet in the QCD plasma via gluon Bremsstrahlung, described by BDMPS-Z formalism in large scattering number limit (175; 176; 177; 178; 179), rests on a single parameter \hat{q} , the jet quenching parameter. It is defined as the transverse momentum diffusion constant of the (emitted) gluon per unit length of the jet trajectory: $\hat{q} = \langle \mathbf{p}_\perp^2 \rangle / dz$ (176). In our computation, we will call any fast moving color charged object with some representation R a jet, since in the eikonal limit the identity of the object should not matter except its color charge (this includes the emitted gluon as well). The same parameter also gives the damping rate of an energetic small dipole of size b by $\Gamma^{dipole} = \frac{1}{2} \hat{q} b^2$ in small b limit. This connection between the two can be understood as follows. The amplitude square of the gluon Bremsstrahlung is

a product of transition amplitude forward in time and its complex conjugate. The conjugate amplitude can be put as

$$(\langle f|U(t)|i\rangle)^* = \langle \bar{f}|(U(t))^*|\bar{i}\rangle, \quad (4.0.1)$$

where $U(t)$ is the time-evolution operator and $|\bar{i}\rangle$ is a time-inversion state of the initial state $|i\rangle$, which in Schrodinger picture is just the complex conjugate wave function of the original wave-function. Since the time-inverse operator $U(t)^*$ describes a negative energy state with opposite color charge, the complex conjugate of transition amplitude can be put as an ordinary transition amplitude of a jet, but with a negative energy and opposite color charge, which evolves with time-reversed propagator $U(t)^*$. Let's call this "anti-jet". This is nothing but the evolution on the second contour in Schwinger-Keldysh formalism for complex conjugate amplitudes. The key element is that the thermally fluctuating soft gauge fields that are the main source of scatterings with the jet are classical fields in nature, which are "r"-type fields in the language of Schwinger-Keldysh formalism: these classical soft r-type fluctuations give leading order contributions to the total scattering rate to the jet, due to Bose-Einstein enhancement in the soft region, $n_B(\omega) \sim T/\omega$ for $\omega \ll T$. As these r-type fields have the same values on both contours in the Schwinger-Keldysh formalism, it doesn't matter on which contour we put the anti-jet for the computation of soft scatterings with them. If we choose to put the jet and anti-jet together, they look just like a color dipole. In BDMPS-Z formalism, we have jet-antijet-gluon three body system during the virtual process, which can be thought of as a collection of three color dipoles. The only difference between this jet-antijet pair and a real color dipole is that the anti-jet has a negative kinetic energy: the damping rate part of the

hamiltonian (i.e. the imaginary part) coming from soft scatterings with thermal fluctuations is the same between the two, since these scatterings care only the color charges of the pair. In large scattering number limit, the small size regime dominates, and the scattering amplitude becomes

$$A^{pair} = (1 - e^{i\mathbf{b}\cdot\mathbf{q}_\perp})A^{single} \approx -i(\mathbf{b}\cdot\mathbf{q}_\perp)A^{single}, \quad (4.0.2)$$

where A_{single} is the scattering amplitude with a single jet, \mathbf{q} is the spatial part of the exchanged momentum, and \mathbf{b} is the transverse size of the color dipole. This gives the damping rate part being

$$\Gamma^{pair} = \Gamma^{dipole} \approx \int d^3\mathbf{q} \frac{d\Gamma^{single}}{d^3\mathbf{q}} (\mathbf{b}\cdot\mathbf{q}_\perp)^2 = \frac{1}{2}b^2 \int d^3\mathbf{q} \frac{d\Gamma^{single}}{d^3\mathbf{q}} q_\perp^2 = \frac{1}{2}b^2\hat{q}, \quad (4.0.3)$$

with the conventional definition of \hat{q} being the transverse momentum diffusion rate of a single jet.

We compute \hat{q} in the presence of strong magnetic field limit $eB \gg T^2$, in both weakly coupled regime at leading order in α_s as well as in strongly coupled regime described by AdS/CFT correspondence. In the former case, we additionally assume $\alpha_s eB \ll T^2$, so that self-energy corrections from lowest Landau level states (LLL) of quarks to the “hard” particles of typical momenta T can be neglected (see later sections for more details). Only with this additional assumption of small enough coupling α_s , a systematic power counting scheme at weak coupling we employ can apply: this scheme was recently introduced in Ref.(180) to compute heavy-quark diffusion constant in strong magnetic field in perturbative QCD (pQCD). We follow the same

scheme in this work. We further neglect small quark mass corrections treating them massless: this is well-justified practically, m_q^2/eB or m_q^2/T^2 is about 10^{-4} for $T \sim 300$ MeV. In both weakly and strongly coupled regimes, we consider the two cases of jet motions: the jet moving parallel to the magnetic field and the one moving perpendicular to the magnetic field.

4.1 Jet Quenching Parameter at Weak Coupling

The leading order computation of \hat{q} in small α_s can be done by first computing the scattering rate per unit momentum transfer, $d\Gamma^{single}/d^3\mathbf{q}$, from leading t-channel gluon exchange between hard thermal quarks or gluons and the jet. Then the jet quenching parameter is computed as

$$\hat{q} = \frac{1}{v} \int d\mathbf{q}^3 \frac{d\Gamma^{single}}{d^3\mathbf{q}} \mathbf{q}_\perp^2, \quad (4.1.4)$$

where \mathbf{q}_\perp is the transverse component of the momentum transfer, and $1/v$ factor is from the translation between the diffusion constants “per unit length” and “per unit time” : $d/dz = (1/v)d/dt$. In the large jet momentum limit $P \gg T$, which is the case for either heavy-quarks ($P^0 = M_Q \gg T$) or for a ultra-relativistic jet ($P \approx E(1, \mathbf{v})$ with $E \gg T$ and $v \approx 1$), the leading power of P in the Feynman diagrams arises only in the t-channel exchange diagrams. For the case of scatterings with thermal gluons, this statement is not gauge-invariant, but is true in the gauge $\epsilon \cdot P = \tilde{\epsilon} \cdot P = 0$ where $\epsilon, \tilde{\epsilon}$ are polarizations of incoming and out-going gluons (181). For a ultra-relativistic jet where P is nearly light-like, this gauge is essentially the light-cone gauge.

The t-channel momentum exchange \mathbf{q} involves a soft scale ($Q \ll T$) for leading log contributions (as we will see), which features logarithmic IR singularity for \hat{q} . This is cured by

gluon self-energy corrections either from thermally excited LLL quarks or from thermally excited hard gluons. Both give the screening masses for t-channel gluon exchange, the former being $m_{D,B}^2 \sim \alpha_s e B$ and the latter $m_D^2 \sim \alpha_s T^2$. Under our assumption of $eB \gg T^2$, we can keep only the former Debye screening from the LLL states. We emphasize that the t-channel exchanged gluons for which we include the self-energy are space-like and soft.

On the other hand, the dispersion relations of scattering hard quarks and hard gluons generally get thermal mass corrections from the same self-energy but evaluated in nearly on-shell kinematic regions. They are of the same order, $\alpha_s e B$ or $\alpha_s T^2$. As our further assumption of $\alpha_s e B \ll T^2$, and hard quarks and gluons have typical momenta T , we can neglect the self-energy (i.e. thermal mass) for these scattering hard thermal particles in leading order computation: the leading order \hat{q} comes from the hard momentum ($\sim T$) region of scattering particles. These hard particles are then free particles in leading order treatment. In turn, this also justifies the computation of self-energy itself from 1-loop of hard particles in the loop: these hard particles in the loop are free particles, their thermal mass corrections give only higher order corrections to the self-energy. This leading order treatment is then self-consistent (180).

We give a brief summary of results we will obtain in the next subsections of detailed computation of \hat{q} . For the case of scattering with thermal gluons, due to an issue of gauge invariance that we mentioned above, one needs to work directly with this formula computing somewhat challenging phase space integrals as done originally in Ref.(181). The leading log contribution is however manageable, can be shown to be $\hat{q}_{gluon} \sim \alpha_s^2 T^3 \log\left(\frac{T^2}{\alpha_s e B}\right)$. On the other hand, the contribution coming from scatterings with LLL quarks will be shown to be

$\hat{q}_{quarks} \sim \alpha_s^2 eBT \log\left(\frac{1}{\alpha_s}\right)$, which is larger than \hat{q}_{gluon} by a factor of $eB/T^2 \gg 1$. The origin of this enhancement is basically the large density of states of LLL quarks which scales linearly with eBT (eB from the density of states of LLL in two transverse dimensions and T from the longitudinal thermal distribution), while the density of states of gluons with thermal distribution scales only with T^3 . Therefore, the leading order \hat{q} is provided by the scatterings with the thermally excited LLL quarks.

The t-channel process with LLL quarks is free of gauge-invariance issue, and in this case one can explore an alternative way of computing the t-channel scattering rate $d\Gamma/d^3\mathbf{q}$ from cutting the 1-loop retarded jet self-energy diagram, which gives the imaginary part of retarded jet self-energy or the damping rate of the jet,

$$-Im[\Sigma^R(P)] \sim \Gamma^{single} = \int d^3\mathbf{q} \frac{d\Gamma^{single}}{d^3\mathbf{q}}, \quad (4.1.5)$$

where \mathbf{q} is nothing but the loop momentum of the gluon line in the jet self-energy computation, and $\Sigma^R(P)$ is the retarded jet self-energy: see Figure 25. The internal gluon line should include its own self-energy coming from 1-loop hard thermal LLL states: that would be the Hard Thermal Loop propagator in the soft t-channel momentum region of \mathbf{q} , but now from the LLL states instead of more conventional free hard fermions/gluons. As argued in the above, the contributions from hard gluons to this t-channel gluon self-energy is subdominant and neglected. Once we compute $d\Gamma^{single}/d^3\mathbf{q}$ in this method, we can compute \hat{q} by weighting the integral by

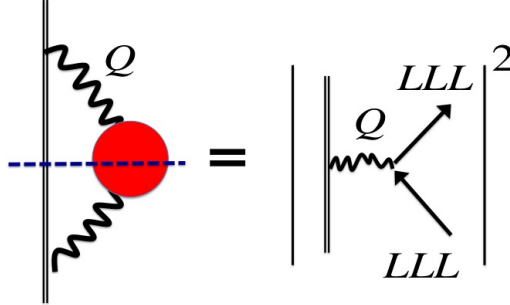


Figure 25. The imaginary cut of the jet self-energy is equal to the damping rate, that is, the total scattering rate with thermal (hard) particles, especially the lowest Landau level quarks. The exchanged gluon line is Debye screened by the same hard LLL states.

an additional factor of q_{\perp}^2 . This method seems much simpler, so we will adopt it in the next subsections.

Scattering rate of the jet from its 1-loop self-energy

For definiteness we assume that the jet is a fast moving fermion with momentum P , but the result in high P limit is independent of this detail, due to eikonal reduction of jet propagation when $P \gg Q$: the only important fact is that the current of the jet in relativistic normalization is

$$\bar{U}(P+Q)\gamma^{\mu}t^a U(P) \approx 2P^{\mu}t^a, \quad (4.1.6)$$

where t^a is the color charge of the jet.

The 1-loop retarded jet self-energy is given by $\Sigma^R(P) = (-i)\Sigma^{ra}(P)$ with "ra"-self-energy in real-time formalism is

$$\Sigma^{ra}(P) = (ig)^2 C_2^J \gamma^\beta \int \frac{d^4 Q}{(2\pi)^4} \left[G_{\alpha\beta}^{rr}(Q) S_{(0)}^{ra}(P+Q) + G_{\alpha\beta}^{ar}(Q) S_{(0)}^{rr}(P+Q) \right] \gamma^\alpha, \quad (4.1.7)$$

where C_2^J is the color Casimir of the jet, and $G_{\alpha\beta}(Q) = \langle A_\alpha(Q) A_\beta(-Q) \rangle$ are the real-time gluon propagators without colors (or the color diagonal part defined by $\langle A_\alpha^a(Q) A_\beta^b(-Q) \rangle \equiv G_{\alpha\beta}(Q) \delta^{ab}$), and $S_{(0)}(Q)$ are the bare jet propagator given by

$$\begin{aligned} S_{(0)}^{ra}(Q) &= (-i) \frac{\gamma^0 P(\mathbf{q})}{q^0 - \sqrt{\mathbf{q}^2 + M^2} + i\epsilon}, \quad S_{(0)}^{ar}(Q) = (-i) \frac{\gamma^0 P(\mathbf{q})}{q^0 - \sqrt{\mathbf{q}^2 + M^2} - i\epsilon}, \\ S_{(0)}^{rr}(Q) &= -\left(\frac{1}{2} - n_F(q^0)\right) (2\pi) \gamma^0 P(\mathbf{q}) \delta\left(q^0 - \sqrt{\mathbf{q}^2 + M^2}\right), \end{aligned} \quad (4.1.8)$$

with the spinor projection operator

$$P(\mathbf{q}) = \frac{1}{2} \left(1 + \frac{\gamma^0(\gamma \cdot \mathbf{q} - iM)}{\sqrt{\mathbf{q}^2 + M^2}} \right), \quad (4.1.9)$$

and M is the rest mass of the jet. We will consider relativistic cases where the jet momentum $\mathbf{p} \gg M$. Our metric convention in this work is $\eta = (-, +, +, +)$. The self-energy re-summed jet propagator $S(P)$ is given by

$$(S^{ra}(P))^{-1} = (S_{(0)}^{ra}(P))^{-1} - \Sigma^{ra}(P), \quad (4.1.10)$$

and the damping rate of the jet Γ^{single} is identified by the ansatz

$$S^{ra}(P) \approx (-i) \frac{\gamma^0 P(\mathbf{p})}{p^0 - \sqrt{\mathbf{p}^2 + M^2} + i\Gamma^{single}/2} \quad (4.1.11)$$

neglecting a mass shift and wave function renormalization which are from the real part of $\Sigma^R(P)$ instead of the imaginary part. This ansatz is equivalent to

$$(S^{ra}(P))^{-1} \approx (-i)P(\mathbf{p})\gamma^0 \left(p^0 - \sqrt{\mathbf{p}^2 + M^2} + i\Gamma^{single}/2 \right) = (S_{(0)}^{ra}(P))^{-1} + P(\mathbf{p})\gamma^0 \Gamma^{single}/2, \quad (4.1.12)$$

and comparing with (Equation 4.1.10) and using $Tr(P(\mathbf{p})) = 2$, we have

$$\Gamma^{single} = Re \left[Tr \left(\Sigma^{ra}(P) \gamma^0 P(\mathbf{p}) \right) \right] \Big|_{p^0 = \sqrt{\mathbf{p}^2 + M^2}} = -Im \left[Tr \left(\Sigma^R(P) \gamma^0 P(\mathbf{p}) \right) \right] \Big|_{p^0 = \sqrt{\mathbf{p}^2 + M^2}}, \quad (4.1.13)$$

which is the desired formula relating the damping rate of the jet with the imaginary part of its retarded self-energy.

Using the explicit expression (Equation 4.1.7) for $\Sigma^{ra}(P)$, and (Equation 4.1.8), and the similar thermal relations for gluon propagators

$$\begin{aligned} G_{\alpha\beta}^{ar}(Q) &= (G_{\beta\alpha}^{ra}(Q))^*, \\ G_{\alpha\beta}^{rr}(Q) &= \left(\frac{1}{2} + n_B(q^0) \right) (G_{\alpha\beta}^{ra}(Q) - G_{\alpha\beta}^{ar}(Q)) \equiv \left(\frac{1}{2} + n_B(q^0) \right) \rho_{\alpha\beta}^g(Q), \end{aligned} \quad (4.1.14)$$

with the gluon spectral density $\rho_{\alpha\beta}^g(Q)$ that is a hermitian matrix in (α, β) , one can finally arrive at after some amount of manipulations (see Appendix 2 in Ref.(182) for the relevant details)

$$\begin{aligned} \Gamma^{single} &= \frac{g^2}{2} C_2^J \int \frac{d^4 Q}{(2\pi)^4} (n_B(q^0) + n_F(p^0 + q^0)) (2\pi) \delta(p^0 + q^0 - \sqrt{(\mathbf{p} + \mathbf{q})^2 + M^2}) \rho_{\alpha\beta}^g(Q) \\ &\times \text{Tr} \left[\gamma^\beta \gamma^0 P(\mathbf{p} + \mathbf{q}) \gamma^\alpha \gamma^0 P(\mathbf{p}) \right], \end{aligned} \quad (4.1.15)$$

which is basically a cut of the self-energy where all internal propagators are replaced by their spectral densities. For the bare jet internal line $S_{(0)}(P + Q)$, it imposes simply the on-shell δ function on the out-going jet state after the scattering, while the spectral density of the internal gluon line encodes the soft t-channel scatterings with hard LLL quarks or hard thermal gluons. A convenient fact for us is that the internal 1-loop momentum \mathbf{q} is nothing but the exchanged momentum in these t-channel scattering with the hard particles, so that one can read off the differential scattering rate $d\Gamma^{single}/d^3\mathbf{q}$ by simply writing the result as

$$\Gamma^{single} = \int d^3\mathbf{q} \frac{d\Gamma^{single}}{d^3\mathbf{q}}. \quad (4.1.16)$$

To find the gluon spectral density after re-summing 1-loop gluon self-energy from the LLL quarks, we start from

$$(G^{ra}(Q))^{-1} = (G_{(0)}^{ra}(Q))^{-1} - \Pi^{ra}(Q), \quad (4.1.17)$$

where the inverse refers to the Lorentz indices, and $\Pi_{\alpha\beta}^{ra}(Q)$ is the ra-type gluon self-energy at 1-loop

$$\Pi_{\alpha\beta}^{ra}(Q) = (ig)^2 T_R N_F \langle j_\alpha^r(Q) j_\beta^a(-Q) \rangle, \quad (4.1.18)$$

where j_α is the quark color current after color indices are stripped off, and the quark color traces gives T_R which is 1/2 for fundamental and N_c for adjoint representation, and N_F is the number of light flavors. In our LLL approximation in massless limit, the above current-current correlation function factorizes into a product of 1+1 dimensional correlation function and the transverse density of the LLL states. The former is then easily computed using the well-known bosonization of 1+1 dimensional fermion into a massless real scalar field. These have been recently computed in Ref.(180) and the result is given by

$$\Pi_{\alpha\beta}^{ra}(Q) = \chi \left(Q_\parallel^2 \eta_{\parallel\alpha\beta} - Q_{\parallel\alpha} Q_{\parallel\beta} \right), \quad \chi \equiv -i \frac{g^2}{\pi} T_R N_F \left(\frac{eB}{2\pi} \right) e^{-\frac{\mathbf{q}_\perp^2}{2eB}} \frac{1}{Q_{\parallel\epsilon}^2}, \quad (4.1.19)$$

where Q_\parallel and $\eta_{\parallel\alpha\beta}$ refer to 1+1 dimensional components of momentum and the metric along the magnetic field direction, \mathbf{q}_\perp is the component perpendicular to the magnetic field direction, and

$$Q_{\parallel\epsilon}^2 \equiv Q_\parallel^2 \Big|_{q^0 \rightarrow q^0 + i\epsilon} = -(q^0 + i\epsilon)^2 + q_z^2. \quad (4.1.20)$$

The $(G_{(0)}^{ra}(Q))^{-1}$ and therefore $G^{ra}(Q)$ needs a gauge-fixing, and we choose to work in the covariant gauge where

$$(G_{(0)}^{ra}(Q))^{-1} = i \left(Q^2 \eta_{\alpha\beta} - Q_\alpha Q_\beta + \frac{1}{\xi} Q_\alpha Q_\beta \right) \Big|_{q^0 \rightarrow q^0 + i\epsilon}, \quad (4.1.21)$$

where ξ is a gauge parameter. Then, $G^{ra}(Q)$ with (Equation 4.1.19) is found to be given by

$$G_{\alpha\beta}^{ra}(Q) = -i \frac{\eta_{\alpha\beta}}{Q_\epsilon^2} + i(1 - \xi) \frac{Q_\alpha Q_\beta}{(Q_\epsilon^2)^2} - \left(Q_\parallel^2 \eta_{\alpha\beta} - Q_{\parallel\alpha} Q_{\parallel\beta} \right) \frac{\chi}{Q_\epsilon^2 (Q_\epsilon^2 + i\chi Q_\parallel^2)}, \quad (4.1.22)$$

where $Q_\epsilon^2 \equiv -(q^0 + i\epsilon)^2 + \mathbf{q}^2$. The gluon spectral density is defined to be twice of the hermitian part of $G^{ra}(Q)$, and since the above is symmetric in Lorentz indices, it is simply twice of the real part: $\rho_{\alpha\beta}^g(Q) = 2 \operatorname{Re} [G_{\alpha\beta}^{ra}(Q)]$.

The second term involving ξ is proportional to Q_α , which vanishes after being contracted with the jet current $\bar{U}(P + Q)\gamma^\alpha U(P)$ in (Equation 4.1.15) by Ward identity, which ensures the gauge invariance of the scattering rate (Equation 4.1.15). From the on-shell constraint in (Equation 4.1.15) the momentum transfer Q is space like, so the real part from the first term in (Equation 4.1.22) which is $\sim \delta(Q^2) \operatorname{sgn}(q^0)$ does not contribute to the scattering rate in (Equation 4.1.15). The contribution from the last term in (Equation 4.1.22) represents the

scatterings with the LLL states we are looking for. A simple, but careful computation as in Ref.(180) gives

$$\rho_{\alpha\beta}^g(Q) \sim \frac{(2\pi)Q_{\parallel\alpha}Q_{\parallel\beta}\frac{g^2}{\pi}T_R N_F\left(\frac{eB}{2\pi}\right)e^{-\frac{q_{\perp}^2}{2eB}}\text{sgn}(q^0)\delta(Q_{\parallel}^2)}{\left(q_{\perp}^2 + \frac{g^2}{\pi}T_R N_F\left(\frac{eB}{2\pi}\right)e^{-\frac{q_{\perp}^2}{2eB}}\right)^2}, \quad (4.1.23)$$

which is a key ingredient in our subsequent computations.

Since

$$\text{sgn}(q^0)\delta(Q_{\parallel}^2) = \frac{1}{2q^0} (\delta(q^0 - q_z) + \delta(q^0 + q_z)) , \quad (4.1.24)$$

where we assume the magnetic field points to the \hat{z} direction, there are two separate pieces in the above spectral function. They reflect the two light-like spectrums of 1+1 dimensional LLL quarks moving in opposite directions, each corresponding to a definite 4D chirality of massless quarks. Since the gluon vertex with the quarks does not mix the two chiralities, the momentum transfer Q should be given by the momentum difference of the two states within the same 1+1 dimensional chiral spectrum, and therefore Q should be also light-like in 1+1 dimensions. The term with $\delta(q^0 - q_z)$ arises from the LLL quarks moving to \hat{z} direction, while the term with $\delta(q^0 + q_z)$ corresponds to the LLL quarks moving to the opposite direction.

Computing the spinor trace in (Equation 4.1.15) gives

$$\begin{aligned} & Tr \left[\gamma^\beta \gamma^0 P(\mathbf{p} + \mathbf{q}) \gamma^\alpha \gamma^0 P(\mathbf{p}) \right] \\ &= \hat{v}_{\mathbf{p}}^\alpha \hat{v}_{\mathbf{p}+\mathbf{q}}^\beta + \hat{v}_{\mathbf{p}+\mathbf{q}}^\alpha \hat{v}_{\mathbf{p}}^\beta - \eta^{\alpha\beta} \frac{(P \cdot Q)}{E_{\mathbf{p}} E_{\mathbf{p}+\mathbf{q}}} \equiv S^{\alpha\beta}, \end{aligned} \quad (4.1.25)$$

where $E_{\mathbf{p}} \equiv \sqrt{\mathbf{p}^2 + M^2}$ and

$$\hat{v}_{\mathbf{p}}^{\alpha} \equiv \frac{P^{\alpha}}{E_{\mathbf{p}}} = (1, \mathbf{p}/E_{\mathbf{p}}) = (1, \mathbf{v}_{\mathbf{p}}), \quad (4.1.26)$$

where $\mathbf{v}_{\mathbf{p}}$ is nothing but the velocity of the jet of momentum P . In deriving the above result, we used the on-shell condition $P^2 = -M^2$. From the above expression, it is straightforward to see the on-shell Ward identity that we claimed before holds

$$S^{\alpha\beta} Q_{\alpha} = \frac{1}{E_{\mathbf{p}} E_{\mathbf{p}+\mathbf{q}}} (2P \cdot Q + Q^2) P^{\beta} = 0, \quad (4.1.27)$$

where we used the fact that the energy δ function in (Equation 4.1.15) imposes the on-shell condition $(P + Q)^2 = -M^2$ which is equivalent to

$$2P \cdot Q + Q^2 = 0, \quad (4.1.28)$$

since $P^2 = -M^2$.

The scattering rate (Equation 4.1.15) with the gluon spectral density (Equation 4.1.23) and the spinor trace (Equation 4.1.25) are the basic ingredients in our computation of jet quenching parameter in weak coupling theory in the following subsections.

\hat{q} when the jet is parallel to the magnetic field

Let us first consider the case where the jet is moving parallel to the magnetic field, say along \hat{z} direction: $\mathbf{p} = p_z \hat{z}$, $p_z > 0$. In this case, the notions of \parallel and \perp from the magnetic field and

the jet coincide, so we can use them for both. From the gluon spectral density (Equation 4.1.23)

and

$$\text{sgn}(q^0)\delta(Q_{\parallel}^2) = \frac{1}{2q^0} (\delta(q^0 - q_z) + \delta(q^0 + q_z)) , \quad (4.1.29)$$

there are two distinct delta-functions which give different characteristic contributions to the jet scattering rate. We will find that the one coming from LLL quarks moving opposite to the jet direction (i.e. the one with $\delta(q^0 + q_z)$) gives the dominant contribution in high energy limit $v \rightarrow 1$.

From (Equation 4.1.15) with (Equation 4.1.23), we see that we need to compute $S^{\alpha\beta}Q_{\parallel\alpha}Q_{\parallel\beta}$. Due to the Ward identity and $Q_{\parallel\alpha} = Q_{\alpha} - Q_{\perp\alpha}$, this is equal to

$$S^{\alpha\beta}Q_{\parallel\alpha}Q_{\parallel\beta} = S^{\alpha\beta}Q_{\perp\alpha}Q_{\perp\beta} = -\frac{1}{E_{\mathbf{p}}E_{\mathbf{p}+\mathbf{q}}}(P \cdot Q)\mathbf{q}_{\perp}^2 = \frac{1}{2E_{\mathbf{p}}E_{\mathbf{p}+\mathbf{q}}}Q^2\mathbf{q}_{\perp}^2 = \frac{(\mathbf{q}_{\perp}^2)^2}{2E_{\mathbf{p}}E_{\mathbf{p}+\mathbf{q}}} , \quad (4.1.30)$$

where we used $P \cdot Q_{\perp} = 0$ and (Equation 4.1.28), as well as $Q^2 = \mathbf{q}_{\perp}^2$ in the last equality due to the $\delta(Q_{\parallel}^2)$ factor in (Equation 4.1.23). The net result is quite simple.

From (Equation 4.1.29), let us consider each delta-function separately, and perform q^0 integral so that we can replace q^0 with $\pm q_z$ where \pm refers to each case of the two delta-functions. Then, the energy delta function in (Equation 4.1.15) is worked out as

$$\begin{aligned} \delta(p^0 + q^0 - \sqrt{(\mathbf{p} + \mathbf{q})^2 + M^2}) &= \delta\left(\sqrt{p_z^2 + M^2} \pm q_z - \sqrt{(p_z + q_z)^2 + \mathbf{q}_{\perp}^2 + M^2}\right) \\ &= \frac{E_{\mathbf{p}+\mathbf{q}}}{E_{\mathbf{p}}(1 \mp v)} \delta\left(q_z \mp \frac{\mathbf{q}_{\perp}^2}{2E_{\mathbf{p}}(1 \mp v)}\right) , \end{aligned} \quad (4.1.31)$$

where $E_{\mathbf{p}+\mathbf{q}}$ should be replaced by

$$E_{\mathbf{p}+\mathbf{q}} = E_{\mathbf{p}} \pm q_z = E_{\mathbf{p}} + \frac{\mathbf{q}_{\perp}^2}{2E_{\mathbf{p}}(1 \mp v)}, \quad (4.1.32)$$

and

$$q^0 = \pm q_z = \frac{\mathbf{q}_{\perp}^2}{2E_{\mathbf{p}}(1 \mp v)}. \quad (4.1.33)$$

Finally, the statistical factor $(n_B(q^0) + n_F(p^0 + q^0))$ in (Equation 4.1.15) is simplified if we assume that the coupling $\alpha_s = g_s^2/(4\pi)$ is small enough that

$$q^0 = \frac{\mathbf{q}_{\perp}^2}{2E_{\mathbf{p}}(1 \mp v)} \ll T, \quad (4.1.34)$$

since we will see shortly that the typical momentum transfer is $\mathbf{q}_{\perp}^2 \sim \alpha_s eB$. Then we have at leading order

$$n_B(q^0) \approx \frac{T}{q^0} = \frac{2TE_{\mathbf{p}}(1 \mp v)}{\mathbf{q}_{\perp}^2}, \quad (4.1.35)$$

while $n_F(p^0 + q^0)$ is exponentially suppressed due to high energy limit $p^0 = E_{\mathbf{p}} \rightarrow \infty$.

Gathering all the above discussions, especially (Equation 4.1.30), (Equation 4.1.31) and (Equation 4.1.35), we finally arrive at a compact result for the scattering rate (Equation 4.1.15)

as

$$\Gamma^{single} = \sum_{\pm} (8\pi) \alpha_s C_2^J (1 \mp v) T \int \frac{d^2 \mathbf{q}_{\perp}}{(2\pi)^2} \frac{\alpha_s T_R N_F \left(\frac{eB}{2\pi} \right) e^{-\frac{\mathbf{q}_{\perp}^2}{2eB}}}{\left(\mathbf{q}_{\perp}^2 + 4\alpha_s T_R N_F \left(\frac{eB}{2\pi} \right) e^{-\frac{\mathbf{q}_{\perp}^2}{2eB}} \right)^2}, \quad (4.1.36)$$

from which we see that the lower sign case (that is, from $\delta(q^0 + q_z)$ piece in the gluon spectral density coming from the LLL quarks moving opposite to the jet direction) gives the dominant contribution in high energy limit $v \rightarrow 1$.

The condition (Equation 5.0.13) we assumed is perfectly fine for the lower sign case (that is, $(1 + v)$, or $\delta(q^0 + q_z)$ case) in high energy limit: $v \rightarrow 1$ and $E_{\mathbf{p}} = M\gamma \rightarrow \infty$. For the uppers sign case, (Equation 5.0.13) will eventually be violated in ultra-high energy limit when

$$\gamma(1 - v) \sim \sqrt{1 - v} \lesssim \frac{\mathbf{q}_{\perp}^2}{TM} \approx \frac{\alpha_s eB}{TM}, \quad (4.1.37)$$

but in this case, $n_B(q^0) \sim e^{-q^0/T} \ll 1$ is exponentially suppressed anyway. Therefore, we always get the dominant contribution from the $\delta(q^0 + q_z)$ piece in the gluon spectral density in high energy limit $v \rightarrow 1$, while $\delta(q^0 - q_z)$ contribution is sub-leading. We will keep only the dominant contribution in the following.

From (Equation 4.1.36), we get the sought-for differential scattering rate of the jet with the LLL quarks

$$\frac{d\Gamma^{single}}{d^2\mathbf{q}_{\perp}} = \frac{2}{\pi} \alpha_s C_2^J (1 + v) T \frac{\alpha_s T_R N_F \left(\frac{eB}{2\pi}\right) e^{-\frac{\mathbf{q}_{\perp}^2}{2eB}}}{\left(\mathbf{q}_{\perp}^2 + 4\alpha_s T_R N_F \left(\frac{eB}{2\pi}\right) e^{-\frac{\mathbf{q}_{\perp}^2}{2eB}}\right)^2}, \quad (4.1.38)$$

and the jet quenching parameter to complete leading order in α_s is finally computed as

$$\hat{q} \equiv \frac{1}{v} \int d^2\mathbf{q}_{\perp} \frac{d\Gamma^{single}}{d^2\mathbf{q}_{\perp}} \mathbf{q}_{\perp}^2 = \frac{1}{\pi} (1 + 1/v) C_2^J T_R N_F \alpha_s^2 (eB) T \left(\log(1/\alpha_s) - 1 - \gamma_E - \log(T_R N_F / \pi) \right), \quad (4.1.39)$$

where $\gamma_E \approx 0.577$ and the leading logarithm is produced from the range

$$\alpha_s eB \ll \mathbf{q}_\perp^2 \ll eB. \quad (4.1.40)$$

In getting the above complete leading order result (leading log and the constant under the log), we used the standard technique (183) of introducing the intermediate scale $\sqrt{\alpha_s eB} \ll q^* \ll \sqrt{eB}$, and divide the integral into two separate regions $|\mathbf{q}_\perp| < q^*$ and $|\mathbf{q}_\perp| > q^*$ where the integrand simplifies to leading order in q^*/\sqrt{eB} and $\sqrt{\alpha_s eB}/q^*$ (see the next section for a more detailed example of the same technique). It is interesting to point out that the UV cut-off is provided by the inverse size of the LLL levels, \sqrt{eB} , from the exponential term $e^{-\frac{\mathbf{q}_\perp^2}{2eB}}$, which is naturally expected since the LLL states cannot provide or absorb transverse momentum greater than this. It should be also remarked that the jet-quenching parameter from the LLL states is finite in the infinite energy limit of $v \rightarrow 1$.

\hat{q} when the jet is perpendicular to the magnetic field

Let us next consider the case where the jet is moving perpendicular to the magnetic field direction. We choose the magnetic field to point to \hat{z} , and the jet to move to \hat{x} direction: $\mathbf{p} = p_x \hat{x}$. What we mean by \mathbf{q}_\perp in the gluon spectral density (Equation 4.1.23) is then $\mathbf{q}_\perp = (q_x, q_y)$, while the parallel component is $Q_\parallel = (q^0, q_z)$. The transverse directions to the jet is (q_y, q_z) , and recall that \hat{q} is defined as a momentum diffusion constant in this transverse space.

The definition of \hat{q} assumes a rotational symmetry around the jet direction \hat{x} , which is clearly broken by the magnetic field along \hat{z} . This means that the transverse momentum diffusion of

the jet along \hat{z} will in general be different from the diffusion along \hat{y} direction. Let us denote the momentum diffusion along \hat{z} as \hat{q}_z , and along \hat{y} as \hat{q}_y . The original definition of \hat{q} assuming the rotational invariance is the sum of momentum diffusion constants along the two transverse directions: $\hat{q} = \hat{q}_z + \hat{q}_y$. The asymmetry in the momentum diffusion constants should affect the BDMPS-Z gluon Bremsstrahlung emission pattern in interesting ways to have an azimuthal asymmetry in the gluon emission spectrum.

From (Equation 4.1.15) with (Equation 4.1.23) and (Equation 4.1.25), we need to compute $S^{\alpha\beta}Q_{\parallel\alpha}Q_{\parallel\beta} = S^{\alpha\beta}Q_{\perp\alpha}Q_{\perp\beta}$ where we again used the Ward identity. We have

$$\begin{aligned} S^{\alpha\beta}Q_{\perp\alpha}Q_{\perp\beta} &= \frac{1}{E_{\mathbf{p}}E_{\mathbf{p}+\mathbf{q}}} (2(P \cdot Q_{\perp})((P+Q) \cdot Q_{\perp}) - (P \cdot Q)Q_{\perp}^2) \\ &= \frac{1}{E_{\mathbf{p}}E_{\mathbf{p}+\mathbf{q}}} \left(2(p_x q_x)(p_x q_x + q_x^2 + q_y^2) + \frac{1}{2} (q_x^2 + q_y^2)^2 \right), \end{aligned} \quad (4.1.41)$$

where we used the on-shell condition $2P \cdot Q + Q^2 = 0$ as well as $Q_{\parallel}^2 = 0$ from (Equation 4.1.23).

We will consider a high jet energy limit such that

$$p_x \sim M\gamma \gg \sqrt{eB} \gg T, \quad (4.1.42)$$

and since we will see later that $Q \lesssim \sqrt{eB}$, this means that the jet energy is much larger than the momentum transfer: $p_x \sim E_{\mathbf{p}} \gg Q$. Then (Equation 4.1.41) is simplified as

$$S^{\alpha\beta}Q_{\perp\alpha}Q_{\perp\beta} \approx 2q_x^2 \frac{p_x^2}{E_{\mathbf{p}}^2} = 2q_x^2 v^2, \quad (4.1.43)$$

where $v = p_x/E_{\mathbf{p}}$ is the velocity of the jet.

As before, the gluon spectral density (Equation 4.1.23) has two separate pieces, each from $\delta(q^0 \mp q_z)$ (see (Equation 4.1.24)). Performing q^0 integration simply replaces q^0 with $\pm q_z$. Then the energy δ -function in (Equation 4.1.15) becomes after some algebra

$$\begin{aligned}
& \delta\left(p^0 + q^0 - \sqrt{(\mathbf{p} + \mathbf{q})^2 + M^2}\right) = \delta\left(\sqrt{p_x^2 + M^2} \pm q_z - \sqrt{(p_x + q_x)^2 + q_y^2 + q_z^2 + M^2}\right) \\
& = \frac{(E_{\mathbf{p}} \pm q_z)}{\sqrt{p_x^2 \pm 2q_z E_{\mathbf{p}} - q_y^2}} \left(\delta(q_x + p_x - \sqrt{p_x^2 \pm 2q_z E_{\mathbf{p}} - q_y^2}) + \delta(q_x + p_x + \sqrt{p_x^2 \pm 2q_z E_{\mathbf{p}} - q_y^2}) \right) \\
& \sim \frac{(E_{\mathbf{p}} \pm q_z)}{\sqrt{p_x^2 \pm 2q_z E_{\mathbf{p}} - q_y^2}} \delta(q_x + p_x - \sqrt{p_x^2 \pm 2q_z E_{\mathbf{p}} - q_y^2}), \tag{4.1.44}
\end{aligned}$$

where in the final form, we dropped the second δ -function, since it would give no contribution due to $Q \ll p_x$. On the other hand, the first δ -function will put q_x to be

$$q_x = \sqrt{p_x^2 \pm 2q_z E_{\mathbf{p}} - q_y^2} - p_x = \frac{\pm 2q_z E_{\mathbf{p}} - q_y^2}{\sqrt{p_x^2 \pm 2q_z E_{\mathbf{p}} - q_y^2} + p_x} \approx \pm q_z \frac{E_{\mathbf{p}}}{p_x} = \pm \frac{q_z}{v}, \tag{4.1.45}$$

where we used $p_x \gg Q$ as before. Since q_x is along the jet direction, while we are interested in computing the transverse momentum diffusion along \hat{z} and \hat{y} (\hat{q}_z and \hat{q}_y), we should integrate over q_x at this stage, and the above energy δ -function simply replaces q_x with $\pm q_z/v$ at leading order. The Jacobian in front of the δ -function (Equation 4.1.44) also simplifies as

$$\frac{(E_{\mathbf{p}} \pm q_z)}{\sqrt{p_x^2 \pm 2q_z E_{\mathbf{p}} - q_y^2}} \approx \frac{E_{\mathbf{p}}}{p_x} = \frac{1}{v}. \tag{4.1.46}$$

With all these, the (Equation 4.1.43) becomes

$$S^{\alpha\beta} Q_{\perp\alpha} Q_{\perp\beta} \approx 2q_x^2 v^2 \approx 2q_z^2, \quad (4.1.47)$$

and the jet scattering rate is given by

$$\Gamma^{single} \approx \sum_{\pm} \frac{2}{\pi v} \alpha_s C_2^J \int dq_z \int dq_y n_B(\pm q_z)(\pm q_z) \frac{\alpha_s T_R N_F \left(\frac{eB}{2\pi} \right) e^{-\frac{(q_z^2/v^2 + q_y^2)}{2eB}}}{\left(\frac{q_z^2}{v^2} + q_y^2 + 4\alpha_s T_R N_F \left(\frac{eB}{2\pi} \right) e^{-\frac{(q_z^2/v^2 + q_y^2)}{2eB}} \right)^2}. \quad (4.1.48)$$

For the lower sign (that is coming from $\delta(q^0 + q_z)$ piece in the gluon spectral density), we can simply change the variable from q_z to $-q_z$ to get the same expression to the upper sign case, which means that the LLL states moving along or opposite directions to the magnetic field give the same contributions to the jet scattering rate and hence to the momentum diffusion constants. Therefore, the total scattering rate should be twice of the one with the upper sign and the differential scattering rate we can use in order to compute the momentum diffusion constants is finally given as

$$\frac{d\Gamma^{single}}{dq_y dq_z} \approx \frac{4}{\pi v} \alpha_s C_2^J n_B(q_z) q_z \frac{\alpha_s T_R N_F \left(\frac{eB}{2\pi} \right) e^{-\frac{(q_z^2/v^2 + q_y^2)}{2eB}}}{\left(\frac{q_z^2}{v^2} + q_y^2 + 4\alpha_s T_R N_F \left(\frac{eB}{2\pi} \right) e^{-\frac{(q_z^2/v^2 + q_y^2)}{2eB}} \right)^2}, \quad (4.1.49)$$

which is our starting point of computing the jet quenching parameters \hat{q}_z and \hat{q}_y in high energy limit:

$$\hat{q}_z = \frac{1}{v} \int dq_y \int dq_z q_z^2 \frac{d\Gamma^{single}}{dq_y dq_z}, \quad \hat{q}_y = \frac{1}{v} \int dq_y \int dq_z q_y^2 \frac{d\Gamma^{single}}{dq_y dq_z}. \quad (4.1.50)$$

One aspect of the above result (Equation 4.1.49) is that it contains the vacuum contribution which can be obtained in $T \rightarrow 0$ limit. In $T \rightarrow 0$ limit, we have

$$n_B(q_z) \rightarrow -\Theta(-q_z), \quad T \rightarrow 0, \quad (4.1.51)$$

which restricts the integral to $q^0 = q_z < 0$ region. The $q^0 < 0$ means that the jet gives the energy to the LLL states, and it is not difficult to find that the only way this is possible in the vacuum is a pair-creation of quark and antiquark pair from the vacuum. In the presence of the magnetic field with the 1+1 dimensional dispersion relation of LLL quarks, this pair-creation by the jet energy transfer to LLL states is consistent with the on-shell kinematics, which gives a finite contribution to the jet scattering rate even in the vacuum, as is given by (Equation 4.1.49) with $n_B(q_z) \rightarrow -\Theta(-q_z)$.

We first compute these vacuum contributions to \hat{q}_z and \hat{q}_y . We show some details for \hat{q}_z^{vacuum} and the computation for \hat{q}_y^{vacuum} is nearly identical. We have

$$\hat{q}_z^{vacuum} = \frac{4}{\pi v^2} \alpha_s C_2^J \int_{-\infty}^{\infty} dq_y \int_{-\infty}^0 dq_z (-q_z)^3 \frac{\alpha_s T_R N_F \left(\frac{eB}{2\pi} \right) e^{-\frac{(q_z^2/v^2 + q_y^2)}{2eB}}}{\left(\frac{q_z^2}{v^2} + q_y^2 + 4\alpha_s T_R N_F \left(\frac{eB}{2\pi} \right) e^{-\frac{(q_z^2/v^2 + q_y^2)}{2eB}} \right)^2}. \quad (4.1.52)$$

Changing $q_z \rightarrow vq_z$, and working in the polar coordinate system of (q_z, q_y) plane, (q, θ) , we have

$$\hat{q}_z^{vacuum} = \frac{4v^2}{\pi} \alpha_s C_2^J \int_{\pi/2}^{3\pi/2} d\theta (-\cos \theta)^3 \int_0^\infty dq q^4 \frac{\alpha_s T_R N_F \left(\frac{eB}{2\pi}\right) e^{-\frac{q^2}{2eB}}}{\left(q^2 + 4\alpha_s T_R N_F \left(\frac{eB}{2\pi}\right) e^{-\frac{q^2}{2eB}}\right)^2}. \quad (4.1.53)$$

Without the exponential factor in the numerator, the q integral is linearly divergent in large q limit, so the exponential factor in the numerator provides a relevant UV cutoff, which implies that the dominant leading contribution to the final result comes from the region $q^2 \sim eB$. Then in the denominator, one can safely neglect the Debye mass term which is $m_{D,B}^2 \sim \alpha_s eB \ll eB \sim q^2$ compared to q^2 at leading order computation. This brings us to leading order

$$\begin{aligned} \hat{q}_z^{vacuum} &= \frac{4v^2}{\pi} \alpha_s C_2^J \int_{\pi/2}^{3\pi/2} d\theta (-\cos \theta)^3 \int_0^\infty dq \alpha_s T_R N_F \left(\frac{eB}{2\pi}\right) e^{-\frac{q^2}{2eB}} \\ &= \frac{16v^2}{3(2\pi)^{3/2}} C_2^J T_R N_F \alpha_s^2 (eB)^{3/2}. \end{aligned} \quad (4.1.54)$$

The next-to-leading order correction is further suppressed by an additional factor of $\sqrt{\alpha_s}$ coming from the region $q \sim \sqrt{\alpha_s eB}$. The almost same computation gives the leading order vacuum contribution to \hat{q}_y as

$$\begin{aligned} \hat{q}_y^{vacuum} &= \frac{4}{\pi} \alpha_s C_2^J \int_{\pi/2}^{3\pi/2} d\theta (-\cos \theta \sin^2 \theta) \int_0^\infty dq \alpha_s T_R N_F \left(\frac{eB}{2\pi}\right) e^{-\frac{q^2}{2eB}} \\ &= \frac{8}{3(2\pi)^{3/2}} C_2^J T_R N_F \alpha_s^2 (eB)^{3/2}. \end{aligned} \quad (4.1.55)$$

We see that $\hat{q}_z^{vacuum} \neq \hat{q}_y^{vacuum}$ at leading order, which implies that the momentum diffusion in the transverse space of the jet direction is asymmetric.

Next, we would like to compute the thermal contributions at finite temperature T . This can be obtained by subtracting the vacuum contribution from (Equation 4.1.49):

$$\frac{d\Gamma_{thermal}^{single}}{dq_y dq_z} \approx \frac{4}{\pi v} \alpha_s C_2^J (n_B(q_z) + \Theta(-q_z)) q_z \frac{\alpha_s T_R N_F \left(\frac{eB}{2\pi}\right) e^{-\frac{(q_z^2/v^2 + q_y^2)}{2eB}}}{\left(\frac{q_z^2}{v^2} + q_y^2 + 4\alpha_s T_R N_F \left(\frac{eB}{2\pi}\right) e^{-\frac{(q_z^2/v^2 + q_y^2)}{2eB}}\right)^2}. \quad (4.1.56)$$

From the fact that

$$n_B(q_z) + \Theta(-q_z) \approx \text{sgn}(q_z) e^{-|q_z|/T}, \quad |q_z| \gg T, \quad (4.1.57)$$

the integration range of q_z is effectively confined into $|q_z| \lesssim T$. Then, due to the hierarchy we are assuming $eB \gg T^2$, we can replace the exponent $e^{-\frac{q_z^2/v^2}{2eB}}$ with 1 at leading order in $T^2/eB \ll 1$:

$$\frac{d\Gamma_{thermal}^{single}}{dq_y dq_z} \approx \frac{4}{\pi v} \alpha_s C_2^J (n_B(q_z) + \Theta(-q_z)) q_z \frac{\alpha_s T_R N_F \left(\frac{eB}{2\pi}\right) e^{-\frac{q_y^2}{2eB}}}{\left(\frac{q_z^2}{v^2} + q_y^2 + 4\alpha_s T_R N_F \left(\frac{eB}{2\pi}\right) e^{-\frac{q_y^2}{2eB}}\right)^2}. \quad (4.1.58)$$

There are three important scales in the above result: 1) $\sqrt{\alpha_s eB}$ which sets the scale of Debye screening mass (that appears in the denominator) which serves an IR cut-off, 2) the temperature T that enters $n_B(q_z) + \Theta(-q_z)$, 3) \sqrt{eB} that gives the ultimate UV cutoff by the exponential suppression $e^{-\frac{q_y^2}{2eB}}$. Recall that our assumption on hierarchy of scales is $\sqrt{\alpha_s eB} \ll T \ll \sqrt{eB}$.

It can be easily seen from the q_y integral in (Equation 6.1.13) that the leading contribution comes from the region

$$|q_y| \sim \sqrt{q_z^2/v^2 + \alpha_s eB} \lesssim T. \quad (4.1.59)$$

This is because q_y integral is UV convergent for both \hat{q}_z and \hat{q}_y due to the denominator, independent of the existence of the $e^{-\frac{q_y^2}{2eB}}$ term. Therefore, to leading order in T^2/eB we again can replace $e^{-\frac{q_y^2}{2eB}}$ with 1, and we finally have

$$\frac{d\Gamma_{thermal}^{single}}{dq_y dq_z} \approx \frac{4}{\pi v} \alpha_s C_2^J (n_B(q_z) + \Theta(-q_z)) q_z \frac{\alpha_s T_R N_F \left(\frac{eB}{2\pi}\right)}{\left(\frac{q_z^2}{v^2} + q_y^2 + 4\alpha_s T_R N_F \left(\frac{eB}{2\pi}\right)\right)^2}, \quad (4.1.60)$$

valid at leading order. This means that the ultimate UV cutoff, \sqrt{eB} , does not play a role at leading order in T^2/eB , and the leading order result comes from the softer scale dynamics between $\sqrt{\alpha_s eB}$ and T .

Let us show some details of our computation of \hat{q}_z with (Equation 4.1.60) at complete leading order in α_s (that is, the leading log as well as the constant under the log):

$$\begin{aligned} \hat{q}_z^{thermal} &\equiv \frac{4}{\pi v^2} \alpha_s C_2^J \int dq_z \int dq_y (n_B(q_z) + \Theta(-q_z)) q_z^3 \frac{\alpha_s T_R N_F \left(\frac{eB}{2\pi}\right)}{\left(\frac{q_z^2}{v^2} + q_y^2 + 4\alpha_s T_R N_F \left(\frac{eB}{2\pi}\right)\right)^2} \\ &= \frac{2}{v^2} \alpha_s^2 C_2^J T_R N_F \left(\frac{eB}{2\pi}\right) \int dq_z (n_B(q_z) + \Theta(-q_z)) q_z^3 \frac{1}{\left(\frac{q_z^2}{v^2} + 4\alpha_s T_R N_F \left(\frac{eB}{2\pi}\right)\right)^{\frac{3}{2}}}, \end{aligned} \quad (4.1.61)$$

where we performed the q_y integration in the last line. It is not difficult to see from the above that the remaining q_z integral produces the logarithm between the IR cutoff $\sqrt{\alpha_s eB}$ and the UV

cutoff T . To handle this, we follow the standard technique (183) of introducing an intermediate scale q^* between $\sqrt{\alpha_s e B}$ and T (that is, $\sqrt{\alpha_s e B} \ll q^* \ll T$), and divide the q_z integral into $|q_z| < q^*$ and $|q_z| > q^*$. In the first integral of $|q_z| < q^*$, since $|q_z| \ll T$ we can replace to leading order

$$n_B(q_z) + \Theta(-q_z) \approx \frac{T}{q_z}, \quad (4.1.62)$$

and we have

$$\begin{aligned} & \frac{2}{v^2} \alpha_s^2 C_2^J T_R N_F \left(\frac{eB}{2\pi} \right) T \int_{-q^*}^{q^*} dq_z q_z^2 \frac{1}{\left(\frac{q_z^2}{v^2} + 4\alpha_s T_R N_F \left(\frac{eB}{2\pi} \right) \right)^{\frac{3}{2}}} \\ &= 2v\alpha_s^2 C_2^J T_R N_F \left(\frac{eB}{2\pi} \right) T \left(\log \left(\frac{(q^*)^2}{\alpha_s T_R N_F \left(\frac{eB}{2\pi} \right) v^2} \right) - 2 + O \left(\frac{\alpha_s e B}{(q^*)^2} \right) \right). \end{aligned} \quad (4.1.63)$$

In the other region of $|q_z| > q^*$, we instead have $|q_z| \gg \sqrt{\alpha_s e B}$, so we can ignore the Debye mass in the denominator at leading order to have

$$\begin{aligned} & 2v\alpha_s^2 C_2^J T_R N_F \left(\frac{eB}{2\pi} \right) \int_{|q_z| > q^*} dq_z (n_B(q_z) + \Theta(-q_z)) \operatorname{sgn}(q_z) \\ &= 2v\alpha_s^2 C_2^J T_R N_F \left(\frac{eB}{2\pi} \right) T \left(\log \left(\frac{T^2}{(q^*)^2} \right) + O \left(\frac{q^*}{T} \right) \right). \end{aligned} \quad (4.1.64)$$

Combining the two regions (Equation 4.1.63) and (Equation 4.1.64), we finally have the thermal contribution to $\hat{q}_z^{thermal}$ at complete leading order as

$$\hat{q}_z^{thermal} = \frac{1}{\pi} v C_2^J T_R N_F \alpha_s^2 (eB) T \left(\log \left(\frac{T^2}{\alpha_s T_R N_F \left(\frac{eB}{2\pi} \right) v^2} \right) - 2 \right), \quad (4.1.65)$$

to leading order in α_s and $\alpha_s eB/T^2$. Recall our assumed hierarchy of scales $\alpha_s eB \ll T^2 \ll eB$.

A similar computation can be done for $\hat{q}_y^{thermal}$:

$$\begin{aligned} \hat{q}_y^{thermal} &\equiv \frac{4}{\pi v^2} \alpha_s C_2^J \int dq_z \int dq_y (n_B(q_z) + \Theta(-q_z)) q_z q_y^2 \frac{\alpha_s T_R N_F \left(\frac{eB}{2\pi} \right)}{\left(\frac{q_z^2}{v^2} + q_y^2 + 4\alpha_s T_R N_F \left(\frac{eB}{2\pi} \right) \right)^2} \\ &= \frac{2}{v^2} \alpha_s^2 C_2^J T_R N_F \left(\frac{eB}{2\pi} \right) \int dq_z (n_B(q_z) + \Theta(-q_z)) q_z \frac{1}{\left(\frac{q_z^2}{v^2} + 4\alpha_s T_R N_F \left(\frac{eB}{2\pi} \right) \right)^{\frac{1}{2}}} . \end{aligned} \quad (4.1.66)$$

From the region $|q_z| < q^*$ we have

$$\begin{aligned} &\frac{2}{v^2} \alpha_s^2 C_2^J T_R N_F \left(\frac{eB}{2\pi} \right) T \int_{-q^*}^{q^*} dq_z \frac{1}{\left(\frac{q_z^2}{v^2} + 4\alpha_s T_R N_F \left(\frac{eB}{2\pi} \right) \right)^{\frac{1}{2}}} \\ &= \frac{2}{v} \alpha_s^2 C_2^J T_R N_F \left(\frac{eB}{2\pi} \right) T \left(\log \left(\frac{(q^*)^2}{\alpha_s T_R N_F \left(\frac{eB}{2\pi} \right) v^2} \right) + O \left(\frac{\alpha_s eB}{(q^*)^2} \right) \right) . \end{aligned} \quad (4.1.67)$$

and from the region $|q_z| > q^*$ we have

$$\begin{aligned} &\frac{2}{v} \alpha_s^2 C_2^J T_R N_F \left(\frac{eB}{2\pi} \right) \int_{|q_z| > q^*} dq_z (n_B(q_z) + \Theta(-q_z)) \operatorname{sgn}(q_z) \\ &= \frac{2}{v} \alpha_s^2 C_2^J T_R N_F \left(\frac{eB}{2\pi} \right) T \left(\log \left(\frac{T^2}{(q^*)^2} \right) + O \left(\frac{q^*}{T} \right) \right) . \end{aligned} \quad (4.1.68)$$

so the final result for $\hat{q}_y^{thermal}$ at complete leading order is given by

$$\hat{q}_y^{thermal} = \frac{1}{\pi v} C_2^J T_R N_F \alpha_s^2 (eB) T \left(\log \left(\frac{T^2}{\alpha_s T_R N_F \left(\frac{eB}{2\pi} \right) v^2} \right) + 0 \right) , \quad (4.1.69)$$

where by 0 in the above, we mean there is no other constant under the log than what is shown in the above result.

Comparing (Equation 4.1.65) and (Equation 4.1.69), we see that $\hat{q}_z^{thermal}$ and $\hat{q}_y^{thermal}$ are in general different, but in the high energy limit $v \rightarrow 1$, they differ only by a constant under the log, while they become equal at leading log order in $T^2/(\alpha_s eB)$.

In summary, the sum of the vacuum and thermal contributions to the \hat{q}_z and \hat{q}_y is given by

$$\begin{aligned}\hat{q}_z &= \frac{16v^2}{3(2\pi)^{3/2}} C_2^J T_R N_F \alpha_s^2 (eB)^{3/2} + \frac{1}{\pi} v C_2^J T_R N_F \alpha_s^2 (eB) T \left(\log \left(\frac{T^2}{\alpha_s T_R N_F \left(\frac{eB}{2\pi}\right) v^2} \right) - 2 \right), \\ \hat{q}_y &= \frac{8}{3(2\pi)^{3/2}} C_2^J T_R N_F \alpha_s^2 (eB)^{3/2} + \frac{1}{\pi v} C_2^J T_R N_F \alpha_s^2 (eB) T \left(\log \left(\frac{T^2}{\alpha_s T_R N_F \left(\frac{eB}{2\pi}\right) v^2} \right) + 0 \right).\end{aligned}\tag{4.1.70}$$

We should note that the next-to-leading order correction to the vacuum contribution (the first term in the above) is further suppressed by $\sqrt{\alpha_s}$ compared to the leading order (see the previous discussion below (Equation 4.1.54)), so it is sub-leading by $\sqrt{\alpha_s eB}/T \ll 1$ compared to the leading order result from the thermal contributions (the second term in the above). Therefore, the above two terms indeed represent the first two leading terms in our assumed hierarchy of scales $\alpha_s eB \ll T^2 \ll eB$.

4.2 Jet Quenching Parameter at Strong Coupling

We compute our jet quenching parameter in strong magnetic field in the AdS/CFT correspondence. We use two well-established methods in literature corresponding to the two different definitions of the jet quenching parameter, albeit the fact that these two definitions agree with

each other at weak coupling regime: 1) the first definition is what we have used in our computation at weak coupling, that is, the transverse momentum diffusion constant, $\hat{q} = \frac{d\langle \mathbf{p}_\perp^2 \rangle}{dz}$, 2) the second definition is in terms of a light-like Wilson loop (179) with a transverse spatial separation \mathbf{b}_\perp in small \mathbf{b}_\perp limit behaving as $\langle W(\mathbf{b}_\perp)^\dagger W(\mathbf{0}) \rangle \sim \exp[-\frac{1}{4\sqrt{2}}\hat{q}\mathbf{b}_\perp^2 x^+]$ where x^+ is the light-like extension of the loop. To see the equivalence heuristically at weak coupling (we will not be precise about color factors and normalizations), let's prepare a fast moving initial state with a transverse momentum \mathbf{p}_\perp written in the position basis $|\mathbf{x}_\perp\rangle$ as

$$|\mathbf{p}_\perp\rangle = \frac{1}{\sqrt{S_\perp}} \int d^2\mathbf{x}_\perp e^{i\mathbf{p}_\perp \cdot \mathbf{x}_\perp} |\mathbf{x}_\perp\rangle, \quad (4.2.71)$$

where S_\perp is the transverse area put to normalize the state. After traversing the light-like distance x^+ , each state $|\mathbf{x}_\perp\rangle$ in the eikonal approximation will pick-up the Wilson line $W(\mathbf{x}_\perp)$, so the final state becomes

$$|\psi_f\rangle = \frac{1}{\sqrt{S_\perp}} \int d^2\mathbf{x}_\perp e^{i\mathbf{p}_\perp \cdot \mathbf{x}_\perp} W(\mathbf{x}_\perp) |\mathbf{x}_\perp\rangle, \quad (4.2.72)$$

and the transition S-matrix to the state with additional momentum kick \mathbf{q}_\perp is

$$\langle \mathbf{p}_\perp + \mathbf{q}_\perp | \psi_f \rangle = \frac{1}{S_\perp} \int d^2\mathbf{x}_\perp e^{-i\mathbf{q}_\perp \cdot \mathbf{x}_\perp} W(\mathbf{x}_\perp). \quad (4.2.73)$$

Then, the probability distribution of transverse momentum $P(\mathbf{q}_\perp)$ after traversing the light distance x^+ becomes

$$P(\mathbf{q}_\perp, x^+) = |\langle \mathbf{p}_\perp + \mathbf{q}_\perp | \psi_f \rangle|^2 = \frac{1}{S_\perp} \int d^2 \mathbf{b}_\perp e^{i \mathbf{q}_\perp \cdot \mathbf{b}_\perp} \langle W(\mathbf{b}_\perp)^\dagger W(\mathbf{0}) \rangle, \quad (4.2.74)$$

where we have used the translational invariance in the transverse space. If the Wilson loop behaves as $\langle W(\mathbf{b}_\perp)^\dagger W(\mathbf{0}) \rangle \sim \exp[-\frac{1}{4\sqrt{2}} \hat{q} \mathbf{b}_\perp^2 x^+]$, the distribution evolves in time (or space z) as

$$\begin{aligned} \frac{\partial P(\mathbf{q}_\perp, x^+)}{\partial z} &= \sqrt{2} \frac{\partial P(\mathbf{q}_\perp, x^+)}{\partial x^+} = \frac{\hat{q}}{4} \frac{1}{S_\perp} \int d^2 \mathbf{b}_\perp (-\mathbf{b}_\perp^2) e^{i \mathbf{q}_\perp \cdot \mathbf{b}_\perp} \langle W(\mathbf{b}_\perp)^\dagger W(\mathbf{0}) \rangle \\ &= \frac{\hat{q}}{4} \frac{1}{S_\perp} \int d^2 \mathbf{b}_\perp (\nabla_{\mathbf{q}_\perp}^2 e^{i \mathbf{q}_\perp \cdot \mathbf{b}_\perp}) \langle W(\mathbf{b}_\perp)^\dagger W(\mathbf{0}) \rangle \\ &= \frac{\hat{q}}{4} \nabla_{\mathbf{q}_\perp}^2 \frac{1}{S_\perp} \int d^2 \mathbf{b}_\perp e^{i \mathbf{q}_\perp \cdot \mathbf{b}_\perp} \langle W(\mathbf{b}_\perp)^\dagger W(\mathbf{0}) \rangle = \frac{\hat{q}}{4} \nabla_{\mathbf{q}_\perp}^2 P(\mathbf{q}_\perp, x^+), \end{aligned} \quad (4.2.75)$$

which is precisely the Fokker-Planck equation coming from the random momentum kicks with the momentum diffusion constant \hat{q} , showing the equivalence of the two definitions.

We compute \hat{q} via the definition of 1) in the AdS/CFT correspondence using a single string world-sheet moving with a velocity v ; the method developed in Refs (184; 341). The momentum diffusion constant is identified from the low frequency limit of the spectral density of color electric field correlators in real-time Schwinger-Keldysh formalism, quite similar to conductivity for current operators. In operator-field mapping in the AdS/CFT, the color electric field operator maps to the transverse displacement of the string world-sheet. Since the low frequency limit of spectral density in AdS/CFT correspondence is given solely by event-horizon properties via membrane paradigm (6), we will skip the details already present in literature, and simply apply

the known expression to our situation with strong magnetic field. The same universality has also been derived by holographic RG formalism in low frequency limit.

We also compute \hat{q} in the definition of 2) from the light-like Wilson loops; the method used in Ref.(343; 187). As is the case without magnetic field in literature, the definition 2) gives a different result from that from 1), which still seems to be an open issue.

The black-hole geometry in AdS space with a magnetic field in z direction takes a form

$$ds^2 = g_{zz}(-f(r)dt^2 + dz^2) + g_{xx}(dx^2 + dy^2) + \frac{1}{p(r)}dr^2. \quad (4.2.76)$$

The Hawking temperature T of the black hole which is identified with the field theory temperature is

$$T = \frac{1}{4\pi} \sqrt{g_{zz}(r_h) f'(r_h) p'(r_h)}, \quad (4.2.77)$$

where r_h is the radius of the black hole horizon which solves $f(r_h) = 0$. In the presence of a strong magnetic field $B \gg T^2$ in the bulk, the black hole metric (Equation 4.2.76) takes the particular form for the region $r \ll \sqrt{B}R^2$ where the scale is much smaller than the magnetic field (280)

$$ds^2 = \frac{r^2}{\mathcal{R}^2} (-f(r)dt^2 + dz^2) + \mathcal{R}^2 \mathcal{B}(dx^2 + dy^2) + \frac{1}{\frac{r^2}{\mathcal{R}^2} f(r)} dr^2, \quad (4.2.78)$$

where $f(r) = 1 - \frac{r_h^2}{r^2}$ with the horizon corresponding to $r = r_h$, and $R^4 = \lambda \alpha'^2$ is the radius of the AdS_5 spacetime ($\lambda = g_{YM}^2 N_c$ is the strong coupling constant and $\alpha' = l_s^2$ is the string length scale which disappears in final physical results). The above metric is a product of 3

dimensional BTZ and trivial flat two dimensions. We identify $\mathcal{R} = \frac{R}{\sqrt{3}}$ as the radius of the AdS_3 spacetime or BTZ black hole, and $\mathcal{B} = \sqrt{3}B = \sqrt{3}F_{xy}$ as the physical magnetic field at the boundary. The Hawking temperature T of the BTZ black hole (Equation 4.2.78) is

$$T = \frac{1}{4\pi} \sqrt{g_{zz}(r_h) f'(r_h) p'(r_h)} = \frac{r_h}{2\pi \mathcal{R}^2}. \quad (4.2.79)$$

\hat{q} from transverse momentum diffusion

The transverse momentum diffusion constant $\kappa(v)$ “per unit time” of a heavy quark moving with velocity v in the strongly coupled regime at zero magnetic field, was first computed in Refs.(184; 341) for $N = 4$ Super Yang-Mills theory, and was generalized to non-conformal theories in Ref.(190). In the eikonal regime of high jet energy, there should be no distinction between heavy-quark and the jet for the momentum diffusion constant, since the scatterings would care only about its color charges. Based on this premise, we can identify

$$\hat{q}(v) = \frac{2}{v} \kappa(v), \quad (4.2.80)$$

where the factor 2 is from the definition of $\kappa(v)$: it is defined by $\langle \xi_T^i(t) \xi_T^j(t') \rangle = \kappa \delta^{ij} \delta(t - t')$,

so that

$$\kappa = \frac{1}{2} \int d^2 \mathbf{q}_\perp^2 \frac{d\Gamma}{d^2 \mathbf{q}_\perp^2} \mathbf{q}_\perp^2, \quad (4.2.81)$$

and $1/v$ is from translating $d/dz = (1/v)d/dt$.

\hat{q} when the jet is parallel to the magnetic field

In the presence of strong magnetic field parallel to the jet, the Nambu-Goto (NG) action is

$$S_{NG}^{\parallel} = \int d\tau d\sigma \mathcal{L}^{\parallel}(\bar{h}_{ab}) = -\frac{1}{2\pi\alpha'} \int d\tau d\sigma \sqrt{-\det \bar{h}_{ab}}, \quad (4.2.82)$$

where the background induced metric on the string \bar{h}_{ab} is given by

$$\bar{h}_{ab} = g_{\mu\nu} \partial_a x^{\mu}(\tau, \sigma) \partial_b x^{\nu}(\tau, \sigma). \quad (4.2.83)$$

Using the embedding $(\tau, \sigma) \Rightarrow (t(\tau, \sigma), 0, 0, z(\tau, \sigma), r = \sigma)$, the background induced metric $\bar{h}_{ab}(\dot{z}, z')$ (Equation 7.5.32) becomes $(\cdot \equiv d/d\tau, ' \equiv d/d\sigma)$

$$\bar{h}_{ab}(\dot{z}, z') = g_{tt} \partial_a t \partial_b t + g_{zz} \partial_a z \partial_b z + g_{rr} \partial_a r \partial_b r. \quad (4.2.84)$$

Using a particular Ansatz of the form $t(\tau, \sigma) = \tau + K(\sigma)$ and $z = v\tau + F(\sigma)$, which represents a “trailing string” configuration moving with velocity v , the background induced metric (Equation 7.5.33) becomes

$$\begin{aligned} \bar{h}_{\tau\tau}(v, z') &= g_{tt} + v^2 g_{zz}, \\ \bar{h}_{\sigma\sigma}(v, z') &= g_{tt} (K')^2 + g_{zz} (z')^2 + g_{rr}, \\ \bar{h}_{\tau\sigma}(v, z') &= g_{tt} K' + g_{zz} z' v. \end{aligned} \quad (4.2.85)$$

Finding the equation of motion from the action, we have

$$\partial_\sigma \left(\frac{g_{tt}g_{zz}(z' - vK')}{\sqrt{-\det \bar{h}_{ab}}} \right) = 0. \quad (4.2.86)$$

There exists a gauge freedom of re-parametrizing the world-sheet coordinate τ : $\tau \rightarrow \tau + h(\sigma)$ for any function $h(\sigma)$, under which we have the transformation $K(\sigma) \rightarrow K(\sigma) + h(\sigma)$ and $z \rightarrow z + vh(\sigma)$. Indeed, the above equation of motion is invariant under this transformation, as it should. Requiring $\bar{h}_{\tau\sigma}(v, z') = 0$ to fix this gauge freedom, we have an additional constraint $K' = -\frac{g_{zz}}{g_{tt}}z'v$, which can be used to diagonalize (Equation 7.5.34) as

$$\begin{aligned} \bar{h}_{\tau\tau}(v, z') &= -g_{zz}f \left(1 - \frac{v^2}{f}\right), \\ \bar{h}_{\sigma\sigma}(v, z') &= g_{zz} \left(1 - \frac{v^2}{f}\right) (z')^2 + g_{rr}, \\ \bar{h}_{\tau\sigma}(v, z') &= 0, \end{aligned} \quad (4.2.87)$$

while the equation of motion in this gauge becomes

$$\frac{g_{zz}^2 f}{\sqrt{-\det \bar{h}_{ab}}} \left(1 - \frac{v^2}{f}\right) z' = \text{constant} \equiv C_{zz}v. \quad (4.2.88)$$

Using $g_{rr} = \frac{1}{g_{zz}f}$ and

$$-\det \bar{h}_{ab} = -\bar{h}_{\tau\tau}(v, z')\bar{h}_{\sigma\sigma}(v, z') = g_{zz}^2 f \left(1 - \frac{v^2}{f}\right)^2 (z')^2 - \left(1 - \frac{v^2}{f}\right), \quad (4.2.89)$$

we find

$$(z')^2 = \frac{C_{zz}^2 v^2}{g_{zz}^4 f^2} \frac{1}{\left(1 - \frac{v^2}{f}\right) \left(1 - \frac{C_{zz}^2 v^2}{g_{zz}^2 f}\right)}. \quad (4.2.90)$$

Since the factor $(1 - \frac{v^2}{f})$ in (Equation 7.5.37) vanishes when $f(r_s) = v^2$, requiring $(z')^2$ to be positive across $r = r_s$, the other factor $(1 - \frac{C_{zz}^2 v^2}{g_{zz}^2 f})$ has to vanish at $r = r_s$ as well, which will fix the integration constant $C_{zz} = g_{zz}(r_s)$. Therefore, (Equation 7.5.37) becomes

$$(z')^2 = \frac{g_{zz}^2(r_s)}{g_{zz}^4(r)} \frac{v^2}{f^2(r)} \frac{1}{\left(1 - \frac{v^2}{f(r)}\right) \left(1 - \frac{g_{zz}^2(r_s)}{g_{zz}^2(r)} \frac{v^2}{f(r)}\right)}, \quad (4.2.91)$$

and using this the metric (Equation 7.5.36) is finally given by

$$\begin{aligned} \bar{h}_{\tau\tau}(v, z') &= g_{zz}(-f + v^2), \\ \bar{h}_{\sigma\sigma}(v, z') &= g_{zz} \left(\frac{1}{g_{zz}^2(r)f(r) - g_{zz}^2(r_s)v^2} \right), \\ \bar{h}_{\tau\sigma}(v, z') &= 0, \end{aligned} \quad (4.2.92)$$

which can be interpreted as a metric of a 2-dimensional black hole with a line element $ds_{(2)}^2$ given by

$$ds_{(2)}^2 = \bar{h}_{\tau\tau} d\tau^2 + \bar{h}_{\sigma\sigma} d\sigma^2 = g_{zz}(-\tilde{f}(r)) d\tau^2 + \frac{1}{\tilde{p}(r)} d\sigma^2, \quad (4.2.93)$$

where $\tilde{f}(r) = f - v^2$, $\tilde{p}(r) = [g_{zz}^2(r)f(r) - g_{zz}^2(r_s)v^2](g_{zz})^{-1}$, and the radius of the horizon r_s of the 2-dimensional black hole is found from $\tilde{f}(r_s) = 0$ or $f(r_s) = v^2$, i.e., $r_s = \gamma r_h$ where $\gamma = \frac{1}{\sqrt{1-v^2}}$.

The Hawking temperature of the 2-dimensional black hole denoted as T_s^\parallel is still given by (Equation 7.1.4) after replacing $T \rightarrow T_s^\parallel$, $f(r) \rightarrow \tilde{f}(r)$ and $p(r) \rightarrow \tilde{p}(r)$, i.e.,

$$T_s^\parallel = \frac{1}{4\pi} \sqrt{g_{zz}(r_s) \tilde{f}'(r_s) \tilde{p}'(r_s)} = \frac{r_h}{2\pi \mathcal{R}^2} \sqrt{1+v^2} = T \sqrt{1+v^2}, \quad (4.2.94)$$

where we used $\tilde{p}'(r_s) = 2g'_{zz}(r_s)v^2 + g_{zz}(r_s)f'(r_s)$ and $r_s = \gamma r_h$.

Note that the drag force acting on the heavy quark F_{drag}^\parallel is simply given by

$$F_{drag}^\parallel = \frac{\delta \mathcal{L}}{\delta z'} = -\frac{C_{zz}}{2\pi\alpha'} v = -\frac{2}{3} \pi \sqrt{\lambda} \gamma^2 T^2 v, \quad (4.2.95)$$

where we used $C_{zz} = g_{zz}(r_s)$ and $r_s = \gamma r_h$ to get the last line. This is independent of the magnetic field in our limit $B \gg T^2$. This could be interpreted as a superfluid nature of the LLL states in strong magnetic field, as discussed in Ref.(205) (see also Refs.(192; 193)).

To obtain the transverse momentum diffusion constant from the color electric field correlators, we consider the fluctuations of the dual field, that is, the fluctuations of transverse position of the string, δx . The transverse fluctuation $\delta h_{ab}(\delta \dot{x}, \delta x')$ around the background induced metric $\bar{h}_{ab}(v, z')$ (Equation 4.2.92) is given by

$$\begin{aligned} \delta h_{\tau\tau}(\delta \dot{x}, \delta x') &= g_{xx}(\delta \dot{x})^2, \\ \delta h_{\sigma\sigma}(\delta \dot{x}, \delta x') &= g_{xx}(\delta x')^2, \\ \delta h_{\tau\sigma}(\delta \dot{x}, \delta x') &= g_{xx}(\delta \dot{x} \delta x')^2. \end{aligned} \quad (4.2.96)$$

Replacing $\bar{h}_{ab}(v, z') \rightarrow \bar{h}_{ab}(v, z') + \delta h_{ab}(\delta \dot{x}, \delta x')$ in S_{NG}^{\parallel} (Equation 7.5.31), and expanding it to linear order in $\delta h_{ab}(\delta \dot{x}, \delta x')$, one finds

$$\begin{aligned}
S_{NG}^{\parallel} &= \int d\tau d\sigma \mathcal{L}^{\parallel}(\bar{h}_{ab}(v, z'), \delta h_{ab}(\delta \dot{x}, \delta x')) , \\
&= -\frac{1}{4\pi\alpha'} \int d\tau d\sigma g_{xx} \sqrt{-\det \bar{h}_{ab}(v, z')} \bar{h}^{ab}(v, z') \delta h_{ab}(\delta \dot{x}, \delta x') , \\
&= -\frac{1}{2} \int d\tau d\sigma \bar{G}_{\parallel}^{ab}(v, z') \partial_a \delta x(\tau, \sigma) \partial_b \delta x(\tau, \sigma) ,
\end{aligned} \tag{4.2.97}$$

where $\bar{G}_{\parallel}^{ab}(v, z') \equiv \frac{1}{2\pi\alpha'} g_{xx} \sqrt{-\det \bar{h}_{ab}(v, z')} \bar{h}^{ab}(v, z')$. Note that the indices a and b are raised and lowered using the background induced metric $\bar{h}_{ab}(v, z')$, and $\bar{h}^{ab}(v, z')$ is the inverse of $\bar{h}_{ab}(v, z')$.

Using the conjugate momenta $\Pi^{\parallel} = \frac{\partial \mathcal{L}^{\parallel}}{\partial \sigma \delta x}$, defining the retarded Green's function $G_R^{\parallel} \equiv -\frac{\Pi^{\parallel}}{\delta x}$ as in Ref.(6), and using the equation of motion for δx in momentum space derived from the action (Equation 4.2.97)

$$\partial_{\sigma} \bar{G}_{\parallel}^{\sigma\sigma} \partial_{\sigma} \delta x - \omega^2 \bar{G}_{\parallel}^{\tau\tau} \delta x = 0 , \tag{4.2.98}$$

one can derive the holographic RG flow equation for the retarded Green's function G_R^{\parallel} to be

$$\partial_{\sigma} G_R^{\parallel} = -\frac{(G_R^{\parallel})^2}{\bar{G}_{\parallel}^{\sigma\sigma}} + \omega^2 \bar{G}_{\parallel}^{\tau\tau} . \tag{4.2.99}$$

Since $\bar{G}_{\parallel}^{\tau\tau}$ and $\frac{1}{\bar{G}_{\parallel}^{\sigma\sigma}}$ diverge at the horizon of the 2-dimensional black hole metric, i.e., at $r = r_s$, we first note that G_R^{\parallel} vanishes at $\omega = 0$, and we expect $G_R^{\parallel} \propto \omega$ for small ω limit. Since the

right-hand side is $O(\omega^2)$, G_R^\parallel becomes a constant in σ in $\omega \rightarrow 0$ limit. Demanding the regularity of the right-hand side at the horizon, we find

$$\begin{aligned}
G_R^\parallel(\omega) &= \pm \omega \sqrt{G_\parallel^{\tau\tau} G_\parallel^{\sigma\sigma}}|_{r=r_s}, \\
&= \pm \frac{\omega}{2\pi\alpha'} g_{xx} \sqrt{-\det \bar{h}_{ab}} \sqrt{\bar{h}^{\tau\tau} \bar{h}^{\sigma\sigma}}|_{r=r_s}, \\
&= -\frac{i\omega}{2\pi\alpha'} g_{xx}(r_s),
\end{aligned} \tag{4.2.100}$$

where the negative sign is chosen for the retarded function (the positive sign would be for the advanced function). Therefore, the velocity dependent transverse momentum diffusion constant per unit time is given by (190)

$$\kappa^\parallel(v) = -2T_s^\parallel \lim_{\omega \rightarrow 0} \frac{\text{Im } G_R^\parallel(\omega)}{\omega} = \frac{T_s^\parallel}{\pi\alpha'} g_{xx}(r_s) = \frac{\sqrt{1+v^2}}{3\pi} \sqrt{\lambda} \mathcal{B} T, \tag{4.2.101}$$

where we used $g_{xx}(r_s) = \mathcal{R}^2 \mathcal{B}$, $\frac{\mathcal{R}^2}{\alpha'} = \frac{\sqrt{\lambda}}{3}$, $T_s^\parallel = T\sqrt{1+v^2}$. Finally, the jet quenching parameter $\hat{q}(v) \equiv 2\frac{\kappa^\parallel(v)}{v}$ is found to be

$$\hat{q}(v) = 2\frac{\kappa^\parallel(v)}{v} = \frac{2}{3\pi} \sqrt{1 + \frac{1}{v^2}} \sqrt{\lambda} \mathcal{B} T. \tag{4.2.102}$$

Note that when $v = 0$, $\kappa^\parallel(0)$ is identified with κ_\perp , the heavy-quark momentum diffusion constant in perpendicular direction to the magnetic field introduced in Ref.(180). Therefore, the \mathcal{B} dependence of $\kappa_\perp = \frac{1}{3\pi} \sqrt{\lambda} \mathcal{B} T$ at strong coupling is similar to $\kappa_\perp \propto \alpha_s^2(eB)T$ found in Ref.(180) at weak coupling.

\hat{q} when the jet is perpendicular to the magnetic field

We next consider a jet moving to x direction, which is perpendicular to the magnetic field direction z . We first find the trailing string background as before. Using the embedding $(\tau, \sigma) \Rightarrow (t(\tau, \sigma), x(\tau, \sigma), 0, 0, r = \sigma)$, and an Ansatz of the form $t(\tau, \sigma) = \tau + K(r)$ and $x = v\tau + F(r)$, the background induced metric becomes

$$\begin{aligned}\bar{h}_{\tau\tau}(v, x') &= g_{tt} + v^2 g_{xx}, \\ \bar{h}_{\sigma\sigma}(v, x') &= g_{tt}(K')^2 + g_{xx}(x')^2 + g_{rr}, \\ \bar{h}_{\tau\sigma}(v, x') &= g_{tt}K' + g_{xx}x'v.\end{aligned}\tag{4.2.103}$$

As in the previous subsection, requiring $\bar{h}_{\tau\sigma}(v, x') = 0$ to fix the residual gauge freedom, we have $\frac{\partial K}{\partial r} = -\frac{g_{xx}}{g_{tt}}x'v$ which can be used to diagonalize (Equation 4.2.103) as

$$\begin{aligned}\bar{h}_{\tau\tau}(v, x') &= -g_{zz}f\left(1 - \frac{v^2}{f}\frac{g_{xx}}{g_{zz}}\right), \\ \bar{h}_{\sigma\sigma}(v, x') &= g_{xx}\left(1 - \frac{v^2}{f}\frac{g_{xx}}{g_{zz}}\right)(x')^2 + g_{rr}, \\ \bar{h}_{\tau\sigma}(v, x') &= 0,\end{aligned}\tag{4.2.104}$$

while the equation of motion becomes

$$\frac{g_{xx}g_{zz}f\left(1 - \frac{v^2}{f}\frac{g_{xx}}{g_{zz}}\right)x'}{\sqrt{-\det \bar{h}_{ab}(v, x')}} = \text{constant} \equiv C_{xx}v.\tag{4.2.105}$$

Using $g_{rr} = \frac{1}{g_{zz}f}$ and

$$- \det \bar{h}_{ab}(v, x') = -\bar{h}_{\tau\tau}(v, x')\bar{h}_{\sigma\sigma}(v, x') = g_{xx}g_{zz}f \left(1 - \frac{v^2}{f} \frac{g_{xx}}{g_{zz}}\right)^2 (x')^2 - \left(1 - \frac{v^2}{f} \frac{g_{xx}}{g_{zz}}\right), \quad (4.2.106)$$

we solve (Equation 4.2.105) to obtain

$$(x')^2 = \frac{C_{xx}^2 v^2}{g_{xx}^2 g_{zz}^2 f^2} \frac{1}{\left(1 - \frac{v^2}{f} \frac{g_{xx}}{g_{zz}}\right) \left(1 - \frac{C_{xx}^2 v^2}{g_{xx} g_{zz} f}\right)}. \quad (4.2.107)$$

As before, the two factors in the denominator should vanish at the same location $r = \tilde{r}_s$, which fixes the integration constant to be $C_{xx} = g_{xx}(\tilde{r}_s) = g_{xx} = \text{constant}$. Therefore, (Equation 4.2.107) becomes

$$(x')^2 = \frac{1}{g_{zz}^2(r)} \frac{v^2}{f^2(r)} \frac{1}{\left(1 - \frac{v^2}{f(r)} \frac{g_{xx}}{g_{zz}(r)}\right)^2}, \quad (4.2.108)$$

and using this, the metric (Equation 4.2.104) finally becomes

$$\begin{aligned} \bar{h}_{\tau\tau}(v, x') &= g_{zz} \left(-f + v^2 \frac{g_{xx}}{g_{zz}} \right), \\ \bar{h}_{\sigma\sigma}(v, x') &= \frac{1}{g_{zz} \left(f - v^2 \frac{g_{xx}}{g_{zz}} \right)}, \\ \bar{h}_{\tau\sigma}(v, x') &= 0, \end{aligned} \quad (4.2.109)$$

which can be interpreted as a 2-dimensional black hole metric with a line element $ds_{(2)}^2$ given by

$$ds_{(2)}^2 = \bar{h}_{\tau\tau} d\tau^2 + \bar{h}_{\sigma\sigma} d\sigma^2 = g_{zz}(-\tilde{f}(r)) d\tau^2 + \frac{1}{\tilde{p}(r)} d\sigma^2, \quad (4.2.110)$$

where $\tilde{f}(r) = f - v^2 \frac{g_{xx}}{g_{zz}}$, $\tilde{p}(r) = g_{zz} \tilde{f}(r)$, and the radius of the horizon \tilde{r}_s of the 2-dimensional black hole is found from $\tilde{f}(\tilde{r}_s) = 0$ or $f(\tilde{r}_s) = v^2 \frac{g_{xx}}{g_{zz}(\tilde{r}_s)}$, i.e.,

$$\tilde{r}_s^2 = r_h^2 + v^2 \mathcal{R}^2 g_{xx} = v^2 \mathcal{R}^4 \mathcal{B} \left(1 + \frac{4\pi^2}{v^2} \frac{T^2}{\mathcal{B}} \right), \quad (4.2.111)$$

using $g_{xx} = \mathcal{B} \mathcal{R}^2$, $g_{zz}(\tilde{r}_s) = \frac{\tilde{r}_s^2}{\mathcal{R}^2}$, and $T = \frac{r_h}{2\pi \mathcal{R}^2}$ from (Equation 4.2.79). The Hawking temperature of this 2-dimensional black hole is given by

$$T_s^\perp = \frac{1}{4\pi} \sqrt{g_{zz}(\tilde{r}_s) \tilde{f}'(\tilde{r}_s) \tilde{p}'(\tilde{r}_s)} = \frac{g_{zz}(\tilde{r}_s) \tilde{f}'(\tilde{r}_s)}{4\pi} = \frac{v\sqrt{\mathcal{B}}}{2\pi} \left(1 + \frac{4\pi^2}{v^2} \frac{T^2}{\mathcal{B}} \right)^{1/2}. \quad (4.2.112)$$

Note that the drag force to the heavy-quark jet F_{drag}^\perp is simply given by

$$F_{drag}^\perp = \frac{\delta \mathcal{L}}{\delta x'} = -\frac{C_{xx}}{2\pi\alpha'} v = -\frac{1}{6\pi} \sqrt{\lambda} \mathcal{B} v, \quad (4.2.113)$$

where we used $C_{xx} = g_{xx}$ in the last equality. It is interesting to note that this drag force exists even at zero temperature. As we explained in the case of weak coupling, this is possible in the case of weak coupling due to the fact that it is kinematically possible to create a quark-antiquark pair from the LLL vacuum by scatterings with the jet. It is interesting that we observe the same feature even at strong coupling.

To find the transverse momentum diffusion along z direction (note that z, y are the two perpendicular directions to the jet motion), we consider fluctuations of string position along the z direction which is dual to the z component of color electric field: δz . The transverse

fluctuation $\delta h_{ab}(\delta\dot{z}, \delta z')$ around the background induced metric $\bar{h}_{ab}(v, x')$ (Equation 4.2.109) is given by

$$\begin{aligned}\delta h_{\tau\tau}(\delta\dot{z}, \delta z') &= g_{zz}(\delta\dot{z})^2, \\ \delta h_{\sigma\sigma}(\delta\dot{z}, \delta z') &= g_{zz}(\delta z')^2, \\ \delta h_{\tau\sigma}(\delta\dot{z}, \delta z') &= g_{zz}(\delta\dot{z}\delta z'),\end{aligned}\tag{4.2.114}$$

and the Nambu-Goto action is expanded to linear order in $\delta h_{ab}(\delta\dot{z}, \delta z')$ as

$$\begin{aligned}S_{NG}^\perp &= \int d\tau d\sigma \mathcal{L}^\perp(\bar{h}_{ab}(v, x'), \delta h_{ab}(\delta\dot{z}, \delta z')), \\ &= -\frac{1}{4\pi\alpha'} \int d\tau d\sigma g_{zz} \sqrt{-\det \bar{h}_{ab}(v, x')} \bar{h}^{ab}(v, x') \delta h_{ab}(\delta\dot{z}, \delta z'), \\ &= -\frac{1}{2} \int d\tau d\sigma \bar{G}_\perp^{ab}(v, x') \partial_a \delta z(\tau, \sigma) \partial_b \delta z(\tau, \sigma),\end{aligned}\tag{4.2.115}$$

where $\bar{G}_\perp^{ab}(v, x') \equiv \frac{1}{2\pi\alpha'} g_{zz} \sqrt{-\det \bar{h}_{ab}(v, x')} \bar{h}^{ab}(v, x')$. Using the conjugate momenta $\Pi^\perp = \frac{\partial \mathcal{L}^\perp}{\partial \sigma \delta z}$, defining the retarded Green's function as $G_R^\perp \equiv -\frac{\Pi^\perp}{\delta z}$, and using the equation of motion for δz in momentum space derived from the action (Equation 4.2.115)

$$\partial_\sigma \bar{G}_\perp^{\sigma\sigma} \partial_\sigma \delta z - \omega^2 \bar{G}_\perp^{\tau\tau} \delta z = 0,\tag{4.2.116}$$

one can derive the holographic RG flow equation for the retarded Green's function G_R^\perp to be

$$\partial_\sigma G_R^\perp = -\frac{(G_R^\perp)^2}{\bar{G}_\perp^{\sigma\sigma}} + \omega^2 \bar{G}_\perp^{\tau\tau}.\tag{4.2.117}$$

By the same reasoning as before, we have in small ω limit

$$\begin{aligned}
G_R^\perp(\omega) &= \pm\omega\sqrt{\overline{G}_\perp^{\tau\tau}\overline{G}_\perp^{\sigma\sigma}}|_{r=r_s}, \\
&= \pm\frac{\omega}{2\pi\alpha'}g_{zz}\sqrt{-\det\bar{h}_{ab}\sqrt{\bar{h}^{\tau\tau}\bar{h}^{\sigma\sigma}}}|_{r=\tilde{r}_s}, \\
&= -\frac{i\omega}{2\pi\alpha'}g_{zz}(\tilde{r}_s).
\end{aligned} \tag{4.2.118}$$

Therefore, the velocity dependent momentum diffusion constant along z per unit time when the jet is moving perpendicular to the magnetic field is given by

$$\kappa_z^\perp(v) = -2T_s^\perp \lim_{\omega \rightarrow 0} \frac{\text{Im } G_R^\perp(\omega)}{\omega} = \frac{T_s^\perp}{\pi\alpha'}g_{zz}(\tilde{r}_s) = \frac{v^3}{6\pi^2}\sqrt{\lambda}\mathcal{B}^{3/2} + v\sqrt{\lambda}\sqrt{\mathcal{B}}T^2, \tag{4.2.119}$$

for $\mathcal{B} \gg T^2$, where we have used $g_{zz}(\tilde{r}_s) = \frac{\tilde{r}_s^2}{\mathcal{R}^2} = v^2\mathcal{R}^2\mathcal{B}\left(1 + \frac{4\pi^2}{v^2}\frac{T^2}{\mathcal{B}}\right)$ from (Equation 4.2.111), $\frac{\mathcal{R}^2}{\alpha'} = \frac{\sqrt{\lambda}}{3}$, $T_s^\perp = \frac{v\sqrt{\mathcal{B}}}{2\pi}\left(1 + \frac{4\pi^2}{v^2}\frac{T^2}{\mathcal{B}}\right)^{1/2}$ from (Equation 4.2.112). Therefore, the jet quenching parameter $\hat{q}_z \equiv \frac{\kappa_z^\perp(v)}{v}$ is given by

$$\hat{q}_z = \frac{\kappa_z^\perp(v)}{v} = \frac{v^2}{6\pi^2}\sqrt{\lambda}\mathcal{B}^{3/2} + \sqrt{\lambda}\sqrt{\mathcal{B}}T^2, \tag{4.2.120}$$

which has a very similar structure to that at weak coupling (Equation 4.1.70). Especially, the first term is the vacuum part that exists even at zero temperature, similarly to the case at weak coupling.

Note that when $v = 0$, $g_{zz}(\tilde{r}_s) = g_{zz}(r_h) = 4\pi^2\mathcal{R}^2T^2$, and $\kappa_z^\perp(0) = \frac{T}{\pi\alpha'}g_{zz}(r_h) = \frac{4\pi}{3}\sqrt{\lambda}T^3$ is identified with κ_\parallel , the heavy-quark momentum diffusion constant along the magnetic field

introduced in Ref.(180). Therefore κ_{\parallel} at strong coupling is independent of \mathcal{B} , which is precisely same to $\kappa_{\parallel} \propto \alpha_s^2 T^3$ in Ref.(180) found at weak coupling pQCD. This seems in line with the idea of superfluid nature of LLL states in Ref.(205).

Following the same steps, one can compute the diffusion constant along the other remaining transverse direction y . We find the momentum diffusion per unit time as

$$\kappa_y^{\perp}(v) = \frac{T_s^{\perp}}{\pi\alpha'} g_{yy}(\tilde{r}_s) = \frac{T_s^{\perp}}{\pi\alpha'} g_{xx} = \frac{v}{6\pi^2} \sqrt{\lambda} \mathcal{B}^{3/2} + \frac{1}{3v} \sqrt{\lambda} \sqrt{\mathcal{B}} T^2, \quad (4.2.121)$$

for $\mathcal{B} \gg T^2$, and we finally have

$$\hat{q}_y = \frac{\kappa_y^{\perp}(v)}{v} = \frac{1}{6\pi^2} \sqrt{\lambda} \mathcal{B}^{3/2} + \frac{1}{3v^2} \sqrt{\lambda} \sqrt{\mathcal{B}} T^2. \quad (4.2.122)$$

It is interesting to compare these results in AdS/CFT, (Equation 4.2.120) and (Equation 4.2.122), with the results at weak coupling (Equation 4.1.70) computed in pQCD.

\hat{q} from light-like Wilson loop

The jet quenching parameter at strong coupling was first computed in Ref.(343; 187) at zero magnetic field using light-like Wilson loops and the AdS/CFT correspondence. See also Ref.(188) for the lattice QCD computation of the jet quenching parameter. Here, we extend the works of Ref.(343; 187) to the case with strong magnetic field by using the general formula for jet quenching parameter derived in Ref.(194). Since the computational steps are already in literature, we simply summarize the general formula and our results in the case of strong magnetic field. We emphasize that the results we obtain from this method are different from those

we obtain in the previous subsection using the heavy-quark trailing string: this discrepancy exists even in the original computations for $N = 4$ SYM without magnetic field. This might be due to possible breakdown of heavy-quark method in ultra-relativistic limit (184), although it has not been fully understood to the best of our knowledge.

\hat{q} when the jet is parallel to the magnetic field

We first make a coordinate transformation $r = \frac{\mathcal{R}^2}{u}$ to rewrite our metric (Equation 4.2.78)

as

$$ds^2 = G_{\mu\nu}dx^\mu dx^\nu = \frac{\mathcal{R}^2}{u^2} (-f(u)dt^2 + dz^2) + \mathcal{R}^2\mathcal{B}(dx^2 + dy^2) + \frac{\mathcal{R}^2}{u^2 f(u)} du^2, \quad (4.2.123)$$

where $f(u) = 1 - \frac{u^2}{u_h^2}$, the horizon corresponds to $u = u_h$, the boundary to $u = 0$, and the Hawking temperature T of the BTZ black hole (Equation 4.3.151) is

$$T = \frac{1}{2\pi u_h}. \quad (4.2.124)$$

The jet quenching parameter \hat{q} for a jet moving along the z direction (with the speed of light $v = 1$) can be directly obtained from the metric by (194),

$$\hat{q} = \frac{1}{\pi\alpha'} \left(\int_0^{u_h} du \frac{1}{G_{xx}} \sqrt{\frac{G_{uu}}{G_{tt} + G_{zz}}} \right)^{-1} = \frac{2}{3} \sqrt{\lambda} \mathcal{B} T \left(\int_0^{u_h} du \sqrt{\frac{1}{u^2 - u^4/u_h^2}} \right)^{-1}. \quad (4.2.125)$$

The integral in the above has a logarithmic UV divergence near $u = 0$, which is easy to understand. Recall that our BTZ metric (Equation 4.3.151) is valid only up to the “UV cutoff”

$u_c \approx 1/\sqrt{B}$ in the full 5 dimensional dual geometry where the energy scale $1/u$ is smaller than the scale of the magnetic field. For $u \ll u_c$, especially near the UV boundary $u = 0$, the full AdS_5 geometry takes over, which makes the above integral finite in the region $u \ll u_c$. Therefore, a large logarithm develops in the above integral between the scale $1/u_h \sim T$ and $1/u_c \sim \sqrt{B}$, and we get the leading-log result of \hat{q} as

$$\hat{q} = \frac{4}{3} \frac{\sqrt{\lambda} \mathcal{B} T}{\log(B/T^2)}. \quad (4.2.126)$$

To find the constant under the log, we need to know the exact geometry interpolating BTZ and AdS_5 , but we will not go into such detail in this work, satisfied with the above leading-log result in our assumed hierarchy $B \gg T^2$.

\hat{q} when the jet is perpendicular to the magnetic field

We compute next the jet quenching parameter when the jet is moving perpendicular to the magnetic field. As we can have two different transverse directions, one along the magnetic field, the other perpendicular to the magnetic field, we should consider the two cases separately as before. Let the magnetic field point to z direction, and the jet move to x direction.

The jet quenching parameter \hat{q}_z for the momentum broadening along the z direction is

$$\hat{q}_z = \frac{1}{2\pi\alpha'} \left(\int_{u_c}^{u_h} du \frac{1}{G_{zz}} \sqrt{\frac{G_{uu}}{G_{tt} + G_{xx}}} \right)^{-1} = \frac{\sqrt{\lambda}}{6\pi} \left(\int_{u_c}^{u_h} du \frac{u^2}{\sqrt{(\mathcal{B}u^2 - 1 + u^2/u_h^2)(1 - u^2/u_h^2)}} \right)^{-1}, \quad (4.2.127)$$

where an extra factor $1/2$ is from our definition of \hat{q}_z (such that in an isotropic case, $\hat{q} = \hat{q}_z + \hat{q}_y = 2\hat{q}_z$), and $u_c \approx 1/\sqrt{B}$ is the UV cutoff of our BTZ metric. From the above, it is easy

to see that the region $u \lesssim u_c$ gives a contribution to the integral which is of order $u_c^3 \sim (1/B)^{3/2}$, that is subleading compared to the contribution from $u_c \ll u < u_h$, where the integral becomes simplified to

$$\int_{u_c}^{u_h} du \frac{u^2}{\sqrt{(\mathcal{B}u^2 - 1 + u^2/u_h^2)(1 - u^2/u_h^2)}} \approx \frac{1}{\sqrt{\mathcal{B}}} \int_0^{u_h} du \frac{u}{\sqrt{1 - u^2/u_h^2}} = \frac{u_h^2}{\sqrt{\mathcal{B}}} = \frac{1}{4\pi^2 \sqrt{\mathcal{B}T^2}}, \quad (4.2.128)$$

so that we have a leading order expression for \hat{q}_z as

$$\hat{q}_z = \frac{2\pi}{3} \sqrt{\lambda} \sqrt{\mathcal{B}T^2}. \quad (4.2.129)$$

Similarly, the momentum broadening along y direction, \hat{q}_y , is

$$\hat{q}_y = \frac{1}{2\pi\alpha'} \left(\int_{u_c}^{u_h} du \frac{1}{G_{yy}} \sqrt{\frac{G_{uu}}{G_{tt} + G_{xx}}} \right)^{-1} = \frac{\sqrt{\lambda}\mathcal{B}}{6\pi} \left(\int_{u_c}^{u_h} du \frac{1}{\sqrt{(\mathcal{B}u^2 - 1 + u^2/u_h^2)(1 - u^2/u_h^2)}} \right)^{-1}. \quad (4.2.130)$$

The integral produces a leading large logarithm between $u_c \ll u \ll u_h$ where the integral becomes

$$\int_{u_c}^{u_h} du \frac{1}{\sqrt{(\mathcal{B}u^2 - 1 + u^2/u_h^2)(1 - u^2/u_h^2)}} \approx \frac{1}{\sqrt{\mathcal{B}}} \int_{u_c}^{u_h} du \frac{1}{u} = \frac{1}{2\sqrt{\mathcal{B}}} \log(B/T^2). \quad (4.2.131)$$

The constant under the log requires a full knowledge of the interpolating metric between BTZ and AdS_5 , and it is easy to see that the UV region $u \lesssim u_c$ also produces a constant under the log. Therefore, we have a leading-log result for \hat{q}_y in $B \gg T^2$ limit as

$$\hat{q}_y = \frac{\sqrt{\lambda} B^{3/2}}{(3\pi) \log(B/T^2)}. \quad (4.2.132)$$

Comparing with (Equation 4.2.129), we see that $\hat{q}_y \gg \hat{q}_z$ in the assumed hierarchy $B \gg T^2$.

Our results are summarized as follows. In weak coupling perturbative QCD, for a jet moving parallel to the strong magnetic field, we have the jet quenching parameter at complete leading order in α_s (the leading log and the constant under the log) as

$$\hat{q} = \frac{1}{\pi} (1 + 1/v) C_2^J T_R N_F \alpha_s^2 (eB) T \left(\log(1/\alpha_s) - 1 - \gamma_E - \log(T_R N_F / \pi) \right). \quad (4.2.133)$$

For a jet moving perpendicular to the magnetic field, there are two different transverse directions due to the presence of the magnetic field. The momentum diffusion along the magnetic field direction, \hat{q}_z , is given by

$$\hat{q}_z = \frac{16v^2}{3(2\pi)^{3/2}} C_2^J T_R N_F \alpha_s^2 (eB)^{3/2} + \frac{1}{\pi} v C_2^J T_R N_F \alpha_s^2 (eB) T \left(\log \left(\frac{T^2}{\alpha_s T_R N_F \left(\frac{eB}{2\pi} \right) v^2} \right) - 2 \right), \quad (4.2.134)$$

while the momentum diffusion along the perpendicular direction, \hat{q}_y , is given by

$$\hat{q}_y = \frac{8}{3(2\pi)^{3/2}} C_2^J T_R N_F \alpha_s^2 (eB)^{3/2} + \frac{1}{\pi v} C_2^J T_R N_F \alpha_s^2 (eB) T \left(\log \left(\frac{T^2}{\alpha_s T_R N_F \left(\frac{eB}{2\pi} \right) v^2} \right) + 0 \right). \quad (4.2.135)$$

In both (Equation 4.2.134) and (Equation 4.2.135), the first term represents the vacuum contribution that exists even at zero temperature, while the second term is the leading thermal contribution to complete leading order (the leading log and the constant under the log). These two terms are the first two leading contributions in the assumed hierarchy of scales, $\alpha_s eB \ll T^2 \ll eB$.

In strong coupling AdS/CFT correspondence, we compute our jet quenching parameters in the two different methods: 1) heavy-quark strings, and 2) light-like Wilson loops. In the method 1), when the jet is moving parallel to the magnetic field, we have ($\lambda \equiv g_s^2 N_c$ and $B = eB$)

$$\hat{q} = \frac{2}{3\pi} \sqrt{1 + \frac{1}{v^2}} \sqrt{\lambda} \mathcal{B} T, \quad (4.2.136)$$

while, in the case the jet is moving perpendicular to the magnetic field, the two different momentum diffusion constants depending on the orientation with respect to magnetic field are

$$\hat{q}_z = \frac{v^2}{6\pi^2} \sqrt{\lambda} \mathcal{B}^{3/2} + \sqrt{\lambda} \sqrt{\mathcal{B}} T^2, \quad (4.2.137)$$

and

$$\hat{q}_y = \frac{1}{6\pi^2} \sqrt{\lambda} \mathcal{B}^{3/2} + \frac{1}{3v^2} \sqrt{\lambda} \sqrt{\mathcal{B}} T^2. \quad (4.2.138)$$

In the method 2) of the AdS/CFT correspondence, for the jet moving parallel to the magnetic field, we have

$$\hat{q} = \frac{4}{3} \frac{\sqrt{\lambda} \mathcal{B} T}{\log(B/T^2)}, \quad (4.2.139)$$

and for the jet moving perpendicular to the magnetic field, we have

$$\hat{q}_z = \frac{2\pi}{3} \sqrt{\lambda} \sqrt{\mathcal{B}} T^2, \quad (4.2.140)$$

and

$$\hat{q}_y = \frac{\sqrt{\lambda} B^{3/2}}{(3\pi) \log(B/T^2)}. \quad (4.2.141)$$

Perhaps, the most useful observations from these results in the assumed hierarchy $T^2 \ll eB$ are 1) the jet quenching is generally larger in the case the jet is moving perpendicular to the magnetic field, compared to the case the jet is moving parallel to the magnetic field, 2) in the case the jet is moving perpendicular to the magnetic field, the transverse momentum diffusion is asymmetric, $\hat{q}_z \neq \hat{q}_y$. The 1) implies that the strong magnetic field tends to suppress more jets in the reaction plane than the jets out-of reaction plane, so it would reduce the elliptic flow of the jets. The 2) implies that the BDMPS-Z/LPM evolution equation of the gluon emission vertex $F(\mathbf{b})$ in the two dimensional impact parameter space \mathbf{b} in large scattering number limit (that is, small \mathbf{b} limit, or harmonic potential limit) becomes an asymmetric harmonic oscillator problem with complex frequencies,

$$i \frac{\partial F(\mathbf{b})}{\partial t} = -\frac{1}{2\omega} \nabla_{\mathbf{b}}^2 F(\mathbf{b}) + \frac{i}{4} (\hat{q}_z \mathbf{b}_z^2 + \hat{q}_y \mathbf{b}_y^2) F(\mathbf{b}), \quad (4.2.142)$$

where $\mathbf{b} = (\mathbf{b}_z, \mathbf{b}_y)$ and ω is the gluon energy. This problem is still solvable analytically both in finite and infinite mediums, which can be plugged into the emission formula to find the azimuthally asymmetric gluon Bremsstrahlung spectrum. We hope to report a detailed numerical analysis of it and its implications in heavy-ion phenomenology of jet spectrum in a near future.

4.3 Energy Loss of Heavy Quark at Strong Coupling

In this section, we will study the energy loss of a heavy quark moving in arbitrary direction in a strongly magnetized $\mathcal{N}=4$ SYM plasma. Before we jump into the energy loss problem, in the following, we will review the effect of external magnetic field on the particle spectrum of $\mathcal{N}=4$ SYM and adjoint QCD.

The field content of $\mathcal{N}=4$ SYM theory, including their $U(1) \subset SU(4)$ R-symmetry charge, is as follows (all of them are in adjoint representation of the gauge group $SU(N_c)$), see for example (280): there are four flavors of Weyl fermions (1 Weyl fermion of charge 1 and 3 Weyl fermions of charge $-\frac{1}{3}$); 3 complex scalar field of charge $\frac{2}{3}$; and 1 vector field of charge 0 (the gauge field). And, the spectrum of single particle excitations of $\mathcal{N}=4$ SYM theory in the presence of a magnetic field pointing in the z direction are given by relativistic Landau levels which are the following (280): for a charge q_ϕ scalar field

$$E_n = \sqrt{|q_\phi \mathcal{B}|(2n+1) + p_z^2}, \quad n = 0, 1, 2, \dots; \quad (4.3.143)$$

for a charge q_ψ Weyl fermion (with $s_z = \pm \frac{1}{2}$)

$$E_n = \sqrt{2|q_\psi \mathcal{B}|(n + \frac{1}{2} - s_z) + p_z^2}, \quad n = 0, 1, 2, \dots \quad (4.3.144)$$

From (Equation 4.3.143) and (Equation 4.3.144) it is clear that in the lowest Landau level (LLL) with zero energy (at vanishing momentum p_z) we only have Weyl fermions but no scalars. Hence, in the strong magnetic field $\mathcal{B} \gg T^2$ regime the whole dynamics of $\mathcal{N} = 4$ SYM theory is entirely dominated by the lowest Landau levels (LLLs) of Weyl fermions with four flavors (in the adjoint representation) since the scalar particles (and higher Landau levels of Weyl fermions) are integrated out in this regime resulting in a (1+1)-dimensional low energy effective field theory of LLLs and the gauge field.

In contrast, the field content of adjoint QCD with four flavors, including their $U(1) \subset SU(4)$ flavor-symmetry charge, is as follows (all of them are in adjoint representation of the gauge group $SU(N_c)$), see for example (207): there are four flavors of Weyl fermions (1 Weyl fermion of charge 1 and 3 Weyl fermions of charge $-\frac{1}{3}$); and 1 vector field of charge 0 (the gauge field). And, the spectrum of single particle excitations of adjoint QCD in the presence of a magnetic field pointing in the z direction are given by the relativistic Landau levels which for a charge q_ψ Weyl fermion (with $s_z = \pm \frac{1}{2}$) are given by

$$E_n = \sqrt{2|q_\psi \mathcal{B}|(n + \frac{1}{2} - s_z) + p_z^2}, \quad n = 0, 1, 2, \dots \quad (4.3.145)$$

Hence, in the strong magnetic field $\mathcal{B} \gg T^2$ regime the whole dynamics of adjoint QCD is entirely dominated by the lowest Landau levels (LLs) of Weyl fermions with four flavors (in the adjoint representation) since the higher Landau levels of Weyl fermions are integrated out in this regime resulting in a (1+1)-dimensional low energy effective field theory of LLs and the gauge field. Note that the beta function for adjoint QCD with four flavors is given by (207), see also (208; 209),

$$\beta = \mu \frac{\partial}{\partial \mu} \lambda(\mu) \equiv -\frac{1}{2} \frac{\lambda^2}{(2\pi)^2} + \frac{5}{4} \frac{\lambda^3}{(2\pi)^4}, \quad (4.3.146)$$

which has vanishing beta function or IR fixed point at $g_{YM}^2 N_c \equiv \lambda = \lambda^* = \frac{8}{5} \pi^2$. Since, the beta function of $\mathcal{N}=4$ SYM vanishes for any 't Hooft coupling λ , we can claim that

$$\begin{aligned} \mathcal{N} = 4 \text{ SYM in strong magnetic field } \mathcal{B} \gg T^2 \text{ at } \lambda = \lambda^* \equiv & \text{adjoint QCD with four flavors in} \\ & \text{strong magnetic field } \mathcal{B} \gg T^2 \text{ at } \lambda = \lambda^*, \end{aligned}$$

where λ^* is defined as the coupling at which the beta function of adjoint QCD with four flavors vanishes. Note that in this article whenever we refer to adjoint QCD we are specifically referring to the adjoint QCD with four flavors and at its conformal IR fixed point $\lambda = \lambda^*$.

Due to the above equivalence, using the AdS/CFT correspondence in order to study the effect of the strong magnetic field $\mathcal{B} \gg T^2$ on a strongly coupled $\mathcal{N}=4$ SYM plasma or vacuum is particularly interesting, since the results found for $\mathcal{N} = 4$ SYM (at strong coupling and large

N_c limit) also apply for adjoint QCD (at strong coupling and large N_c limit). Therefore, we can conclude that the entropy density (280)

$$s = \frac{1}{3\sqrt{3}} N_c^2 \mathcal{B} T, \quad (4.3.147)$$

conductivity (210)

$$\sigma^{\parallel} = \frac{1}{32\sqrt{3}\pi^3} \frac{\mathcal{B}}{T}, \quad (4.3.148)$$

shear viscosity to entropy density ratio (212)

$$\frac{\eta^{\parallel}}{s} = \pi \frac{T^2}{\mathcal{B}}, \quad (4.3.149)$$

and Chern-Simons diffusion rate (213)

$$\Gamma = \frac{\lambda^2}{384\sqrt{3}\pi^5} \mathcal{B} T^2, \quad (4.3.150)$$

of $\mathcal{N} = 4$ SYM plasma, in the strong magnetic field $\mathcal{B} \gg T^2$ regime, are also the entropy density, conductivity, shear viscosity to entropy density ratio, and Chern-Simons diffusion rate of adjoint QCD plasma in strong magnetic field $\mathcal{B} \gg T^2$ at $\lambda = \lambda^*$.

It would be very interesting to check the above claim numerically using the lattice adjoint QCD (214) in strong magnetic field $\mathcal{B} \gg T^2$ regime (for lattice QCD in magnetic field see (215; 195)) which would also be a nice numerical verification of the AdS/CFT correspondence

in a set up where supersymmetry is totally broken unlike the previous numerical tests of the AdS/CFT correspondence which rely on supersymmetry (216).

4.3.1 Drag Force

It is well known that a quark moving at a constant velocity v , for example, through a strongly coupled $\mathcal{N}=4$ SYM vacuum, doesn't lose its energy, even though it does in a plasma at finite temperature T . The rates of energy and momentum loss of a heavy quark moving at constant velocity v through a strongly coupled $\mathcal{N}=4$ SYM plasma, with no magnetic field, were first computed in (217; 218) using the AdS/CFT correspondence. Effects of fluid velocity gradients and axial chemical potential on heavy quark energy loss has also been investigated in (219; 220). And, the rates of energy and momentum loss of an accelerating quark moving through a strongly coupled $\mathcal{N}=4$ SYM vacuum, with no magnetic field, was found in (221; 222; 223), see also (224; 225; 226; 227).

In this thesis, using the AdS/CFT correspondence, we show that in the presence of a strong magnetic field \mathcal{B} , even a nonaccelerating quark moving at a constant velocity v , through a strongly coupled $\mathcal{N}=4$ SYM vacuum at $T = 0$, loses its energy at a rate linearly dependent on \mathcal{B} .

We will study the rates of energy and momentum loss of a heavy quark of mass M moving with velocity v , in arbitrary direction, through a strongly magnetized plasma in the strong coupling regime. The effect of the magnetic field directly on the heavy quark moving through a non-magnetized plasma (ignoring the effect of the magnetic field on the plasma) was studied in (228; 229). In this article, we rather ignore the effect of the magnetic field \mathcal{B} directly on the

heavy quark of relativistic mass $\gamma M \gg \sqrt{\mathcal{B}}$, where the Lorentz factor $\gamma = \frac{1}{\sqrt{1-v^2}}$, and only consider the effect of the strong magnetic field $\mathcal{B} \gg T^2$ on the plasma. In other words, we will work on the more physical limit $\gamma M \gg \sqrt{\mathcal{B}} \gg T$.

Specifically, we will study the rates of energy and momentum loss of a heavy quark of mass M moving at constant velocity v through a strongly coupled $N = 4$ SYM plasma in the presence of strong magnetic field $\mathcal{B} \gg T^2$ using its 5-dimensional gravity dual.

The 5-dimensional background metric in the presence of strong magnetic field $\mathcal{B} \gg T^2$ is given by (280),

$$ds^2 = g_{MN} dx^M dx^N = \frac{\mathcal{R}^2}{u^2} (-f(u) dt^2 + dz^2) + \mathcal{R}^2 \mathcal{B} (dx^2 + dy^2) + \frac{\mathcal{R}^2}{u^2 f(u)} du^2, \quad (4.3.151)$$

where $f(u) = 1 - \frac{u^2}{u_h^2}$, the horizon corresponds to $u = u_h$, the boundary to $u = 0$, the Hawking temperature T of the BTZ black hole is $T = \frac{1}{2\pi u_h}$, we identify $\mathcal{R} = \frac{R}{\sqrt{3}}$ as the radius of the AdS_3 spacetime or BTZ black hole, and $\mathcal{B} = \sqrt{3}eB = \sqrt{3}F_{xy}$ as the physical magnetic field at the boundary. Also, note that (Equation 4.3.151) is valid only near the horizon, i.e., in the regime $u \gg u_0 = \frac{1}{\sqrt{\mathcal{B}}}$. And, for an arbitrary strength of \mathcal{B} , the metric numerically interpolates between the AdS_3 spacetime or BTZ black hole (Equation 4.3.151) near the horizon (IR) and AdS_5 spacetime near the boundary (UV)(280).

We will further rewrite the metric (Equation 4.3.151) as

$$ds^2 = \frac{\mathcal{R}^2}{u^2} \left(-F dt^2 + dz^2 + H(dx^2 + dy^2) + \frac{du^2}{F} \right), \quad (4.3.152)$$

where $F = f(u) = 1 - \frac{u^2}{u_h^2}$, and $H = u^2 \mathcal{B}$, so that, it resembles the anisotropic metric used in (230), which we will follow closely in the following derivation of the energy and momentum losses of a heavy quark.

On the gravity side the rates of energy and momentum loss of a heavy quark are described by a string propagating in the background (Equation 4.3.152) governed by the equation of motion for the string which is derived from the Nambu-Goto action

$$S = -\frac{1}{2\pi\alpha'} \int d\tau d\sigma \sqrt{-\det h_{ab}} = \int d\tau d\sigma L, \quad (4.3.153)$$

where $h_{ab} = g_{MN} \partial_a X^M(\tau, \sigma) \partial_b X^N(\tau, \sigma)$ is the induced worldsheet metric. In the following expressions, we set $\mathcal{R}^2/2\pi\alpha' = \sqrt{\lambda}/6\pi$ to one, and reinstate it at the end.

From the action (Equation 4.3.153), we determine the spacetime momentum flow Π_M along the string to be

$$\Pi_M = \frac{\partial L}{\partial(\partial_\sigma X^M)}. \quad (4.3.154)$$

Since, we have rotational symmetry in the xy -directions, we can set $y = 0$. Then, identifying $(t, u) = (\tau, \sigma)$ and considering a string embedding of the form

$$x(t, u) \rightarrow (vt + x(u)) \cos \varphi, \quad (4.3.155)$$

$$z(t, u) \rightarrow (vt + z(u)) \sin \varphi, \quad (4.3.156)$$

which corresponds to a quark moving with velocity v in the xz -plane at an angle φ with the x -axis, the Lagrangian takes the form

$$\begin{aligned}
L = & -\frac{1}{u^2\sqrt{F}} \left[F + \sin^2 \varphi (F^2 z'^2 - v^2) \right. \\
& \left. + H \cos^2 \varphi \left[F^2 x'^2 - v^2 - F v^2 (z' - x')^2 \sin^2 \varphi \right] \right]^{1/2}, \quad (4.3.157)
\end{aligned}$$

and, the rates at which energy and momentum flow from the boundary to the horizon along the string become

$$\begin{aligned}
-\Pi_t &= \frac{1}{Lu^4} Fv \left[x' \sin^2 \mathbf{p} + H z' \cos^2 \mathbf{p} \right], \\
\Pi_x &= \frac{1}{Lu^4} H \left[F x' + v^2 (z' - x') \sin^2 \varphi \right] \cos \varphi, \\
\Pi_z &= \frac{1}{Lu^4} \left[F z' + H v^2 (x' - z') \cos^2 \varphi \right] \sin \varphi, \quad (4.3.158)
\end{aligned}$$

where $'$ denotes differentiation with respect to u . Note that

$$-\Pi_t = \Pi_x v \cos \mathbf{p} + \Pi_z v \sin \mathbf{p} = \vec{\Pi} \cdot \vec{v}. \quad (4.3.159)$$

Moreover, from the equation of motion $\partial_u \Pi_M = 0$ (which is valid only when the end of the string or the heavy quark is nonaccelerating), we find that Π_M is a constant independent of u or the mass of the quark $M = \frac{\sqrt{\lambda}}{2\pi} \left(\frac{1}{u} - \frac{1}{u_c} \right)$ (218) where u is the radial location at which the end of the string is attached to, say, a D7 brane. And, u_c is the radius of the worldsheet horizon with

$u_c = u_h$ for $v = 0$, and constrained by $u \leq u_c$ which is determined by requiring the time-time component of the worldsheet metric to always be negative or zero. Therefore, we are free to fix M to any value as long as it satisfies the bound $\sqrt{\lambda}\sqrt{\mathcal{B}} \gg M \gg \sqrt{\lambda}T$ which is the result of the geometrical bound $u_0 \ll u \ll u_h$, on the gravity side, and the physical requirement that the mass of the heavy quark M must be much larger than the temperature T of the plasma, i.e., $M \gg \sqrt{\lambda}T$ or $u \ll u_h$, so that the heavy quark can be considered a legitimate external probe of the plasma.

In addition, we should note that, since requiring the time-time component of the worldsheet metric at $T = 0$ and $B = 0$ (for the pure AdS_5 bulk metric) to always be negative or zero would result in the constraint $1 - v^2 \geq 0$, we could conclude that the $u = u_c$ or $M = 0$ limit must be accompanied by the $v = 1$ limit. So, in the vacuum at $T = 0$, the bound on M becomes $\sqrt{\lambda}\sqrt{\mathcal{B}} \gg M \geq 0$, hence we are free to set the mass of the quark $M = 0$, if we would like to, as long as we also set its velocity $v = 1$.

In order to find the background solution of the string, we invert the relations (Equation 4.3.158) to find

$$x' = \pm \frac{v}{F\sqrt{H}} \frac{N_x}{\sqrt{N_z N_x - D}}, \quad z' = \pm \frac{Hv}{F\sqrt{H}} \frac{N_z}{\sqrt{N_z N_x - D}}, \quad (4.3.160)$$

where

$$N_x = -\Pi_x(F \text{Sec. } \mathbf{p} - H v^2 \cos \mathbf{p}) + \Pi_z H v^2 \sin \mathbf{p}, \quad (4.3.161)$$

$$N_z = -\Pi_z(F \csc \mathbf{p} - v^2 \sin \mathbf{p}) + \Pi_x v^2 \cos \mathbf{p}, \quad (4.3.162)$$

$$\begin{aligned} D &= \frac{F \csc \mathbf{p} \text{Sec. } \mathbf{p}}{u^4} \left[\Pi_z \Pi_x u^4 - H v^2 \cos \mathbf{p} \sin \mathbf{p} \right] \\ &\times \left[F - v^2 \left(H \cos^2 \mathbf{p} + \sin^2 \mathbf{p} \right) \right]. \end{aligned} \quad (4.3.163)$$

Since, $F(H)$ is monotonically decreasing (increasing) from the boundary to the horizon, the last factor in square brackets in (Equation 4.3.163) is positive at the boundary and negative at the horizon. Therefore, there exists a critical value u_c in between such that

$$F_c - v^2 (H_c \cos^2 \mathbf{p} + \sin^2 \mathbf{p}) = 0, \quad (4.3.164)$$

where $H_c = H(u_c)$, and $F_c = F(u_c)$. Note that at $u = u_c$, $D = 0$, and

$$N_z N_x|_{u_c} = -v^4 (H_c \Pi_z \cos \mathbf{p} - \Pi_x \sin \mathbf{p})^2, \quad (4.3.165)$$

is negative unless the momenta are related through

$$\frac{\Pi_z}{\Pi_x} = \frac{\tan \mathbf{p}}{H_c}, \quad (4.3.166)$$

in which case it vanishes.

Then, requiring the first square bracket in (Equation 4.3.163) also vanishes at $u = u_c$, and using (Equation 4.3.166), we find

$$\Pi_x = H_c \frac{v \cos \mathbf{p}}{u_c^2}, \quad \Pi_z = \frac{v \sin \mathbf{p}}{u_c^2}. \quad (4.3.167)$$

Therefore, the drag force or the rate of momentum loss of a heavy quark, defined as $\vec{F}_{drag} = \frac{d\vec{p}}{dt} \equiv (-\Pi_x, -\Pi_z)$ is (after reinstating the factor $\mathcal{R}^2/2\pi\alpha' = \sqrt{\lambda}/6\pi$)

$$\vec{F}_{drag} = -\frac{\sqrt{\lambda}}{6\pi} \frac{v}{u_c^2} (H_c \cos \mathbf{p}, \sin \mathbf{p}), \quad (4.3.168)$$

which is exactly Eq. 3.22 in (230), up to an overall minus sign, once we exchange the x and z components of the drag force.

Solving (Equation 4.3.164) for u_c , we find

$$u_c^2 = \frac{1}{\mathcal{B}} \left(\frac{1 - v^2 \sin^2 \mathbf{p}}{\frac{4\pi^2 T^2}{\mathcal{B}} + v^2 \cos^2 \mathbf{p}} \right), \quad (4.3.169)$$

which can be used in (Equation 4.3.168), to find

$$\vec{F}_{drag} = -\frac{\sqrt{\lambda}\mathcal{B}v}{6\pi} \left(\cos \mathbf{p}, \sin \mathbf{p} \left(\frac{\frac{4\pi^2 T^2}{\mathcal{B}} + v^2 \cos^2 \mathbf{p}}{1 - v^2 \sin^2 \mathbf{p}} \right) \right). \quad (4.3.170)$$

Note that (Equation 4.3.170), exactly reduces to Eq. 3.113 and Eq. 3.95 of (206), by the current author, Li, and Yee, when $\mathbf{p} = 0$ (which corresponds to a heavy quark moving in the

x -direction or perpendicular to the magnetic field) and $\mathbf{p} = \pi/2$ (which corresponds to a heavy quark moving in the z -direction or parallel to the magnetic field), respectively.

In the vacuum at $T = 0$, the rate of momentum loss $\frac{d\vec{p}}{dt}$ (Equation 4.3.170) reduces to

$$\frac{d\vec{p}}{dt} = -\frac{\sqrt{\lambda}\mathcal{B}v}{6\pi} \left(\cos \mathbf{p}, \sin \mathbf{p} \left(\frac{v^2 \cos^2 \mathbf{p}}{1 - v^2 \sin^2 \mathbf{p}} \right) \right), \quad (4.3.171)$$

which for $v = 1$ (and $M = 0$) becomes

$$\frac{d\vec{p}}{dt} = -\frac{\sqrt{\lambda}\mathcal{B}}{6\pi} (\cos \mathbf{p}, \sin \mathbf{p}). \quad (4.3.172)$$

Therefore, the rate of energy loss $\frac{dE}{dt} = \Pi_t = \frac{d\vec{p}}{dt} \cdot \vec{v}$, for a massless quark moving at the speed of light $v = 1$ in $\mathcal{N}=4$ SYM vacuum at $T = 0$, is

$$\frac{dE}{dt} = -\frac{\sqrt{\lambda}\mathcal{B}}{6\pi}. \quad (4.3.173)$$

Similarly, for $T \neq 0$ but $\mathcal{B} \gg T^2$ and $v^2 = v_*^2 = 1 - \frac{4\pi^2 T^2}{\mathcal{B}}$, the drag force (Equation 4.3.170) reduces to

$$\vec{F}_{drag} = \frac{d\vec{p}}{dt} = -\frac{\sqrt{\lambda}\mathcal{B}v_*}{6\pi} (\cos \mathbf{p}, \sin \mathbf{p}) = -\frac{\sqrt{\lambda}\mathcal{B}}{6\pi} \vec{v}_*. \quad (4.3.174)$$

Therefore, the rate of energy loss $\frac{dE}{dt} = \Pi_t = \vec{F}_{drag} \cdot \vec{v}$, for a heavy quark of mass M moving at near the speed of light $v^2 = v_*^2 = 1 - \frac{4\pi^2 T^2}{\mathcal{B}} \simeq 1$ in $\mathcal{N}=4$ SYM plasma at $T \ll \sqrt{\mathcal{B}}$, becomes

$$\frac{dE}{dt} = -\frac{\sqrt{\lambda}\mathcal{B}}{6\pi} v_*^2 \simeq -\frac{\sqrt{\lambda}\mathcal{B}}{6\pi}. \quad (4.3.175)$$

In summary, we have found that a massless quark moving at the speed of light $v = 1$, in arbitrary direction, through a strongly coupled and magnetized $\mathcal{N}=4$ SYM vacuum at $T = 0$ loses its energy at a rate linearly dependent on \mathcal{B} (Equation 4.3.173)

$$\frac{dE}{dt} = -\frac{\sqrt{\lambda}}{6\pi}\mathcal{B}. \quad (4.3.176)$$

We have also found that a heavy quark moving at near the speed of light $v \simeq 1$, in arbitrary direction, through a strongly coupled and magnetized $\mathcal{N}=4$ SYM plasma at $T \neq 0$ loses its energy at a rate linearly dependent on \mathcal{B} (Equation 4.3.175)

$$\frac{dE}{dt} \simeq -\frac{\sqrt{\lambda}}{6\pi}\mathcal{B}. \quad (4.3.177)$$

We should also note that the results found in this article for $\mathcal{N} = 4$ SYM (Equation 4.3.176) and (Equation 4.3.177) are also the results one would find for adjoint QCD with four flavors and at IR fixed point $\lambda = \lambda^*$.

From the phenomenological point of view the results (Equation 4.3.176) and (Equation 4.3.177) are also very interesting since knowing the rate of energy loss in the presence of a strong magnetic field B is crucial for a complete understanding and numerical simulations of the energy loss mechanisms of the hard probes of the quark-gluon plasma (QGP) produced in heavy ion collisions.

CHAPTER 5

THERMALIZATION OF MAGNETIZED QUARK-GLUON PLASMA

(Previously published as Kiminad A. Mamo and Ho-Ung Yee, “Thermalization of Quark-Gluon Plasma in Magnetic Field at Strong Coupling,” Phys. Rev. D 92, no. 10, 105005 (2015))

In this chapter, we study the effect of external magnetic field on the thermalization of QGP at strong coupling regime using the AdS/CFT correspondence. Magnetic field can potentially be important in the thermalization of QGP in heavy-ion collisions, since the thermalization occurs at an early stage of heavy-ion collisions when the magnetic field is strong, before it dies out with time.

In our study, the QGP that undergoes thermalization is modeled by falling of a thin spatial mass shell to the bottom of AdS space, forming a black-hole at the end of thermalization (231). See Refs. (232; 233; 234; 235; 236; 237) for other approaches. We treat the magnetic field as external, and use known solutions of AdS geometries with magnetic field at zero and finite temperatures. In a thin-shell approximation, we join two static solutions, one with zero temperature and the other with finite temperature, across the falling shell via the Israel junction condition (238). At each time, the location of the shell in the energy coordinate (holographic coordinate) divides the AdS space into two regions: one with the geometry of zero temperature that is not yet thermalized, and the other with finite temperature that is thermalized. As the shell falls down towards infrared, eventually forming a black-hole, the AdS space becomes filled with the geometry with finite temperature, representing dynamical thermalization. The proper

time (or Eddington-Finkelstein time) by which the shell forms a black-hole can be a reasonable definition of thermalization time in the model (125).

Magnetic AdS geometries with zero and finite temperatures

For joining of two static solutions across a thin falling shell to work, each static solution one uses for the two different regions that the shell divides the space-time into, must be isotropic and homogeneous: this requirement is seen in the Israel junction condition in the subsequent analysis. The underlying reason for this requirement can be understood by the Einstein-Maxwell equations with a source (the shell) viewed as an initial value problem. The shell (which is assumed to be neutral) starting from rest at initial time and moving along its trajectory would normally source metric perturbations inside its future light cone while it falls down by its own gravity. There is no a priori reason to expect that the resulting geometry in the future will simply be given by joining of two static geometries across the falling shell: one instead expects gravitational waves emanating from the shell. In the presence of isotropy and homogeneity however, a powerful uniqueness theorem of Einstein-Maxwell theory dictates that a (neutral) homogeneous and isotropic solution in a connected region with no sources is completely fixed by its conserved energy density, and must take a form of static black-hole with that conserved energy density. The two regions bounded by the shell have constant energy densities differing by the energy density of the shell, and since these energies are conserved, the geometries in each region are fixed by the uniqueness theorem to be those static geometries with conserved energy densities. This is the physical reason why the falling shell ansatz works: simply put, no gravitational radiation is possible in isotropic and homogeneous collapse (239).

We look for AdS geometries with magnetic field which possess isotropy and homogeneity. In dimension $D = 5$ (corresponding to 4-dimensional QGP) a single magnetic field necessarily breaks isotropy. To overcome this difficulty, we consider $\mathcal{N} = 4$ super-Yang-Mills gauge theory with global $SO(6)_R$ R-symmetry that allows three orthogonal magnetic fields from each $U(1)^3 \subset SO(6)_R$ of equal magnitude. Although our model for the magnetic field from R-symmetry of $\mathcal{N} = 4$ super Yang-Mills theory has differences from QCD, such as the charge content of the matter fields, we expect that the universal feature we observe in this model could indicate the similar trend in real QCD in strong coupling regime.

The corresponding theory in AdS is the gauged $U(1)^3$ supergravity which is a particular Einstein-Maxwell-Scalar theory. It admits an exact solution with three orthogonal magnetic fields of equal magnitude that ensures isotropy and homogeneity of the energy-momentum tensor (240). The action is given by

$$(16\pi G_5)\mathcal{L} = (R - V) - \frac{1}{2} \sum_{I=1}^2 (\partial\phi_I)^2 - \frac{1}{4} \sum_{a=1}^3 X_a^{-2} (F^a)^2 + \frac{1}{4\sqrt{-g_5}} \epsilon^{\mu\nu\rho\sigma\lambda} F_{\mu\nu}^1 F_{\rho\sigma}^2 A_\lambda^3, \quad (5.0.1)$$

where $F_{\mu\nu}^a = \partial_\mu A_\nu^a - \partial_\nu A_\mu^a$ and

$$V = -\frac{4}{L^2} \sum_{a=1}^3 X_a^{-1}$$

$$X_1 = e^{-\frac{1}{\sqrt{6}}\phi_1 - \frac{1}{\sqrt{2}}\phi_2}, \quad X_2 = e^{-\frac{1}{\sqrt{6}}\phi_1 + \frac{1}{\sqrt{2}}\phi_2}, \quad X_3 = e^{\frac{2}{\sqrt{6}}\phi_1}. \quad (5.0.2)$$

We will set $L = 1$ in the following. The field equations derived from the Lagrangian (Equation 7.4.26) admit an exact magnetically charged AdS₅ black hole solution (240)

$$ds_5^2 = \frac{dz^2}{f(z)z^2} - \frac{f(z)}{z^2} dt^2 + \frac{(d\vec{x})^2}{z^2},$$

$$F_{ij}^a = \epsilon^{aij} B, \quad \phi_I = 0, \quad (5.0.3)$$

where $a = 1, 2, 3$ labels three $U(1)$ R-symmetries and $i, j = 1, 2, 3$ are spatial indices. The function $f(z)$ is

$$f(z) = 1 - mz^4 + \frac{1}{8}B^2z^4 \log(mz^4), \quad (5.0.4)$$

with $z_H = m^{-\frac{1}{4}}$ being the location of the black hole horizon solving $f(z_H) = 0$. The parameters (m, B) are related to the temperature T by

$$T = -\frac{f'(z_H)}{4\pi} = \frac{8m - B^2}{8\pi m^{3/4}}. \quad (5.0.5)$$

Note that at $m = \frac{1}{8}B^2$, the temperature of the black hole (Equation 5.0.5) goes to zero, and hence the extremal zero temperature solution in the presence of magnetic fields is given by

$$f_0(z) = 1 - \frac{1}{8}B^2z^4 + \frac{1}{8}B^2z^4 \log\left(\frac{1}{8}B^2z^4\right). \quad (5.0.6)$$

We map this to the field theory vacuum in the presence of magnetic field. We must have $m \geq \frac{1}{8}B^2$ for thermodynamic stability.

In 4-dimensional AdS space (corresponding to a field theory in 3-dimensions), one can realize isotropy and homogeneity with a single magnetic field $F_{12} = B$. The exact black hole solution with magnetic field in the Einstein-Maxwell theory is known (241)

$$ds_4^2 = \frac{dz^2}{f(z)z^2} - \frac{f(z)}{z^2} dt^2 + \frac{(d\vec{x})^2}{z^2}, \quad (5.0.7)$$

where

$$f(z) = 1 - mz^3 + B^2 z^4. \quad (5.0.8)$$

The location of the black hole horizon is given by $f(z_H) = 0$, and the temperature T is

$$T = -\frac{f'(z_H)}{4\pi} = \frac{3 - B^2 z_H^4}{4\pi z_H^3}. \quad (5.0.9)$$

When $m = m_0 \equiv \frac{4}{3^{3/4}} B^{3/2}$, the temperature of the black hole solution (Equation 5.0.9) becomes zero, and hence the extremal zero temperature solution is given by the blackening factor,

$$f_0(z) = 1 - \frac{4}{3^{3/4}} B^{3/2} z^3 + B^2 z^4. \quad (5.0.10)$$

The metric (Equation 5.0.7) with $m = 0$, that is $f(z) = 1 + B^2 z^4$, is a solution of the Einstein-Maxwell equation without black-hole horizon. The reason why it can not be the solution for zero temperature is its violation of causality: the speed of light in the bulk AdS with respect to the field theory coordinates (t, \vec{x}) at position z is $c(z) = f(z)$, which has to be

less than 1 to respect causality of the field theory (242). This means that this geometry should be excluded in a meaningful AdS/CFT correspondence.

Holographic thermalization with magnetic field

The thin shell initially starting from rest at a position $z_i = 1/\pi Q_s$ collapses from the UV region of small z to the IR region of large z under its own gravity, eventually passing through its black-hole horizon by which we have thermalization. The geometry is constructed by joining a black hole solution with finite temperature (Equation 5.0.4) above the shell in the UV region with the zero temperature solution (Equation 5.0.6) below the shell, across the trajectory of the shell in (t, z) coordinates that is determined by Israel junction conditions.

The metric induced on the 4-dimensional world-volume Σ of the shell can be written in a conformal form

$$ds_{\Sigma}^2 = \frac{-d\tau^2 + (d\vec{x})^2}{(z(\tau))^2}, \quad (5.0.11)$$

where $z(\tau)$ is the position of the shell in z coordinate at a conformal time τ . Continuity of the metric across the shell requires identifying \vec{x} on Σ with \vec{x} in the background. The trajectory of the shell with respect to (t_U, z) coordinates in the upper (UV) region of space-time parameterized by the conformal time τ , that is $(t_U(\tau), z(\tau))$, determines the induced metric on Σ . Comparing time component of that with (Equation 7.5.32) gives

$$f(z(\tau)) \dot{t}_U^2(\tau) - \frac{\dot{z}^2(\tau)}{f(z(\tau))} = 1, \quad (5.0.12)$$

where $\cdot \equiv \frac{d}{d\tau}$. This relates t_U and τ , given a trajectory $z(\tau)$. Similarly, the same trajectory with respect to the IR coordinates $(t_L(\tau), z(\tau))$ should satisfy the condition

$$f_0(z(\tau)) \dot{t}_L^2(\tau) - \frac{\dot{z}^2(\tau)}{f_0(z(\tau))} = 1, \quad (5.0.13)$$

that gives a relation between t_L and τ once the trajectory $z(\tau)$ is found. Finally the Israel junction condition is

$$[K_{ij} - \gamma_{ij}K] = -8\pi G_5 S_{ij}, \quad (5.0.14)$$

where $[A] \equiv A_L - A_U$, S_{ij} is the energy-momentum tensor on the shell, and γ_{ij} is the induced metric on the shell with respect to the shell coordinate $\xi^i = (\tau, \vec{x})$. The $K_{ij}^{U/L}$ are extrinsic curvatures evaluated on the shell from the upper and lower regions respectively,

$$K_{ij} = \frac{\partial x^\alpha}{\partial \xi^i} \frac{\partial x^\beta}{\partial \xi^j} \nabla_\alpha n_\beta = -n_\alpha \left(\frac{\partial^2 x^\alpha}{\partial \xi^i \partial \xi^j} + \Gamma_{\beta\gamma}^\alpha \frac{\partial x^\beta}{\partial \xi^i} \frac{\partial x^\gamma}{\partial \xi^j} \right), \quad (5.0.15)$$

with the unit normal vectors $n_{L/R}^\mu$ to the surface Σ pointing to the direction of increasing z .

They are given by

$$\begin{aligned} n_U &= \left(\frac{z\dot{z}}{f(z)} \right) \frac{\partial}{\partial t} + (zf(z)\dot{t}) \frac{\partial}{\partial z}, \\ n_L &= \left(\frac{z\dot{z}}{f_0(z)} \right) \frac{\partial}{\partial t} + (zf_0(z)\dot{t}) \frac{\partial}{\partial z}, \end{aligned} \quad (5.0.16)$$

where all quantities are evaluated on the shell. The non-vanishing components of $K_{ij}^{U/L}$ are

$$\begin{aligned}
K_{\tau\tau}^U &= -\frac{\dot{t}_U}{z} \left(\frac{f(f' + 2\ddot{z})}{2(f + \dot{z}^2)} - \frac{f}{z} \right), \\
K_{ij}^U &= -\frac{\dot{t}_U f}{z^2} \delta_{ij}, \quad i, j = 1, 2, 3, \\
K_{\tau\tau}^L &= -\frac{\dot{t}_L}{z} \left(\frac{f_0(f'_0 + 2\ddot{z})}{2(f_0 + \dot{z}^2)} - \frac{f_0}{z} \right), \\
K_{ij}^L &= -\frac{\dot{t}_L f_0}{z^2} \delta_{ij}, \quad i, j = 1, 2, 3.
\end{aligned} \tag{5.0.17}$$

where $' \equiv \frac{d}{dz}$. Assuming energy-momentum tensor on the shell of a conformal form,

$$S_{ij} = 4p(z)u_i u_j + \gamma_{ij}p(z), \quad u_i = \left(\frac{1}{z}, 0, 0, 0 \right), \tag{5.0.18}$$

with the pressure $p(z)$ to be determined, the junction condition becomes

$$\begin{aligned}
f_0 \dot{t}_L - f \dot{t}_U &= 8\pi G_5 p(z), \\
\dot{t}_L \frac{z f_0 \left(\frac{f'_0}{2} + \ddot{z} \right)}{(f_0 + \dot{z}^2)} - \dot{t}_U \frac{z f \left(\frac{f'}{2} + \ddot{z} \right)}{(f + \dot{z}^2)} &= 4 \cdot 8\pi G_5 p(z).
\end{aligned} \tag{5.0.19}$$

Removing $p(z)$ from the above equations and using

$$\dot{t}_L = \frac{\sqrt{f_0 + \dot{z}^2}}{f_0}, \quad \dot{t}_U = \frac{\sqrt{f + \dot{z}^2}}{f}, \tag{5.0.20}$$

$B \text{ (fm}^{-2}\text{)}$	$z_H \text{ (fm)}$	$m \text{ (fm}^{-4}\text{)}$	$C \text{ (fm}^{-4}\text{)}$
0	0.209	525.5	263.7
2.06	0.209	527.6	262.6
5.16	0.208	538.7	260.2
25.81	0.187	810.6	272.1
51.61	0.162	1469.1	331.0

TABLE I

(AdS₅) Parameters of our numerical solutions for RHIC with a late-time temperature $T = 300$ MeV and several exemplar values of $B = 0; 0.08 \text{ GeV}^2; 0.2 \text{ GeV}^2; 1 \text{ GeV}^2; 2 \text{ GeV}^2$.

from (Equation 5.0.12) and (Equation 5.0.13), the resulting equation for \dot{z} is integrable to give

$$\dot{z} = \sqrt{\left(\frac{Cz^4}{2} + \frac{f_0(z) - f(z)}{2Cz^4}\right)^2 - f_0(z)}, \quad (5.0.21)$$

with a constant of motion $C > 0$. This reproduces the one in Ref. (125). We choose to express the falling trajectory in terms of the boundary time t_U which can be identified with the field theory (QCD) time on the boundary. Using the relation (Equation 5.0.12), the solution (Equation 5.0.21) translates to

$$\frac{dz}{dt_U} = f(z) \sqrt{\frac{\left(\frac{Cz^4}{2} + \frac{f_0(z) - f(z)}{2Cz^4}\right)^2 - f_0(z)}{\left(\frac{Cz^4}{2} + \frac{f_0(z) - f(z)}{2Cz^4}\right)^2 - (f_0(z) - f(z))}}, \quad (5.0.22)$$

which we solve numerically. More precisely, the thermalization time is defined as the Eddington-Finkelstein time when the mass shell passes through its black-hole horizon (125).

Following (125), we set our initial condition of the falling mass shell in terms of the saturation scale Q_s , which governs the initial gluon distribution, as

$$z(t_U = 0) = z_i = \frac{1}{\pi Q_s}, \quad \dot{z}(t_U = 0) = 0. \quad (5.0.23)$$

We measure z in units of fm. For RHIC, we take $Q_s = 0.87 \text{ GeV} = 4.42 \text{ fm}^{-1}$, and for LHC we have $Q_s = 1.23 \text{ GeV} = 6.24 \text{ fm}^{-1}$. In Table I, we show parameters of our numerical solutions after fixing the final thermalization temperature to be $T = 300 \text{ MeV}$ for RHIC for several exemplar values of magnetic field. In Figure 26, we show the time history of falling mass shell in the field theory (QCD) time t_U for a few exemplar values of magnetic field B with a fixed final temperature. The plots clearly indicate that the presence of magnetic field speeds up the thermalization of the plasma: the stronger the magnetic field, the shorter the thermalization time. More precisely, the thermalization time is defined as the Eddington-Finkelstein time when the mass shell passes through its black-hole horizon (125). However, it is qualitatively similar to the time in Schwarz coordinate t_U we show when the mass shell falls close to the horizon.

Instead of fixing final temperature, we also study the case where the energy density measured from zero temperature but finite B state is fixed while we vary magnetic field, that is we fix $\Delta\epsilon \equiv \epsilon(T, B) - \epsilon(T = 0, B)$, which can be interpreted as the energy density thrown by colliding nuclei into the background magnetic field. Explicitly, we have

$$\Delta\epsilon = \frac{N_c^2}{4\pi^2} \left(\frac{3}{2}m + \frac{3}{16}B^2 \left(\log \left(\frac{B^2}{8m} \right) - 1 \right) \right), \quad (5.0.24)$$

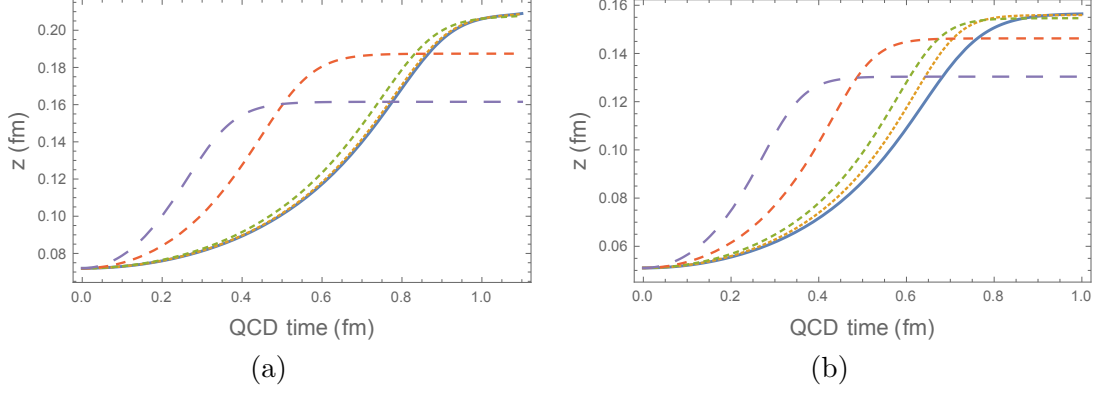


Figure 26. (AdS_5) Thermalization history of falling mass shell for RHIC (left) and LHC (right). The late-time temperature is fixed to be $T = 300$ (400) MeV for RHIC (LHC), and the magnetic fields are $B = 0$ (0) (*solid blue*); 0.08 (0.3) (*orange*); 0.2 (0.52) (*green*); 1 (1.32) (*red*); 2 (2.64) (*violet*) GeV^2 for RHIC (LHC). Thermalization time is when the curve reaches its plateau at the horizon.

which determines the parameter m in the geometry, given a fixed $\Delta\epsilon$ and varying B . In Figure 27, we show the resulting time trajectories of energy shell with $\Delta\epsilon$ chosen to be the energy density of $T = 300$ MeV, $B = 0$ state. Our observation of faster thermalization with magnetic field seems robust.

To examine whether our conclusion depends on the number of dimensions the field theory resides in, we study the thermalization of plasma in magnetic field in one less dimension. In AdS_4 (corresponding to 3-dimensional field theory), the analysis is the same with (Equation 5.0.8) in

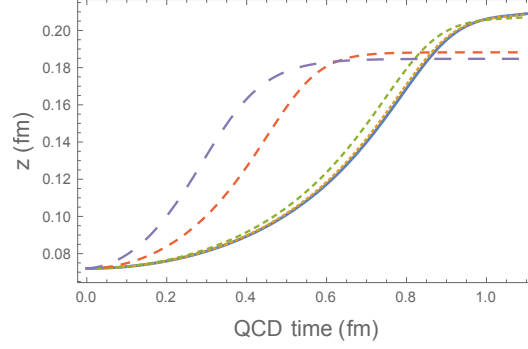


Figure 27. (AdS₅) Thermalization history of falling mass shell for fixed energy density, and varying magnetic field $B = 0$ (*solid blue*); 0.08 (*orange*); 0.2 (*green*); 1 (*red*); 2 (*violet*) GeV^2 for RHIC.

the place of (Equation 5.0.4), and (Equation 5.0.10) in the place of (Equation 5.0.6), but with the energy-momentum tensor on the shell taking a 3-dimensional conformal form,

$$S_{ij} = 3p(z)u_i u_j + \gamma_{ij}p(z), \quad u_i = \left(\frac{1}{z}, 0, 0\right). \quad (5.0.25)$$

We arrive at

$$\frac{dz}{dt_U} = f(z) \sqrt{\frac{\left(\frac{Cz^3}{2} + \frac{f_0(z)-f(z)}{2Cz^3}\right)^2 - f_0(z)}{\left(\frac{Cz^3}{2} + \frac{f_0(z)-f(z)}{2Cz^3}\right)^2 - (f_0(z) - f(z))}}, \quad (5.0.26)$$

which can be solved numerically given the constant C which, as before, should be determined from initial conditions. In Figure 28, we show the time history of falling mass shell trajectory in field theory time t_U for a few exemplar values of magnetic field B for 3-dimensional gauge theory with a fixed final temperature. Again, the plots clearly demonstrate that the presence of magnetic field hastens the thermalization.

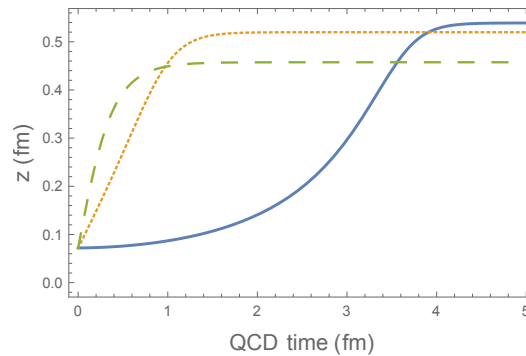


Figure 28. (AdS_4) Thermalization history of falling mass shell in AdS_4 for a late-time temperature of $T = 300$, and the magnetic fields are $B = 0$ (*solid blue*); 0.08 (*orange*); 0.2 (*green*) GeV^2 .

In summary, in the framework of AdS/CFT correspondence, we have studied the thermalization of strongly coupled gauge theory plasma in the presence of magnetic field, utilizing simplified picture of thermalization as falling of a thin homogeneous energy-shell towards the black-hole horizon. Our results in various dimensions have revealed that magnetic field universally hastens thermalization in strong coupling regime. At weak coupling, a strong magnetic field causes the dimensional reduction of the system into 1-dimensional one with lowest Landau levels, and one may study the effects of magnetic field to thermalization at weak coupling in this context. It would be interesting to see how weak coupling result compares with our conclusion in this work at strong coupling.

CHAPTER 6

CONFINEMENT-DECONFINEMENT PHASE TRANSITION IN EXTERNAL MAGNETIC FIELD

(Previously published as Kiminad A. Mamo and Ho-Ung Yee, “Inverse magnetic catalysis in holographic models of QCD,” JHEP 1505, 121 (2015))

Recently, the study of the QCD phase diagram for magnetic field B has attracted considerable attention (243; 244; 245; 246; 247; 248; 249; 250; 251; 252; 253; 254; 258; 255; 256; 257; 259; 260; 195), see (67) for a review. The main motivation for studying the QCD phase diagram under external magnetic field B stems from the fact that strong magnetic field B is produced in heavy ion collisions experiments at RHIC $eB \sim 0.01 \text{ GeV}^2$ and LHC $eB \sim 0.25 \text{ GeV}^2$ (54), due to the charged spectator particles, which has interesting effects on the quark-gluon plasma created during these heavy ion collision experiments (152; 153; 261; 262; 263; 103), see (67) for a review. A strong magnetic field $eB \sim 4 \text{ GeV}^2$ is also produced during the electroweak phase transition of the early Universe (264), and relatively weaker magnetic field $eB \sim 1 \text{ MeV}^2$ is produced in the interior of dense neutron stars (265).

Another motivation comes from the fact that the study of the QCD phase diagram with magnetic field B is amenable to numerical simulations of QCD on the lattice, without facing the sign problem of lattice QCD that exist in the case of non-zero baryon chemical potential μ_B , creating an opportunity to compare the holographic and low energy effective models of QCD directly with QCD itself.

Regarding the study of the QCD phase diagram for magnetic field B , most of the models for QCD (243; 244; 245; 246; 247; 248; 249; 250; 251; 252), including the holographic ones (253; 254; 258; 255; 256; 257), have studied chiral-symmetry-restoration transition and have predicted that the critical temperature T_c of the transition increases with increasing magnetic field B at zero chemical potential $\mu = 0$. This enhancing effect of the magnetic field B on the critical temperature T_c has been termed *magnetic catalysis*. However, recent lattice QCD result (195) has indicated the opposite effect, that is, the critical temperature T_c decreases with increasing magnetic field B , for $B \lesssim 1 \text{ GeV}^2$ and zero chemical potential $\mu = 0$. This inhibiting effect of the magnetic field B on the critical temperature T_c has been termed *inverse magnetic catalysis*.

Even though, the recent lattice QCD result (195) has also indicated that the confinement-deconfinement and chiral symmetry breaking phase transitions occur at the same critical temperature $T_c(B)$ at least for $B \lesssim 1 \text{ GeV}^2$, most holographic calculations so far (253; 254; 258; 255; 256; 257; 259) have been concerned only with $T_c(B)$ of the chiral symmetry breaking phase transition.

However, recently, reference (260), inspired by the recent lattice QCD result (195), has a priori assumed confinement and chiral symmetry breaking transitions to occur at the same critical temperature T_c in Sakai-Sugimoto model, and has argued that, in this case, $T_c(B)$ must be a decreasing function of B , consistent with the recent lattice QCD result (195), but has not provided a direct computation of $T_c(B)$.

In this thesis, we give a direct computation of the critical temperature $T_c(B)$ of the confinement-deconfinement phase transition in hard-wall AdS/QCD, and holographic duals of flavored and unflavored $\mathcal{N} = 4$ SYM on $\mathbb{R}^3 \times S^1$ where S^1 is a circle of length l in one of the spatial directions. (Note that, at finite temperature T , \mathbb{R}^3 is really $S_\tau^1 \times \mathbb{R}^2$ where S_τ^1 is the thermal circle with length $\frac{1}{T}$.) Also, note that, since the fermions of both the flavored and unflavored $\mathcal{N} = 4$ SYM on $\mathbb{R}^3 \times S^1$ obey antiperiodic boundary conditions around the circle S^1 , they acquire a tree-level mass $m \sim \frac{1}{l}$. The scalars are periodic around the circle, hence they acquire masses only at the quantum level through their couplings to the fermions (53). The gluons, however, do not acquire masses, therefore, at low-energy, both flavored and unflavored $\mathcal{N} = 4$ SYM on $\mathbb{R}^3 \times S^1$ reduce to pure 3D Yang-Mills theory.

It is well known that both flavored and unflavored $\mathcal{N} = 4$ super-Yang Mills theories (SYM) on flat spacetime \mathbb{R}^4 are not confining gauge theories. However, they can be made confining in the large- N_c limit by placing them on a compact space with length l , and the confinement-deconfinement phase transition occurs at critical temperature $T_c = \frac{1}{l}$ (266; 269; 267), see (53; 363) for a review. In our case, the compact space is $\mathbb{R}^3 \times S^1$, that is, we compactify one of the spatial dimensions into a circle of length l .

The confinement-deconfinement phase transition both in flavored and unflavored $\mathcal{N} = 4$ SYM on $\mathbb{R}^3 \times S^1$ is holographically modeled by a phase transition between a black hole solution with radius of horizon $r = r_h$, and AdS_5 -soliton solution which smoothly ends at $r = r_0$. However, to study the confinement-deconfinement phase transition in QCD on \mathbb{R}^4 at strong coupling, we use the hard-wall AdS/QCD model where the confinement-deconfinement phase

transition, of QCD on \mathbb{R}^4 , is holographically modeled by a phase transition between a black hole solution with radius of horizon $r = r_h$, and thermal- AdS_5 solution with hard-wall IR cut-off $r = r_0$.

We derive the corresponding thermal- AdS_5 solution which is the holographic dual to the confined phase of QCD on \mathbb{R}^4 by starting from a black hole solution, which corresponds to the deconfined phase of strongly coupled QCD on \mathbb{R}^4 , by setting the mass of the black hole to zero (277). And, we derive the corresponding AdS_5 -soliton solution, which is the holographic dual to the confined phase of flavored and unflavored $\mathcal{N} = 4$ SYM on $\mathbb{R}^3 \times S^1$, by "double Wick rotating" a black hole solution (53; 363).

In this thesis, we use two black hole solutions in the presence of constant magnetic field B . First, we use the black hole solution in the presence of constant magnetic field $B \ll T^2$ found in (93) to study the confinement-deconfinement phase transition in strongly coupled QCD on \mathbb{R}^4 and unflavored $\mathcal{N} = 4$ SYM on $\mathbb{R}^3 \times S^1$. Then, we use the black hole solution in the presence of constant magnetic field B , including the backreaction of N_f flavor or D7-branes for $N_f \ll N_c$, found in (272) to study the confinement-deconfinement phase transition in flavored $\mathcal{N} = 4$ SYM on $\mathbb{R}^3 \times S^1$.

The effect of magnetic field B on different observables has also been studied in (213; 210; 273; 212; 274) using the backreacted black hole solution of (93) without flavor D7-branes.

Depending on the specific holographic models to QCD, various length and energy scales appear throughout this paper. Some of the relevant length and energy scales are: the radius of the AdS_5 spacetime L which we set to $L = 1$, the radius of the black hole horizon r_h

which is related to the Hawking temperature T_H of the black hole (which is dual to the field theory temperature $T = T_H$), the radial position of the canonical singularity of the AdS_5 -soliton $r_0 = \pi T_c(B = 0) = \pi \times 0.175 \text{ GeV} = 0.55 \text{ GeV}$ for flavored and unflavored $\mathcal{N} = 4$ SYM on $\mathbb{R}^3 \times S^1$, the radial position of the hard-wall $r_0 = \frac{m_\rho}{2.405} = 0.323 \text{ GeV}$ in the thermal- AdS_5 solution for the hard-wall AdS/QCD, and an external magnetic field B in the range of $0 - 0.35 \text{ GeV}^2$ for the hard-wall AdS/QCD model and $0 - 4.2 \text{ GeV}^2$ for the flavored $\mathcal{N} = 4$ SYM on $\mathbb{R}^3 \times S^1$.

6.1 Einstein-Maxwell Theory in 5D

In this section, we review elements of Einstein-Maxwell theory in 5D which will, subsequently, be used to study confinement-deconfinement phase transitions in hard-wall AdS/QCD and holographic dual of unflavored $\mathcal{N} = 4$ SYM on $\mathbb{R}^3 \times S^1$.

The action of five-dimensional Einstein-Maxwell theory with a negative cosmological constant is (93)

$$S = S_{bulk} + S_{bdy} , \quad (6.1.1)$$

where the bulk action S_{bulk} is

$$S_{bulk} = \frac{1}{16\pi G_5} \int d^5x \sqrt{-g} \left(R - F^{MN} F_{MN} + \frac{12}{L^2} \right) , \quad (6.1.2)$$

and the boundary action S_{bdy} is

$$S_{bdy} = \frac{1}{8\pi G_5} \int d^4x \sqrt{-\gamma} \left(K - \frac{3}{L} + \frac{L}{2} \left(\ln \frac{r}{L} \right) F^{\mu\nu} F_{\mu\nu} \right) \Big|_{r=r_\Lambda} . \quad (6.1.3)$$

In the boundary action S_{bndy} (Equation 6.1.3), the first term is the Gibbons-Hawking surface term, and the other terms are the counter terms needed to cancel the UV($r_\Lambda \rightarrow \infty$) divergences in the bulk action in accordance with the holographic renormalization procedure (11). Note that the counter terms are entirely constructed from the induced metric $\gamma_{\mu\nu}$ on the boundary surface at $r = r_\Lambda$, that is,

$$\gamma_{\mu\nu}(r_\Lambda) = \text{diag}(g_{tt}(r_\Lambda), g_{xx}(r_\Lambda), g_{yy}(r_\Lambda), g_{zz}(r_\Lambda)) . \quad (6.1.4)$$

And, K is the trace, with respect to $\gamma_{\mu\nu}$, of the extrinsic curvature of the boundary given by $K_{\mu\nu} = (\partial_r \gamma_{\mu\nu}) / (2\sqrt{g_{rr}})$. Using the matrix formula $\partial_\mu(\det M) = \det M \text{tr}(M^{-1} \partial_\mu M)$ (363), we can write $K = \gamma^{\mu\nu} K_{\mu\nu} = \frac{\sqrt{g^{rr}} \partial_r \sqrt{\gamma}}{\sqrt{\gamma}}$ (93; 363).

In addition to the Bianchi identity, the field equations are (93)

$$R_{MN} = -\frac{4}{L^2} g_{MN} - \frac{1}{3} F^{PQ} F_{PQ} g_{MN} + 2 F_{MP} F_N^P , \quad (6.1.5)$$

$$\nabla^M F_{MN} = 0 . \quad (6.1.6)$$

From now on we set the AdS radius to unity, that is, $L = 1$.

Turning on a constant bulk magnetic field, in the z -direction, $B_z = F_{xy} = \partial_x A_y - \partial_y A_x = B$, where the bulk gauge potential $A_\mu(x, r) = \frac{1}{2} B(x \delta_\mu^y - y \delta_\mu^x)$, which solves Maxwell's equation

(Equation 6.1.6), and contracting Einstein's field equation (Equation 6.1.5), one can find the Ricci scalar $R = g^{MN} R_{MN}$ to be

$$R = -20 + \frac{2}{3} B^2 g^{xx} g^{yy}. \quad (6.1.7)$$

So, the on-shell Euclidean action S_E (which can be found from the Lorentzian action (Equation 6.1.1) by analytic continuation in the imaginary time direction, i.e., $t_E = it$) takes the form

$$S_E = S_{bulk}^E + S_{bndy}^E, \quad (6.1.8)$$

where the on-shell Euclidean bulk action S_{bulk}^E is

$$S_{bulk}^E = \frac{V_3}{8\pi G_5} \int_0^\beta dt_E \int_{r'}^{r_\Lambda} dr \sqrt{g} \left(4 + \frac{2}{3} B^2 g^{xx} g^{yy} \right), \quad (6.1.9)$$

and, the on-shell Euclidean boundary action S_{bndy}^E is

$$S_{bndy}^E = -\frac{V_3}{8\pi G_5} \int_0^\beta dt_E \sqrt{\gamma} \left(K - 3 + B^2 g^{xx} g^{yy} \ln r_\Lambda \right), \quad (6.1.10)$$

and, r_Λ is the UV cut-off while r' is the radius of the horizon $r' = r_h$ for a black hole solution, and IR cut-off $r' = r_0$ for a thermal- AdS_5 or AdS_5 -soliton solutions. From now on we set $V_3 = 8\pi G_5 = 1$. Also, note that the on-shell Euclidean action S_E is related to the free energy F by $S_E = \beta F$.

Background solutions with $B \ll T^2$

Here, we review the black hole solution in the presence of constant magnetic field $B \ll T^2$ found in (93) which corresponds to the deconfined phase of strongly coupled QCD on \mathbb{R}^4 (flat spacetime) and unflavored $\mathcal{N} = 4$ SYM on $\mathbb{R}^3 \times S^1$. Then, starting from the black hole solution, by setting the mass of the black hole to zero (277), we derive the corresponding thermal- AdS_5 solution which is the holographic dual to the confined phase of strongly coupled QCD on flat spacetime \mathbb{R}^4 . And, by "double Wick rotating" the black hole solution (53; 363), we derive the corresponding AdS_5 -soliton solution which is the holographic dual to the confined phase of unflavored and strongly coupled $\mathcal{N} = 4$ SYM on $\mathbb{R}^3 \times S^1$.

Black hole

For $B \ll T^2$ and electric charge density ρ , the perturbative black hole solution in powers of B , up to an integration constant a_3 is given in Eq. 6.1 and 6.16 of Ref. (93). Here, we set the electric charge density $\rho = 0$ and fix the integration constant $a_3 = -\frac{2}{3}$ so that the perturbative solution in powers of B matches the near boundary solution which is also given in Eq. 4.4, 4.5 and 6.16 of (93). Therefore, the black hole solution in Eq. 6.1 and 6.16 of Ref. (93), for vanishing electric charge density $\rho = 0$ and $a_3 = -\frac{2}{3}$, takes the form

$$\begin{aligned}
 ds_{bh}^2 &= r^2 \left(-f(r)dt^2 + q(r)dz^2 + h(r)(dx^2 + dy^2) \right) + \frac{dr^2}{f(r)r^2}, \quad (6.1.11) \\
 f(r) &= 1 - \frac{M}{r^4} - \frac{2}{3}B^2 \frac{\ln r}{r^4} + \mathcal{O}(B^4), \\
 q(r) &= 1 - \frac{2}{3}B^2 \frac{\ln r}{r^4} + \mathcal{O}(B^4), \\
 h(r) &= 1 + \frac{1}{3}B^2 \frac{\ln r}{r^4} + \mathcal{O}(B^4),
 \end{aligned}$$

and, the Hawking temperature T becomes

$$T = \frac{1}{\beta} = U'(r_h) = \frac{r_h}{2\pi} \left(1 + \frac{M}{r_h^4} - \frac{2}{3} B^2 \left(\frac{1}{2r_h^4} - \frac{\ln r_h}{r_h^4} \right) \right) + \mathcal{O}(B^4) , \quad (6.1.12)$$

where M is the mass of the black hole, $U(r) = r^2 f(r)$, the radius of the horizon r_h is defined by requiring $f(r = r_h) = 0$, T is the Hawking temperature of the black hole, and β is the length of the thermal circle which acquired a fixed value as a function of r_h in order to avoid the canonical singularity at the horizon $r = r_h$. One can also check that (Equation 6.1.11) indeed satisfies the Einstein field equation (Equation 6.1.5) or its contracted version (Equation 6.1.7).

Thermal- AdS_5

The thermal- AdS_5 solution can be found from a black hole solution by setting the mass of the black hole M to zero, see (277) for the electrically charged black hole case. Therefore, from the black hole solution for $B \ll T^2$ (Equation 6.1.11), we can determine the thermal-AdS solution for $B \ll \Lambda_{IR}^2 \sim r_0^2$ by setting the mass of the black hole $M = 0$,

$$\begin{aligned} ds_{thermal}^2 &= r^2 \left(-f_0(r) dt^2 + q(r) dz^2 + h(r) (dx^2 + dy^2) \right) + \frac{dr^2}{f_0(r)r^2} , \quad (6.1.13) \\ f_0(r) &= 1 - \frac{2}{3} B^2 \frac{\ln r}{r^4} + \mathcal{O}(B^4) , \\ q(r) &= 1 - \frac{2}{3} B^2 \frac{\ln r}{r^4} + \mathcal{O}(B^4) , \\ h(r) &= 1 + \frac{1}{3} B^2 \frac{\ln r}{r^4} + \mathcal{O}(B^4) . \end{aligned}$$

AdS_5 -soliton

The AdS_5 -soliton solution (268; 269) can be determined from the black hole solution (Equation 6.1.11) by "double Wick rotation" $t = iz'$ and $z = it'$ (53; 363). Therefore, for $B \ll \Lambda_{IR}^2 \sim r_0^2$ the AdS_5 -soliton solution is,

$$\begin{aligned}
 ds_{soliton}^2 &= r^2 (f_s(r) dz'^2 - q(r) dt'^2 + h(r) (dx^2 + dy^2)) + \frac{dr^2}{f_s(r)r^2}, \quad (6.1.14) \\
 f_s(r) &= 1 - \frac{M}{r^4} - \frac{2}{3} B^2 \frac{\ln r}{r^4} + \mathcal{O}(B^4), \\
 q(r) &= 1 - \frac{2}{3} B^2 \frac{\ln r}{r^4} + \mathcal{O}(B^4), \\
 h(r) &= 1 + \frac{1}{3} B^2 \frac{\ln r}{r^4} + \mathcal{O}(B^4), \\
 \frac{1}{l} &= \frac{U'(r_0)}{4\pi} = \frac{r_0}{2\pi} \left(1 + \frac{M}{r_0^4} + \frac{2}{3} B^2 \left(\frac{\ln r_0}{r_0^4} - \frac{1}{2r_0^4} \right) \right) + \mathcal{O}(B^4).
 \end{aligned}$$

where l is the length of the circle in the compactified z' direction which is arbitrary for the black hole solution but in order to avoid the canonical singularity at $r = r_0$ (where r_0 is defined by requiring $f_s(r = r_0) = 0$), it acquires a finite value which is given in terms of r_0 for the AdS_5 -soliton solution (Equation 6.1.14).

On-shell Euclidean actions with $B \ll T^2$

Here, we determine the on-shell Euclidean actions (free energies) for the black hole, thermal- AdS_5 , and AdS_5 -soliton solutions. And, we compute the difference between the on-shell Euclidean actions of the deconfining geometry (which is the black hole geometry for both hard-wall AdS/QCD and holographic dual of unflavored $\mathcal{N} = 4$ SYM on $\mathbb{R}^3 \times S^1$) and the confining ge-

ometry (which is the thermal- AdS_5 geometry for hard-wall AdS/QCD, and the AdS_5 -soliton geometry for holographic dual of unflavored $\mathcal{N} = 4$ SYM on $\mathbb{R}^3 \times S^1$).

Black hole

The on-shell Euclidean action $S_E = S_{bh}$ (Equation 6.1.8) for the black hole solution with $B \ll T^2$ (Equation 6.1.11) is

$$S_{bh} = S_{bulk} + S_{bndy}, \quad (6.1.15)$$

where the on-shell Euclidean bulk action of the black hole S_{bulk} for $B \ll T^2$ is

$$S_{bulk} = \int_0^\beta dt_E \int_{r_h}^{r_\Lambda} dr \sqrt{g} \left(4 + \frac{2}{3} B^2 g^{xx} g^{yy} \right), \quad (6.1.16)$$

and the on-shell Euclidean boundary action of the black hole S_{bndy} for $B \ll T^2$ is

$$S_{bndy} = - \int_0^\beta dt_E \sqrt{\gamma} \left(\frac{\sqrt{g^{rr}} \partial_r \sqrt{\gamma}}{\sqrt{\gamma}} - 3 + B^2 g^{xx} g^{yy} \ln r_\Lambda \right). \quad (6.1.17)$$

The bulk action S_{bulk} (Equation 6.1.16) (after using the black hole metric for $B \ll T^2$ (Equation 6.1.11), using the fact that $h(r)\sqrt{q(r)} = 1 + \mathcal{O}(B^4)$, evaluating the integrals, and simplifying) become

$$S_{bulk} = -\beta \left(r_h^4 - r_\Lambda^4 - \frac{2}{3} B^2 \ln r_\Lambda + \frac{2}{3} B^2 \ln r_h \right) + \mathcal{O}(B^4), \quad (6.1.18)$$

which diverges when $r_\Lambda \rightarrow \infty$, and the boundary action S_{bndy} (Equation 6.1.17) becomes

$$S_{bndy} = -\beta(r_\Lambda^4 + \frac{2}{3}B^2 \ln r_\Lambda - \frac{1}{2}M - \frac{1}{3}B^2) + \mathcal{O}(B^4), \quad (6.1.19)$$

where we ignored terms which goes to zero in the $r_\Lambda \rightarrow \infty$ limit. Also note that (Equation 6.1.19) diverges when $r_\Lambda \rightarrow \infty$, but the sum of S_{bulk} (Equation 6.1.18) and S_{bndy} (Equation 6.1.19) is finite. Hence, the black hole on-shell Euclidean action S_{bh} (Equation 6.1.15) is

$$S_{bh} = S_{bulk} + S_{bndy} = -\beta \left(r_h^4 - \frac{1}{2}M + \frac{2}{3}B^2 \ln r_h - \frac{1}{3}B^2 \right) + \mathcal{O}(B^4). \quad (6.1.20)$$

Thermal- AdS_5

The on-shell Euclidean action $S_E = S_{thermal}$ (Equation 6.1.8) for the thermal- AdS_5 solution with $B \ll \Lambda_{IR}^2 \sim r_0^2$ (Equation 6.1.13) is

$$S_{thermal} = S_{tbulk} + S_{tbndy}, \quad (6.1.21)$$

where the on-shell Euclidean bulk action S_{tbulk} of the thermal- AdS_5 for $B \ll \Lambda_{IR}^2 \sim r_0^2$ is

$$S_{tbulk} = \int_0^{\beta'} dt_E \int_{r_0}^{r_\Lambda} dr \sqrt{g} \left(4 + \frac{2}{3}B^2 g^{xx} g^{yy} \right), \quad (6.1.22)$$

and the on-shell Euclidean boundary action S_{tbndy} of the thermal- AdS_5 for $B \ll T^2$ is

$$S_{tbndy} = - \int_0^{\beta'} dt_E \sqrt{\gamma} \left(\frac{\sqrt{g^{rr}} \partial_r \sqrt{\gamma}}{\sqrt{\gamma}} - 3 + B^2 g^{xx} g^{yy} \ln r_\Lambda \right). \quad (6.1.23)$$

The thermal- AdS_5 bulk action S_{tbulk} (Equation 6.1.22) (after using the thermal- AdS_5 metric for $B \ll T^2$ (Equation 6.1.13), using the fact that $h(r)\sqrt{q(r)} = 1 + \mathcal{O}(B^4)$, evaluating the integrals, and simplifying) becomes

$$S_{tbulk} = -\beta' \left(r_0^4 - r_\Lambda^4 - \frac{2}{3} B^2 \ln r_\Lambda + \frac{2}{3} B^2 \ln r_0 \right) + \mathcal{O}(B^4), \quad (6.1.24)$$

which diverges when $r_\Lambda \rightarrow \infty$, and the thermal- AdS_5 boundary action S_{tbndy} (Equation 6.1.23) becomes

$$S_{tbndy} = -\beta' \left(r_\Lambda^4 + \frac{2}{3} B^2 \ln r_\Lambda - \frac{1}{3} B^2 \right) + \mathcal{O}(B^4), \quad (6.1.25)$$

which diverges as well when $r_\Lambda \rightarrow \infty$. But, the sum of S_{tbulk} (Equation 6.1.24) and S_{tbndy} (Equation 6.1.25) is finite. Hence, the thermal on-shell Euclidean action $S_{thermal}$ (Equation 6.1.21) becomes

$$S_{thermal} = -\beta \left(r_0^4 + \frac{2}{3} B^2 \ln r_0 - \frac{1}{3} B^2 \right) + \mathcal{O}(B^4). \quad (6.1.26)$$

where we used $\beta' = \beta\sqrt{f} = \beta$ at the boundary $r_\Lambda \rightarrow \infty$.

Therefore, ΔS_E (which is the difference between the AdS_5 black hole (Equation 6.1.20) and thermal- AdS_5 (Equation 6.1.26) on-shell Euclidean actions) becomes

$$\Delta S_E = S_{bh} - S_{thermal} = -\beta \left(r_h^4 - r_0^4 - \frac{1}{2}M + \frac{2}{3}B^2 \ln\left(\frac{r_h}{r_0}\right) \right) + \mathcal{O}(B^4) . \quad (6.1.27)$$

AdS_5 -soliton

Since, black hole (Equation 6.1.11) and AdS_5 -soliton (Equation 6.1.14) are equivalent Euclidean geometries, their on-shell Euclidean actions take similar form. In fact, the on-shell Euclidean action of AdS_5 -soliton can be found by merely replacing r_h by r_0 in the on-shell Euclidean action for the black hole (363). Therefore, the difference between the on-shell actions S_{bh} of the black hole (Equation 6.1.20) and $S_{soliton}$ of AdS_5 -soliton geometries is simply

$$\Delta S_E = S_{bh} - S_{soliton} = -\beta \left(r_h^4 - r_0^4 + \frac{2}{3}B^2 \ln\frac{r_h}{r_0} \right) + \mathcal{O}(B^4) . \quad (6.1.28)$$

6.2 Hard-Wall AdS/QCD

For hard-wall AdS/QCD(93), we determine the critical temperature $T_c(B)$ of the confinement-deconfinement phase transition by first determining the critical radius of the horizon $r_h = r_{hc}$ from the condition that the difference between the Euclidean actions for the black hole and thermal- AdS_5 solutions vanish at $r_h = r_{hc}$, i.e., $\Delta S_E(r_h = r_{hc}) = 0$. For $B \ll T^2$, requiring

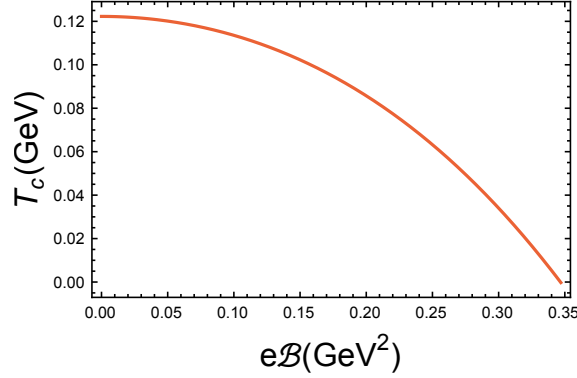


Figure 29. Critical temperature $T_c(B)$ of the hard-wall AdS/QCD with $r_0 = \frac{m_\rho}{2.405} = 0.323 \text{ GeV}$ Note: $\mathcal{B} = \sqrt{3}B$ is the physical magnetic field at the boundary.

$\Delta S_E(r_{hc}) = 0$ in (Equation 6.1.27), we find the constraint equation for the critical radius of the horizon r_{hc} to be

$$r_{hc}^4 + \frac{2}{3}B^2 \ln\left(\frac{r_{hc}}{r_0}\right) - 2r_0^4 + \mathcal{O}(B^4) = 0, \quad (6.2.29)$$

which can be solved numerically for $r_{hc}(B, r_0)$. Note that, we have fixed $M = 2r_0^4$ in (Equation 6.1.27), so that (Equation 6.2.29) reduces to the constraint equation found in (278; 279) at $B = 0$, which is $r_{hc}^4 = 2r_0^4$. Once we find the solution for r_{hc} from the constraint equation (Equation 6.2.29), we can use (Equation 6.1.12) to find $T_c = T(r_h = r_{hc}, M = 2r_0^4)$. The plot of the numerical solution for $T_c(B, r_0)$ for $B \ll T^2$ is given in Figure 29, and the numerical plot clearly shows that $T_c(B)$ decreases with increasing $B \ll T^2$ in agreement with the *inverse magnetic catalysis* recently found in lattice QCD for $B \lesssim 1 \text{ GeV}^2$ (195).

6.3 Unflavored $\mathcal{N}=4$ SYM Plasma on Compact Space

For the holographic dual of unflavored $\mathcal{N} = 4$ SYM on $\mathbb{R}^3 \times S^1$, we study the confinement-deconfinement phase transition by using the same Einstein-Maxwell action in $5D$ as we used for the hard-wall AdS/QCD, and the analysis will be similar to the hard-wall AdS/QCD case but, for the unflavored $\mathcal{N} = 4$ SYM on $\mathbb{R}^3 \times S^1$ case, we compactify the black hole solution in the z direction into a circle of length l , and compare its free energy with the free energy of AdS_5 -soliton solution (Equation 6.1.14) instead of the thermal- AdS_5 solution (Equation 6.1.13) that we used for the hard-wall AdS/QCD.

It is easy to see from (Equation 6.1.28) that the critical radius of the horizon $r_h = r_{hc}$ at which $\Delta S_E(r_h = r_{hc}) = 0$ is given by $r_h = r_{hc} = r_0$. Therefore, using (Equation 6.1.12), the critical temperature $T_c = T(r_h = r_{hc} = r_0)$ becomes,

$$T_c = \frac{r_0}{2\pi} \left(1 + \frac{M}{r_0^4} - \frac{2}{3} B^2 \left(\frac{1}{2r_0^4} - \frac{\ln r_0}{r_0^4} \right) \right) + \mathcal{O}(B^4) = \frac{1}{l}. \quad (6.3.30)$$

Fixing $M = r_0^4$ so that we reproduce the correct $B = 0$ result $T_c(B = 0) = \frac{r_0}{\pi}$, and fixing r_0 from the value of T_c at $B = 0$, which we denote as T_c^0 , we can write (Equation 6.3.30) in terms of $T_c^0 = \frac{r_0}{\pi}$ as

$$T_c = T_c^0 \left(1 - \left(\frac{B}{B_c} \right)^2 \right) + \mathcal{O}(B^4) \quad (6.3.31)$$

where we defined the critical magnetic field $B_c = \frac{\sqrt{6}\pi^2(T_c^0)^2}{1-2\ln(LT_c^0\pi)}$ and L is the radius of the AdS spacetime. From (Equation 6.3.31), it is easy to see that T_c is a decreasing function with increasing $B \ll T^2$ in qualitative agreement with the recent lattice QCD result (195).

6.4 Flavored $\mathcal{N}=4$ SYM Plasma on Compact Space

Previously, we have studied the confinement-deconfinement phase transition in the holographic dual of unflavored $\mathcal{N} = 4$ SYM on $\mathbb{R}^3 \times S^1$ using the backreacted black hole and AdS_5 -soliton geometries, from which, we can infer a simple prescription of finding T_c in any backreacted black hole and AdS_5 -soliton based models.

The prescription is, first find the backreacted metric and the Hawking temperature $T(r_h)$ of the black hole, then the critical temperature T_c is simply given by $T_c = T(r_h = r_0)$ where r_0 can be fixed by the value of $T_c^0 = T_c(B = 0)$.

Therefore, using this prescription, we can determine $T_c(N_f, B)$ of the holographic dual of flavored $\mathcal{N} = 4$ SYM on $\mathbb{R}^3 \times S^1$. To this end we will use the backreacted metric of $D3/D7$ model given in (272) where the authors have also found the Hawking temperature $T(\frac{N_f}{N_c}, B)$ including the backreaction of N_f $D7$ -branes and magnetic field B to be, see Eq. 3.1 of (272),

$$T = \frac{r_h}{\pi} \left(1 + \frac{\lambda_h}{64\pi^2} \frac{N_f}{N_c} \left(1 - 2\sqrt{1 + \frac{B^2}{r_h^4}} \right) \right) + \mathcal{O}((N_f/N_c)^2). \quad (6.4.32)$$

Since the on-shell Euclidean action of the black hole solution (including the backreaction of N_f $D7$ -branes and magnetic field B) has also been given in Eq. 3.14 of (272), in order to find the corresponding Euclidean action of the AdS_5 -soliton, all we need to do is replace r_h by r_0 in Eq. 3.14 of (272). Hence, the difference between the two on-shell Euclidean actions vanishes at the critical radius of the horizon $r_h = r_{hc} = r_0$. And, using $r_h = r_{hc} = r_0$ in (Equation 6.4.32), the

critical temperature $T_c = T(r_h = r_{hc} = r_0)$ of the confinement-deconfinement phase transition in flavored $\mathcal{N} = 4$ SYM on $\mathbb{R}^3 \times S^1$ becomes

$$T_c = \frac{r_0}{\pi} \left(1 + \frac{\lambda_h}{64\pi^2} \frac{N_f}{N_c} \left(1 - 2\sqrt{1 + \frac{B^2}{r_0^4}} \right) \right) + \mathcal{O}((N_f/N_c)^2), \quad (6.4.33)$$

which can be written in terms of $T_c^0 = T_c(N_f = 0, B = 0) = \frac{r_0}{\pi}$ as

$$T_c = T_c^0 \left(1 + \frac{\lambda_h}{64\pi^2} \frac{N_f}{N_c} \left(1 - 2\sqrt{1 + \frac{1}{\pi^4} \frac{B^2}{(T_c^0)^4}} \right) \right) + \mathcal{O}((N_f/N_c)^2), \quad (6.4.34)$$

where λ_h is the value of the 't Hooft coupling fixed at the horizon r_h , that is, $\lambda_h = 4\pi g_s e^{\phi_h} N_c$ where g_s is the string coupling constant and $\phi(r)$ is the dilaton scalar field.

Note that, for $B = 0$, (Equation 6.4.34) reduces to

$$T_c = T_c^0 \left(1 - \frac{\lambda_h}{64\pi^2} \frac{N_f}{N_c} \right) + \mathcal{O}((N_f/N_c)^2), \quad (6.4.35)$$

which is in a qualitative agreement with the hard-wall AdS/QCD (281), functional renormalization group study of QCD (282), and lattice QCD (283) results which show that T_c decreases with increasing number of flavors N_f at zero magnetic field $B = 0$ and chemical potential $\mu = 0$.

We have plotted (Equation 6.4.34) in Figure 30 which clearly shows that $T_c(B)$ decreases with increasing $B \ll T^2$ in agreement with the *inverse magnetic catalysis* recently found in lattice QCD for $B \lesssim 1 \text{ GeV}^2$ (195).

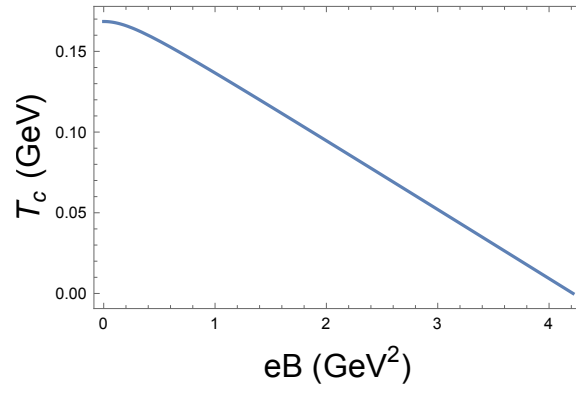


Figure 30. Critical temperature $T_c(B)$ of flavored $\mathcal{N} = 4$ SYM on $R^3 \times S^1$ (Equation 6.4.34) using $T_c^0 = 0.175 \text{ GeV}$ and $\lambda_h = 23 \times \frac{N_c}{N_f}$.

CHAPTER 7

$\mathcal{N}=4$ SUPER YANG-MILLS GAUGE THEORY ON THE COULOMB BRANCH

Despite the success of the AdS/CFT correspondence, as it was demonstrated in the previous chapters, in understanding the strongly coupled regime of gauge theories such as $\mathcal{N} = 4$ super Yang-Mills (SYM), we still lack an exact string theory dual to QCD even though there are various works which explored different non-conformal deformations of $\mathcal{N} = 4$ SYM both on the top-down (where both the details of the deformation of $\mathcal{N} = 4$ SYM and its string theory dual are known) (297; 298; 299; 266; 300; 301; 266; 347; 348; 304; 305; 306; 307; 308), and bottom-up approaches (where the details of the deformation of $\mathcal{N} = 4$ SYM and its string theory dual are unknown) (275; 289; 290; 291; 292; 344; 345; 346; 296).

In this chapter, we will present a new top-down approach which is based on the string theory dual to $\mathcal{N} = 4$ SYM on the Coulomb branch (cSYM). And, in the following, we will first give a brief introduction to $\mathcal{N} = 4$ cSYM and its supergravity dual.

In $\mathcal{N} = 4$ cSYM at zero temperature, a scale is introduced dynamically through the Higgs mechanism where the scalar particles Φ_i ($i=1\dots 6$) of $\mathcal{N} = 4$ SYM acquire a non-zero vacuum expectation value (VEV) that breaks the conformal symmetry, and the gauge symmetry $SU(N_c)$ to its subgroup $U(1)^{N_c-1}$ without breaking the supersymmetry, and without resulting in a running of the coupling constant (347). At finite temperature, the mechanism is the same except the fact that supersymmetry will be broken as well.

The string theory dual for $\mathcal{N} = 4$ cSYM at zero temperature is well known. Among various Type IIB supergravity background solutions that are dual to the strongly coupled $\mathcal{N} = 4$ cSYM at zero temperature (347; 348; 304; 305), in this thesis, we will study a Type IIB supergravity background solution that describes non-extremal rotating black 3-branes (with mass parameter m and single rotational parameter r_0) which, in the extremal limit, i.e., $r_0 \gg m^{1/4}$, is dual to $\mathcal{N} = 4$ SYM on the Coulomb branch at zero temperature that arises from N_c D3-branes distributed uniformly in the angular direction, inside a 3-sphere of radius r_0 (348).

So far the studies of the non-extremal rotating black 3-brane supergravity backgrounds has been limited to the grand canonical ensemble (which is described by fixed temperature T and angular velocity Ω or chemical potential μ), and canonical ensemble (which is described by fixed temperature T and angular momentum density J or charge density $\langle J^0 \rangle = \rho$), see (349; 354; 350; 351; 352; 314; 355; 356; 357; 353; 319). The two ensembles have different physics, for example, in planar rotating black 3-branes, Hawking-Page phase transition does not exist in the grand canonical ensemble even though it does exist in the canonical ensemble (352; 353).

In this thesis, we will introduce a new ensemble which is described by a fixed temperature T and an energy scale Λ which is directly related to the rotation parameter r_0 of the rotating black 3-brane background through $\Lambda \equiv \frac{r_0}{\pi R^2}$ where R is the radius of the AdS_5 space. From the field theory side the energy scale Λ is related to the expectation value of dimension 4 operator $\mathcal{O} = Tr \Phi_{i_1} \Phi_{i_2} \Phi_{i_3} \Phi_{i_4}$, that is, $\langle \mathcal{O} \rangle \sim \lim_{r \rightarrow \infty} \sqrt{-g} g^{rr} \partial_r h \sim \Lambda^4$ of the massless metric fluctuation $h = \bar{g}^{\mu\nu} h_{\mu\nu} = 1 - \bar{g}^{\mu\nu} g_{\mu\nu}$, where $\bar{g}_{\mu\nu}$ is the metric component of pure

$AdS_5 \times S^5$ space while $g_{\mu\nu}$ is our 10-dimensional metric (Equation 7.2.14) (347). We will see that the energy scale Λ in $\mathcal{N} = 4$ cSYM plays similar role as Λ_{QCD} in QCD.

7.1 Thermodynamics and a Second-Order Phase Transition

The rotating black 3-brane solution of the 5-dimensional Einstein-Maxwell-scalar action found from the $U(1)^3$ consistent truncation of Type IIB supergravity on S^5 (358; 359), see also (240; 322; 360), is given by

$$ds_{(5)}^2 = \frac{r^2}{R^2} H^{1/3} \left(-f dt^2 + dx^2 + dy^2 + dz^2 \right) + \frac{H^{-2/3}}{\frac{r^2}{R^2} f} dr^2, \quad (7.1.1)$$

where

$$f = 1 - \frac{r_h^4}{r^4} \frac{H(r_h)}{H(r)}, \quad H = 1 - \frac{r_0^2}{r^2}, \quad (7.1.2)$$

$$\begin{aligned} \varphi_1 &= \frac{1}{\sqrt{6}} \ln H, \quad \varphi_2 = \frac{1}{\sqrt{2}} \ln H, \\ A_t^1 &= i \frac{r_0}{R^2} \frac{r_h^2 \sqrt{H(r_h)}}{r^2 H(r)}, \\ r_h^2 &= \frac{1}{2} \left(r_0^2 + \sqrt{r_0^4 + 4m} \right), \end{aligned} \quad (7.1.3)$$

$\kappa = \frac{r_0^2}{r_h^2}$, m is the mass parameter, and $A_t^2 = A_t^3 = 0$. Note that our metric (Equation 7.1.1) is equivalent to the metric used in (356) after analytically continuing $r_0 \rightarrow -i\sqrt{q}$. We should also note that having an imaginary gauge potential, in our ensemble, is not a problem, since all physical quantities in the 5-dimensional spacetime are given in terms of $(\partial_r A_t^1)^2$.

The Hawking temperature T of the black hole (rotating black 3-brane) solution (Equation 7.1.1) is given by

$$\frac{T}{\Lambda} = \frac{1 - \frac{1}{2}\kappa}{\sqrt{\kappa - \kappa^2}}, \quad (7.1.4)$$

where $T_0 = \frac{r_h}{\pi R^2}$, $\Lambda = \frac{r_0}{\pi R^2}$, and $\kappa = \frac{r_0^2}{r_h^2} = \frac{\Lambda^2}{T_0^2}$. We have plotted $\frac{T}{\Lambda}$ in Figure 31. We can also invert (Equation 7.1.4) to find

$$\kappa = \frac{1 + \frac{T^2}{\Lambda^2} \left(1 \mp \sqrt{\frac{T^2}{\Lambda^2} - 2}\right)}{\frac{1}{2} + 2\frac{T^2}{\Lambda^2}}. \quad (7.1.5)$$

Note that in (Equation 7.1.5) ” $-$ ” corresponds to large black hole branch and ” $+$ ” corresponds to small black hole branch.

The entropy density $s(T, \Lambda)$, for our ensemble where T and Λ are held fixed, is given by

$$\begin{aligned} s(T, \Lambda) &= \frac{A_H}{4G_5 V_3} = \frac{1}{4G_5} \sqrt{g_{xx}(r_h)g_{yy}(r_h)g_{zz}(r_h)} \\ &= \frac{\pi^2 N_c^2 T_0^3}{2} (1 - \kappa)^{1/2}, \end{aligned} \quad (7.1.6)$$

where $G_5 = \pi R^3 / 2N_c^2$, and V_3 is the three-dimensional volume. And, the corresponding free energy density $f(T, \Lambda)$ of our ensemble can be determined by integrating the entropy density $s(T, \Lambda)$ as (344; 296)

$$\begin{aligned} f(T, \Lambda) &= - \int_{r_{hmin}}^{r_h} \frac{dT'}{dr'_h} s(r'_h, \Lambda) dr'_h \\ &= - \frac{\pi^2 N_c^2 T_0^4}{8} \left(1 - \kappa - \frac{3}{4}\kappa^2 - \kappa^2 \log\left(\frac{2}{\kappa} - 2\right)\right), \end{aligned} \quad (7.1.7)$$

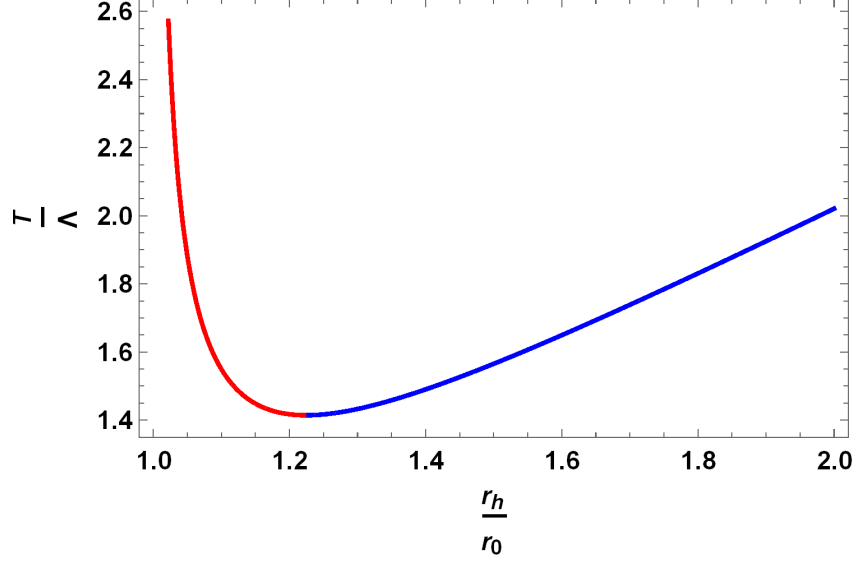


Figure 31. Hawking temperature (Equation 7.1.4).

where we choose $r_{hmin} = \sqrt{\frac{3}{2}}r_0$, and set the integration constant $f(T_{min}, \Lambda) = 0$. Note that it is possible to find the free energy f by simply integrating the entropy density s because the source $h = \bar{g}^{\mu\nu}h_{\mu\nu}$ to $\langle \mathcal{O} \rangle \sim \Lambda^4$ is normalized to vanish at the boundary. We have plotted the free energy density $f(T, \Lambda)$ (Equation 7.1.7) in Figure 32.

The other thermodynamic quantities can be determined from the free energy density $f(T, \Lambda)$ (Equation 7.1.7) as: pressure $p = -f$, energy density $\epsilon = p + Ts$, specific heat $C_\Lambda = T \left(\frac{\partial s}{\partial T} \right)_\Lambda$, and speed of sound $c_s^2 = \frac{\partial p}{\partial \epsilon} = \frac{s}{C_\Lambda}$. We have plotted the thermodynamics quantities in Figure 34, Figure 35, Figure 36, Figure 37. To compare our results with pure Yang-Mills theory on the lattice and improved holographic QCD see Fig.5-9 in (296).

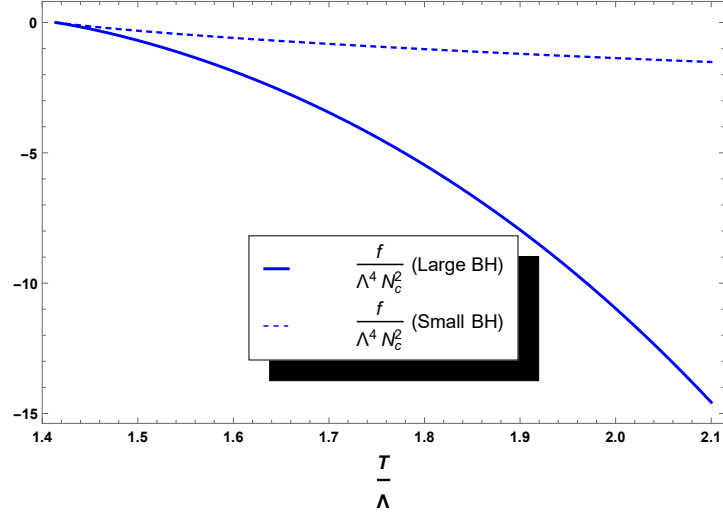


Figure 32. The free energy density $\frac{f}{\Lambda^4 N_c^2}$ of $\mathcal{N} = 4$ cSYM plasma (Equation 7.1.7) for the large and small black holes.

7.2 Cornell Potential and Glueball Mass Spectrum

The Nambu-Goto (NG) action is

$$S_{NG} = \int d\tau d\sigma \mathcal{L}(h_{ab}) = -\frac{1}{2\pi\alpha'} \int d\tau d\sigma \sqrt{-\det h_{ab}}, \quad (7.2.8)$$

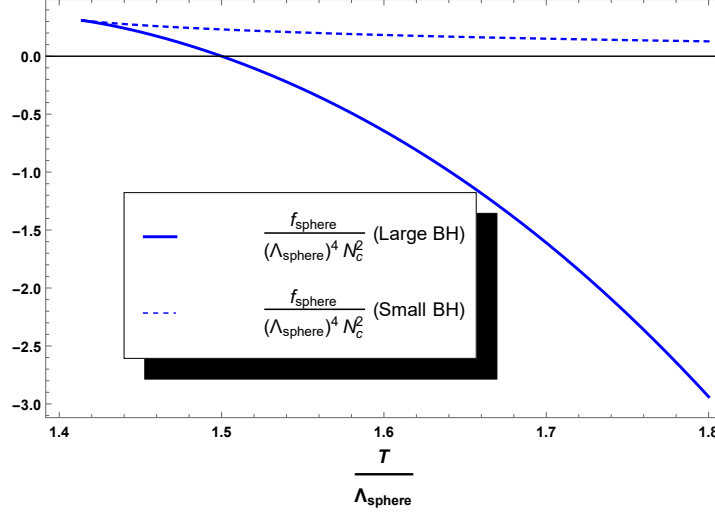


Figure 33. The free energy density $\frac{f_{\text{sphere}}}{(\Lambda_{\text{sphere}})^4 N_c^2}$ of $\mathcal{N} = 4$ SYM plasma on 3-sphere of radius R (Equation 7.3.16) for the large and small black holes.

where the background induced metric on the string $h_{ab} = g_{\mu\nu} \partial_a x^\mu(\tau, \sigma) \partial_b x^\nu(\tau, \sigma)$. Using the embedding $(\tau, \sigma) \Rightarrow (t(\tau, \sigma), 0, 0, x(\tau, \sigma), r = \sigma)$, the background induced metric $h_{ab}(x')$ becomes ($' \equiv d/d\sigma$)

$$\begin{aligned} h_{\tau\tau}(x') &= g_{tt}, \\ h_{\sigma\sigma}(x') &= g_{rr} \left(\frac{1}{1 + \frac{C^2}{g_{xx}g_{tt}}} \right), \end{aligned} \quad (7.2.9)$$

where we used

$$(x')^2 = \frac{-C^2 g_{rr}}{g_{xx}g_{tt}} \frac{1}{\left(1 + \frac{C^2}{g_{tt}g_{xx}}\right)}. \quad (7.2.10)$$

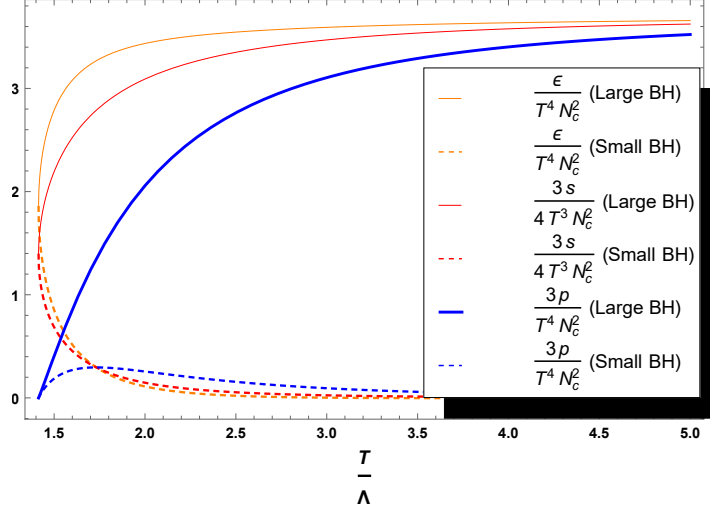


Figure 34. The energy density $\frac{\epsilon}{T^4}$, entropy density $\frac{3}{4} \frac{s}{T^3 N_c^2}$, and pressure $\frac{3p}{T^4 N_c^2}$ of $\mathcal{N} = 4$ cSYM plasma for the large and small black holes.

which is the solution of the NG equation of motion, and the integration constant C is related to the conjugate momenta $\Pi = \frac{\partial \mathcal{L}}{\partial x'} = -\frac{C}{2\pi\alpha'}$.

Cornell Potential

Considering a string configuration where a heavy quark is attached to each ends of the string, we can extract the potential energy $V(L)$, of the two quarks separated by length L , from the on-shell Nambu-Goto action S_{NG} as

$$V(L) = \frac{-2S_{NG}}{\mathcal{T}}, \quad (7.2.11)$$

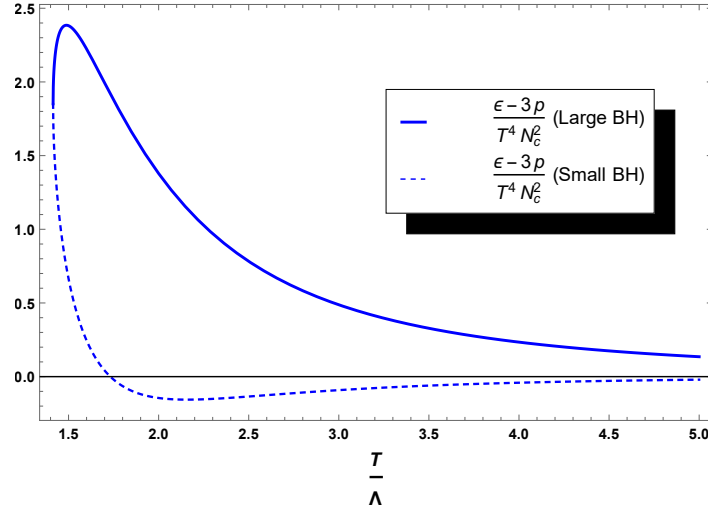


Figure 35. The trace anomaly $\frac{\epsilon - 3p}{T^4 N_c^2}$ of $\mathcal{N} = 4$ cSYM plasma for the large and small black holes.

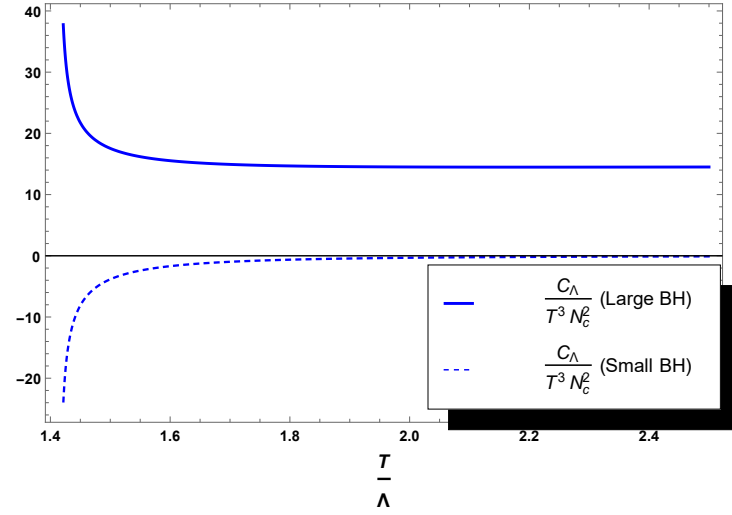


Figure 36. The specific heat C_Λ of $\mathcal{N} = 4$ cSYM plasma for the large and small black holes.

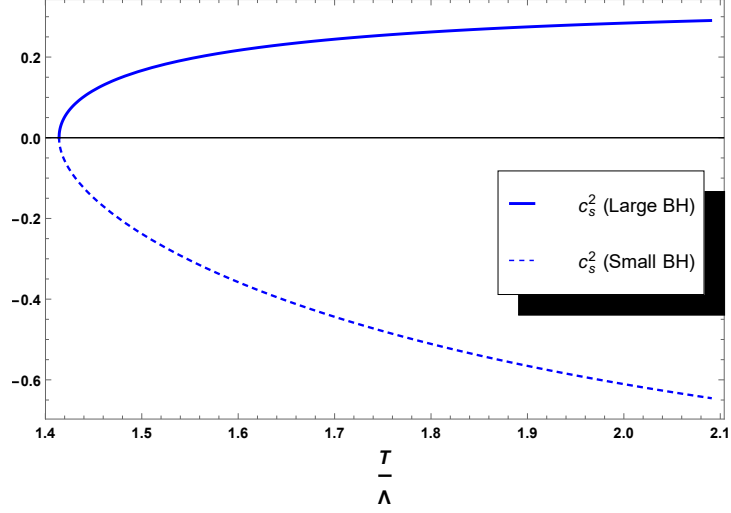


Figure 37. The speed of sound c_s^2 of $\mathcal{N} = 4$ cSYM plasma for the large and small black holes.

where

$$\begin{aligned}
 -\frac{2\pi\alpha'}{\mathcal{T}}S_{NG} &= \int_{r_m}^{\infty} dr \left(\sqrt{-\det h_{ab}(x')} - \sqrt{-\det h_{ab}(0)} \right) \\
 &\quad - \int_{r_h}^{r_m} dr \sqrt{-\det h_{ab}(0)},
 \end{aligned} \tag{7.2.12}$$

and r_m is related to L through the boundary condition $\frac{L}{2} = \int_{r_m}^{\infty} x' dr$, and we also fix the integration constant C by demanding $x' |_{r=r_m} \rightarrow \infty$ which is satisfied only when $C^2 = -g_{tt}(r_m)g_{xx}(r_m)$. Note that we have a factor of 2 in (Equation 7.2.11) because our gauge covers only half of the full string configuration which accounts to only half of the full potential energy between the

quarks, see (363) for discussion on how to compute $V(L)$ in the $x(r)$ gauge instead of the widely used $r(x)$ gauge of (335).

For $r \gg r_m$, after approximating $h_{\sigma\sigma}(x') \cong h_{\sigma\sigma}(0) = g_{rr}$,

$$\begin{aligned} V(L) &\simeq -\frac{1}{\pi\alpha'} \int_{r_0}^{r_m} dr \sqrt{-\det h_{ab}(0)} \\ &\simeq -\frac{2\sqrt{\lambda}}{3\pi} \frac{1}{L} + \frac{\pi\sqrt{\lambda}\Lambda^2}{4} L + \frac{5\Lambda}{6} + \mathcal{O}(r_0^4), \end{aligned} \quad (7.2.13)$$

where we used $\frac{L}{2} = \int_{r_m}^{\infty} x' dr \cong \frac{1}{3} \frac{R^2}{r_m}$ with $x' \cong \frac{g_{xx}(r_m)}{g_{xx}} \sqrt{\frac{g_{rr}}{g_{xx}}} \cong \frac{r_m^2 R^2}{r^4}$ for $r \gg r_m$, and we have set $r_h = r_0$ and $f = 1$ in the extremal limit.

Uplifting the 5D metric to 10D

The 5-dimensional metric (Equation 7.1.1) can be uplifted to the full 10-dimensional metric as (347; 348; 355)

$$\begin{aligned} ds_{(10)}^2 &= \frac{r^2}{R^2} \tilde{H}^{1/2} \left(-\tilde{f} dt^2 + dx^2 + dy^2 + dz^2 \right) + \frac{\tilde{H}^{1/2} H^{-1}}{\frac{r^2}{R^2} f} dr^2 \\ &+ R^2 \left(\tilde{H}^{1/2} d\theta^2 + H \tilde{H}^{-1/2} \sin^2 \theta d\phi^2 + \tilde{H}^{-1/2} \cos^2 \theta d\Omega_3^2 \right) \\ &+ 2A_t^1 H \tilde{H}^{-1/2} R^2 \sin^2 \theta dt d\phi, \end{aligned} \quad (7.2.14)$$

where

$$\tilde{H} = \sin^2 \theta + H \cos^2 \theta, \text{ and } \tilde{f} = 1 - \frac{r_h^4}{r^4} \frac{H(r_h)}{\tilde{H}(r)}, \quad (7.2.15)$$

f and H are the same as in (Equation 7.1.1). Our 10-dimensional metric (Equation 7.2.14) is equivalent to Eq.2.21 of (355) after analytically continuing the rotation parameter $r_0 \rightarrow -ir_0$,

and re-writing (Equation 7.2.14) in terms of $\mu \equiv m^{1/4}$. Note that the $g_{t\phi}$ component of (Equation 7.2.14) is imaginary and one could make it real by analytically continuing $t \rightarrow -it$ as in (351; 348). However, since we are also interested in real-time dynamics, such as computation of transport coefficients (360), we refrain from analytically continuing $t \rightarrow -it$, and we treat our 10-dimensional metric (Equation 7.2.14) as a complex saddle point. Also note that $g_{t\phi} = A_t^1 = 0$ in the extremal limit $r_h = r_0$, hence does not affect the computation of $V(L)$ and mass of the glueballs.

In (348), the heavy quark-antiquark potential energy $V(L)$ was computed for the 10-dimensional background metric (Equation 7.2.14) after analytically continuing $t \rightarrow -it$ and in the extremal limit where $r_h = r_0$ or $\tilde{f} = f = 1$ case. The authors have shown that, for $\theta = \frac{\pi}{2}$, $V(L)$ smoothly interpolates between a Coulombic potential $V(L) = -\frac{2\Gamma(3/4)^2\sqrt{\lambda}}{\Gamma(1/4)^2} \frac{1}{L}$ for small L and a confining potential $V(L) = \frac{\pi\sqrt{\lambda}\Lambda^2}{2}L$ for large L . See curve (b) in Fig.5 of (348). Their numerical result agrees qualitatively with our analytic result (Equation 7.2.13) on the 5-dimensional metric (Equation 7.1.1).

Glueball Mass Spectrum

It can easily be shown that bulk fluctuations in the 5-dimensional metric (Equation 7.1.1), at least in the near boundary limit where the metric is essentially AdS_5 space with IR cut-off at $r = r_0$, have mass-gap and quantized mass spectrum proportional to $\Lambda = \frac{r_0}{\pi R^2}$.

In (348), it was shown that a scalar bulk fluctuation in a 10-dimensional metric (Equation 7.2.14), after analytically continuing $t \rightarrow -it$, indeed has mass gap proportional to Λ and a quantized mass spectrum $M_n^2 = 4\pi^2\Lambda^2 n(n+1)$, see Eq.54 in (348). Since, a scalar bulk fluc-

tuation in (Equation 7.2.14) has the same 5-dimensional bulk equation of motion as in (348) which is the Jacobi equation, we can use this result to calculate the mass spectrum of glueballs in $\mathcal{N} = 4$ cSYM.

The transverse gravitational tensor fluctuation $h_y^x(t, z, r)$ in the 10-dimensional metric (Equation 7.2.14), which is a source to dimension 4 stress-energy tensor operator T_x^y , also has the same 5-dimensional bulk equation of motion as the scalar field which is the Jacobi equation. Therefore, we can infer that the operator T_x^y which corresponds to spin-2 glueballs of $J^{PC} = 2^{++}$ (336) has mass spectrum given by $M_n^2 = 4\pi^2\Lambda^2 n(n+1)$ for $n = 1, 2, \dots$

The real and imaginary parts of the bulk fluctuation of a massless complex scalar field $\Phi = e^{-\phi} + i\chi$, in the 10-dimensional metric (Equation 7.2.14), are sources to the dimension 4 scalar operators $\mathcal{O}_4 = Tr F^2$ and $\tilde{\mathcal{O}}_4 = Tr F \wedge F$, respectively (337), and its 5-dimensional bulk equation of motion is the Jacobi equation. Therefore, \mathcal{O}_4 and $\tilde{\mathcal{O}}_4$ which correspond to the scalar glueballs of $J^{PC} = 0^{++}$ and $J^{PC} = 0^{-+}$, respectively, have a degenerate mass spectrum given by $M_n^2 = 4\pi^2\Lambda^2 n(n+1)$ for $n = 1, 2, \dots$

7.3 Hadronization

The EoS plotted in Figure 32 and Figure 34 has interesting physical interpretation, that is, a localized large black hole shrinks and cools down until its temperature reaches the critical temperature T_c at which $p(T_c) = 0$, and the large black hole smoothly turns in to a localized small black hole (a second-order phase transition). Since, the small black hole has negative specific heat and is unstable even classically, it starts Hawking radiating hadrons and eventually its energy and entropy vanishes and turn in to thermal AdS or gas of hadrons.

We would like to stress that in the small black hole phase, i.e., the hadronization phase where the entropy decreases due to bound-state formation, the plasma "fire ball" is reheating and thereby again reducing its free energy below that of the thermal AdS or hadron gas phase. The temperature evolution of the small black hole may also be compared to the temperature evolution during hadronization in experimental high-energy collisions.

Since, this entire process (the production of plasma in a hadron-hadron collision, and its subsequent decay via hadronization) is unitary, there is no information loss. Therefore, the small black hole information paradox (323; 324) is resolved in AdS/CFT correspondence.

As a comparison to $\mathcal{N} = 4$ cSYM, let us look at what happens for $\mathcal{N} = 4$ SYM on sphere based on its free energy density f_{sphere} plotted in Fig. Figure 33 and given by (266), see also (363),

$$f_{sphere} = \frac{F_{sphere}}{V_3} = -\frac{\pi^2 N_c^2 T_0^4}{8} (1 - \kappa_{sphere}), \quad (7.3.16)$$

where $\kappa_{sphere} = \frac{R^2}{r_h^2} = \frac{\Lambda_{sphere}^2}{T_0^2}$, and the Hawking temperature $\frac{T}{\Lambda_{sphere}} = \frac{1 + \frac{1}{2}\kappa_{sphere}}{\sqrt{\kappa_{sphere}}}$. A localized large black hole with spherical horizon shrinks and cools down until its temperature reaches the critical temperature T_c at which $p_{sphere}(T_c) = 0$ and abruptly changes to thermal AdS (a first-order phase transition also known as Hawking-Page transition (326; 266)). Since, this entire process is unitary, there is no information loss in $\mathcal{N} = 4$ SYM on sphere and its holographic dual, see (142; 327).

Sufficiently small black hole with spherical horizon in $AdS_5 \times S^5$ suffers a Gregory and Laflamme (GL) instability (328) for $r_h \ll R$ where R is the radius of the compact extra dimensions S^5 (329; 330; 331). The presence of GL instability in sufficiently small black hole

with spherical horizon is expected since in the $r_h \ll R$ limit the small black hole resembles an unstable 10-dimensional Schwarzschild black hole where the extra dimensions are 5-dimensional flat space \mathbb{R}^5 (329).

However, small black hole with planar horizon in (Equation 7.2.14) does not suffer a GL instability because in the $R \ll r_h < r_{hmin} = \sqrt{\frac{3}{2}}r_0$ limit the small black hole resembles a stable 10-dimensional Schwarzschild black hole where the extra dimensions are 5-dimensional compact space with radius $R \ll r_h < r_{hmin} = \sqrt{\frac{3}{2}}r_0$, i.e., the GL instability is stabilized due to the compactification of the extra dimensions (328).

Finally, we propose the following formula to compute the number of thermal hadrons emitted per unit volume in the local rest frame from $\mathcal{N} = 4$ cSYM plasma in its hadronizing phase (or small black hole with temperature

$$(2\pi)^3 \frac{d\Gamma_{hadron}}{d^3\mathbf{k}} \equiv \frac{1}{\sigma(0)} \frac{d\Gamma_{Hawking}}{d^3\mathbf{k}}, \quad (7.3.17)$$

where (332)

$$(2\pi)^3 \frac{d\Gamma_{Hawking}}{d^3\mathbf{k}} = \frac{\sigma(\omega, \mathbf{k})}{e^{\omega/T} \mp 1}, \quad (7.3.18)$$

is the Hawking radiation rate of the black hole with temperature T , and $\sigma(\omega, \mathbf{k})$ is the cross-section for a hadron (bulk fluctuation) of energy ω and momentum \mathbf{k} coming in from infinity

to be absorbed by $\mathcal{N} = 4$ cSYM plasma in its hadronizing phase (or the small black hole). The absorption cross-section $\sigma(\omega, \mathbf{k})$ is given by

$$\sigma(\omega, \mathbf{k}) = -\frac{16\pi G_5}{\omega} \text{Im } G^R(\omega, \mathbf{k}), \quad (7.3.19)$$

where $G^R(\omega, \mathbf{k})$ is the retarded two-point function of an operator \mathcal{O} corresponding to the hadron, (20)

$$G^R(\omega, \mathbf{k}) = -i \int d^4x e^{-ikx} \theta(t) \langle [\mathcal{O}(t, \mathbf{x}), \mathcal{O}(0, 0)] \rangle, \quad (7.3.20)$$

which can be computed using the dictionary of AdS/CFT correspondence in real-time (333; 6). For example, for spin-2 glueballs $\mathcal{O} = T_x^y$ is the energy-momentum tensor operator with a source transverse metric bulk fluctuation (graviton) h_y^x .

In the hydrodynamic limit $\omega \ll T$, (Equation 7.3.17) reduces to the Cooper-Frye formula in the local rest frame (Bose or Fermi distribution), see Eq.A1 of (334),

$$(2\pi)^3 \frac{d\Gamma_{hadron}}{d^3\mathbf{k}} \simeq \frac{1}{e^{\omega/T} \mp 1}, \quad (7.3.21)$$

where $\omega^2 = M_h^2 + |\mathbf{k}|^2$, M_h is the mass of the hadron, and \mathbf{k} is its momentum.

We would like to emphasize that in the presence of local thermal equilibrium with temperature distribution $T(t, \mathbf{x})$ for the black hole, the 3-dimensional volume integral of (Equation 7.3.21), i.e.,

$$(2\pi)^3 \frac{d\Gamma_{hadron}}{d^3\mathbf{k}} \simeq \frac{1}{e^{\omega/T(t, \mathbf{x})} \mp 1} d^3\mathbf{x}, \quad (7.3.22)$$

should be carried out over a freeze-out or isothermal hypersurface defined by the constraint equation $T(t, \mathbf{x}) = T_f$ where $T_f \geq T_{min} = T_c$, and can be used to eliminate the explicit time t dependence from the integrand, i.e., $t = t_f(\mathbf{x})$. Therefore, the hadron emission rate at this freeze-out or isothermal hypersurface is given by

$$(2\pi)^3 \frac{d\Gamma_{hadron}}{d^3\mathbf{k}} \simeq \frac{1}{e^{\omega/T_f} \mp 1} d^3\mathbf{x}. \quad (7.3.23)$$

Note that the same argument applies in the boosted frame which justifies the application of similar constraint equation $T(t, \mathbf{x}) = T_f$ in the hydrodynamic models that use Cooper-Frye formula (Equation 7.3.23) in the boosted frame, see for example (338).

Note that, in (339) Castorina, Kharzeev, and Satz have conjectured that a QCD counterpart of Hawking radiation by black holes provides a common mechanism for thermal hadron production in high energy interactions, from e^+e^- annihilation to heavy ion collisions. Our result (Equation 7.3.17) is the AdS/CFT version of their conjecture.

We have shown that the large black hole branch of the non-extremal rotating black 3-brane background solution (Equation 7.1.1) has pure Yang-Mills-like equation of state: the pressure p vanishes at critical temperature $T_c = T_{min} = \sqrt{2}\Lambda$, see Figure 34; the trace anomaly $\epsilon - 3p$ have a maxima around T_c and vanishes at very high temperature, see Figure 35; and the speed of sound c_s^2 approaches its conformal limit $1/3$ from below. In order to compare our results with pure Yang-Mills theory on the lattice and improved holographic QCD see Fig.5-9 in (296).

In summary, we have computed the heavy quark-antiquark potential energy $V(L)$ of $\mathcal{N} = 4$ cSYM at $T = 0$ and have shown that it is given by Cornell potential, see (Equation 7.2.13). We have also shown that the mass spectrums of the scalar and spin-2 glueballs of $\mathcal{N} = 4$ cSYM at $T = 0$ are degenerate and given by $M_n^2 = 4\pi^2\Lambda^2 n(n+1)$ for $n = 1, 2, \dots$

We have found a second-order phase transition from the large black hole branch with positive specific heat to the small black hole branch with negative specific heat. From the gravity side, the reason why we have this second-order phase transition is due to the fact that, as can be seen from the free energy depicted in Figure 32, the small black hole branch has lower (or negative) free energy compared to the thermal AdS space or extremal black hole.

We have conjectured that the small black hole is dual to $\mathcal{N} = 4$ cSYM plasma in its hadronizing phase, and we have proposed a formula (Equation 7.3.17) that relates the Hawking radiation rate with the thermal hadron emission rate, and in the hydrodynamic limit $\omega \ll T$ reduces to Cooper-Frye formula in the local rest frame. See (340) for analogous phenomena where unstable plasma-balls decay by thermally radiating hadrons.

7.4 Transport Coefficients

The transverse metric fluctuation $h_{xy}(t, z, r)$ decouples from other fluctuations, hence the shear viscosity for a general background metric $g_{\mu\nu}$ is given by (51)

$$\eta = \frac{1}{16\pi G_5} \sqrt{g_{xx}(r_h)g_{yy}(r_h)g_{zz}(r_h)} \frac{g_{xx}(r_h)}{g_{yy}(r_h)} = \frac{s}{4\pi} \frac{g_{xx}(r_h)}{g_{yy}(r_h)}. \quad (7.4.24)$$

Since, for our background metric (Equation 7.1.1) $g_{xx} = g_{yy}$, the shear viscosity η of $\mathcal{N} = 4$ cSYM is simply

$$\frac{\eta}{s} = \frac{1}{4\pi}. \quad (7.4.25)$$

Bulk viscosity ζ can be computed by closely following (345). To this end, we first replace $\varphi_1 \rightarrow \frac{1}{2}\tilde{\varphi}_1$ followed by $\varphi_2 \rightarrow \frac{\sqrt{3}}{2}\tilde{\varphi}_1$, to bring the Einstein-Maxwell-scalar part of our action (Equation 6.1.1) in the same form as the action used in (345), i.e.,

$$(16\pi G_5) \frac{\mathcal{L}}{\sqrt{-g_5}} = (\mathcal{R} - \tilde{V}(\tilde{\varphi}_1)) - \frac{1}{2} (\partial\tilde{\varphi}_1)^2 + \dots, \quad (7.4.26)$$

where

$$\tilde{V}(\tilde{\varphi}_1) = -\frac{4}{R^2} \left(e^{\frac{2}{\sqrt{6}}\tilde{\varphi}_1} \left(1 + \frac{\kappa(1-\kappa)}{2\kappa^3} (e^{-\frac{3}{\sqrt{6}}\tilde{\varphi}_1} - 1)^3 \right) + 2e^{-\frac{1}{\sqrt{6}}\tilde{\varphi}_1} \right). \quad (7.4.27)$$

In the $\tilde{r} = \varphi_1(r)$ gauge, the bulk viscosity ζ up to a constant is (345)

$$\frac{\zeta}{s} \propto \frac{1}{4\pi} \frac{\tilde{V}'(\tilde{r}_h)^2}{\tilde{V}(\tilde{r}_h)^2}, \quad (7.4.28)$$

where $'$ denotes the derivative with respect to $\tilde{r} = \tilde{\varphi}_1(r)$. Note that, in the gauge $\tilde{r} = \tilde{\varphi}_1(r) = \frac{2}{\sqrt{6}} \ln H(r)$, the horizon of the black hole is located at $\tilde{r} = \tilde{r}_h = \frac{2}{\sqrt{6}} \ln H(r_h) = \frac{2}{\sqrt{6}} \ln(1 - \kappa)$ where κ is still given by (Equation 7.1.5). We have plotted $\frac{\zeta}{s}$ in Figure 38

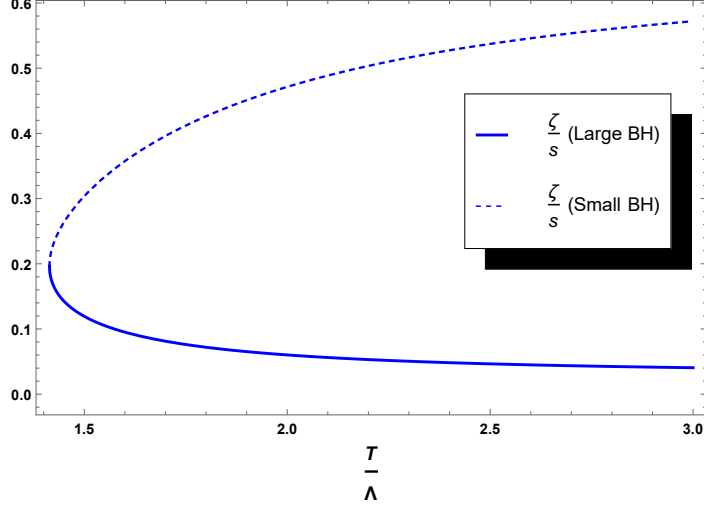


Figure 38. The bulk viscosity to entropy density ratio $\frac{\zeta}{s}$ of $\mathcal{N} = 4$ SYM plasma on the Coulomb branch for both large and small black holes (Equation 7.4.28).

The conductivity σ_f of a $U(1)$ flavor charge can simply be computed using the general formula (6; 210)

$$\sigma_f = \frac{1}{g_5^2} \sqrt{g_{xx}(r_h)g_{yy}(r_h)g_{zz}(r_h)g^{xx}(r_h)} = \frac{N_c N_f T_0}{4\pi} (1 - \kappa)^{1/6}, \quad (7.4.29)$$

where we used $g_5^2 = \frac{4\pi^2 R}{N_c N_f}$ and a bulk $U(1)$ flavor action of the form $S_f = -\frac{1}{4g_5^2} \int d^5x \sqrt{-g} F^2$ which can be derived from the low-energy limit of the Dirac-Born-Infeld action of probe N_f D7-branes (364). Note that there is no mixing between the gravitational and flavor gauge field fluctuations. We have plotted σ_f in Figure 39.

The conductivity σ_R of a single R-charge can be computed by directly computing the two-point retarded correlation functions $G^{\mu\nu}$ of the spatial component of the R-current J^μ , in the presence background A_t^1 which results in mixing between the gravitational and gauge field fluctuations, and using Kubo formula, i.e.,

$$\sigma_R = \lim_{\omega \rightarrow 0} -\frac{1}{\omega} \text{Im} G^{xx}(\omega, \mathbf{k} = 0) = \frac{N_c^2 T_0}{32\pi} \frac{(2 - \kappa)^2}{\sqrt{1 - \kappa}}, \quad (7.4.30)$$

where in the last line we used $G^{xx} = \frac{-i(2-\kappa)^2 N_c^2 T_0 \omega}{32\pi\sqrt{1-\kappa}}$ which is nothing but Eq.4.34 of (356) after replacing $\kappa \rightarrow -\kappa$, and $G^{xx} \rightarrow \frac{1}{2}G^{xx}$ to compensate for the different normalisation we have for the gauge fields. We have plotted σ_R in Figure 39.

7.5 Hard Probes

The Nambu-Goto (NG) action is

$$S_{NG} = \int d\tau d\sigma \mathcal{L}(h_{ab}) = -\frac{1}{2\pi\alpha'} \int d\tau d\sigma \sqrt{-\det h_{ab}}, \quad (7.5.31)$$

where the background induced metric on the string h_{ab} is given by

$$h_{ab} = g_{\mu\nu} \partial_a x^\mu(\tau, \sigma) \partial_b x^\nu(\tau, \sigma). \quad (7.5.32)$$

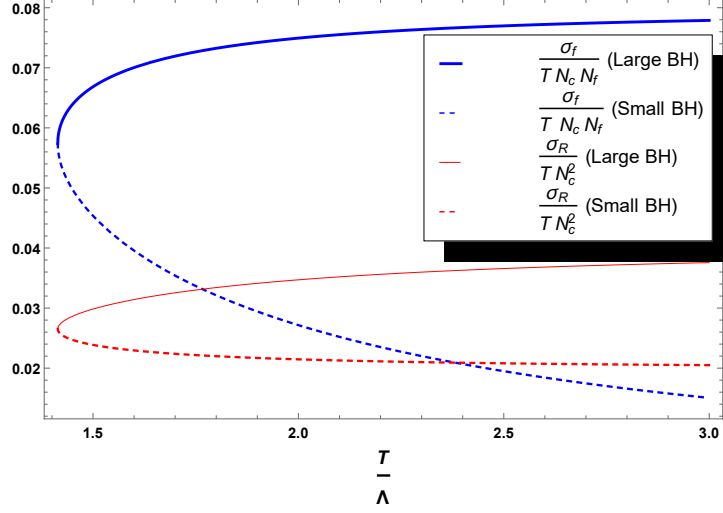


Figure 39. The conductivity $\frac{\sigma_f}{T N_c N_f}$ of a $U(1)$ flavor charge (Equation 7.4.29), and $\frac{\sigma_R}{T N_c^2}$ of a single R-charge (Equation 7.4.30) of flavored and unflavored $\mathcal{N} = 4$ SYM plasma, respectively, on the Coulomb branch for both large and small black holes.

Using the embedding $(\tau, \sigma) \Rightarrow (t(\tau, \sigma), 0, 0, x(\tau, \sigma), r = \sigma)$, the background induced metric $h_{ab}(\dot{z}, z')$ (Equation 7.5.32) becomes ($\cdot \equiv d/d\tau, ' \equiv d/d\sigma$)

$$h_{ab}(\dot{x}, x') = g_{tt} \partial_a t \partial_b t + g_{xx} \partial_a x \partial_b x + g_{rr} \partial_a r \partial_b r. \quad (7.5.33)$$

Using a particular Ansatz of the form $t(\tau, \sigma) = \tau + K(\sigma)$ and $z = v\tau + F(\sigma)$, which represents a “trailing string” configuration moving with velocity v , the background induced metric (Equation 7.5.33) becomes (206)

$$\begin{aligned} h_{\tau\tau}(v, x') &= g_{tt} + v^2 g_{xx}, \\ h_{\sigma\sigma}(v, x') &= g_{tt}(K')^2 + g_{xx}(x')^2 + g_{rr}, \\ h_{\tau\sigma}(v, x') &= g_{tt}K' + g_{xx}x'v. \end{aligned} \tag{7.5.34}$$

Finding the equation of motion from the action, we have

$$\partial_\sigma \left(\frac{g_{tt}g_{xx}(x' - vK')}{\sqrt{-\det h_{ab}}} \right) = 0. \tag{7.5.35}$$

Requiring $h_{\tau\sigma}(v, x') = 0$ to fix this gauge freedom, we have an additional constraint $K' = -\frac{g_{xx}}{g_{tt}}x'v$, which can be used to diagonalize (Equation 7.5.34) as (206)

$$\begin{aligned} h_{\tau\tau}(v, x') &= g_{tt} \left(1 + v^2 \frac{g_{xx}}{g_{tt}} \right), \\ h_{\sigma\sigma}(v, x') &= \left(1 + v^2 \frac{g_{xx}}{g_{tt}} \right) g_{xx}(x')^2 + g_{rr}. \end{aligned} \tag{7.5.36}$$

Solving the equation of motion, in this gauge, for x' , we find

$$(x')^2 = \frac{-C^2 g_{rr}}{g_{xx}^2 g_{tt}} \frac{1}{\left(1 + v^2 \frac{g_{xx}}{g_{tt}} \right) \left(1 + \frac{C^2}{g_{tt}g_{xx}} \right)}. \tag{7.5.37}$$

where the integration constant C is related to the conjugate momenta $\Pi = \frac{\partial \mathcal{L}}{\partial x'} = -\frac{C}{2\pi\alpha'}$. Since the factor $1 + v^2 \frac{g_{xx}}{g_{tt}}$ in (Equation 7.5.37), for $v \neq 0$, vanishes when $-\frac{g_{tt}(r_s)}{g_{xx}(r_s)} = v^2$, requiring $(x')^2$ to be positive across $r = r_s$, the other factor $1 + \frac{C^2}{g_{tt}g_{tt}}$ has to vanish at $r = r_s$ as well, which will fix the integration constant $C^2 = -g_{tt}(r_s)g_{xx}(r_s)$ for $v \neq 0$.

So, the induced metric (Equation 7.5.36) for $v \neq 0$ becomes

$$\begin{aligned} h_{\tau\tau}(v, x') &= g_{tt} \left(1 - \frac{g_{tt}(r_s)}{g_{tt}} \frac{g_{xx}}{g_{xx}(r_s)} \right), \\ h_{\sigma\sigma}(v, x') &= g_{rr} \left(\frac{1}{1 - \frac{g_{xx}(r_s)g_{tt}(r_s)}{g_{xx}g_{tt}}} \right). \end{aligned} \quad (7.5.38)$$

which can be interpreted as a metric of a 2-dimensional black hole with a line element $ds_{(2)}^2$ given by

$$ds_{(2)}^2 = h_{\tau\tau}d\tau^2 + h_{\sigma\sigma}d\sigma^2 = -g_{tt}(-\tilde{f}(r))d\tau^2 + \frac{1}{\tilde{p}(r)}d\sigma^2, \quad (7.5.39)$$

where $\tilde{f}(r) = 1 - \frac{g_{tt}(r_s)}{g_{tt}} \frac{g_{xx}}{g_{xx}(r_s)}$, $\tilde{p}(r) = g_{rr} \left(1 - \frac{g_{xx}(r_s)g_{tt}(r_s)}{g_{xx}g_{tt}} \right)$. The radius of the horizon r_s of the 2-dimensional black hole is found by solving the algebraic equation $-\frac{g_{tt}(r_s)}{g_{xx}(r_s)} = v^2$. And, the Hawking temperature of the 2-dimensional black hole denoted as T_s is

$$T_s = \frac{1}{4\pi} \sqrt{-g_{tt}(r_s)\tilde{f}'(r_s)\tilde{p}'(r_s)}. \quad (7.5.40)$$

The drag force is given by (217; 218), see also (206),

$$F_{drag} = -\frac{C}{2\pi\alpha'} = -\frac{1}{2}\pi\sqrt{\lambda}T_0^2\gamma v Q(\kappa, \gamma), \quad (7.5.41)$$

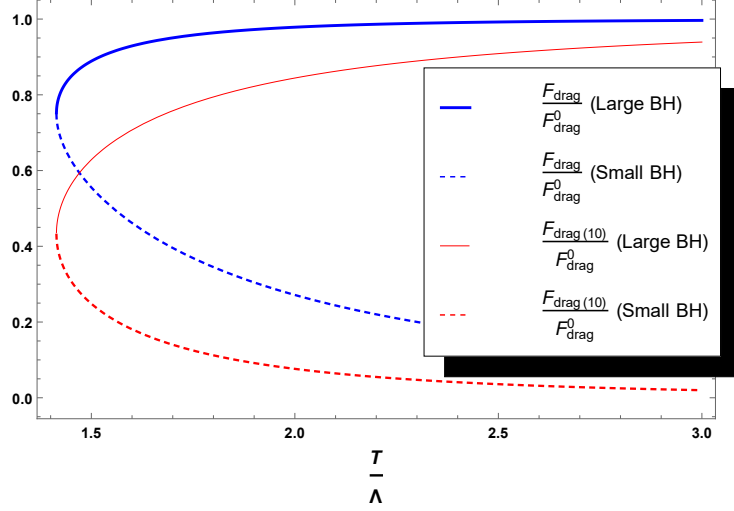


Figure 40. The drag forces $\frac{F_{drag}}{F_{drag}^0}$ (Equation 7.5.41), and $\frac{F_{drag(10)}}{F_{drag}^0}$ of $\mathcal{N} = 4$ SYM plasma on the Coulomb branch for both large and small black holes, normalized by the drag force $F_{drag}^0 = -\frac{1}{2}\sqrt{\lambda}\pi T^2\gamma v$ of the conformal $\mathcal{N} = 4$ SYM plasma.

where $Q(\kappa, \gamma) = \frac{\kappa}{2\gamma} \left(1 + \sqrt{1 + 4\gamma^2 \frac{1-\kappa}{\kappa^2}} \right)$, and we have used $r_s^2 = \gamma r_h^2 Q(\kappa, \gamma)$ which solves the algebraic equation $-\frac{g_{tt}(r_s)}{g_{xx}(r_s)} = v^2$. We have plotted F_{drag} in Figure 40

The velocity dependent transverse momentum diffusion constant per unit time $\kappa^\perp(v)$ is given by (206)

$$\kappa^\perp(v) = \frac{T_s}{\pi\alpha'} g_{xx}(r_s), \quad (7.5.42)$$

and the longitudinal momentum diffusion constant per unit time $\kappa^\parallel(v)$ is (365)

$$\kappa^\parallel(v) = \frac{T_s}{\pi\alpha'} \frac{1}{g_{xx}} \frac{(g_{tt}g_{xx})'}{(g_{tt}/g_{xx})'} \Big|_{r=r_s}. \quad (7.5.43)$$

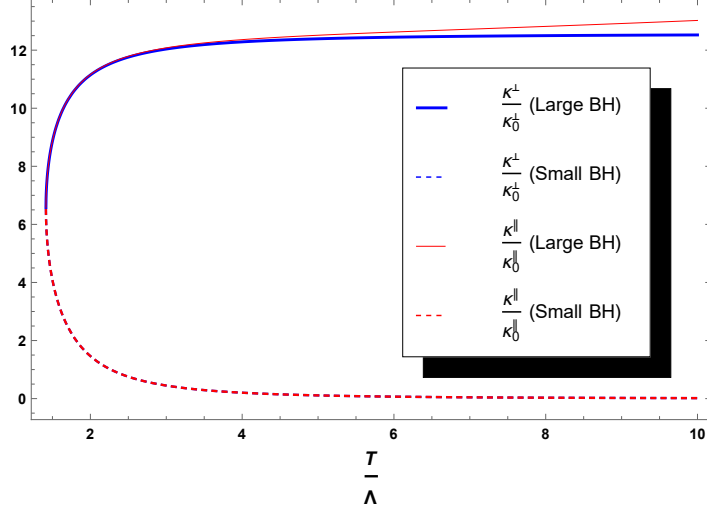


Figure 41. The transverse and longitudinal momentum diffusion constants $\frac{\kappa^\perp(0)}{\kappa_0(v)}$ (Equation 7.5.42) and $\frac{\kappa^\parallel(0)}{\kappa_0(v)}$ (Equation 7.5.43), respectively, of $\mathcal{N} = 4$ SYM plasma on the Coulomb branch for both large and small black holes, normalized by the momentum diffusion constant $\kappa_0 = \kappa_0^\perp(0) = \kappa_0^\parallel(0) = \sqrt{\lambda}\pi T^3$ of the conformal $\mathcal{N} = 4$ SYM plasma.

We have plotted $\kappa^\perp(0)$ and $\kappa^\parallel(0)$ in Figure 41. Note from Figure 41 that $\kappa^\perp(v) \neq \kappa^\parallel(v)$ even at $v = 0$ in $\mathcal{N} = 4$ cSYM plasma, even though they are equal to each other at $v = 0$ in $\mathcal{N} = 4$ SYM plasma. Also note that, as can be seen in Figure 41, the difference between $\kappa^\perp(v)$ and $\kappa^\parallel(v)$ gets enhanced with increasing T and v .

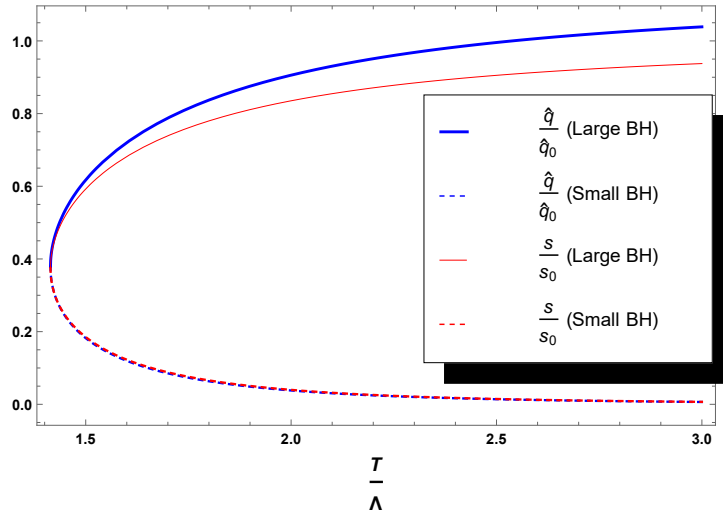


Figure 42. The jet quenching parameter $\frac{\hat{q}}{\hat{q}_0}$ (Equation 7.5.45) and entropy density $\frac{s}{s_0}$ of $\mathcal{N} = 4$ SYM plasma on the Coulomb branch for both large and small black holes, normalized by the jet quenching parameter $\hat{q}_0 = \frac{\pi^{3/4}\Gamma(3/4)}{\sqrt{2}\Gamma(5/4)}\sqrt{\lambda}T^3$ and entropy density $s_0 = \frac{1}{2}\pi^2 N_c^2 T^3$ of the conformal $\mathcal{N} = 4$ SYM plasma.

In (367) the drag force was studied using the 10-dimensionnal metric (Equation 7.2.14), and it was shown that the drag force $F_{drag(10)}$ is (shown below after re-writing it in terms of κ , and making the analytic continuation $r_0 \rightarrow -ir_0$ which is equivalent to replacing $\kappa \rightarrow -\kappa$)

$$F_{drag(10)} = -\frac{1}{2}\sqrt{\lambda}\pi T_0^2\sqrt{1-\kappa}\gamma v. \quad (7.5.44)$$

Note that (Equation 7.5.44) is equivalent to the $\gamma \rightarrow \infty$ limit of (Equation 7.5.41), and it has similar $\sqrt{1-\kappa}$ dependence as the entropy density (Equation 7.1.6) indicating that the drag force (Equation 7.5.44) could be the measure of the color degrees of freedom of the plasma (187). We have plotted (Equation 7.5.44) in Figure 40.

And, in (355), it was shown that the jet quenching parameter \hat{q} , studied using the 10-dimensionnal metric (Equation 7.2.14), is (shown below after re-writing it in terms of κ , and making the analytic continuation $r_0 \rightarrow -ir_0$ which is equivalent to replacing $\kappa \rightarrow -\kappa$)

$$\frac{\hat{q}}{\hat{q}_0} = \frac{\mathbf{K}(1/\sqrt{2})}{\mathbf{K}(n)}(2n^2)^2(2n'^2)^{1/2}, \quad (7.5.45)$$

where $\mathbf{K}(n)$ is the complete elliptic integral of the first kind, $n^2 = \frac{1-\kappa}{2-\kappa}$, $n' = \sqrt{1-n^2}$, and $\hat{q}_0 = \frac{\pi^{3/4}\Gamma(3/4)}{\sqrt{2}\Gamma(5/4)}\sqrt{\lambda}T^3$ (343; 187). In Mathematica, the complete elliptic integral of the first kind is implemented using $\text{EllipticK}[n^2] \equiv \mathbf{K}(n)$. We have plotted \hat{q} in Figure 42.

Note that, for the small black hole branch, we have

$$\frac{F_{drag(10)}}{F_{drag}^0} \simeq \frac{\hat{q}}{\hat{q}_0} = \frac{s}{s_0} = \sqrt{a\left(\lambda, \frac{T}{\Lambda}\right)}, \quad (7.5.46)$$

where $a(\lambda, \frac{T}{\Lambda}) = 1 - \kappa$ is our a-function defined in Eq. 6.29 and 6.38 of (187), similar to the c-function of a two dimensional conformal field theory, which measures the number of degrees of freedom of a theory at an energy scale T and decreases monotonically with renormalization group flow. Note that $\frac{F_{drag(10)}}{F_{drag}^0} \simeq \frac{s}{s_0}$ since $T_0 \simeq T$. For the small black hole branch, it is easy to see from Fig. Figure 40 and Fig. Figure 42 that $a(\lambda, \frac{T}{\Lambda})$ decreases monotonically with the energy scale $\frac{T}{\Lambda}$. Therefore, the a-function $a(\lambda, \frac{T}{\Lambda})$ measures the color degrees of freedom of the small black hole branch ($\mathcal{N} = 4$ cSYM in its hadronizing phase) which is decreasing due to Hawking radiation or thermal hadron emission.

In summary, we have studied the transport coefficients of the non-extremal rotating black 3-brane dual to strongly coupled $\mathcal{N} = 4$ cSYM plasma, such as bulk viscosity to entropy density ratio $\frac{\zeta}{s}$ (Equation 7.4.28), and conductivity σ (Equation 7.4.29)(Equation 7.4.30), see Figure 38 and Figure 39, respectively. We have found that the bulk viscosity of the large black hole has a maxima around T_c , and its conductivity σ asymptotes to its conformal value starting from below it. For the small black hole (which is dual to $\mathcal{N} = 4$ cSYM plasma in its hadronizing phase), the bulk viscosity increases with temperature while the conductivity decreases.

We have also computed the transport coefficients of the hard probes of the $\mathcal{N} = 4$ cSYM plasma. We have shown that the drag force F_{drag} , momentum diffusion coefficient κ , and jet quenching parameter \hat{q} increase with temperature for the large black hole but decrease with temperature for the small black hole ($\mathcal{N} = 4$ cSYM plasma in its hadronizing phase), see Figure 40, Figure 41 and Figure 42.

We would also like to point out that a recent hydrodynamic simulation (366) indicates that a drag force that decreases with temperature near T_c could explain the so called 'heavy quark puzzle', which is consistent with our finding that the drag force decreases with temperature when the plasma is in its hadronizing phase.

APPENDICES



Open Access and Copyright Terms

Present-day scientific publishing operates with various legal and financial models. JHEP is presently an open access journal, fully sponsored by the consortium SCOAP³ (www.scoap3.org) and published by Springer (www.springer.com). Articles are distributed under the creative commons license CC-BY 4.0 (<http://creativecommons.org/licenses/by/4.0/>) which permits any use, distribution, and reproduction in any medium, provided the original author(s) and source are credited. In this sense copyright is retained by the authors by default.

Notwithstanding the aforementioned and in any case the submission of an article to JHEP implies that:

- the work described has not been published before (except in form of non-peer-reviewed material such as “preprints”, theses, lectures, reports, etc. publicly posted on institutional or community repositories such as university and arXiv, and not subject to any copyright protection); that it is not under consideration for publication, and will not be published, in any other refereed publication; that its publication has been approved by all co-authors, if any, as well as — tacitly or explicitly — by the responsible authorities at the institution where the work was carried out.
- the author warrants that his/her contribution is original and that he/she has full power to make this grant. The author, by accepting the terms and conditions, signs for and accepts responsibility for releasing this material on behalf of any and all co-authors.

copytrnsfr 02/11

AMERICAN PHYSICAL SOCIETY

DN11672
Manuscript NumberSpin polarized photons from an axially charged plasma at weak coupling: Complete leading order
Article TitleKiminad A. Mamo and Ho-Ung Yee
Names of All Authors**TRANSFER OF COPYRIGHT AGREEMENT**

Copyright to the above-listed unpublished and original article submitted by the above author(s), the abstract forming part thereof, and any subsequent errata (collectively, the "Article") is hereby transferred to the American Physical Society (APS) for the full term thereof throughout the world, subject to the Author Rights (as hereinafter defined) and to acceptance of the Article for publication in a journal of APS. This transfer of copyright includes all material to be published as part of the Article (in any medium), including but not limited to tables, figures, graphs, movies, other multimedia files, and all supplemental materials. APS shall have the right to register copyright to the Article in its name as claimant, whether separately or as part of the journal issue or other medium in which the Article is included.

The author(s), and in the case of a Work Made For Hire, as defined in the U.S. Copyright Act, 17 U.S.C. §101, the employer named below, shall have the following rights (the "Author Rights"):

- (1) All proprietary rights other than copyright, such as patent rights.
- (2) The nonexclusive right, after publication by APS, to give permission to third parties to republish print versions of the Article or a translation thereof, or excerpts therefrom, without obtaining permission from APS, provided the APS-prepared version is not used for this purpose, the Article is not republished in another journal, and the third party does not charge a fee. If the APS version is used, or the third party republishes in a publication or product charging a fee for use, permission from APS must be obtained.
- (3) The right to use all or part of the Article, including the APS-prepared version without revision or modification, on the author(s)' web home page or employer's website and to make copies of all or part of the Article, including the APS-prepared version without revision or modification, for the author(s)' and/or the employer's use for educational or research purposes.
- (4) The right to post and update the Article on free-access e-print servers as long as files prepared and/or formatted by APS or its vendors are not used for that purpose. Any such posting made or updated after acceptance of the Article for publication shall include a link to the online abstract in the APS journal or to the entry page of the journal. If the author wishes the APS-prepared version to be used for an online posting other than on the author(s)' or employer's website, APS permission is required; if permission is granted, APS will provide the Article as it was published in the journal, and use will be subject to APS terms and conditions.
- (5) The right to make, and hold copyright in, works derived from the Article, as long as all of the following conditions are met: (a) at least one author of the derived work is an author of the Article; (b) the derived work includes at least ten (10) percent of new material not covered by APS's copyright in the Article; and (c) the derived work includes no more than fifty (50) percent of the text (including equations) of the Article. If these conditions are met, copyright in the derived work rests with the authors of that work, and APS (and its successors and assigns) will make no claim on that copyright. If these conditions are not met, explicit APS permission must be obtained. Nothing in this Section shall prevent APS (and its successors and assigns) from exercising its rights in the Article.
- (6) If the Article was prepared under a U.S. Government contract, the government shall have the rights under the copyright to the extent required by the contract.

All copies of part or all of the Article made under any of the Author Rights shall include the appropriate bibliographic citation and notice of the APS copyright.

By signing this Agreement, the author(s), and in the case of a Work Made For Hire, the employer, jointly and severally represent and warrant that the Article is original with the author(s) and does not infringe any copyright or violate any other right of any third parties, and that the Article has not been published elsewhere, and is not being considered for publication elsewhere in any form, except as provided herein. If each author's signature does not appear below, the signing author(s) represent that they sign this Agreement as authorized agents for and on behalf of all authors who have the legal right to transfer copyright and that this Agreement and authorization is made on behalf of the same. The signing author(s) (and, in the case of a Work Made For Hire, the signing employer) also represent and warrant that they have the full power to enter into this Agreement and to make the grants contained herein.

Kiminad Mamo
ELECTRONICALLY SIGNED25Jan2016 11:42:24
Date

Figure 44. Copyright agreement for PRD.

CITED LITERATURE

1. B. Mller, Phys. Scripta T 158, 014004 (2013) [arXiv:1309.7616 [nucl-th]].
2. J. M. Maldacena, Adv. Theor. Math. Phys. 2, 231 (1998) [hep-th/9711200].
3. S. S. Gubser, I. R. Klebanov and A. M. Polyakov, Phys. Lett. B 428, 105 (1998) [hep-th/9802109].
4. E. Witten, Adv. Theor. Math. Phys. 2, 253 (1998) [hep-th/9802150].
5. D. T. Son and A. O. Starinets, JHEP 0209, 042 (2002) [hep-th/0205051].
6. N. Iqbal and H. Liu, Phys. Rev. D 79, 025023 (2009) [arXiv:0809.3808 [hep-th]].
7. J. Kapusta and C. Gale, “Finite-Temperature Field Theory: Principles and Applications,”.
8. L. Susskind and E. Witten, hep-th/9805114.
9. A. W. Peet and J. Polchinski, Phys. Rev. D 59, 065011 (1999) [hep-th/9809022].
10. S. de Haro, S. N. Solodukhin and K. Skenderis, Commun. Math. Phys. 217, 595 (2001) [hep-th/0002230].

11. K. Skenderis, *Class. Quant. Grav.* 19, 5849 (2002) [hep-th/0209067].
12. M. Bianchi, D. Z. Freedman and K. Skenderis, *Nucl. Phys. B* 631, 159 (2002) [hep-th/0112119].
13. C. P. Herzog and D. T. Son, *JHEP* 0303, 046 (2003) [hep-th/0212072].
14. E. Barnes, D. Vaman, C. Wu and P. Arnold, “Real-time finite-temperature correlators from AdS/CFT,” *Phys. Rev. D* 82, 025019 (2010).
15. K. Skenderis and B. C. van Rees, *JHEP* 0905, 085 (2009) [arXiv:0812.2909 [hep-th]].
16. J. Adams et al. [STAR Collaboration], *Nucl. Phys. A* 757, 102 (2005); [nucl-ex/0501009].
17. K. Adcox et al. [PHENIX Collaboration], *Nucl. Phys. A* 757, 184 (2005). [nucl-ex/0410003].
18. P. Kovtun, D. T. Son and A. O. Starinets, *Phys. Rev. Lett.* 94, 111601 (2005) [hep-th/0405231].
19. T. Damour, Thèse de Doctorat d’Etat, Université Pierre et Marie Curie, Paris VI, 1979.
20. G. Policastro, D. T. Son and A. O. Starinets, *Phys. Rev. Lett.* 87, 081601 (2001) [hep-th/0104066].
21. P. Kovtun, D. T. Son and A. O. Starinets, *JHEP* 0310, 064 (2003) [hep-th/0309213].

- 22. P. Kovtun, G. D. Moore and P. Romatschke, Phys. Rev. D 84, 025006 (2011)
[arXiv:1104.1586 [hep-ph]].
- 23. R. C. Myers, M. F. Paulos and A. Sinha, JHEP 0906, 006 (2009); [arXiv:0903.2834 [hep-th]].
- 24. S. Cremonini and P. Szepietowski, JHEP 1202, 038 (2012); [arXiv:1111.5623 [hep-th]].
- 25. A. Buchel and S. Cremonini, JHEP 1010, 026 (2010). [arXiv:1007.2963 [hep-th]].
- 26. S. Cremonini, Mod. Phys. Lett. B 25, 1867 (2011) [arXiv:1108.0677 [hep-th]].
- 27. P. Basu, et al., Phys. Lett. B 689, 45 (2010); [arXiv:0911.4999 [hep-th]].
- 28. M. Ammon, et al., Phys. Lett. B 686, 192 (2010). [arXiv:0912.3515 [hep-th]].
- 29. M. Natsuume and M. Ohta, Prog. Theor. Phys. 124, 931 (2010); [arXiv:1008.4142 [hep-th]].
- 30. P. Basu and J. -H. Oh, JHEP 1207, 106 (2012) arXiv:1109.4592 [hep-th].
- 31. J. Erdmenger, P. Kerner and H. Zeller, Phys. Lett. B 699, 301 (2011); [arXiv:1011.5912
[hep-th]].
- 32. W. Florkowski, Phys. Lett. B 668, 32 (2008) [arXiv:0806.2268 [nucl-th]].
- 33. W. Florkowski and R. Ryblewski, Acta Phys. Polon. B 40, 2843 (2009) [arXiv:0901.4653
[nucl-th]].

- 34. T. Azeyanagi, W. Li and T. Takayanagi, JHEP 0906, 084 (2009) [arXiv:0905.0688 [hep-th]].
- 35. D. Mateos and D. Trancanelli, JHEP 1107, 054 (2011) [arXiv:1106.1637 [hep-th]].
- 36. A. Rebhan and D. Steineder, Phys. Rev. Lett. 108, 021601 (2012) [arXiv:1110.6825 [hep-th]].
- 37. T. Faulkner, H. Liu and M. Rangamani, JHEP 1108, 051 (2011) [arXiv:1010.4036 [hep-th]].
- 38. I. Heemskerk and J. Polchinski, JHEP 1106, 031 (2011) [arXiv:1010.1264 [hep-th]].
- 39. S. Grozdanov, JHEP 1206, 079 (2012) [arXiv:1112.3356 [hep-th]].
- 40. E. T. Akhmedov, hep-th/0202055.
- 41. E. T. Akhmedov, Phys. Lett. B 442, 152 (1998) [hep-th/9806217].
- 42. S. -J. Sin and Y. Zhou, JHEP 1105, 030 (2011) [arXiv:1102.4477 [hep-th]].
- 43. Y. Matsuo, S. -J. Sin and Y. Zhou, JHEP 1201, 130 (2012) [arXiv:1109.2698 [hep-th]].
- 44. S. Jain, JHEP 1011, 092 (2010) [arXiv:1008.2944 [hep-th]].
- 45. S. K. Chakrabarti, S. Chakraborty and S. Jain, JHEP 1102, 073 (2011) [arXiv:1011.3499 [hep-th]].

- 46. J. -H. Oh, JHEP 1206, 103 (2012) [arXiv:1201.5605 [hep-th]].
- 47. S. Carroll, G. Field and R. Jackiw, Phys. Rev. D 41, 1231 (2009).
- 48. K. Landsteiner and J. Mas, JHEP 0707, 088 (2007) [arXiv:0706.0411 [hep-th]].
- 49. A. Adams, K. Balasubramanian and J. McGreevy, JHEP 0811, 059 (2008) [arXiv:0807.1111 [hep-th]].
- 50. A. Buchel, J. T. Liu and A. O. Starinets, “Coupling constant dependence of the shear viscosity in N=4 supersymmetric Yang-Mills theory,” Nucl. Phys. B 707, 56 (2005) [hep-th/0406264].
- 51. K. A. Mamo, “Holographic RG flow of the shear viscosity to entropy density ratio in strongly coupled anisotropic plasma,” JHEP 1210, 070 (2012) [arXiv:1205.1797 [hep-th]].
- 52. S. C. Huot, S. Jeon and G. D. Moore, “Shear viscosity in weakly coupled $N = 4$ super Yang-Mills theory compared to QCD,” Phys. Rev. Lett. 98, 172303 (2007) [hep-ph/0608062].
- 53. J. Casalderrey-Solana, H. Liu, D. Mateos, K. Rajagopal and U. A. Wiedemann, “Gauge/String Duality, Hot QCD and Heavy Ion Collisions,” arXiv:1101.0618 [hep-th].

- 54. V. Skokov, A. Y. Illarionov and V. Toneev, “Estimate of the magnetic field strength in heavy-ion collisions,” *Int. J. Mod. Phys. A* 24, 5925 (2009) [arXiv:0907.1396 [nucl-th]].
- 55. K. Fukushima, D. E. Kharzeev and H. J. Warringa, “The Chiral Magnetic Effect,” *Phys. Rev. D* 78, 074033 (2008) [arXiv:0808.3382 [hep-ph]].
- 56. D. E. Kharzeev, L. D. McLerran and H. J. Warringa, “The Effects of topological charge change in heavy ion collisions: ‘Event by event P and CP violation’,” *Nucl. Phys. A* 803, 227 (2008) [arXiv:0711.0950 [hep-ph]].
- 57. D. T. Son and A. R. Zhitnitsky, “Quantum anomalies in dense matter,” *Phys. Rev. D* 70, 074018 (2004) [hep-ph/0405216].
- 58. H. -U. Yee, “Holographic Chiral Magnetic Conductivity,” *JHEP* 0911, 085 (2009) [arXiv:0908.4189 [hep-th]].
- 59. A. Rebhan, A. Schmitt and S. A. Stricker, “Anomalies and the chiral magnetic effect in the Sakai-Sugimoto model,” *JHEP* 1001, 026 (2010) [arXiv:0909.4782 [hep-th]].
- 60. D. E. Kharzeev and H. -U. Yee, “Chiral Magnetic Wave,” *Phys. Rev. D* 83, 085007 (2011) [arXiv:1012.6026 [hep-th]].
- 61. G. M. Newman, “Anomalous hydrodynamics,” *JHEP* 0601, 158 (2006) [hep-ph/0511236].

- 62. K. Landsteiner, E. Megias, L. Melgar and F. Pena-Benitez, “Holographic Gravitational Anomaly and Chiral Vortical Effect,” JHEP 1109, 121 (2011) [arXiv:1107.0368 [hep-th]].
- 63. G. Basar and D. E. Kharzeev, “The Chern-Simons diffusion rate in strongly coupled N=4 SYM plasma in an external magnetic field,” Phys. Rev. D 85, 086012 (2012) [arXiv:1202.2161 [hep-th]].
- 64. G. Basar, D. Kharzeev, and V. Skokov, “Conformal anomaly as a source of soft photons in heavy ion collisions,” arXiv:1206.1334 [hep-ph].
- 65. A. Bzdak and V. Skokov, “Anisotropy of photon production: initial eccentricity or magnetic field,” arXiv:1208.5502 [hep-ph].
- 66. K. Tuchin, “Electromagnetic radiation by quark-gluon plasma in magnetic field,” arXiv:1206.0485 [hep-ph].
- 67. D. E. Kharzeev, K. Landsteiner, A. Schmitt and H. -U. Yee, “‘Strongly interacting matter in magnetic fields’: an overview,” arXiv:1211.6245 [hep-ph].
- 68. S. Turbide, C. Gale, E. Frodermann and U. Heinz, “Electromagnetic radiation from nuclear collisions at RHIC energies,” Phys. Rev. C 77, 024909 (2008) [arXiv:0712.0732 [hep-ph]].

69. J. Manninen, E. L. Bratkovskaya, W. Cassing and O. Linnyk, “Dilepton production in p+p, Cu+Cu and Au+Au collisions at 200 AGeV,” *Eur. Phys. J. C* 71, 1615 (2011) [arXiv:1005.0500 [nucl-th]].

70. A. Adare et al. [PHENIX Collaboration], “Enhanced production of direct photons in Au+Au collisions at $\sqrt{s_{NN}} = 200$ GeV and implications for the initial temperature,” *Phys. Rev. Lett.* 104, 132301 (2010) [arXiv:0804.4168 [nucl-ex]].

71. A. Adare et al. [PHENIX Collaboration], “Detailed measurement of the e^+e^- pair continuum in $p+p$ and Au+Au collisions at $\sqrt{s_{NN}} = 200$ GeV and implications for direct photon production,” *Phys. Rev. C* 81, 034911 (2010) [arXiv:0912.0244 [nucl-ex]].

72. S. S. Adler et al. [PHENIX Collaboration], “Centrality dependence of direct photon production in $\sqrt{s_{NN}} = 200$ GeV Au + Au collisions,” *Phys. Rev. Lett.* 94, 232301 (2005) [nucl-ex/0503003].

73. P. B. Arnold, G. D. Moore and L. G. Yaffe, “Photon emission from quark gluon plasma: Complete leading order results,” *JHEP* 0112, 009 (2001) [hep-ph/0111107].

74. F. -M. Liu, T. Hirano, K. Werner and Y. Zhu, “Centrality-dependent direct photon $p(t)$ spectra in Au + Au collisions at RHIC,” *Phys. Rev. C* 79, 014905 (2009) [arXiv:0807.4771 [hep-ph]].

- 75. R. J. Fries, B. Muller and D. K. Srivastava, “Centrality dependence of direct photons in Au+Au collisions at $\sqrt{s_{NN}} = 200$ GeV,” Phys. Rev. C 72, 041902 (2005) [nucl-th/0507018].
- 76. G. Policastro, D. T. Son and A. O. Starinets, “From AdS / CFT correspondence to hydrodynamics,” JHEP 0209, 043 (2002) [hep-th/0205052].
- 77. S. Caron-Huot, P. Kovtun, G. D. Moore, A. Starinets and L. G. Yaffe, “Photon and dilepton production in supersymmetric Yang-Mills plasma,” JHEP 0612, 015 (2006) [hep-th/0607237].
- 78. K. Jo and S. -J. Sin, “Photo-emission rate of sQGP at finite density,” Phys. Rev. D 83, 026004 (2011) [arXiv:1005.0200 [hep-th]].
- 79. D. Mateos and L. Patino, “Bright branes for strongly coupled plasmas,” JHEP 0711, 025 (2007) [arXiv:0709.2168 [hep-th]].
- 80. J. Mas, J. P. Shock, J. Tarrio and D. Zoakos, “Holographic Spectral Functions at Finite Baryon Density,” JHEP 0809, 009 (2008) [arXiv:0805.2601 [hep-th]].
- 81. B. Hassanain and M. Schvellinger, “Diagnostics of plasma photoemission at strong coupling,” Phys. Rev. D 85, 086007 (2012) [arXiv:1110.0526 [hep-th]].

- 82. B. Hassanain and M. Schvellinger, “Plasma photoemission from string theory,” JHEP 1212, 095 (2012) [arXiv:1209.0427 [hep-th]].
- 83. B. Hassanain and M. Schvellinger, “Plasma conductivity at finite coupling,” JHEP 1201, 114 (2012) [arXiv:1108.6306 [hep-th]].
- 84. R. Baier, S. A. Stricker, O. Taanila and A. Vuorinen, “Production of Prompt Photons: Holographic Duality and Thermalization,” Phys. Rev. D 86, 081901 (2012) [arXiv:1207.1116 [hep-ph]].
- 85. D. Steineder, S. A. Stricker and A. Vuorinen, “Thermalization at intermediate coupling,” arXiv:1209.0291 [hep-ph].
- 86. L. Patino and D. Trancanelli, “Thermal photon production in a strongly coupled anisotropic plasma,” JHEP 1302, 154 (2013) [arXiv:1211.2199 [hep-th]].
- 87. A. Rebhan and D. Steineder, “Electromagnetic signatures of a strongly coupled anisotropic plasma,” JHEP 1108, 153 (2011) [arXiv:1106.3539 [hep-th]].
- 88. P. V. Buividovich, M. N. Chernodub, D. E. Kharzeev, T. Kalaydzhyan, E. V. Luschevskaya and M. I. Polikarpov, “Magnetic-Field-Induced insulator-conductor transition in SU(2) quenched lattice gauge theory,” Phys. Rev. Lett. 105, 132001 (2010) [arXiv:1003.2180 [hep-lat]].

89. M. I. Polikarpov, O. V. Larina, P. V. Buividovich, M. N. Chernodub, T. K. Kalaydzhyan, D. E. Kharzeev and E. V. Luschevskaya, “Conductivity of SU(2) gluodynamics vacuum induced by magnetic field,” AIP Conf. Proc. 1343 (2011) 630.
90. W. -T. Deng and X. -G. Huang, “Event-by-event generation of electromagnetic fields in heavy-ion collisions,” Phys. Rev. C 85, 044907 (2012) [arXiv:1201.5108 [nucl-th]].
91. A. Czajka and S. Mrowczynski, “N=4 Super Yang-Mills Plasma,” Phys. Rev. D 86, 025017 (2012) [arXiv:1203.1856 [hep-th]].
92. E. D’Hoker and P. Kraus, “Magnetic Brane Solutions in AdS,” JHEP 0910, 088 (2009) [arXiv:0908.3875 [hep-th]].
93. E. D’Hoker and P. Kraus, “Charged Magnetic Brane Solutions in AdS (5) and the fate of the third law of thermodynamics,” JHEP 1003, 095 (2010) [arXiv:0911.4518 [hep-th]].
94. S. -i. Nam, “Electrical conductivity of quark matter at finite T under external magnetic field,” Phys. Rev. D 86, 033014 (2012) [arXiv:1207.3172 [hep-ph]].
95. B. O. Kerbikov and M. A. Andreichikov, “Dense Quark Matter Conductivity in Ultra-Intense Magnetic Field,” arXiv:1206.6044 [hep-ph].
96. K. Tuchin, “Photon decay in strong magnetic field in heavy-ion collisions,” Phys. Rev. C 83, 017901 (2011) [arXiv:1008.1604 [nucl-th]].

- 97. D. Kharzeev and A. Zhitnitsky, “Charge separation induced by P-odd bubbles in QCD matter,” Nucl. Phys. A 797, 67 (2007).
- 98. M. A. Metlitski and A. R. Zhitnitsky, “Anomalous axion interactions and topological currents in dense matter,” Phys. Rev. D 72, 045011 (2005).
- 99. D. Kharzeev, A. Krasnitz and R. Venugopalan, “Anomalous chirality fluctuations in the initial stage of heavy ion collisions and parity odd bubbles,” Phys. Lett. B 545, 298 (2002).
- 100. T. Lappi and L. McLerran, “Some features of the glasma,” Nucl. Phys. A 772, 200 (2006).
- 101. S. A. Voloshin, “Parity violation in hot QCD: How to detect it,” Phys. Rev. C 70, 057901 (2004).
- 102. B. I. Abelev et al. [STAR Collaboration], “Azimuthal Charged-Particle Correlations and Possible Local Strong Parity Violation,” Phys. Rev. Lett. 103, 251601 (2009).
- 103. I. Selyuzhenkov [ALICE Collaboration], “Anisotropic flow and other collective phenomena measured in Pb-Pb collisions with ALICE at the LHC,” Prog. Theor. Phys. Suppl. 193, 153 (2012).
- 104. M. Asakawa, A. Majumder and B. Muller, “Electric Charge Separation in Strong Transient Magnetic Fields,” Phys. Rev. C 81, 064912 (2010).

105. A. Bzdak, V. Koch and J. Liao, “Remarks on possible local parity violation in heavy ion collisions,” *Phys. Rev. C* 81, 031901 (2010).
106. F. Wang, “Effects of Cluster Particle Correlations on Local Parity Violation Observables,” *Phys. Rev. C* 81, 064902 (2010).
107. S. Pratt, S. Schlichting and S. Gavin, “Effects of Momentum Conservation and Flow on Angular Correlations at RHIC,” *Phys. Rev. C* 84, 024909 (2011).
108. E. V. Gorbar, V. A. Miransky and I. A. Shovkovy, “Normal ground state of dense relativistic matter in a magnetic field,” *Phys. Rev. D* 83, 085003 (2011).
109. Y. Burnier, D. E. Kharzeev, J. Liao and H. -U. Yee, “Chiral magnetic wave at finite baryon density and the electric quadrupole moment of quark-gluon plasma in heavy ion collisions,” *Phys. Rev. Lett.* 107, 052303 (2011).
110. Y. Burnier, D. E. Kharzeev, J. Liao and H. -U. Yee, “From the chiral magnetic wave to the charge dependence of elliptic flow,” [arXiv:1208.2537 [hep-ph]].
111. G. Wang [STAR Collaboration], “Search for Chiral Magnetic Effects in High-Energy Nuclear Collisions,” [arXiv:1210.5498 [nucl-ex]].
112. H. Ke [STAR Collaboration], “Charge asymmetry dependency of π^+/π^- elliptic flow in Au + Au collisions at $\sqrt{s_{NN}} = 200$ GeV,” *J. Phys. Conf. Ser.* 389, 012035 (2012).

113. J. C. Dunlop, M. A. Lisa and P. Sorensen, “Constituent quark scaling violation due to baryon number transport,” Phys. Rev. C 84, 044914 (2011).
114. A. Bzdak and P. Bozek, “Contributions to the event-by-event charge asymmetry dependence for the elliptic flow of π^+ and π^- in heavy-ion collisions,” arXiv:1303.1138 [nucl-th].
115. M. Stephanov and H. -U. Yee, “Charged elliptic flow at zero charge asymmetry,” arXiv:1304.6410 [nucl-th].
116. X. -G. Huang and J. Liao, “Axial Current Generation from Electric Field: Chiral Electric Separation Effect,” Phys. Rev. Lett. 110, 232302 (2013).
117. R. Loganayagam, “Anomalies and the Helicity of the Thermal State,” arXiv:1211.3850 [hep-th].
118. D. E. Kharzeev and H. J. Warringa, “Chiral Magnetic conductivity,” Phys. Rev. D 80, 034028 (2009).
119. A. Adare et al. [PHENIX Collaboration], “Observation of direct-photon collective flow in $\sqrt{s_{NN}} = 200$ GeV Au+Au collisions,” Phys. Rev. Lett. 109, 122302 (2012).
120. D. Lohner [ALICE Collaboration], “Measurement of Direct-Photon Elliptic Flow in Pb-Pb Collisions at $\sqrt{s_{NN}} = 2.76$ TeV,” arXiv:1212.3995 [hep-ex].

- 121. K. Fukushima and K. Mameda, “Wess-Zumino-Witten action and photons from the Chiral Magnetic Effect,” *Phys. Rev. D* 86, 071501 (2012).
- 122. K. A. Mamo, “Enhanced thermal photon and dilepton production in strongly coupled $N=4$ SYM plasma in strong magnetic field,” *arXiv:1210.7428* [hep-th].
- 123. Y. Bu, “Electromagnetic signature in holographic plasma with B field,” *Phys. Rev. D* 87, 026005 (2013).
- 124. H. -U. Yee, “Flows and polarization of early photons with magnetic field at strong coupling,” *arXiv:1303.3571* [nucl-th].
- 125. S. Lin and H. -U. Yee, “Out-of-Equilibrium Chiral Magnetic Effect at Strong Coupling,” *arXiv:1305.3949* [hep-ph].
- 126. Y. Akamatsu and N. Yamamoto, “Chiral Plasma Instabilities,” *arXiv:1302.2125* [nucl-th].
- 127. T. Sakai and S. Sugimoto, “Low energy hadron physics in holographic QCD,” *Prog. Theor. Phys.* 113, 843 (2005).
- 128. G. Mandal and T. Morita, “Gregory-Laflamme as the confinement/deconfinement transition in holographic QCD,” *JHEP* 1109, 073 (2011).

- 129. D. T. Son and N. Yamamoto, “Berry Curvature, Triangle Anomalies, and the Chiral Magnetic Effect in Fermi Liquids,” *Phys. Rev. Lett.* 109, 181602 (2012).
- 130. M. A. Stephanov and Y. Yin, “Chiral Kinetic Theory,” *Phys. Rev. Lett.* 109, 162001 (2012).
- 131. J. -W. Chen, S. Pu, Q. Wang and X. -N. Wang, “Berry curvature and 4-dimensional monopole in relativistic chiral kinetic equation,” [arXiv:1210.8312 [hep-th]].
- 132. J. Ghiglieri, J. Hong, A. Kurkela, E. Lu, G. D. Moore and D. Teaney, “Next-to-leading order thermal photon production in a weakly coupled quark-gluon plasma,” *JHEP* 1305, 010 (2013).
- 133. S. Caron-Huot, P. M. Chesler and D. Teaney, “Fluctuation, dissipation, and thermalization in non-equilibrium AdS5 black hole geometries,” *Phys. Rev. D* 84, 026012 (2011).
- 134. P. M. Chesler and D. Teaney, “Dilaton emission and absorption from far-from-equilibrium non-abelian plasma,” arXiv:1211.0343 [hep-th].
- 135. K. Dusling, “Photons as a viscometer of heavy ion collisions,” *Nucl. Phys. A* 839, 70 (2010).
- 136. A. K. Chaudhuri and B. Sinha, “Direct photon production from viscous QGP,” *Phys. Rev. C* 83, 034905 (2011).

- 137. S. Mitra, P. Mohanty, S. Sarkar and J. -eAlam, “Thermal radiation from an expanding viscous medium,” arXiv:1107.2500 [nucl-th].
- 138. M. Dion, J. -F. Paquet, B. Schenke, C. Young, S. Jeon and C. Gale, “Viscous photons in relativistic heavy ion collisions,” Phys. Rev. C 84, 064901 (2011).
- 139. C. Shen, U. W. Heinz, J. -F. Paquet, I. Kozlov and C. Gale, “Anisotropic flow of thermal photons as a quark-gluon plasma viscometer,” arXiv:1308.2111 [nucl-th].
- 140. M. Lekaveckas and K. Rajagopal, “Effects of Fluid Velocity Gradients on Heavy Quark Energy Loss,” JHEP 1402, 068 (2014).
- 141. S. Lin and E. Shuryak, “Toward the AdS/CFT gravity dual for High Energy Collisions: I.Falling into the AdS,” Phys. Rev. D 77, 085013 (2008)
- 142. J. M. Maldacena, “Eternal black holes in anti-de Sitter,” JHEP 0304, 021 (2003).
- 143. P. Arnold and D. Vaman, “Jet quenching in hot strongly coupled gauge theories revisited: 3-point correlators with gauge-gravity duality,” JHEP 1010, 099 (2010).
- 144. B. Sahoo and H. -U. Yee, “Electrified plasma in AdS/CFT correspondence,” JHEP 1011, 095 (2010).

- 145. J. de Boer, V. E. Hubeny, M. Rangamani and M. Shigemori, “Brownian motion in AdS/CFT,” JHEP 0907, 094 (2009).
- 146. D. T. Son and D. Teaney, “Thermal Noise and Stochastic Strings in AdS/CFT,” JHEP 0907, 021 (2009).
- 147. S. Bhattacharyya, V. E. Hubeny, S. Minwalla and M. Rangamani, “Nonlinear Fluid Dynamics from Gravity,” JHEP 0802, 045 (2008).
- 148. M. Torabian and H. -U. Yee, “Holographic nonlinear hydrodynamics from AdS/CFT with multiple/non-Abelian symmetries,” JHEP 0908, 020 (2009).
- 149. A. Mukhopadhyay, “Nonequilibrium fluctuation-dissipation relation from holography,” Phys. Rev. D 87, no. 6, 066004 (2013).
- 150. D. Kharzeev, A. Krasnitz and R. Venugopalan, “Anomalous chirality fluctuations in the initial stage of heavy ion collisions and parity odd bubbles,” Phys. Lett. B 545, 298 (2002).
- 151. D. Kharzeev and A. Zhitnitsky, “Charge separation induced by P-odd bubbles in QCD matter,” Nucl. Phys. A 797, 67 (2007).
- 152. D. E. Kharzeev, L. D. McLerran and H. J. Warringa, “The Effects of topological charge change in heavy ion collisions: ‘Event by event P and CP violation’,” Nucl. Phys.

- A 803, 227 (2008).
153. K. Fukushima, D. E. Kharzeev and H. J. Warringa, “The Chiral Magnetic Effect,” *Phys. Rev. D* 78, 074033 (2008).
154. K. A. Mamo and H. U. Yee, “Spin polarized photons and dileptons from axially charged plasma,” *Phys. Rev. D* 88, no. 11, 114029 (2013).
155. K. A. Mamo and H. U. Yee, “Spin polarized photons from an axially charged plasma at weak coupling: Complete leading order,” *Phys. Rev. D* 93, no. 6, 065053 (2016) [arXiv:1512.01316 [hep-ph]].
156. A. Ipp, A. Di Piazza, J. Evers and C. H. Keitel, “Photon polarization as a probe for quark-gluon plasma dynamics,” *Phys. Lett. B* 666, 315 (2008).
157. D. Bodeker, “On the effective dynamics of soft nonAbelian gauge fields at finite temperature,” *Phys. Lett. B* 426, 351 (1998).
158. P. B. Arnold, D. T. Son and L. G. Yaffe, “Effective dynamics of hot, soft nonAbelian gauge fields. Color conductivity and $\log(1/\alpha)$ effects,” *Phys. Rev. D* 59, 105020 (1999).
159. M. Stephanov and H.-U. Yee, unpublished.

- 160. D. E. Kharzeev and H. J. Warringa, “Chiral Magnetic conductivity,” *Phys. Rev. D* 80, 034028 (2009).
- 161. H. -U. Yee, “Holographic Chiral Magnetic Conductivity,” *JHEP* 0911, 085 (2009).
- 162. A. Jimenez-Alba and H. U. Yee, “Second order transport coefficient from the chiral anomaly at weak coupling: Diagrammatic resummation,” *Phys. Rev. D* 92, no. 1, 014023 (2015).
- 163. R. Baier, H. Nakkagawa, A. Niegawa and K. Redlich, “Production rate of hard thermal photons and screening of quark mass singularity,” *Z. Phys. C* 53, 433 (1992).
- 164. J. I. Kapusta, P. Lichard and D. Seibert, “High-energy photons from quark - gluon plasma versus hot hadronic gas,” *Phys. Rev. D* 44, 2774 (1991) [*Phys. Rev. D* 47, 4171 (1993)].
- 165. P. B. Arnold, G. D. Moore and L. G. Yaffe, “Photon emission from ultrarelativistic plasmas,” *JHEP* 0111, 057 (2001).
- 166. P. B. Arnold, G. D. Moore and L. G. Yaffe, “Photon emission from quark gluon plasma: Complete leading order results,” *JHEP* 0112, 009 (2001).
- 167. G. Baym, H. Monien, C. J. Pethick and D. G. Ravenhall, “Transverse Interactions and Transport in Relativistic Quark - Gluon and Electromagnetic Plasmas,” *Phys. Rev.*

- Lett. 64, 1867 (1990).
168. G. D. Moore, “Transport coefficients in large $N(f)$ gauge theory: Testing hard thermal loops,” JHEP 0105, 039 (2001).
169. E. Braaten and R. D. Pisarski, “Soft Amplitudes in Hot Gauge Theories: A General Analysis,” Nucl. Phys. B 337, 569 (1990).
170. E. Braaten and T. C. Yuan, “Calculation of screening in a hot plasma,” Phys. Rev. Lett. 66, 2183 (1991).
171. J. P. Blaizot and E. Iancu, “The Quark gluon plasma: Collective dynamics and hard thermal loops,” Phys. Rept. 359, 355 (2002).
172. G. Aarts and J. M. Martinez Resco, “Ward identity and electrical conductivity in hot QED,” JHEP 0211, 022 (2002).
173. P. Aurenche, F. Gelis and H. Zaraket, “A Simple sum rule for the thermal gluon spectral function and applications,” JHEP 0205, 043 (2002).
174. P. Aurenche, F. Gelis, G. D. Moore and H. Zaraket, “Landau-Pomeranchuk-Migdal resummation for dilepton production,” JHEP 0212, 006 (2002).

- 175. R. Baier, Y. L. Dokshitzer, A. H. Mueller, S. Peigne and D. Schiff, “Radiative energy loss of high-energy quarks and gluons in a finite volume quark - gluon plasma,” Nucl. Phys. B 483, 291 (1997).
- 176. R. Baier, Y. L. Dokshitzer, A. H. Mueller, S. Peigne and D. Schiff, “Radiative energy loss and $p(T)$ broadening of high-energy partons in nuclei,” Nucl. Phys. B 484, 265 (1997).
- 177. B. G. Zakharov, “Radiative energy loss of high-energy quarks in finite size nuclear matter and quark - gluon plasma,” JETP Lett. 65, 615 (1997).
- 178. M. Gyulassy, P. Levai and I. Vitev, “Reaction operator approach to nonAbelian energy loss,” Nucl. Phys. B 594, 371 (2001).
- 179. C. A. Salgado and U. A. Wiedemann, “Calculating quenching weights,” Phys. Rev. D 68, 014008 (2003).
- 180. K. Fukushima, K. Hattori, H. U. Yee and Y. Yin, “Heavy Quark Diffusion in Strong Magnetic Fields at Weak Coupling and Implications for Elliptic Flow,” Phys. Rev. D 93, no. 7, 074028 (2016).
- 181. G. D. Moore and D. Teaney, “How much do heavy quarks thermalize in a heavy ion collision?,” Phys. Rev. C 71, 064904 (2005).

- 182. A. Jimenez-Alba and H. U. Yee, “Second order transport coefficient from the chiral anomaly at weak coupling: Diagrammatic resummation,” *Phys. Rev. D* 92, no. 1, 014023 (2015).
- 183. E. Braaten and T. C. Yuan, “Calculation of screening in a hot plasma,” *Phys. Rev. Lett.* 66, 2183 (1991).
- 184. J. Casalderrey-Solana and D. Teaney, “Transverse Momentum Broadening of a Fast Quark in a N=4 Yang Mills Plasma,” *JHEP* 0704, 039 (2007).
- 185. S. S. Gubser, “Momentum fluctuations of heavy quarks in the gauge-string duality,” *Nucl. Phys. B* 790, 175 (2008).
- 186. H. Liu, K. Rajagopal and U. A. Wiedemann, “Calculating the jet quenching parameter from AdS/CFT,” *Phys. Rev. Lett.* 97, 182301 (2006).
- 187. H. Liu, K. Rajagopal and U. A. Wiedemann, “Wilson loops in heavy ion collisions and their calculation in AdS/CFT,” *JHEP* 0703, 066 (2007).
- 188. M. Panero, K. Rummukainen and A. Schfer, “Lattice Study of the Jet Quenching Parameter,” *Phys. Rev. Lett.* 112, no. 16, 162001 (2014).
- 189. E. D’Hoker and P. Kraus, “Magnetic Brane Solutions in AdS,” *JHEP* 0910, 088 (2009).

- 190. U. Gursoy, E. Kiritsis, L. Mazzanti and F. Nitti, “Langevin diffusion of heavy quarks in non-conformal holographic backgrounds,” JHEP 1012, 088 (2010).
- 191. A. V. Sadofyev and Y. Yin, “Chiral Magnetic ”Superfluidity”,” [arXiv:1511.08794 [hep-th]].
- 192. K. Rajagopal and A. V. Sadofyev, “Chiral drag force,” JHEP 1510, 018 (2015).
- 193. M. A. Stephanov and H. U. Yee, “No-Drag Frame for Anomalous Chiral Fluid,” Phys. Rev. Lett. 116, no. 12, 122302 (2016).
- 194. D. Giataganas, “Probing strongly coupled anisotropic plasma,” JHEP 1207, 031 (2012).
- 195. G. S. Bali, et al, “The QCD phase diagram for external magnetic fields,” JHEP 1202, 044 (2012) [arXiv:1111.4956 [hep-ph]].
- 196. K. A. Mamo, “Inverse magnetic catalysis in holographic models of QCD,” JHEP 1505, 121 (2015) [arXiv:1501.03262 [hep-ph]].
- 197. D. Dudal, D. R. Granado and T. G. Mertens, “No inverse magnetic catalysis in the QCD hard and soft wall models,” arXiv:1511.04042 [hep-th].
- 198. Z. Fang, “Anomalous dimension, chiral phase transition and inverse magnetic catalysis in soft-wall AdS/QCD,” Phys. Lett. B 758, 1 (2016).

- 199. R. Rougemont, R. Critelli and J. Noronha, “Holographic calculation of the QCD crossover temperature in a magnetic field,” *Phys. Rev. D* 93, no. 4, 045013 (2016) doi:10.1103/PhysRevD.93.045013 [arXiv:1505.07894 [hep-th]].
- 200. S. w. Li and T. Jia, “Dynamically flavored description of holographic QCD in the presence of a magnetic field,” arXiv:1604.07197 [hep-th].
- 201. N. Evans, C. Miller and M. Scott, “Inverse Magnetic Catalysis in Bottom-Up Holographic QCD,” arXiv:1604.06307 [hep-ph].
- 202. J. F. Fuini and L. G. Yaffe, “Far-from-equilibrium dynamics of a strongly coupled non-Abelian plasma with non-zero charge density or external magnetic field,” *JHEP* 1507, 116 (2015) [arXiv:1503.07148 [hep-th]].
- 203. K. A. Mamo and H. U. Yee, “Thermalization of Quark-Gluon Plasma in Magnetic Field at Strong Coupling,” *Phys. Rev. D* 92, no. 10, 105005 (2015) [arXiv:1505.01183 [hep-ph]].
- 204. M. A. Stephanov and H. U. Yee, “No-Drag Frame for Anomalous Chiral Fluid,” *Phys. Rev. Lett.* 116, no. 12, 122302 (2016) doi:10.1103/PhysRevLett.116.122302 [arXiv:1508.02396 [hep-th]].
- 205. A. V. Sadofyev and Y. Yin, “Chiral Magnetic ”Superfluidity”,” [arXiv:1511.08794 [hep-th]].

206. S. Li, K. A. Mamo and H. U. Yee, “Jet quenching parameter of quark-gluon plasma in strong magnetic field: perturbative QCD and AdS/CFT correspondence,” [arXiv:1605.00188 [hep-ph]].
207. M. Shifman, “Remarks on Adjoint QCD with k Flavors, $k \geq 2$,” Mod. Phys. Lett. A 28, 1350179 (2013) [arXiv:1307.5826 [hep-th]].
208. D. R. T. Jones, “Two-loop diagrams in Yang-Mills theory,” Nucl. Phys. B 75, 531 (1974).
209. W. E. Caswell, “Two-loop diagrams in Yang-Mills theory,” Phys.Rev. Lett. 33, 244 (1974).
210. K. A. Mamo, “Enhanced thermal photon and dilepton production in strongly coupled $N = 4$ SYM plasma in strong magnetic field,” JHEP 1308, 083 (2013) [arXiv:1210.7428 [hep-th]].
211. K. A. Mamo, Phys. Rev. D 94, no. 4, 041901 (2016) doi:10.1103/PhysRevD.94.041901 [arXiv:1606.01598 [hep-th]].
212. R. Critelli, S. I. Finazzo, M. Zaniboni and J. Noronha, “Anisotropic shear viscosity of a strongly coupled non-Abelian plasma from magnetic branes,” Phys. Rev. D 90, no. 6, 066006 (2014) [arXiv:1406.6019 [hep-th]].
213. G. Basar and D. E. Kharzeev, “The Chern-Simons diffusion rate in strongly coupled $N=4$ SYM plasma in an external magnetic field,” Phys. Rev. D 85, 086012 (2012)

[arXiv:1202.2161 [hep-th]].

214. T. DeGrand, Y. Shamir and B. Svetitsky, “Infrared fixed point in $SU(2)$ gauge theory with adjoint fermions,” *Phys. Rev. D* 83, 074507 (2011) [arXiv:1102.2843 [hep-lat]].
215. G. S. Bali, F. Bruckmann, G. Endrudi, S. D. Katz and A. Schfer, “The QCD equation of state in background magnetic fields,” *JHEP* 1408, 177 (2014) [arXiv:1406.0269 [hep-lat]].
216. D. Kadoh, “Recent progress in lattice supersymmetry: from lattice gauge theory to black holes,” *PoS LATTICE 2015*, 017 (2015) [arXiv:1607.01170 [hep-lat]].
217. S. S. Gubser, “Drag force in AdS/CFT,” *Phys. Rev. D* 74, 126005 (2006) [hep-th/0605182].
218. C. P. Herzog, A. Karch, P. Kovtun, C. Kozcaz and L. G. Yaffe, “Energy loss of a heavy quark moving through $N=4$ supersymmetric Yang-Mills plasma,” *JHEP* 0607, 013 (2006) [hep-th/0605158].
219. K. Rajagopal and A. V. Sadofyev, “Chiral drag force,” *JHEP* 1510, 018 (2015) [arXiv:1505.07379 [hep-th]].
220. M. Lekaveckas and K. Rajagopal, “Effects of Fluid Velocity Gradients on Heavy Quark Energy Loss,” *JHEP* 1402, 068 (2014) [arXiv:1311.5577 [hep-th]].

- 221. A. Mikhailov, “Nonlinear waves in AdS / CFT correspondence,” hep-th/0305196.
- 222. M. Chernicoff and A. Guijosa, “Acceleration, Energy Loss and Screening in Strongly-Coupled Gauge Theories,” JHEP 0806, 005 (2008) [arXiv:0803.3070 [hep-th]].
- 223. K. B. Fadafan, H. Liu, K. Rajagopal and U. A. Wiedemann, “Stirring Strongly Coupled Plasma,” Eur. Phys. J. C 61, 553 (2009) [arXiv:0809.2869 [hep-ph]].
- 224. B. Fiol, B. Garolera and A. Lewkowycz, “Exact results for static and radiative fields of a quark in N=4 super Yang-Mills,” JHEP 1205, 093 (2012) [arXiv:1202.5292 [hep-th]].
- 225. A. Lewkowycz and J. Maldacena, “Exact results for the entanglement entropy and the energy radiated by a quark,” JHEP 1405, 025 (2014) [arXiv:1312.5682 [hep-th]].
- 226. P. Banerjee and B. Sathiapalan, “Holographic Brownian Motion in 1+1 Dimensions,” Nucl. Phys. B 884, 74 (2014) [arXiv:1308.3352 [hep-th]].
- 227. P. Banerjee and B. Sathiapalan, “Zero Temperature Dissipation and Holography,” JHEP 1604, 089 (2016) [arXiv:1512.06414 [hep-th]].
- 228. T. Matsuo, D. Tomino and W. Y. Wen, “Drag force in SYM plasma with B field from AdS/CFT,” JHEP 0610, 055 (2006) [hep-th/0607178].

- 229. E. Kiritsis and G. Pavlopoulos, “Heavy quarks in a magnetic field,” JHEP 1204, 096 (2012) [arXiv:1111.0314 [hep-th]].
- 230. M. Chernercoff, D. Fernandez, D. Mateos and D. Trancanelli, “Drag force in a strongly coupled anisotropic plasma,” JHEP 1208, 100 (2012) [arXiv:1202.3696 [hep-th]].
- 231. S. Lin and E. Shuryak, “Toward the AdS/CFT Gravity Dual for High Energy Collisions. 3. Gravitationally Collapsing Shell and Quasiequilibrium,” Phys. Rev. D 78, 125018 (2008), [arXiv:0808.0910 [hep-th]].
- 232. S. Bhattacharyya and S. Minwalla, “Weak Field Black Hole Formation in Asymptotically AdS Spacetimes,” JHEP 0909, 034 (2009), [arXiv:0904.0464 [hep-th]].
- 233. P. M. Chesler and L. G. Yaffe, “Holography and colliding gravitational shock waves in asymptotically AdS5 spacetime,” Phys. Rev. Lett. 106, 021601 (2011), [arXiv:1011.3562 [hep-th]].
- 234. M. P. Heller, et al, “Strong Coupling Isotropization of Non-Abelian Plasmas Simplified,” Phys. Rev. Lett. 108, 191601 (2012), [arXiv:1202.0981 [hep-th]].
- 235. B. Wu and P. Romatschke, “Shock wave collisions in AdS5: approximate numerical solutions,” Int. J. Mod. Phys. C 22, 1317 (2011), [arXiv:1108.3715 [hep-th]].

- 236. D. Garfinkle and L. A. Pando Zayas, “Rapid Thermalization in Field Theory from Gravitational Collapse,” *Phys. Rev. D* 84, 066006 (2011), [arXiv:1106.2339 [hep-th]].
- 237. D. Garfinkle, L. A. Pando Zayas and D. Reichmann, “On Field Theory Thermalization from Gravitational Collapse,” *JHEP* 1202, 119 (2012), [arXiv:1110.5823 [hep-th]].
- 238. W. Israel, “Singular hypersurfaces and thin shells in general relativity,” *Nuovo Cim. B* 44S10, 1 (1966) [Erratum-ibid. B 48, 463 (1967)] [*Nuovo Cim. B* 44, 1 (1966)].
- 239. K. S. Thorne, The general relativistic theory of stellar structure and dynamics, in: C. Dewitt, E. Schatzman, P. Vron (Eds.), *High Energy Astrophysics*, vol. 3, 1967, p. 259.
- 240. A. Donos, J. P. Gauntlett and C. Pantelidou, “Spatially modulated instabilities of magnetic black branes,” *JHEP* 1201, 061 (2012), [arXiv:1109.0471 [hep-th]].
- 241. L. J. Romans, “Supersymmetric, cold and lukewarm black holes in cosmological Einstein-Maxwell theory,” *Nucl. Phys. B* 383, 395 (1992), [hep-th/9203018].
- 242. D. Bak, M. Gutperle, S. Hirano and N. Ohta, “Dilatonic repulsons and confinement via the AdS / CFT correspondence,” *Phys. Rev. D* 70, 086004 (2004), [hep-th/0403249].
- 243. V. P. Gusynin, V. A. Miransky and I. A. Shovkovy, Catalysis of dynamical flavor symmetry breaking by a magnetic field in (2+1)-dimensions, *Phys. Rev. Lett.* 73 (1994) 3499,

hep-ph:9405262.

244. V. A. Miransky and I. A. Shovkovy, Magnetic catalysis and anisotropic confinement in QCD, Phys. Rev. D66 (2002) 045006, hep-ph:0205348.
245. A. J. Mizher, M. N. Chernodub, and E. S. Fraga, Phase diagram of hot QCD in an external magnetic field: possible splitting of deconfinement and chiral transitions, Phys. Rev. D82 (2010) 105016, arXiv:1004.2712.
246. E. S. Fraga and A. J. Mizher, Can a strong magnetic background modify the nature of the chiral transition in QCD?, Nucl. Phys.A820 (2009) 103c–106c, arXiv:0810.3693.
247. R. Gatto and M. Ruggieri, Deconfinement and Chiral Symmetry Restoration in a Strong Magnetic Background, Phys. Rev.D83 (2011) 034016, arXiv:1012.1291.
248. R. Gatto and M. Ruggieri, Dressed Polyakov loop and phase diagram of hot quark matter under magnetic field, Phys. Rev.D82 (2010) 054027, arXiv:1007.0790.
249. A. Osipov, B. Hiller, A. Blin, and J. da Providencia, Dynamical chiral symmetry breaking by a magnetic field and multi-quark interactions, Phys.Lett. B650 (2007) 262–267, hep-ph/0701090.
250. K. Kashiwa, Entanglement between chiral and deconfinement transitions under strong uniform magnetic background field, Phys. Rev.D83 (2011) 117901, arXiv:1104.5167.

- 251. K. G. Klimenko, Three-dimensional Gross-Neveu model at nonzero temperature and in an external magnetic field, *Theor. Math. Phys.* 90 (1992) 1–6.
- 252. J. Alexandre, K. Farakos, and G. Koutsoumbas, Magnetic catalysis in QED(3) at finite temperature: Beyond the constant mass approximation, *Phys. Rev. D* 63 (2001) 065015, hep-th/0010211.
- 253. V. G. Filev, C. V. Johnson, R. C. Rashkov and K. S. Viswanathan, Flavoured large N gauge theory in an external magnetic field, *JHEP* 0710 (2007) 019, hep-th:0701001.
- 254. T. Albash, V. G. Filev, C. V. Johnson and A. Kundu, Finite temperature large N gauge theory with quarks in an external magnetic field, *JHEP* 0807 (2008) 080, arXiv:0709.1547.
- 255. C. V. Johnson and A. Kundu, External Fields and Chiral Symmetry Breaking in the Sakai-Sugimoto Model, *JHEP* 12 (2008) 053, arXiv:0803.0038.
- 256. O. Bergman, G. Lifschytz and M. Lippert, “Response of Holographic QCD to Electric and Magnetic Fields,” *JHEP* 0805, 007 (2008), [arXiv:0802.3720 [hep-th]].
- 257. N. Evans, T. Kalaydzhyan, K.-y. Kim, and I. Kirsch, Non-equilibrium physics at a holographic chiral phase transition, *JHEP* 1101 (2011) 050, arXiv:1011.2519.

- 258. M. S. Alam, V. S. Kaplunovsky and A. Kundu, Chiral Symmetry Breaking and External Fields in the Kuperstein-Sonnenschein Model, JHEP 1204 (2012) 111, arXiv:1202.3488.
- 259. F. Preis, A. Rebhan and A. Schmitt, “Inverse magnetic catalysis in dense holographic matter,” JHEP 1103, 033 (2011), arXiv:1012.4785.
- 260. A. Ballon-Bayona, “Holographic deconfinement transition in the presence of a magnetic field,” JHEP 1311, 168 (2013), [arXiv:1307.6498 [hep-th]].
- 261. D. Kharzeev, Parity violation in hot QCD: Why it can happen, and how to look for it, Phys.Lett. B633 (2006) 260–264, hep-ph/0406125.
- 262. STAR Collaboration Collaboration, S. A. Voloshin, Probe for the strong parity violation effects at RHIC with three particle correlations, Indian J.Phys. 85 (2011) 1103–1107, arXiv:0806.0029.
- 263. STAR Collaboration Collaboration, B. Abelev *et. al.*, Azimuthal Charged-Particle Correlations and Possible Local Strong Parity Violation, Phys.Rev.Lett. 103 (2009) 251601, arXiv:0909.1739.
- 264. T. Vachaspati, Magnetic fields from cosmological phase transitions, Phys. Lett. B265 (1991) 258–261.

- 265. R. C. Duncan and C. Thompson, Formation of very strongly magnetized neutron stars - implications for gamma-ray bursts, *Astrophys. J.* 392 (1992) L9.
- 266. E. Witten, “Anti-de Sitter space, thermal phase transition, and confinement in gauge theories,” *Adv. Theor. Math. Phys.* 2, 505 (1998), [hep-th/9803131].
- 267. J. Sonnenschein, “Stringy confining Wilson loops,” *PoS tnr 2000*, 008 (2000), [hep-th/0009146].
- 268. G. T. Horowitz and R. C. Myers, “The AdS / CFT correspondence and a new positive energy conjecture for general relativity,” *Phys. Rev. D* 59, 026005 (1998), [hep-th/9808079].
- 269. S. Surya, K. Schleich and D. M. Witt, “Phase transitions for flat AdS black holes,” *Phys. Rev. Lett.* 86, 5231 (2001), [hep-th/0101134].
- 270. M. Natsuume, “AdS/CFT Duality User Guide,” [arXiv:1409.3575 [hep-th]].
- 271. C. Hoyos, T. Nishioka and A. O’Bannon, “A Chiral Magnetic Effect from AdS/CFT with Flavor,” *JHEP* 1110, 084 (2011), [arXiv:1106.4030 [hep-th]].
- 272. M. Ammon, V. G. Filev, J. Tarrio and D. Zoakos, “D3/D7 Quark-Gluon Plasma with Magnetically Induced Anisotropy,” *JHEP* 1209 (2012) 039, [arXiv:1207.1047 [hep-th]].

273. G. Arciniega, P. Ortega and L. Patio, “Brighter Branes, enhancement of photon production by strong magnetic fields in the gauge/gravity correspondence,” JHEP 1404, 192 (2014), [arXiv:1307.1153 [hep-th]].
274. R. Rougemont, R. Critelli and J. Noronha, “Anisotropic heavy quark potential in strongly-coupled $\mathcal{N} = 4$ SYM in a magnetic field,” arXiv:1409.0556 [hep-th].
275. J. Erlich, E. Katz, D. T. Son and M. A. Stephanov, “QCD and a holographic model of hadrons,” Phys. Rev. Lett. 95 (2005) 261602, [hep-ph/0501128].
276. G. F. de Teramond and S. J. Brodsky, “Hadronic spectrum of a holographic dual of QCD,” Phys. Rev. Lett. 94 (2005) 201601, [hep-th/0501022].
277. B. H. Lee, C. Park and S. J. Sin, “A Dual Geometry of the Hadron in Dense Matter,” JHEP 0907, 087 (2009), [arXiv:0905.2800 [hep-th]].
278. C. P. Herzog, “A Holographic Prediction of the Deconfinement Temperature,” Phys. Rev. Lett. 98, 091601 (2007), [hep-th/0608151].
279. C. A. Ballon Bayona, H. Boschi-Filho, N. R. F. Braga and L. A. Pando Zayas, “On a Holographic Model for Confinement/Deconfinement,” Phys. Rev. D 77, 046002 (2008), [arXiv:0705.1529 [hep-th]].

- 280. E. D'Hoker and P. Kraus, "Magnetic Brane Solutions in AdS," JHEP 0910, 088 (2009), [arXiv:0908.3875 [hep-th]].
- 281. Y. Kim, B. H. Lee, S. Nam, C. Park and S. J. Sin, "Deconfinement phase transition in holographic QCD with matter," Phys. Rev. D 76, 086003 (2007), [arXiv:0706.2525 [hep-ph]].
- 282. J. Braun and H. Gies, "Chiral phase boundary of QCD at finite temperature," JHEP 0606, 024 (2006), hep-ph:0602226.
- 283. F. Karsch, E. Laermann and A. Peikert, "Quark mass and flavor dependence of the QCD phase transition," Nucl. Phys. B 605, 579 (2001), [hep-lat/0012023].
- 284. M. Ferreira, P. Costa, O. Loureno, T. Frederico and C. Providncia, "Inverse magnetic catalysis in the (2+1)-flavor Nambu-Jona-Lasinio and Polyakov-Nambu-Jona-Lasinio models," Phys. Rev. D 89 (2014) 116011, [arXiv:1404.5577 [hep-ph]].
- 285. J. Braun, W. A. Mian and S. Rechenberger, "Delayed Magnetic Catalysis," [arXiv:1412.6025 [hep-ph]].
- 286. E. S. Fraga and L. F. Palhares, "Deconfinement in the presence of a strong magnetic background: an exercise within the MIT bag model," Phys. Rev. D 86 (2012) 016008, [arXiv:1201.5881 [hep-ph]].

287. N. O. Agasian and S. M. Fedorov, “Quark-hadron phase transition in a magnetic field,” Phys. Lett. B 663 (2008) 445, [arXiv:0803.3156 [hep-ph]].
288. E. S. Fraga, J. Noronha and L. F. Palhares, “Large N_c Deconfinement Transition in the Presence of a Magnetic Field,” Phys. Rev. D 87 (2013) 114014, [arXiv:1207.7094 [hep-ph]].
289. G. F. de Teramond and S. J. Brodsky, Phys. Rev. Lett. 94, 201601 (2005) [hep-th/0501022].
290. A. Karch, E. Katz, D. T. Son and M. A. Stephanov, Phys. Rev. D 74, 015005 (2006) [hep-ph/0602229].
291. H. Liu, K. Rajagopal and Y. Shi, JHEP 0808, 048 (2008) [arXiv:0803.3214 [hep-ph]].
292. K. Chelabi, Z. Fang, M. Huang, D. Li and Y. L. Wu, JHEP 1604, 036 (2016) [arXiv:1512.06493 [hep-ph]].
293. S. S. Gubser, A. Nellore, S. S. Pufu and F. D. Rocha, Phys. Rev. Lett. 101, 131601 (2008) [arXiv:0804.1950 [hep-th]].
294. S. S. Gubser, S. S. Pufu and F. D. Rocha, JHEP 0808, 085 (2008) [arXiv:0806.0407 [hep-th]].

- 295. R. Rougemont, A. Ficnar, S. Finazzo and J. Noronha, JHEP 1604, 102 (2016) [arXiv:1507.06556 [hep-th]].
- 296. U. Gursoy, E. Kiritsis, L. Mazzanti, G. Michalogiorgakis and F. Nitti, Lect. Notes Phys. 828, 79 (2011) [arXiv:1006.5461 [hep-th]].
- 297. A. Karch and E. Katz, JHEP 0206, 043 (2002) [hep-th/0205236].
- 298. D. Mateos, R. C. Myers and R. M. Thomson, Phys. Rev. Lett. 97, 091601 (2006) [hep-th/0605046].
- 299. J. Erdmenger, N. Evans, I. Kirsch and E. Threlfall, Eur. Phys. J. A 35, 81 (2008) [arXiv:0711.4467 [hep-th]].
- 300. T. Sakai and S. Sugimoto, Prog. Theor. Phys. 113, 843 (2005) [hep-th/0412141].
- 301. A. Rebhan, EPJ Web Conf. 95, 02005 (2015) [arXiv:1410.8858 [hep-th]].
- 302. P. Kraus, F. Larsen and S. P. Trivedi, JHEP 9903, 003 (1999) [hep-th/9811120].
- 303. A. Brandhuber and K. Sfetsos, Adv. Theor. Math. Phys. 3, 851 (1999) [hep-th/9906201].
- 304. M. Cvetič, S. S. Gubser, H. Lu and C. N. Pope, Phys. Rev. D 62, 086003 (2000) [hep-th/9909121].

- 305. I. Bakas and K. Sfetsos, Nucl. Phys. B 573, 768 (2000) [hep-th/9909041].
- 306. I. R. Klebanov and M. J. Strassler, JHEP 0008, 052 (2000) [hep-th/0007191].
- 307. J. Polchinski and M. J. Strassler, hep-th/0003136.
- 308. J. M. Maldacena and C. Nunez, Phys. Rev. Lett. 86, 588 (2001) [hep-th/0008001].
- 309. S. S. Gubser, Nucl. Phys. B 551, 667 (1999) [hep-th/9810225].
- 310. K. Behrndt, M. Cvetič and W. A. Sabra, Nucl. Phys. B 553, 317 (1999) [hep-th/9810227].
- 311. M. Cvetič and S. S. Gubser, JHEP 9904, 024 (1999) [hep-th/9902195].
- 312. M. Cvetič and S. S. Gubser, JHEP 9907, 010 (1999) [hep-th/9903132].
- 313. R. G. Cai and K. S. Soh, Mod. Phys. Lett. A 14, 1895 (1999) [hep-th/9812121].
- 314. A. Chamblin, R. Emparan, C. V. Johnson and R. C. Myers, Phys. Rev. D 60, 064018 (1999) [hep-th/9902170].
- 315. S. D. Avramis and K. Sfetsos, JHEP 0701, 065 (2007) [hep-th/0606190].
- 316. D. T. Son and A. O. Starinets, JHEP 0603, 052 (2006) [hep-th/0601157].

- 317. O. DeWolfe, S. S. Gubser and C. Rosen, Phys. Rev. D 84, 126014 (2011) [arXiv:1108.2029 [hep-th]].
- 318. X. Wu, Phys. Rev. D 90, no. 6, 066008 (2014) [arXiv:1401.2701 [hep-th]].
- 319. S. I. Finazzo, R. Rougemont, M. Zaniboni, R. Critelli and J. Noronha, arXiv:1610.01519 [hep-th].
- 320. M. Cvetič et al., Nucl. Phys. B 558, 96 (1999) [hep-th/9903214].
- 321. M. Cvetič, H. Lu, C. N. Pope, A. Sadrzadeh and T. A. Tran, Nucl. Phys. B 586, 275 (2000) [hep-th/0003103].
- 322. K. A. Mamo and H. U. Yee, Phys. Rev. D 92, no. 10, 105005 (2015) [arXiv:1505.01183 [hep-ph]].
- 323. S. W. Hawking, Commun. Math. Phys. 43, 199 (1975) Erratum: [Commun. Math. Phys. 46, 206 (1976)].
- 324. S. W. Hawking, Phys. Rev. D 14, 2460 (1976).
- 325. M. Natsuume, Lect. Notes Phys. 903, pp.1 (2015) [arXiv:1409.3575 [hep-th]].
- 326. S. W. Hawking and D. N. Page, Commun. Math. Phys. 87, 577 (1983).

- 327. S. W. Hawking, Phys. Rev. D 72, 084013 (2005) [hep-th/0507171].
- 328. R. Gregory and R. Laflamme, Phys. Rev. Lett. 70, 2837 (1993) [hep-th/9301052].
- 329. T. Banks, M. R. Douglas, G. T. Horowitz and E. J. Martinec, [hep-th/9808016].
- 330. V. E. Hubeny and M. Rangamani, JHEP 0205, 027 (2002) [hep-th/0202189].
- 331. A. Buchel and L. Lehner, Class. Quant. Grav. 32, no. 14, 145003 (2015) [arXiv:1502.01574 [hep-th]].
- 332. O. Aharony, S. S. Gubser, J. M. Maldacena, H. Ooguri and Y. Oz, Phys. Rept. 323, 183 (2000) [hep-th/9905111].
- 333. G. Policastro, D. T. Son and A. O. Starinets, “From AdS / CFT correspondence to hydrodynamics,” JHEP 0209, 043 (2002) [hep-th/0205052].
- 334. F. Cooper and G. Frye, Phys. Rev. D 10, 186 (1974).
- 335. J. M. Maldacena, Phys. Rev. Lett. 80, 4859 (1998) [hep-th/9803002].
- 336. N. R. Constable and R. C. Myers, JHEP 9910, 037 (1999) [hep-th/9908175].
- 337. C. Csaki, H. Ooguri, Y. Oz and J. Terning, JHEP 9901, 017 (1999) [hep-th/9806021].

338. S. Jeon and U. Heinz, *Int. J. Mod. Phys. E* 24, no. 10, 1530010 (2015) [arXiv:1503.03931 [hep-ph]].
339. P. Castorina, D. Kharzeev and H. Satz, *Eur. Phys. J. C* 52, 187 (2007) [arXiv:0704.1426 [hep-ph]].
340. O. Aharony, S. Minwalla and T. Wiseman, *Class. Quant. Grav.* 23, 2171 (2006) [hep-th/0507219].
341. S. S. Gubser, “Momentum fluctuations of heavy quarks in the gauge-string duality,” *Nucl. Phys. B* 790, 175 (2008) [hep-th/0612143].
342. J. Casalderrey-Solana and D. Teaney, “Heavy quark diffusion in strongly coupled $N=4$ Yang-Mills,” *Phys. Rev. D* 74, 085012 (2006) [hep-ph/0605199].
343. H. Liu, K. Rajagopal and U. A. Wiedemann, “Calculating the jet quenching parameter from AdS/CFT,” *Phys. Rev. Lett.* 97, 182301 (2006) [hep-ph/0605178].
344. S. S. Gubser, A. Nellore, S. S. Pufu and F. D. Rocha, “Thermodynamics and bulk viscosity of approximate black hole duals to finite temperature quantum chromodynamics,” *Phys. Rev. Lett.* 101, 131601 (2008) [arXiv:0804.1950 [hep-th]].
345. S. S. Gubser, S. S. Pufu and F. D. Rocha, “Bulk viscosity of strongly coupled plasmas with holographic duals,” *JHEP* 0808, 085 (2008) [arXiv:0806.0407 [hep-th]].

- 346. R. Rougemont, A. Ficnar, S. Finazzo and J. Noronha, “Energy loss, equilibration, and thermodynamics of a baryon rich strongly coupled quark-gluon plasma,” JHEP 1604, 102 (2016) [arXiv:1507.06556 [hep-th]].
- 347. P. Kraus, F. Larsen and S. P. Trivedi, “The Coulomb branch of gauge theory from rotating branes,” JHEP 9903, 003 (1999) [hep-th/9811120].
- 348. A. Brandhuber and K. Sfetsos, “Wilson loops from multicenter and rotating branes, mass gaps and phase structure in gauge theories,” Adv. Theor. Math. Phys. 3, 851 (1999) [hep-th/9906201].
- 349. S. S. Gubser, “Thermodynamics of spinning D3-branes,” Nucl. Phys. B 551, 667 (1999) [hep-th/9810225].
- 350. M. Cvetič and S. S. Gubser, “Phases of R charged black holes, spinning branes and strongly coupled gauge theories,” JHEP 9904, 024 (1999) [hep-th/9902195].
- 351. M. Cvetič and S. S. Gubser, “Thermodynamic stability and phases of general spinning branes,” JHEP 9907, 010 (1999) [hep-th/9903132].
- 352. R. G. Cai and K. S. Soh, “Critical behavior in the rotating D-branes,” Mod. Phys. Lett. A 14, 1895 (1999) [hep-th/9812121].

- 353. X. Wu, “Holographic entanglement entropy and thermodynamic instability of planar R-charged black holes,” *Phys. Rev. D* 90, no. 6, 066008 (2014) [arXiv:1401.2701 [hep-th]].
- 354. K. Behrndt, M. Cvetič and W. A. Sabra, “Nonextreme black holes of five-dimensional $N=2$ AdS supergravity,” *Nucl. Phys. B* 553, 317 (1999) [hep-th/9810227].
- 355. S. D. Avramis and K. Sfetsos, “Supergravity and the jet quenching parameter in the presence of R-charge densities,” *JHEP* 0701, 065 (2007) [hep-th/0606190].
- 356. D. T. Son and A. O. Starinets, “Hydrodynamics of r-charged black holes,” *JHEP* 0603, 052 (2006) [hep-th/0601157].
- 357. O. DeWolfe, S. S. Gubser and C. Rosen, “Dynamic critical phenomena at a holographic critical point,” *Phys. Rev. D* 84, 126014 (2011) [arXiv:1108.2029 [hep-th]].
- 358. M. Cvetič et al., “Embedding AdS black holes in ten-dimensions and eleven-dimensions,” *Nucl. Phys. B* 558, 96 (1999) [hep-th/9903214].
- 359. M. Cvetič, H. Lu, C. N. Pope, A. Sadrzadeh and T. A. Tran, “Consistent $SO(6)$ reduction of type IIB supergravity on S^5 ,” *Nucl. Phys. B* 586, 275 (2000) [hep-th/0003103].
- 360. K. A. Mamo, “Holographic Hadronization and Thermal Hadron Emission Rate in $\mathcal{N} = 4$ super Yang-Mills Plasma on the Coulomb Branch,” arXiv:1610.09792 [hep-th].

- 361. K. A. Mamo, “Transport coefficients and hard probes of strongly coupled $\mathcal{N} = 4$ super Yang-Mills plasma on the Coulomb branch,” arXiv:1610.09793 [hep-th].
- 362. K. A. Mamo and H. U. Yee, “Gradient Correction to Photon Emission Rate at Strong Coupling,” Phys. Rev. D 91, no. 8, 086011 (2015) [arXiv:1409.7674 [nucl-th]].
- 363. M. Natsuume, “AdS/CFT Duality User Guide,” Lect. Notes Phys. 903, pp.1 (2015) [arXiv:1409.3575 [hep-th]].
- 364. D. Mateos and L. Patino, “Bright branes for strongly coupled plasmas,” JHEP 0711, 025 (2007) [arXiv:0709.2168 [hep-th]].
- 365. S. I. Finazzo, R. Critelli, R. Rougemont and J. Noronha, “Momentum transport in strongly coupled anisotropic plasmas in the presence of strong magnetic fields,” Phys. Rev. D 94, no. 5, 054020 (2016) [arXiv:1605.06061 [hep-ph]].
- 366. S. K. Das, F. Scardina, S. Plumari and V. Greco, “Toward a solution to the R_{AA} and v_2 puzzle for heavy quarks,” Phys. Lett. B 747, 260 (2015) [arXiv:1502.03757 [nucl-th]].
- 367. E. Caceres and A. Guijosa, “Drag force in charged N=4 SYM plasma,” JHEP 0611, 077 (2006) [hep-th/0605235].

VITA

Kiminad Abebe Mamo

Department of Physics

University of Illinois

Chicago, IL, 60607

E-mail: kabebe2@uic.edu

RESEARCH INTERESTS

My research interests lie in **high energy nuclear physics** and **string theory**. I am particularly interested in using the **AdS/CFT** correspondence and thermal perturbative QCD (**pQCD**) to study heavy-ion physics. I am also interested in the application of the **AdS/CFT** correspondence to quantum gravity and condensed matter physics problems.

PUBLICATIONS

Publications in refereed journals

9. Kiminad A. Mamo,

Energy loss of a nonaccelerating quark moving through a strongly coupled $N=4$ super Yang-Mills vacuum or plasma in strong magnetic field,

Physical Review D 94, 041901 (**Rapid Communications**) (2016)

8. Shiyong Li, Kiminad A. Mamo and Ho-Ung Yee,

Jet quenching parameter of quark-gluon plasma in strong magnetic field: Perturbative QCD

and *AdS/CFT* correspondence,

Physical Review D 94, 085016 (2016)

7. Kiminad A. Mamo and Ho-Ung Yee,

Spin Polarized Photons from Axially Charged Plasma at Weak Coupling: Complete Leading Order,

Physical Review D 93, 065053 (2016)

6. Kiminad A. Mamo and Ho-Ung Yee,

Thermalization of quark-gluon plasma in magnetic field at strong coupling,

Physical Review D 92, 105005 (2015)

5. Kiminad A. Mamo,

Inverse magnetic catalysis in holographic models of QCD,

Journal of High Energy Physics 1505, 121 (2015)

4. Kiminad A. Mamo and Ho-Ung Yee,

Gradient correction to photon emission rate at strong coupling,

Physical Review D 91, 086011 (2015)

3. Kiminad A. Mamo and Ho-Ung Yee,

Spin polarized photon and dilepton from axially charged plasma,

Physical Review D 88, 114029 (2013)

2. Kiminad A. Mamo,

Enhanced thermal photon and dilepton production in strongly coupled $N=4$ SYM plasma in

strong magnetic field,

Journal of High Energy Physics 1308, 083, (2013)

1. Kiminad A. Mamo,

Holographic RG flow of the shear viscosity to entropy density ratio in strongly coupled anisotropic plasma,

Journal of High Energy Physics 1210, 070, (2012)

Preprints on arXiv

2. Kiminad A. Mamo,

Transport coefficients and hard probes of strongly coupled $\mathcal{N} = 4$ super Yang-Mills plasma on the Coulomb branch,

(2016), arXiv:1610.09793 [hep-th]

1. Kiminad A. Mamo,

Holographic Hadronization and Thermal Hadron Emission Rate in $\mathcal{N} = 4$ super Yang-Mills Plasma on the Coulomb Branch,

(2016), arXiv:1610.09792 [hep-th]

Undergraduate thesis and manuscripts

2. Kiminad A. Mamo,

The theory of perturbations near the Schwarzschild black hole,

undergraduate thesis project, (2008)

1. Kiminad A. Mamo,

A series of new exactly solvable potentials: from supersymmetric quantum mechanics,
unpublished, (2008)

ACADEMIC APPOINTMENTS

Dean's Scholar Fellow, Department of Physics, University of Illinois, Chicago, IL 2016-2017

Research Assistant, Department of Physics, University of Illinois, Chicago, IL 2013 - 2016

Teaching Assistant, Department of Physics, University of Illinois, Chicago, IL 2009 - 2013

Instructor, Department of Physics, Samara University, Samara, Ethiopia 2008 - 2009

EDUCATION

University of Illinois, Chicago, IL, Ph.D., Physics, December 2017

Addis Ababa University, Addis Ababa, Ethiopia, B.Sc., Physics, July 2008

AWARDS

2. Dean's Scholar Fellowship (2016-17)

1. LAS Travel Award (2016), GSC Travel Award (2016), Student Presenter Award (2016)

SYNERGISTIC ACTIVITIES

Refereed three papers for Physical Review D

CONFERENCES AND SCHOOLS ATTENDED

9. Midwest Theory Get-Together, Argonne National Laboratory, IL, USA (September 30-October 1, 2016)

8. Hot Quarks, South Padre Island, TX, USA (September 12-17, 2016)

7. XIIth Quark Confinement and the Hadron Spectrum, Thessaloniki Greece (August 28-September 4, 2016)
6. QCD Workshop on Chirality, Vorticity and Magnetic Field in Heavy Ion Collisions UCLA, Los Angeles, CA, USA (February 23-26, 2016)
5. Great Lakes Strings Conference 2015, University of Michigan, Ann Arbor, MI, USA (March 27-29, 2015)
4. ECT* Doctorial Training Program (Heavy Ion Collisions : exploring nuclear matter under extreme conditions) Trento, Italy (April 7-May 16, 2014)
3. Spring School on Sperstring Theory and Related Topics, ICTP, Trieste, Italy (March 31-April 8, 2014)
2. Great Lakes Strings Conference 2013, University of Kentucky, Lexington, KY, USA (May 17-19, 2013)
1. Great Lakes Strings Conference 2012, Purdue University, West Lafayette, IN, USA (March 2-4, 2012)

CONFERENCE AND SEMINAR TALKS

15. *Holographic hadronization, transport coefficients, and hard probes of $N = 4$ super Yang-Mills plasma on the Coulomb branch,*
MIT, Cambridge, MA, USA (October 21, 2016)
14. *Energy loss of a quark moving in a strongly magnetized QGP,*
Midwest Theory Get-Together, Argonne National Laboratory, IL, USA (September 30-October 1, 2016)

13. *Jet quenching in strongly magnetized QGP: pQCD vs. AdS/CFT*,
Hot Quarks, South Padre Island, TX, USA (September 12-17, 2016)
12. *Inverse magnetic catalysis in holographic models of QCD*,
XIIth Quark Confinement and the Hadron Spectrum, Thessaloniki, Greece (August 28-September 4, 2016)
11. *Holographic connection between string theory and the real world*,
Physics Festival, University of Illinois, Chicago, IL, USA (March 11, 2016)
10. *Holographic thermalization and deconfinement Transition*,
QCD Workshop on Chirality, UCLA, Los Angeles, CA, USA (February 25, 2016)
9. *Viscous velocity gradient correction to thermal photon emission rate at strong coupling*,
RIKEN Lunch Seminar, Brookhaven National Laboratory, Upton, NY, USA (November 19, 2015)
8. *Deconfinement phase transition in the presence of a magnetic field in holographic models of QCD*,
Lunch Seminar, Stony Brook University, Stony Brook, NY, USA (November 17, 2015)
7. *Gradient correction to photon emission rate at strong coupling*,
Great Lakes Strings Conference 2015, University of Michigan, Ann Arbor, MI, USA (March 27-29, 2015)
6. *Inverse magnetic catalysis in hard-wall AdS/QCD*
High energy physics seminar, University of Illinois, Chicago, IL, USA (November 5, 2014)

5. *Transport coefficients and thermal photon production rate at strong coupling,*

DTP Seminar, European Center for Theoretical Studies, Trento, Italy (April 8 2014)

4. *Non-universal shear viscosities in strongly coupled anisotropic plasma,*

Great Lakes Strings Conference 2013, University of Kentucky, Lexington, KY, USA (May 17-19, 2013)

3. *De-confinement, chiral symmetry restoration, and photo-emission in Sakai-Sugimoto model of string theory*

High energy physics seminar, University of Illinois, Chicago, IL, USA (March 11, 2013)

2. *Strongly enhanced photon and di-lepton production in strongly coupled $N=4$ super-Yang-Mills plasma in strong external magnetic field*

High energy physics seminar, University of Illinois, Chicago, IL, USA (November 15, 2012)

1. *Holographic Wilsonian RG flow and sliding membrane paradigm*

High energy physics seminar, University of Illinois, Chicago, IL, USA (February 6, 2012))

REFERENCES

Prof. Ho-Ung Yee: Ph.D supervisor, University of Illinois at Chicago and RIKEN-BNL,
Email: hyee@uic.edu

Prof. Wai-Yee Keung: University of Illinois at Chicago, Email: keung@uic.edu

Prof. Arthur Licht: University of Illinois at Chicago, Email: licht@uic.edu

Prof. Misha Stephanov: University of Illinois at Chicago, Email: misha@uic.edu